

Dissecting functions of *Arabidopsis thaliana* IQD and KLCR proteins in the control of microtubule-related processes

Dissertation

zur Erlangung des

Doktorgrades der Naturwissenschaften (Dr. rer. nat.)

der

Naturwissenschaftlichen Fakultät I – Biowissenschaften –

der Martin-Luther-Universität

Halle-Wittenberg



vorgelegt

von **Frau Pratibha Kumari**

geb. am 20.05.1990 in Buxar, Bihar Indien

Reviewers

I. Prof. Dr. Steffen Abel

Leibniz institute of Plant Biochemistry, Martin Luther University,
Halle-Wittenberg, Germany

II. Prof. Dr. Ingo Heilmann

Department of Cellular Biochemistry, Martin Luther University,
Halle-Wittenberg, Germany

III. Prof. Dr. David Bouchez

INRA Centre de Versailles-Grignon, Institut Jean-Pierre Bourgin,
UMR1318 INRA-AgroParisTech-ERL3559 CNRS, Versailles
Cedex France

Date of thesis defense-09.03.2020

(Datum der Verteidigung der Dissertation-09.03.2020)

Table of Contents

List of Abbreviations:	III
Summary	1
1 General introduction	2
1.1 Calcium signaling in plants	2
1.2 Decoding mechanisms of Ca ²⁺ signals.....	3
1.3 Function of Ca ²⁺ in growth regulation at the microtubule cytoskeleton	5
1.4 Microtubule assembly and dynamics	6
1.5 Organizations of microtubule arrays during plant growth and development	8
1.6 Regulation of microtubule organization and dynamics	10
1.7 Spatial regulation of cytokinesis in plants	13
1.7.1 Cell division in plants	13
1.7.2 Division plane selection	14
1.7.3 Division plane establishment	16
1.7.4 Phragmoplast guidance	19
1.7.5 MAPs and their roles in spatial regulation of cytokinesis	21
1.8 CaM interacting MAPs in the regulation of microtubule organization and dynamics	25
1.9 IQD proteins, plant-specific CaM interacting MAPs	28
1.10 KLCRs as IQD interactors.....	33
1.11 Thesis aims.....	35
2 Functional characterization of Arabidopsis IQD6 to IQD8	36
2.1 Introduction:	36
2.1.1 IQD: A novel class of microtubule-associated, Ca ²⁺ -CaM interacting protein.....	36
2.2 Results	39
2.2.1 Phenotypic characterization of <i>iqd6</i> , <i>iqd7</i> , and <i>iqd8</i> mutants	39
2.2.2 Subcellular localization of IQD8 and related proteins during cell division and their expression domains	46
2.2.3 Impairment in IQD8 function leads to defects in microtubule array orientation and formation ...	51
2.2.4 IQDs interact with key players of cytokinesis.....	57
2.2.5 IQD8 plays roles in the efficient recruitment of POKs and PHGAPs to the division site.....	65
2.2.6 IQDs interact genetically with POKs and PHGAPs.....	70
2.3 Discussion.....	73
2.3.1 Impairment of IQD function affects cell wall positioning primarily in the epidermis.....	73
2.3.2 Requirement of IQD8 during cell division.....	75
2.3.3 IQDs interaction with division site markers and its requirement for proper localization	80
2.3.4 Conclusion and outlook.....	81
3 Characterization of KLCR interacting Arabidopsis kinesins	83
3.1 Introduction	83
3.1.1 KLCR as kinesin subunit.....	83
3.1.2 Kinesins: microtubule localized motor proteins for trafficking of cargoes along microtubules. ...	85
3.2 Results	88
3.2.1 Selection of candidate kinesins	88
3.2.2 Localization and interaction analysis of kinesin-1 protein	89
3.2.3 Localization and interaction analysis of kinesin-4 proteins	94
3.2.4 Localization and interaction analysis of kinesin-5 proteins	100
3.2.5 Localization and interaction analysis of kinesin-7 proteins	102
3.2.6 Localization and interaction analyses of kinesin-12, kinesin-13 and kinesin-14 proteins	106
3.3 Discussion.....	110
3.3.1 Regulation of kinesin-KLCR complex formation in Arabidopsis.....	110

3.3.2	Alternative functions of Arabidopsis KLCRs	113
3.3.3	Potential novel functions of kinesin motor proteins in plants	113
3.3.4	Roles of kinesins in organelles transport	116
3.3.5	Roles of kinesins in plasma membrane-microtubule continuum.....	117
3.3.6	The potential functions of kinesins in the nucleus.....	119
4	Materials and methods	120
4.1	Chemicals and other supplies	120
4.2	Media	125
4.2.1	Solid medium (SM) for sterile growth of Arabidopsis seedlings.....	125
4.2.2	Lysogeny broth (LB) medium.....	126
4.2.3	Super optimal broth with catabolite repression (SOC) medium, pH 7.0	126
4.2.4	Preparation of YPD medium for cultivation of yeast cells, pH 6.5.....	126
4.2.5	Preparation of synthetic defined (SD) medium	127
4.3	Plant cultivation and growth conditions	127
4.3.1	Sterile growth of Arabidopsis seedlings on agar plates	127
4.3.2	Cultivation of <i>A. thaliana</i> and <i>N. benthamiana</i> on soil	127
4.3.3	Stable transformation of <i>A. thaliana</i> via the floral dip method.....	128
4.3.4	Transient transformation of <i>N. benthamiana</i> leaves.....	128
4.3.5	Generation of mutant lines.....	129
4.4	Cultivation of bacteria and yeast.....	129
4.4.1	Cultivation of <i>Escherichia coli</i> (<i>E. coli</i>).....	129
4.4.2	Cultivation of <i>A. tumefaciens</i>	129
4.4.3	Growth and transformation of <i>S. cerevisiae</i> cultures for Y2H assays.....	130
4.5	Transformation of bacteria and yeast	130
4.5.1	Transformation of chemical competent <i>E. coli</i> cells.....	130
4.5.2	Transformation of chemical competent <i>A. tumefaciens</i>	130
4.5.3	Transformation of <i>Saccharomyces cerevisiae</i> (<i>S. cerevisiae</i>).....	131
4.6	Molecular biological methods.....	132
4.6.1	DNA-based methods.....	132
4.6.2	RNA-based methods.....	135
4.7	Microscopic analysis	136
4.7.1	Confocal laser scanning microscopy (CLSM)	136
4.7.2	Whole-mount immunofluorescence and DAPI staining.....	137
4.7.3	Subcellular distribution of IQD8-GFP	137
4.7.4	Plot profile.....	137
4.7.5	Microtubule pattern analysis and quantification	138
4.7.6	Analysis of width of IQD8-GFP at the division site.....	138
4.7.7	Localization of IQD6-GFP and IQD8-GFP	138
4.7.8	Analysis of cell number, meristem size and root diameter.....	138
4.8	Analysis of growth morphology of mutants and WT.....	139
4.9	Cell wall deviation study and quantification	139
5	Supplemental figures.....	140
	References	153
	Acknowledgements	VII
	CURRICULUM VITAE	VIII
	Erklärung zur Dissertation	XI

List of Abbreviations:

Abbreviation	Description
%	Percentage
°	Degree
μ	Micro
Δ	Deleted
μm	Micrometer
μM	Micromolar
A	Ampere
AD	Activation domain
ADE	Adenin
ANOVA	Analysis of variance
APS	Ammonium persulfate
At(gene name)	<i>Arabidopsis thaliana</i> (gene name)
ATP	Adenosine triphosphate
BiFC	Bimolecular fluorescence complementation assay
bp	Base pairs
BASTA	A brand name for Glufosinate or phosphinothricin
BSA	Bovine serum albumin
°C	Degree celsius
Ca ²⁺	Calcium ion
CaM	Calmodulin
cDNA	Complementary deoxyribonucleic acid
CDS	Cortical division site
CDZ	Cortical division zone
35S promoter	Promoter of 35S RNA coding region in CaMV genome
CLSM	Confocal laser scanning microscopy
CML	Calmodulin-LIKES
Col-0	Arabidopsis ecotype Columbia-0
C-terminal	Carboxy-terminal
DAPI	4',6-diamidino-2-phenylindole
DBD	Deoxyribonucleic acid binding domain
DEST	Destination vector
DMF	Dimethylformamide
DMSO	Dimethyl sulfoxide

DNA	Deoxyribonucleic acid
dNTP	Deoxyribonucleotide
DONR	Donor vector
DTT	Dithiothreitol
<i>E. coli</i>	<i>Escherichia coli</i>
EDTA	Ethylenediaminetetraacetic acid
ENTR	Entry vector
EXP	Expression vector
F-actin	Filamentous actin
FM4-64	<i>N</i> -(3-triethylammoniumpropyl)-4-(6-(4-(diethylamino phenyl hexatrienyl) pyridinium dibromide
FWD	Forward
g	Gram
GFP	Green fluorescent protein
Gh(gene name)	<i>Gossypium hirsutum</i> (gene name)
GTP	Guanosine triphosphate
GUS	β -Glucuronidase
GW	Gateway
h	hour
HEPES	2- (4-(2-hydroxyethyl)-1-piperazinyl) ethanesulfonic acid
HIS	Histidine
IQD	IQ67-DOMAIN
IQR	Interquartile range
Kb	Kilobases
KD	Kilodalton
KHC	KINESINHEAVYCHAIN
KLC(R)	KINESIN LIGHT CHAIN-(RELATED)
L	Liter
LB	Lysogeny broth
LEU	Leucine
LiOAc	Lithium acetate
LSM	Laser scanning microscope
MAP	Microtubule-associated protein
Δ MD	Deleted motor domain
MES	2-(<i>N</i> -Morpholino)ethanesulfonic acid

MilliQ	Ultrapure water
min	Minute
MBD	Microtubule binding domain
n	Nano/Number
OD ₆₀₀	Optical density at 600 nm wavelength
Os(gene name)	<i>Oryza sativa</i>
PAGE	Polyacrylamide gel electrophoresis
PCR	Polymerase chain reaction
PEG	Polyethyleneglycol
PHGAP	PLECKSTRIN HOMOLOGY GTPase ACTIVATING PROTEIN
PI	Propidium iodide
POK	PHRAGMOPLAST ORIENTING KINESIN
PPB	Preprophase band
QC	Quiescent center
RANGAP	Ran GTPase- ACTIVATING PROTEIN
REV	Reverse
Rho	Rat sarcoma homolog
RFP	Red Fluorescent Protein
RNA	Ribonucleic acid
ROP	RHO GTPase from plants
rpm	Revolutions per minute
RT	Room temperature
s	Second
SD	Synthetic defined
SDS	Sodium dodecyl sulfate
S.O.B	Super optimal broth
S.O.C	Super optimal broth with catabolite repression
ssDNA	Single stranded DNA
TAN	TANGLED
TAE	Tris acetate EDTA
TBS	Tris-buffered saline
TBST	TBS with tween20
T-DNA	Transfer deoxyribonucleic acid
TE	Tris-EDTA buffers
TEMED	Tetramethylethylenediamine

Tris	Tris(hydroxymethyl)aminomethane
TRP	Tryptophan
TTP	TON-TRM-PP2A
TZ	Transition zone
V	Volt
v/v	Volume per volume
W	Watt
w/v	Weight per volume
WT	Wild type
Y2H	Yeast-two hybrid
YFP	Yellow fluorescent protein
YPDA	Yeast, peptone, dextrose, adenine

Summary

Calcium (Ca^{2+}) is a ubiquitous second messenger, which plays a very important role in various aspects of plant growth and development. Ca^{2+} sensor proteins such as calmodulin (CaM) and CaM-LIKE (CML) proteins sense spatio-temporal oscillations of Ca^{2+} . Extensive analysis in our group established IQ67-DOMAIN (IQD) proteins as one of the largest known class of CaM binding proteins in plants. IQD proteins mostly localize to microtubules, while some also localize to membrane subdomains or to the cell nucleus, where they recruit CaM to their distinct subcellular sites. IQDs contain regions of intrinsic disorder, which is a feature of scaffold proteins. In co-recruitment assay in *Nicotiana benthamiana*, IQD1 was found to directly interact with KINESIN LIGHT CHAIN (KLC)-RELATED1 (KLCR1) inside the nucleus and at microtubules. Arabidopsis KLCR proteins share sequence and structural similarity with mammalian KLCs, which are functional subunits of animal type-1 kinesins. Taken together, we propose that IQD proteins may act as scaffolds to coordinate Ca^{2+} -CaM signaling at the microtubule-membrane continuum to regulate microtubule dynamics and organization, thereby contributing to plant growth and development. In support of this hypothesis, previous studies showed that the impairment of IQD functions results in various microtubule-related growth defects. However, the precise mechanisms of IQDs functions are largely elusive.

In the first part of this dissertation, using a reverse genetic approach, we aimed to characterize the functions of IQD6, IQD7 and IQD8. Our data revealed IQD8 as a potential scaffold, which plays a multifunctional role during spatial control of cytokinesis starting from division plane selection, establishment, and up to the directed expansion of phragmoplast via association with PHRAGMOPLAST ORIENTING KINESINS and PLECKSTRIN HOMOLOGY GTPase ACTIVATING PROTEIN. Our results imply an interplay between IQDs mediated Ca^{2+} and ROP signaling to fine-tune directed cell wall positioning. Despite the defects in mitotic microtubule arrays at various stages of cell division in the *iqd678* triple mutants, the overall growth and morphology of the plant was not hampered. Therefore, *iqd678* triple mutants may serve as a tool for studying open questions concerning division plane selection, establishment and the guided expansion of phragmoplast. In addition, there is no direct evidence for Ca^{2+} -CaM functions in the regulation of microtubule dynamics during cell division in plants so far. The *iqd678* triple mutants may provide a tool to study the regulation of Ca^{2+} signaling during plant cell division.

In the second part of this dissertation work, we investigated KLCRs functions in terms of their predicted role as a subunit of animal type-1 kinesin-like complexes in plants using targeted interaction studies. In our extensive analysis, we could not identify KLCRs-interacting kinesins. However, we observed the direct interactions of IQD1 and IQD8 with KIN4A. Therefore, our data suggested a possible function of IQDs as a scaffold in the formation of KLCRs-kinesins complexes or alternatively in regulating kinesin mediated intracellular transport of cargoes through direct interaction with kinesins. In addition, this work revealed localization information of candidate kinesins and their interactions. Some of these candidates are entirely uncharacterized. Data from our research will help towards a better understanding of kinesins functions in plants.

1 General introduction

1.1 Calcium signaling in plants

Calcium ions (Ca^{2+}) act as ubiquitous second messengers that play important roles in many cellular processes in response to developmental and environmental cues (Edel and Kudla, 2015; Hepler, 2005; Hepler and Wayne, 1985; Kudla et al., 2010). While calcium (Ca) is the most abundant element in the earth's crust and is involved in almost all signaling and processes, high Ca^{2+} levels are toxic and even lethal (Blackstone, 2015; Case et al., 2007; Kazmierczak et al., 2013).

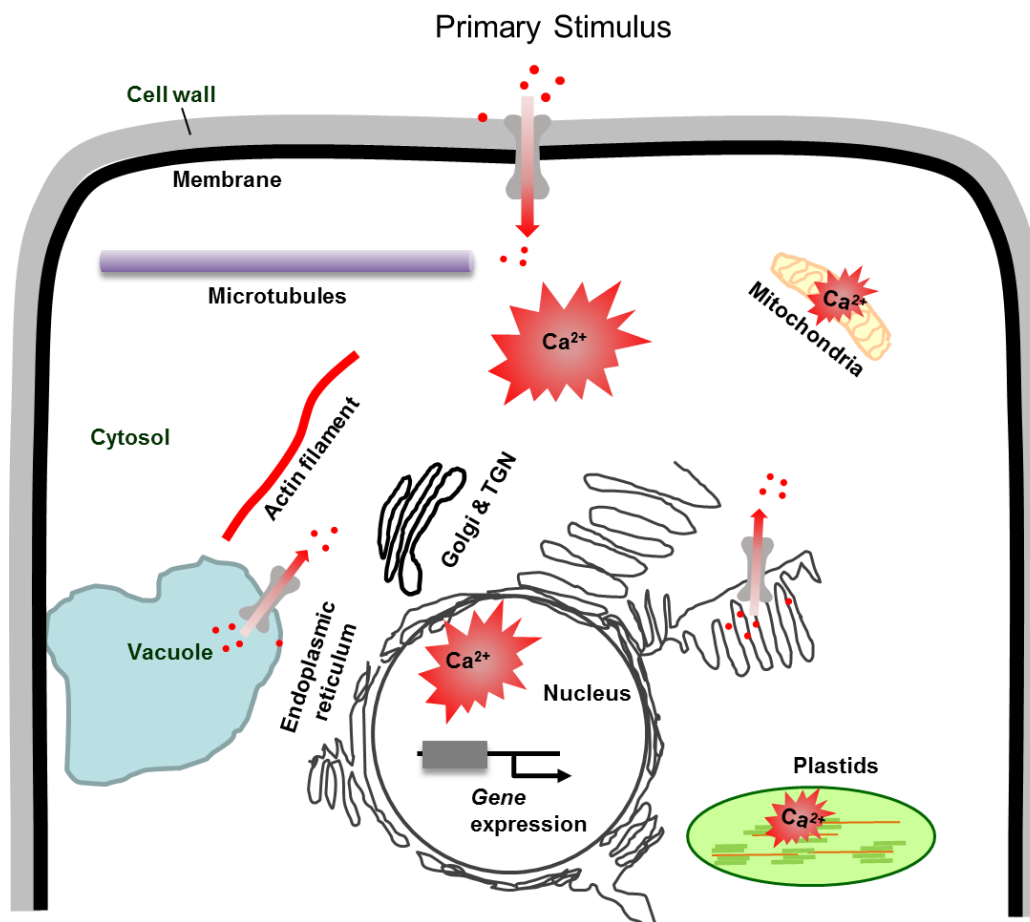


Figure 1.1 Schematic representation of Ca^{2+} distribution and signaling in plants.

In response to primary stimuli, a Ca^{2+} spike is generated within plant cell, which in turn causes downstream response in the nucleus. Ca^{2+} signaling occurs in the cytosol, nucleus, mitochondria and plastids. Ca^{2+} is primarily release of from ER, vacuole and apoplast in response to various stimuli.

The most important reason is that Ca^{2+} at high concentration forms highly insoluble complexes with phosphate. Phosphate is very important for cellular energy metabolism in all life forms (Harold, 2014), and together with Ca^{2+} forms insoluble precipitates, which hinders energy metabolism. Ca^{2+} concentrations above the physiological levels often cause chromosome condensation, protein aggregation and impair several other intracellular

activities (Blackstone, 2015; Case et al., 2007). Under normal physiological conditions, cells maintain a submicromolar concentration of Ca^{2+} in the cytosol by withdrawing Ca^{2+} from the cytosol to the apoplast or the lumen of organelles such as the ER and the vacuole. In response to various stimuli, Ca^{2+} levels in the cells vary spatially and temporally. Such triggers include both abiotic and biotic stress as well as signals from the developmental program. A 10-fold increase in Ca^{2+} level (to 1 μM) is enough to activate the developmental events, without affecting the phosphate energy metabolism (Hepler, 2016, 2005; Hepler and Wayne, 1985). Specific Ca^{2+} signatures that are characterized by amplitude, frequency and duration are produced spatially and temporarily in response to diverse stimuli (Figure 1.1). Signatures of Ca^{2+} are generated by the coordinated action of voltage and ligand-gated channels and transporters present at membranes of different organelles and at the plasma membrane (Dodd et al., 2010; Kudla et al., 2010; Sanders et al., 1999). Ca^{2+} channels, pumps and transporters are encoded by approximately 80 genes in *Arabidopsis*, indicating the diversity in the generation of Ca^{2+} signatures.

1.2 Decoding mechanisms of Ca^{2+} signals

The information encoded in Ca^{2+} signatures is perceived and transduced by a variety of Ca^{2+} binding proteins that eventually coordinate cellular responses (Figure 1.2). Most of the Ca^{2+} binding proteins possess EF-hand motifs, which upon binding to Ca^{2+} undergo conformational changes that either affect their affinity to target proteins or modulate their own enzymatic activity in order to transduce the signals into stimulus-specific responses. *Arabidopsis thaliana* (*A. thaliana*) encodes about 250 EF hand containing Ca^{2+} sensor proteins, which are further grouped into sensor responders and sensor relays (Day et al., 2002; Ranty et al., 2006; Sanders et al., 2002; Xu and Huang, 2017). Sensor responders are bifunctional sensors which consist of both Ca^{2+} binding motifs and a kinase domain, thus capable of transducing Ca^{2+} signals directly by phosphorylation of targets. By definition sensor responders act by intramolecular interactions. Ca^{2+} -dependent protein kinases (CDPKs) are an example of sensor responders that contain Ca^{2+} -dependent Ser/Thr protein kinases as well as 4 EF-hand motifs (Harmon et al., 2000; Hrabak et al., 2003). CDPKs are known to catalyze Ca^{2+} -dependent phosphorylation of their target proteins via its intrinsic catalytic activity (Day et al., 2002). CDPKs are encoded by 34 genes in *A. thaliana*, 31 in *Oryza sativa* (*O. sativa*) (Cai et al., 2015; Hrabak et al., 2003; Ray et al., 2007; Romeis et al., 2001; Saijo et al., 2000; Sheen, 1996), about 20 in *Triticum aestivum* (*T. aestivum*), 35 in *Zea mays* (*Z. mays*) and 20 in *Populus trichocarpa* (*P. trichocarpa*) (Boudsocq et al., 2012; Cai et al., 2015) and are known to play crucial roles in stress and hormone signaling pathways (Boudsocq et al., 2012; Xu and Huang, 2017).

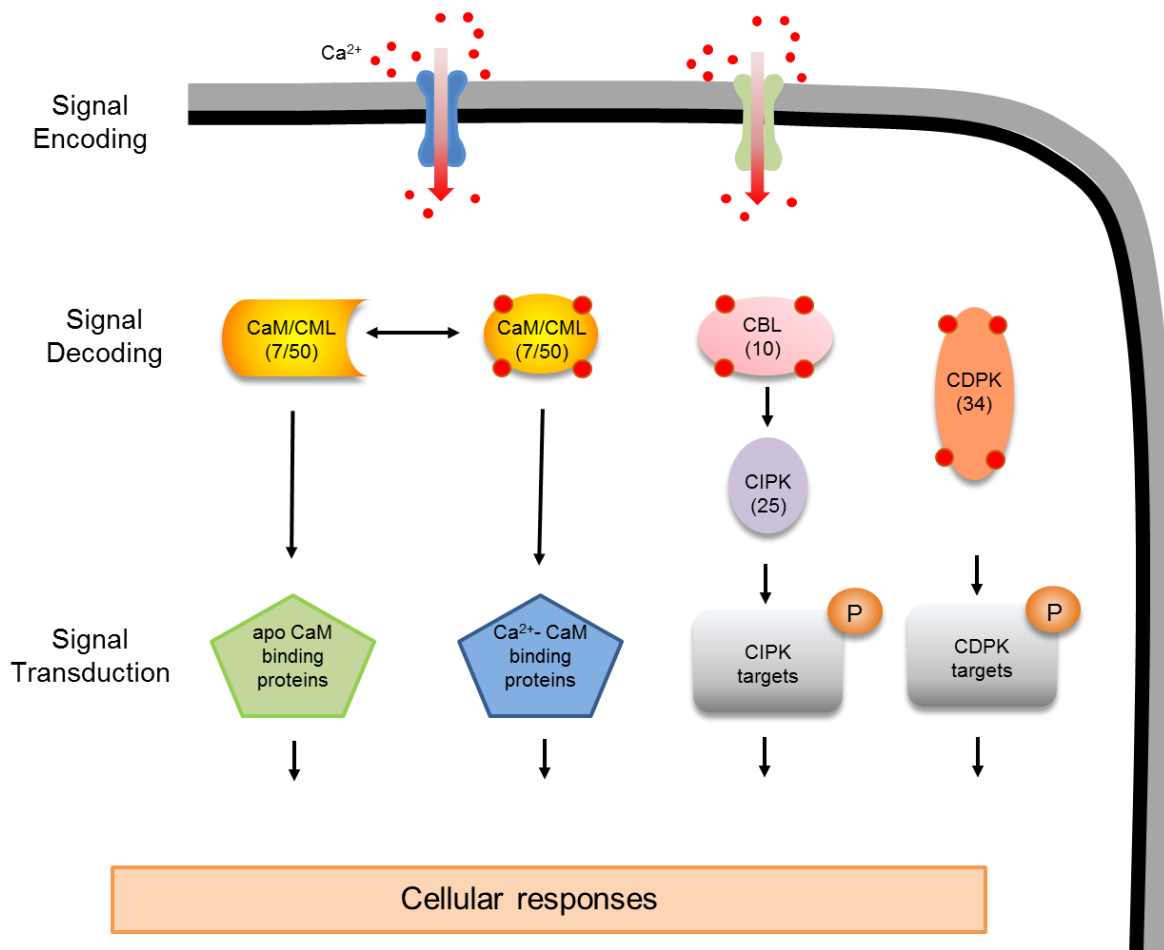


Figure 1.2 Ca²⁺ signaling pathways in plants.

Schematic representation showing different types of Ca²⁺ sensor proteins and their downstream pathways. Numbers in the parenthesis indicate the number of genes encoding respective Ca²⁺ sensor proteins. CaM/CMLs, calmodulin/CaM-LIKE; CDPK, Ca²⁺-DEPENDENT PROTEIN KINASE; CBL, CALCINEURIN B-LIKE; CIPK, CBL-INTERACTING PROTEIN KINASE; P, phosphorylation.

Ca²⁺ sensor relays are sensors which do not contain a catalytic activity. Calmodulin (CaM) and CaM-LIKE proteins (CMLs), and CALCINEURIN B-LIKE (CBLs) are categorized as Ca²⁺ sensor relays. They undergo Ca²⁺-induced conformational changes and subsequently interact with target proteins to regulate the biochemical activities of their targets. CaM and CMLs also interact with target proteins even in the absence of Ca²⁺. The target proteins then modulate various cellular activities to yield cellular responses. Sensor relays decode the signals via bimolecular interactions (Dodd et al., 2010; Kudla et al., 2010; Luan et al., 2002; Sanders et al., 1999). In Arabidopsis, 10 CBLs regulate a specific class of target proteins, the CBL-INTERACTING PROTEIN KINASES (CIPKs), in a Ca²⁺-dependent fashion. CIPKs comprise a family of 26 SNF1-like Ser/Thr protein kinases. CBL-CIPK interaction modules have been considered as bimolecular sensor responders, which play roles in the integration of plant responses to environmental stimuli (Halfter et al., 2000; Hashimoto and Kudla, 2011; Kolukisaoglu et al., 2004; Luan et al., 2002).

The second group of Ca²⁺ sensor relays includes CaM and CMLs, encoded by 7 and 50 genes, respectively, in Arabidopsis. In contrast to CBLs, CaM/CMLs regulate a broad range of functionally diverse proteins, which include transcription factors, enzymes involved in signaling and metabolic pathways, microtubule-associated proteins (MAP) and proteins involved in generating Ca²⁺ signatures (Bouché et al., 2005; Ranty et al., 2006). The potential number of CaM/CML binding proteins (CaMBPs) exceeds more than 300 in plants (Bouché et al., 2005; McCormack et al., 2005; Reddy et al., 2011). CaM/CML family members alter the activity of target proteins by Ca²⁺-dependent/independent protein-protein interactions (Bouché et al., 2005; Ranty et al., 2006). CaM interacting domains of target proteins vary in terms of their primary structure, suggesting the versatility of CaM/CML signaling modules. Typical CaM binding domains are composed of a short (16-35 residues) basic amphiphilic helix which binds to a flexible hydrophobic pocket that forms upon Ca²⁺ binding to apo-CaM/CMLs. Three consensus CaM recruitment motifs are found in many CaMBP, which include the IQ motif (IQxxxRGxxxR) and two related motifs, 1-(5)-10 and 1-(8)-14, which mediate interaction with CaM in Ca²⁺-independent and Ca²⁺-dependent manner, respectively (Bähler and Rhoads, 2002; Hoeflich and Ikura, 2002).

1.3 Function of Ca²⁺ in growth regulation at the microtubule cytoskeleton

Ca²⁺ plays roles in various aspects of plant growth and development by fine-tuning incoming signals during developmental processes of plants. Several studies have shown a role of Ca²⁺ in the regulation and dynamics of microtubules (Hepler, 2016, 2005). Microtubules are components of the cytoskeletal network that form highly dynamic structures and play central roles in cell division, cell expansion, intracellular transport and cellular organization (Akhmanova and Hammer, 2010; Hussey et al., 2006; Lloyd and Hussey, 2001; Sedbrook and Kaloriti, 2008; Wasteneys and Yang, 2004). Microtubule stability is sensitive in vitro to concentration <1 µM of Ca²⁺ ions, indicating direct regulation of the microtubule cytoskeleton by Ca²⁺ (Weisenberg, 1972). It has also been found that much lower amounts of Ca²⁺ are required to depolymerize microtubules in crude extract, which suggested the presence of some proteins in the crude extract that could facilitate microtubule depolymerization (Weisenberg, 1972). Marcum et al. (1978) further showed that Ca²⁺ concentration required for the depolymerization of purified microtubules was decreased by two orders of magnitude, which indicated that CaM increase the sensitivity of microtubules to Ca²⁺. It has been shown that the pressure microinjection of CaM into the living fibroblast cells leads to the localized disruption of microtubules at a relatively small elevation of intracellular Ca²⁺ concentrations. CaM possibly control the lability of Ca²⁺ to microtubule at a molar ratio (CaM: tubulin) that can be achieved locally within the cell. (Keith et al., 1983).

CaM binds to microtubules with very low affinity (Wu et al., 2006), suggesting the involvement of CaM interacting MAPs in Ca²⁺-CaM-dependent regulation of microtubules. Binding of CaM to these MAPs may alter their activities which in turn would result in changes in the stabilization and organization of microtubule (Lloyd and Hussey, 2001; Oda, 2018; Vos et al., 2000). Indeed, past research has shown a differential effect of CaM on microtubule stabilization in the presence or absence of MAPs (Fisher et al., 1996; Lee and Wolff, 1982). In addition, generation of Ca²⁺ in response to various stress conditions such as cold, touch response, gravistimulus, and biotic stress, such as pathogen attack correlates with changes in microtubule organization and stability (Bergey et al., 2014; Hardham, 2013; Nick, 2013; Wang et al., 2011). Several studies have shown that elevation of Ca²⁺ is associated with specific stages of cell division, which may ultimately help in regulating microtubule organization and dynamics (Hepler and Wolniak, 1984; Whitaker, 2008, 2006; Zhang et al., 1990). Ca²⁺ has also been shown to play important roles in regulation of cell wall rigidity as it forms complexes with pectins and stabilizes interaction between pectins (Hepler, 2005). Changes in cell wall composition, in particular in pectin methylesterification precede changes in microtubule organization as has been shown during symmetry breaking in hypocotyl cells (Peaucelle et al., 2015).

1.4 Microtubule assembly and dynamics

Microtubules are components of the cytoskeleton which are vital for various cellular activities of eukaryotic organisms and required for plant growth and development via regulation of cell division, cell expansion and cell differentiation (de Keijzer et al., 2017; Liu et al., 2015; Paredez et al., 2006). Microtubules are 25 nm hollow cylinders made up of a lateral combination of 13 protofilaments. Each protofilament is assembled from alpha (α) and beta (β) tubulin heterodimers in head to tail orientation (Figure 1.3A). Microtubule filaments are polar structures that possess a plus, β -tubulin exposing end, and a minus end, at which α -tubulin is exposed (Goddard et al., 1994; Ledbetter and Porter, 1963). The Guanosine triphosphate (GTP) bound to β -tubulin is hydrolyzed to Guanosine diphosphate (GDP) upon addition of novel α + β -tubulin heterodimers to the plus end of microtubules. In contrast, α -tubulin bound GTP is relatively stable and not hydrolyzed (Figure 1.3B). The GTP-bound form of α - β dimers is more stable than the GDP-bound form. This explains the dynamic nature of plus ends of microtubule filaments, which undergo constant switches between growth and shrinkage (Dixit and Cyr, 2004a; Drechsel and Kirschner, 1994; Horio and Murata, 2014; Kirschner and Mitchison, 1986).

When GTP-bound β -tubulin is present at the plus ends of microtubule filaments, the resulting structure is termed as GTP cap which stabilizes microtubule plus ends and is required for microtubule polymerization (Drechsel and Kirschner, 1994; Weisenberg, 1972). Hydrolysis of GTP leads to conformational changes and subsequent loss of GDP end subunits (Nogales and Wang, 2006; Wang and Nogales, 2005). When microtubules transition from growth to shrinkage, the event is termed catastrophe.

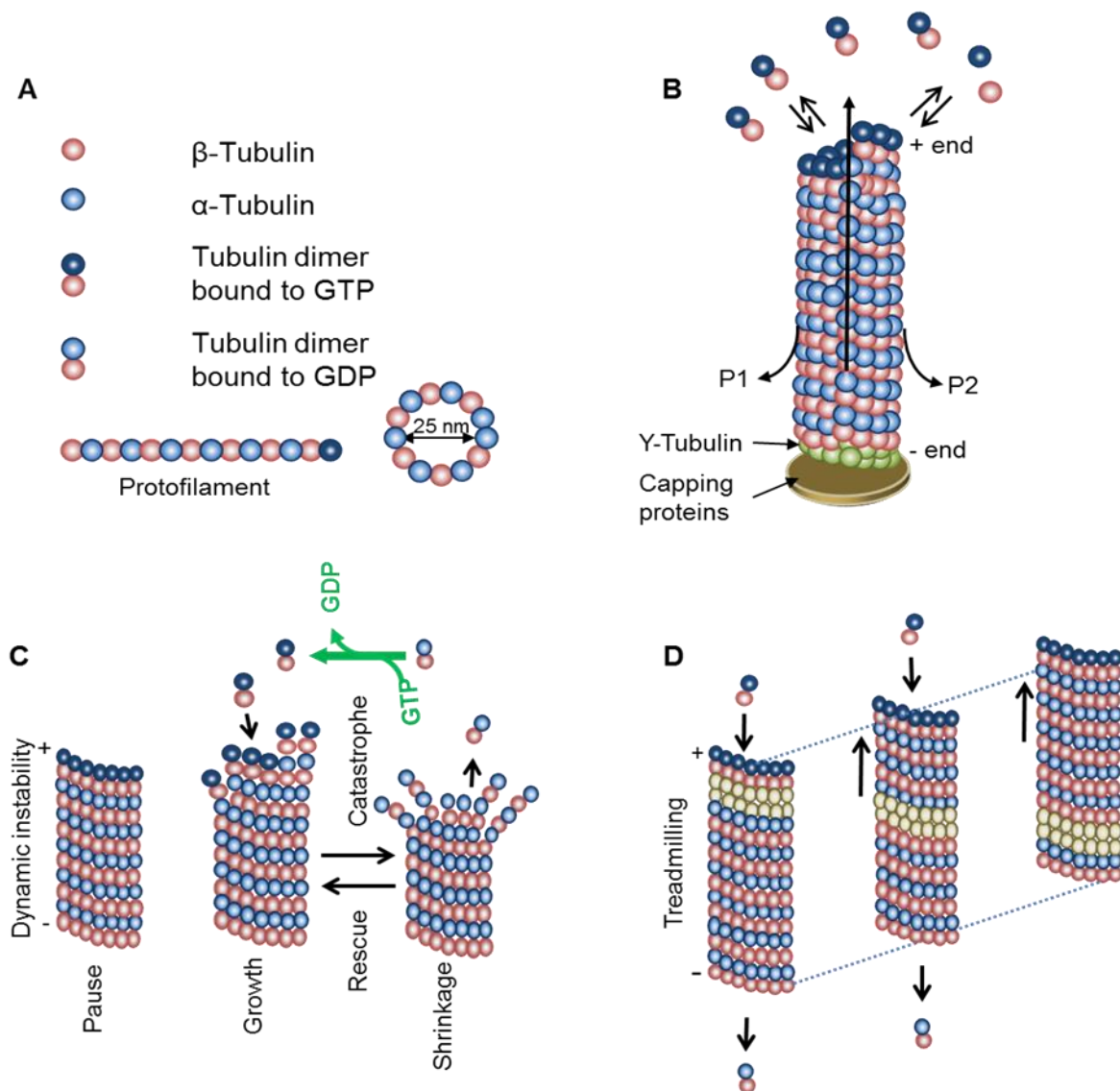


Figure 1.3 Structure and dynamics of microtubules.

Formation of protofilaments from α and β tubulin heterodimers (A), and subsequent formation of microtubule filament (B). Diagrams in (C) and (D) represent processes of dynamic instability and treadmilling. GDP, guanosine triphosphate; GTP, guanosine triphosphate. Direction of yellow subunits represent directional subunit flux in the case of treadmilling. Modified from (Dixit and Cyr, 2004a; Horio and Murata, 2014).

On addition of GTP-bound tubulin to the plus end of microtubule, polymerization is achieved, termed as rescue. Stochastic changes between growth and shrinkage phases are called

dynamic instability (Figure 1.3C). Also, microtubules possess the property of treadmilling in certain circumstances where minus-ends depolymerize (Figure 1.3D) (Dixit and Cyr, 2004a; Drechsel and Kirschner, 1994; Horio and Murata, 2014; Shaw, 2003). Capping or attachment of minus-ends to certain organelles or structure stabilizes these ends (Akhmanova and Hammer, 2010; Dammermann et al., 2003; Shu and Joshi, 1995). Dynamic instability is regulated by plus (+) end tracking proteins, called +TIPs, via promoting either polymerization or depolymerization (Lansbergen and Akhmanova, 2006).

1.5 Organizations of microtubule arrays during plant growth and development

Plant cells are surrounded by a semi-rigid pecto-cellulosic cell wall, which restricts their relative position within the tissue, so the new cell walls must be formed in the position where they are needed. For that plants adapt to the spatial control of cytokinesis. Proper orientation of cell division provides robustness in the structures and functions of plants. To form organized arrays of cells plants acquired specific arrays of microtubules, which spatially control the division plane even before the onset of mitosis in the G2/M phase of the cell cycle (Pickett-Heaps and Northcote, 1966). In interphase, cortical microtubules are aligned nearly perpendicular to the growth axis (Figure 1.4A) and correspondingly control cell expansion. However, in interphase cells of isodiametric cells, microtubule arrays are oriented randomly. These highly dynamic interphase cortical microtubules are organized into an ordered array during G2/M phase, called preprophase band PPB (PPB) (Vos et al., 2004). The PPB is a plant-specific structure consisting mainly of microtubules and actin filaments and girdles around the nucleus at the cell cortex during preprophase stage of cell division (Figure 1.4B). The PPB disappears during the transition from prophase to metaphase leaving behind the site, called cortical division zone (CDZ) which retains the positional memory of PPB (Gunning and Wick, 1985; Rasmussen et al., 2013). Later during cell division, the wide cortical division zone (CDZ) further narrows to the cortical division site (CDS) which locates the precise position of the future division site (Van Damme, 2009).

Several PPB-localized proteins have been identified, which remain at the division site after PPB disintegration and serve as positive markers for the recognition of former PPB position (Lipka et al., 2014; Walker et al., 2007; Xu et al., 2008). The disintegration of PPB microtubules promotes the formation of bipolar spindle microtubules. The Polar cap is formed by polar accumulation of microtubules around the nucleus which guides the bipolarity of the spindle. In animal cells the bipolar spindles are tightly focused, while in plants, spindles are barrel-shaped with somewhat diffuse spindle poles (Figure 1.4C). The spindle helps in the equal distribution of chromosomes towards the spindle poles as in animal cells. Cytokinesis

is accomplished by the formation of the phragmoplast during anaphase. The phragmoplast is a plant-specific structure comprised primarily of antiparallel microtubules and actin filaments, endoplasmic reticulum and Golgi derived vesicles. Phragmoplast guides the delivery of Golgi-derived vesicle carrying cell wall material towards the midzone where these vesicles fuse to form the cell plate (Figure 1.4E) (Smith, 2001; Staehelin and Hepler, 1996). The midbodies in animals are analogous to phragmoplasts of plants. Midbodies associated with the endo-membrane system are required for the furrow ingression and scission during late cytokinesis. (Buschmann and Zachgo, 2016; Otegui et al., 2005; Otegui and Staehelin, 2004). The early phragmoplast is cylindrical in shape. As cytokinesis proceeds, the phragmoplast expands towards the cell periphery, with depolymerization of microtubules at the center of the phragmoplast and formation of new microtubules at the leading zone of the expanding phragmoplast. In the cross section of a plant cell, the expanding phragmoplast appears as a ring and becomes discontinuous before fusion to the cell cortex. The expanding phragmoplast directs the expansion of newly formed cell plate. The cell plate formation starts from the center and expands centrifugally towards the parental plasma membrane, which eventually fuses at the CDS to produce two daughter cells. CDS is formerly occupied by the PPB.

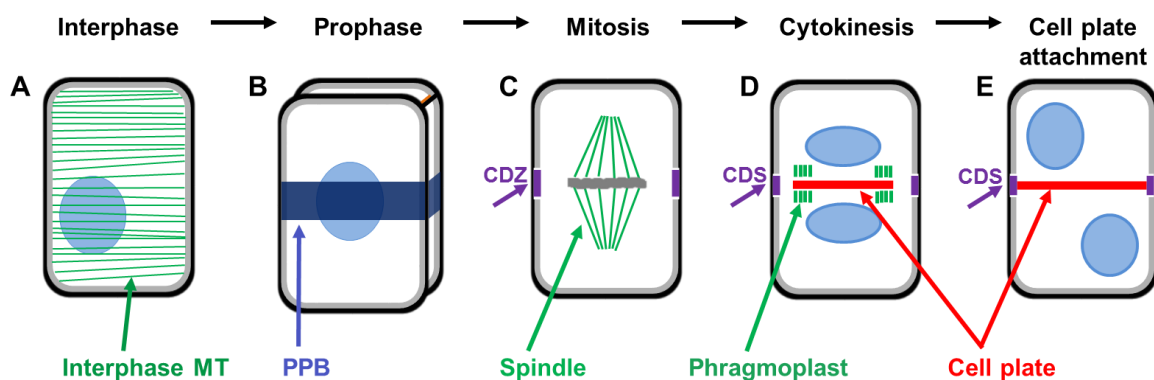


Figure 1.4 Cytoskeletal organization during plant cell cycle.

Diagrams showing specific arrangements of mitotic microtubule arrays during plant cell cycle. Prophase was represented in 3D view while all other stages are in single optical plane. Names of the stages and the specific microtubule arrays are shown. PPB, preprophase band; CDZ, cortical division zone; CDS, cortical division site. Modified from (Müller et al., 2009).

Ultimately, the shape of the plant cell is determined by its axis of expansion. The direction of cellular expansion is regulated by alignment of cytoskeletal arrays in interphase cells (Endler and Persson, 2011). In interphase cells, cortical microtubules align perpendicular to the direction of the growth axis of the cell. These cortical microtubules are tethered to the plasma membrane and serve as a track for the guidance of the cellulose synthase complexes (CSCs) and thus determine the alignment of cellulose microfibrils (Liu et al., 2015; Paredez

et al., 2006). that restrict the growth of cells parallel to its orientation. Cells expand perpendicularly to the direction of cellulose microfibrils. Deposition of cellulose fibers determine the direction of turgor pressure in the cell, which is the primary driving force for cellular expansion. Thus the microtubule cytoskeleton is essential during a plant cell division and cell expansion and therefore is a critical factor in plant morphogenesis. All four microtubule arrays, named interphase, PPB, spindle and phragmoplast are made up of the same α and β subunits. However, their organizations and the positions are changed specifically to each stage of cell division. These highly dynamic transitions require sets of organizing factors, which play roles in organization and dynamics of microtubules.

1.6 Regulation of microtubule organization and dynamics

Most crucial factors responsible for intracellular organization and dynamics of microtubules are proteins which control the activity of microtubule nucleation sites, and MAPs; which regulate the polymerization/depolymerization of microtubule polymers as well as the control of microtubule forms and function. Unlike animals, plants do not contain centrosomes, which is the prime microtubule-organizing center (MTOC) of animals. In contrast, the microtubule organization in plants is more dispersed. Even in the absence of an MTOC, plants are able to form organized cortical microtubules. It is stated that nucleation of organized cortical microtubules is caused by dispersed nucleation sites at the plasma membrane, the nuclear and other organelle surfaces and microtubule strands (Binarová et al., 2000; Dibbayawan et al., 2001; Lee and Liu, 2019). Microtubule nucleation events throughout the cell cycle of plants are depicted in Figure 1.5. Unlike animal cells, the positions of MTOCs in plant cells are rather dynamic than fixed at one place (Chan et al., 2003a). In plants, gamma (γ) tubulin is the most prominent nucleation factor. It is conserved among all eukaryotes. γ tubulin, together with five structurally related proteins, collectively named γ tubulin complex proteins (GCPs), form a γ tubulin ring complex (γ -TuRC) to mediate its microtubule nucleation function (Teixidó-Travesa et al., 2010).

Activation and targeting of the γ -TuRC complex to microtubules is mediated primarily by AUGMIN (AUG1) and NEURAL PRECURSOR CELL EXPRESSED DEVELOPMENTALLY DOWN-REGULATED1 (NEDDI), respectively (Lee and Liu, 2019). The mechanism of targeting the complex at membranes, yet need to be resolved. In addition, γ tubulin (MOZART1) also joins the complex (Hutchins et al., 2010). Based on drug-induced depolymerization experiments in *Nitella tasmanica* (*N. tasmanica*) a charalian algae, it is hypothesized that the γ tubulin complex is recruited to extant microtubules, where it nucleates the new microtubules after branching (Wasteneys and Williamson, 1989). Roles of γ tubulin in the nucleation of cortical microtubules have been investigated extensively (Lee

and Liu, 2019; Murata et al., 2005; Shaw, 2003; Van Bruaene et al., 2004). γ tubulin shuttles between cytosol and microtubules. Upon nucleation events, cytosolic γ tubulin is recruited to the microtubules where it helps to polymerize new microtubules from extant microtubules (Figure 1.5A). The angle of branching decides the orientation of newly formed microtubules. This observation suggests the possibility of microtubule-dependent microtubule nucleation mediated via γ tubulin. However, microtubule-independent nucleation at the cortical site has also been evident in some cases (Murata et al., 2005).

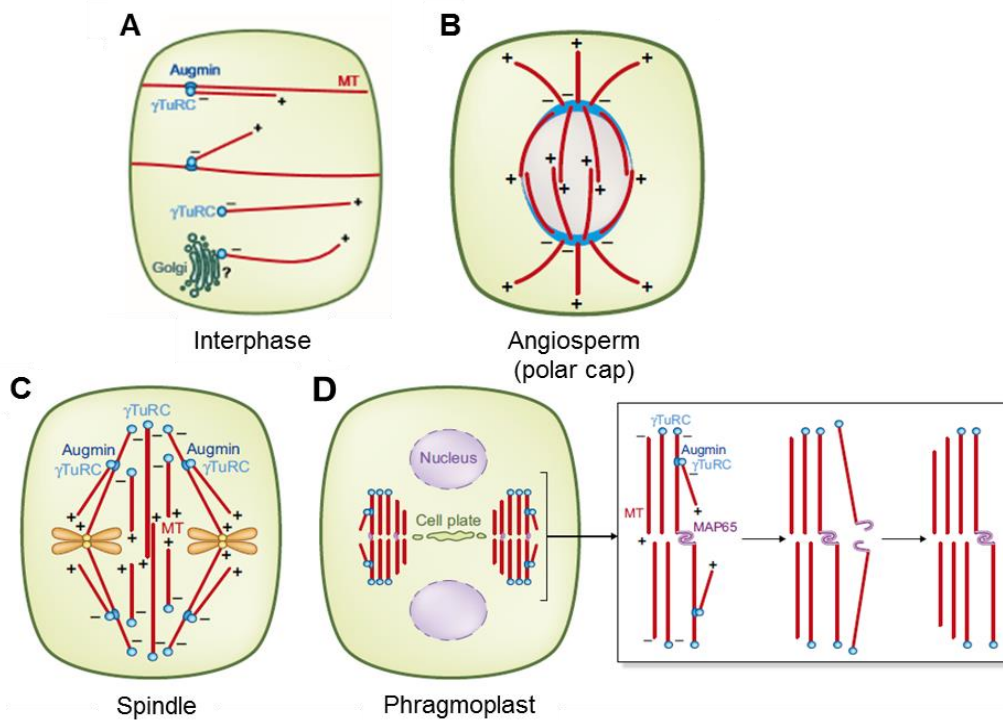


Figure 1.5 Microtubule nucleation in plant cells.

Schematic representation showing events of microtubule nucleation during distinct stages of the cell cycle; (A) interphase cells, (B) prometaphase, (C) metaphase and (D) cytokinesis. γ TuRC, Y tubulin ring complex; MT, microtubule; MAP65-3, MICROTUBULE-ASSOCIATED PROTEIN65-3. (Lee and Liu, 2019).

Although γ tubulin has been detected on PPB microtubules (Liu et al., 1993), it is not yet clear whether new microtubules arise from localized plasma membrane or from preexisting PPB microtubules (Lee and Liu, 2019). Concomitantly, with the formation of PPB, microtubules start nucleating from the nuclear membrane (Wick and Duniec, 1983) and later reorganize into polar caps on the prospindle (Figure 1.5B). γ tubulin and associated proteins are detected on this structure (polar cap), indicating microtubule nucleation events at the nuclear envelope. After breakdown of the nuclear envelope, γ complexes move towards spindle microtubules and later to phragmoplast microtubules, with more pronounced

localization towards the microtubule minus end (Liu et al., 1994, 1993) (Figure 1.5C, D). In addition, early land plants like *Marchantia polymorpha* (*M. polymorpha*) contain centriole-like polar organizers as focused and distinct MTOCs, which eventually determine spindle poles (Apostolakos and Galatis, 1985). The polar organizers also contain γ -TuRC. Likewise, moss [*Physcomitrella patens*(*P. patens*)] cells possess a gametosome, a cytoplasmic transient MTOC, which directs spindle orientation and cell division plane determination (Kosetsu et al., 2017). Coincidentally with above two cases, angiosperm cells also form polar caps during formation of the prospindle. This polar cap mainly determines the orientation of the spindle and thus cell division orientation (Liu et al., 1993).

Beside roles of microtubule nucleation, MAPs play crucial roles in regulating microtubule forms and function (Hamada, 2007; Sedbrook, 2004). Several MAPs have been shown to mediate bundling, crosslinking, nucleation of microtubules as well as regulate microtubule turnover (Ambrose and Cyr, 2008; Chan et al., 1999; Dhonukshe and Gadella, 2003; Dixit and Cyr, 2004a, 2004b; Perrin et al., 2007; Shaw, 2003). Many MAPs are associated directly with the plus ends of microtubules to regulate dynamics of microtubules. One such plus end binding protein is the END BINDING PROTEIN1 (EB1), which directly bind to growing plus ends to regulate microtubule polymerization, their dynamics as well as to mediate the association of other proteins to the plus ends (Korinek, 2000; Rogers et al., 2002; Tirnauer, 2002). MICROTUBULE ORGANIZATION1 (MOR1), a conserved MAP of the MAP215/Dis1 family present throughout eukaryotes, is shown to cause microtubule shortening in spindles and phragmoplasts at restrictive temperatures. In addition to its role in maintaining the length of microtubules, MOR1 also promotes microtubule stabilization at the plus ends of interdigitated microtubule ends of the midzone. At restrictive temperature, *mor1* mutations affect PPB formation. It was proposed that MOR1 regulates cortical microtubules universally as well as other mitotic arrays at the restrictive temperature of 29° and above (Kawamura et al., 2006).

Apart from the role of microtubule plus end binding MAPs in the regulation and dynamics of microtubules, certain other MAPs regulate microtubule activity through their effect on minus ends of microtubules. SPIRAL1 (SPR1) and SPIRAL2 (SPR2) are two plant-specific proteins that bind to the minus ends of microtubules and are involved in cortical microtubule organization. SPR2 binds to the free minus ends to prevent subunit loss. Minus ends are generated by severing activity of p60 subunit of katanin at microtubule crossover sites (Nakamura et al., 2010; Nakamura and Hashimoto, 2009). In response to blue light, SPR2 promotes array reorientation by reducing severing opportunity time and by promoting Katanin activity at crossover sites. Besides its action at minus ends, SPR2 also increases

catastrophe at the plus ends of microtubules (Nakamura et al., 2018). MAPs also play roles in severing and cutting of microtubules to generate new microtubule ends. At crossover sites of microtubules, katanin plays an essential role in microtubule severing. Katanin is a microtubule severing protein that has been first identified in the mitotic extract of *Xenopus laevis* (Vale, 1991). Katanin is the AAA (ATPase associated with diverse cellular activities) type family of ATPases that possesses microtubule severing activity through ATP hydrolysis. It is a heterodimer of a 60 KD (Kilodalton) (p60) catalytic subunit, and an 80 KD (p80) regulatory subunit. The 60 KD catalytic subunit alone is sufficient for both microtubule severing activity and ATP hydrolysis (Hartman et al., 1998; McNally and Vale, 1993). Arabidopsis *KATANIN1* (*KTN1*) encodes a katanin-like protein that possesses similarity to katanin only in its C-terminal ATP binding module (Burk et al., 2001; Hartman et al., 1998). *KTN1* represents only catalytic p60 subunit, and the regulatory p80 subunit appears to be lacking (Keech et al., 2010). The Arabidopsis *KTN1* p60 alone is shown to have microtubule severing activity (Stoppin-Mellet et al., 2002).

KTN1 helps to generate free minus ends of nascent microtubule strands and promotes reorganization (Komis et al., 2017; McNally and Vale, 1993). Loss of *KTN1* leads to defects in the organization of cortical microtubule arrays in interphase cells and at the PPB. However, roles of katanin in organization of spindle and phragmoplast microtubules have not been evident beside their noticeable rotation compared to equatorial plane of cells (Komis et al., 2017). The process also helps in generating free microtubule fragments that serve as substrates for new microtubule assembly (Lyle et al., 2009). CLIP170-ASSOCIATING PROTEIN (CLASP) is a microtubule plus end binding protein, which is shown to play roles in organization of microtubules via interaction with EB1b (Kirik et al., 2007). It also has a credential role in cell division, where it localizes to division structures. During prophase, it is shown to be associated with the PPB. CLASPs are evolutionarily conserved and also essential for microtubule organization in fungi and animals (Akhmanova et al., 2001; Galjart, 2005; Maiato et al., 2003; Máthé et al., 2003; Wittmann and Waterman-Storer, 2005). CLASP localizes to mitotic microtubule arrays and to cortical microtubules in interphase cells. CLASP regulates the transition frequency and controls plus end depolymerization (Kirik et al., 2007).

1.7 Spatial regulation of cytokinesis in plants

1.7.1 Cell division in plants

In contrast to animal cells, where cells are divided by the formation of cleavage furrow through the constriction of the plasma membrane, plant cells are divided by the formation of the cell plate in the center of the cell that grows centrifugally and fuses with the parent cell

wall to generate two daughter cells. Because of the structural differences between plant and animal, plants acquire different mechanisms for determining the division plane than animals. The spindle position in anaphase/metaphase determines the plane of division in animal cells, while the plane of division in plant cells is determined at the cortex before the cell's entry into mitosis. The positioning of the new cell walls in plants is accomplished into following steps. First, division plane selection followed by division plane establishment and, eventually, the guidance of phragmoplast and thus the cell plate to the CDS which is formerly occupied by PPB.

1.7.2 Division plane selection

The PPB is considered to be essentially responsible for setting the cortical division site. The PPB disassembles during the transition from prophase to metaphase and leaves behind a positional memory at which the cell plate fuses with the parental plasma membrane. Until recently, PPB was considered essential for the establishment and maintenance of the division site by recruiting factors directly or indirectly. However, the study provided by Schaefer et al. (2017) showed evidence of the division site establishment even in the case of massive PPB loss. The study showed that cell wall positioning defects in *trm678* mutants do not correspond to the frequency of PPB loss, concluding that the PPB is required for the robustness of division plane as a stabilizer but not an organizer of division plane. Numerous studies have reported many PPB-localized proteins and their ultimate effect on PPB formation and function. These proteins include those, which are involved in microtubule nucleation as well as in the regulation of microtubule turnover (Buschmann et al., 2015; Camilleri et al., 2002; Müller et al., 2006; Walker et al., 2007; Xu et al., 2008). However, factors which at first place act as signals for the formation of PPB remain elusive. Previous studies have implicated the coordinated role of cell geometry, mechanical stress and polarity cues as the early signal for selection of division site (Livanos and Müller, 2019 and references therein). In the case of symmetrical division, the default mechanism of division plane selection is determined by cell's geometry, by using shortest path rule; however, this theory is not true in case of complex cells. According to the geometry rule, cells with fixed volume adapt the division plane with the minimal surface area. Since elements in the dividing cells are under tension, these tensed elements with mobile attachment points adopt the shortest axis of cells. Tension in cytoskeleton elements and nuclear positioning are likely factors that are responsible for geometry sensing of cells.

Nuclear positioning also plays crucial roles in division plane selection. Centrifugation experiments in the protonema of *Adiantum* have shown that the repositioning of the nucleus leads to the formation of a PPB from displaced nuclear position (Mineyuki et al., 1991;

Murata and Wada, 1991). A similar case has been reported for wheat root cells (Burgess, J. & Northcote, 1968). However, whether the position of the nucleus will lead or follows division plane determination, depends upon cell types. Nuclear migration depends primarily on microtubules and/or microfilaments (Frey et al., 2010; Mineyuki and Palevitz, 1990). A cytoplasmic disc, rich in microtubules and actin filament, develops in premitotic cells between the nucleus and cell cortex. The cytoplasmic disc shows tension and forms in the direction and position with minimal area. Later it interacts with cortical microtubules that form the PPB and phragmosome. It is thought that this cytoplasmic disc helps to position the nucleus that eventually becomes the position of PPB (Flanders et al., 1990; Lloyd and Traas, 1988; Sinnott and Bloch, 1940). The filamentous-actin (F-actin) and microtubules sense the tensional force generated in the phragmosome and likely is responsible for selecting its the minimal path (Flanders et al., 1990; Goodbody et al., 1991; Lloyd, 1991). The geometry-based mechanism is further supported by mathematical and computer-based calculations (Besson and Dumais, 2011). Alternative division patterns arise because of distinct cells aspect ratios.

Mechanical forces that determine the division plane are caused by radial microtubules emanating from the nucleus in premitotic cells. Again here, the configuration with the shortest distance rule is stabilized, and the PPB is formed coincidentally with the edge of heavily populated microtubules (Besson and Dumais, 2011). Heterogeneity in the composition of the cell wall induces unequal turgidity forces produced by the cell on the neighboring cells, which likely affects division plane orientation by coaligning of microtubules to the principle direction of the tensile strength (Livanos and Müller, 2019 and references therein). Beside geometrical and mechanical factors of division plane selection, other intriguing factors are hormonal and external cues (Elliott and Shaw, 2018). The functions of auxin have been explained well in the determination of division planes during asymmetric growth in the lateral root (Ditengou et al., 2008; Vermeer and Geldner, 2015) and embryo development (Bayer et al., 2017; Yoshida et al., 2014). Auxin also plays a partial role in deciding the division plane in response to polarity cues. Polar auxin flow can cause the change in the orientation of division in response to environmental and developmental cues (Chakraborty et al., 2018; Dhonukshe et al., 2005a; Willemsen et al., 2003). In addition, the Ca^{2+} and ROP signaling noticeably affect microtubule and actin filament dynamics and organizations (Bürstenbinder et al., 2017; Craddock et al., 2012; Hepler, 2016; Himschoot et al., 2015), which ultimately effects division plane selection.

Division in response to wounds as well as asymmetric divisions during stomatal development in grass (development of subsidiary mother cells) follow external signals to determine the

division plane (Goodbody and Lloyd, 1990; Panteris et al., 2004; Smith, 2001; Venverloo and Libbenga, 1987). It is also possible that localized modifications at the cortex occur before PPB formation, to which PPB microtubules interact later on. Evidence of centripetally inward growing wall stubs in the cell cortex of algae further strengthens this concept. Together it is hypothesized that evolution of the PPB possibly fine-tuned the refinement of the preexisting mechanisms of division plane selection to accurately position factors or alternatively to position or orient spindle (Buschmann and Zachgo, 2016; Colasanti et al., 1993; Mineyuki and Gunning, 1990).

1.7.3 Division plane establishment

1.7.3.1 PPB formation and assembly

Cortical microtubules dispersed throughout the cortex of interphase cell are confined to a band at the cortex during the formation of the PPB in the G2/M phase of the cell cycle. PPB microtubules are newly polymerized microtubules from the free tubulin pool (Cleary et al., 1992; Panteris et al., 1995). These tubulin pools are not synthesized de-novo but generated from the disintegration of preexisting microtubule strands (Hardham and Gunning, 1978). PPB forms coincidentally with phragmosome. In one study, it has been shown that the incomplete or complete PPB is associated with incomplete or complete phragmosomes, respectively, indicating the possible interplay of both structures (Ververloo and Libbenga, 1987). During interphase, growth and shrinkage rate of microtubules are 5 $\mu\text{m}/\text{min}$ and 20 $\mu\text{m}/\text{min}$, respectively and catastrophe and rescue frequency are 0.2 (event/second) and 0.8 (event/second), respectively. Further, during prophase, this growth rate and catastrophe frequency doubles while shrinkage rate and rescue frequency remain the same, indicating faster microtubule turnover resulting in short microtubules. This change in microtubule dynamics contributes to the formation of the PPB via microtubule rearrangement (Dhonukshe and Gadella, 2003; Vos et al., 2004).

The Initial PPB displays an overlapping region of actin filaments and microtubule strands. In the early step of PPB formation, short actin microfilaments help to bundle microtubules of PPB (Takeuchi et al., 2016). As the cell progresses through mitosis, the initial broad PPB narrows progressively throughout prophase (Marcus et al., 2005). Similarly, actin filaments disassemble from the center of the PPB coinciding with the narrow PPB band, the region formed is called actin depleted zone (ADZ). On both sides of the PPB, actin displays twin pick structures indicating region of maximum intensity at the edge of PPB band. Both actin filaments and microtubules are interdependent on each other for PPB form and function. Pharmacological analysis with the actin-depolymerizing drug showed that the loss of actin leads to a defect in PPB narrowing and thus maturation of PPB, which eventually causes

division plane defects (Mineyuki and Palevitz, 1990). However, loss of actin does not affect PPB formation (Cleary et al., 1992; Eleftheriou and Palevitz, 1992; C. L. Granger and Cyr, 2001). The dynamic instability of the timely regulated process of PPB formation is regulated by microtubule-stabilizing/destabilizing and microtubule severing proteins (Dhonukshe and Gadella, 2003). One of such protein is MOR1, a member of MAP215 family, which is postulated to control the length of microtubule (Hussey and Hawkins, 2001; Kawamura et al., 2006; Whittington et al., 2001). The 50% of cells in MOR1 mutants do not form PPBs, indicating the importance of microtubule length in PPB formation. Moreover, MOR1 regulates forms of all microtubule arrays (interphase cortical and mitotic microtubule arrays) (Kawamura et al., 2006). Another protein known to affect PPB microtubules is microtubule severing protein KTN1. The *ktn1-2* mutant produces abnormal PPBs in which microtubules emanate from the PPB and enter other areas of the cortex. Besides, *ktn1-2* mutants also display defects in narrowing of the PPB (Komis et al., 2017). KTN1 regulates the length of PPB microtubules through its severing activity (Burk et al., 2007; Hamada, 2007).

Other candidates are protein kinases such as CYCLIN-DEPENDENT KINASE (CDC) which phosphorylates microtubule-stabilizing protein and catastrophe inhibiting proteins to inactivate them, as well as dephosphorylating enzymes to activate microtubule severing proteins (Belmont et al., 1990; Hush et al., 1996; Verde et al., 1992; Weingartner et al., 2017). In addition, the role of a PP2A phosphatase complex has been reported during PPB formation. Arabidopsis TON2, a regulatory subunit of the PP2A complex, plays crucial roles in the formation of the PPB (Camilleri et al., 2002; Kirik et al., 2012). Researching on PP2A target proteins will address several issues related to the PPB formation and its regulation. Consistent with this, application of phosphatase inhibitors, endothall, also leads to defects in the organization of interphase cortical microtubules, PPB assembly, premature spindle microtubule organization and disrupted phragmoplasts in alfalfa cell cultures (Ayaydin et al., 2000). Likewise, the application of cantharidin, another phosphatase inhibitor, to the cortical microtubules in the section of maize root cells, also induces depolymerization of microtubules (Tian et al., 2004). In contrast, the use of kinase inhibitors has been shown to promote microtubule stabilization (Liu et al., 2017; Tian et al., 2004), suggesting that the control of microtubule stability through activation and inactivation of target MAPs is essential for the formation of PPB (Dhonukshe and Gadella, 2003). While several other proteins and regulating factors of PPB have been identified, the spatial and temporal relationship between them is elusive. In addition, several factors have yet to be discovered, to fully understand the mechanism of PPB formation.

Several studies in higher plants have proven the direct relationship between the location of PPB position and cell plate fusion site. The PPB helps in polar accumulation of perinuclear microtubules perpendicular to the plane of PPB, which is later transformed into spindle poles (Ambrose and Cyr, 2008; Chan et al., 2005). In line with the hypothesis, the importance of the PPB in spindle morphology and orientation has been demonstrated in *Arabidopsis* cells lacking *TRM* gene function (Schaefer et al., 2017). Based on this fact, it is proposed that the PPB helps in tuning the spindle orientation as the centrosome and astral microtubules of animal cells (Schaefer et al., 2017). Until now, the perspicuous relation between spindle orientation and cell plate position has not been evident. Very often wild type cells produced in spindles out of focus orientation, which is eventually corrected during telophase by correct positioning of the phragmoplast (Ambrose and Cyr, 2007; Komaki et al., 2010).

1.7.3.2 Establishment of PPB memory

As mentioned before the PPB specifies the site of cell plate fusion, and thus establishes the plane of division. After PPB disintegration, the site formerly occupied by the PPB is marked either by recruitment of critical factors of the division site or possibly via unidentified membrane modifications. The changed architecture of the former PPB site remains as memory marker of division site for newly growing cell plates. Plants showing loss of these critical markers of division site showed oblique cell walls, primarily because of a loss of phragmoplast guidance towards the cell plate fusion site. Not much is known about the molecular identity of the plasma membrane region left behind after PPB disassembly. An increased endocytic activity is reported at the PPB that could lead to the modification of the plasma membrane in the vicinity of the PPB, and thus establish the cortical mark (Dhonukshe et al., 2005a). Such cortical modification plausibly assists in establishing the PPB memory. In late prophase, the narrow PPB band with dense microtubule strands coincides with a local F-actin depleted zone, ADZ, which persists throughout the cell division and may help to set a memory marker after PPB disintegration. The ADZ acts as a continuous negative markers of the division site (Cleary, 1995; Cleary et al., 1992; Liu and Palevitz, 1992; Sano et al., 2005; Valster and Hepler, 1997; Vanstraelen et al., 2006).

Beside changes in the membrane and cytoskeleton components of the division site, several other factors are known to preserve the memory of PPB after its disassembly at prometaphase. The PPB recruits various factors by direct or indirect interaction with microtubules. TANGLED (TAN) is the very first positive marker of the division site that is recruited to the PPB and remains at their position throughout cytokinesis. Impairment of TAN function leads to division plane defect primarily due to failure of phragmoplast guidance, suggesting its role in division site establishment and maintenance (Smith et al., 1996; Walker

et al., 2007). After TAN, RANGAP1 (Ran GTPase ACTIVATING PROTEIN1) is the second known early positive marker of division site. Like TAN, RANGAP1 also decorates the cortical ring coincident with the PPB in preprophase cells and remains at the division site after disassembly of the PPB (Xu et al., 2008). Impairment of RANGAP1 and closely related RANGAP2 function leads to cytokinetic defects, which indicate the importance of the proteins in the establishment of the division plane (Xu et al., 2008). PHRAGMOPLAST ORIENTING KINESIN1 (POK1) and POK2, a pair of kinesin-12 family proteins is very well studied for their function in division site establishment and maintenance. POK1 has been shown to interact with division site-resident proteins such as TAN and RANGAP and maintains their retention at the division site throughout cytokinesis (Lipka et al., 2014; Müller et al., 2006; Walker et al., 2007; Xu et al., 2008). Loss of POK1/2 functions in *pok12* double mutants results in a dwarf plants with highly disorganized cell orientation profiles. *pok12* double mutants show more frequent defects in phragmoplast orientation than misplaced PPB. Altogether this suggests that misoriented division patterns observed in these mutants are most likely due to loss of reference information from the division site and subsequent failure of phragmoplast guidance. These findings indicate the role of POKs in the establishment as well as maintenance of the division plane for timely and directed expansion of the phragmoplast and thus positioning of the cell plate towards the CDS.

In addition, a member of the kinesin-14 family, kinesin CDKA; 1-associated1 (KCA1) serves as a continuous negative marker of the division site (Cleary et al., 1992; Mineyuki and Palevitz, 1990; Vanstraelen et al., 2006). KCA1 accumulates at the plasma membrane and forms an area depleted of KCA1 called KCA1 depleted zone (KDZ) corresponding to the ADZ and late PPB. The KDZ is formed before the formation of ADZ and remains as it is throughout completion of cytokinesis (Vanstraelen et al., 2006) and is likely to retain the positional information of the PPB. KCA1 was shown to interact with Plant A-type CYCLIN-DEPENDENT KINASE (CDK), such as CDKA1, which is localized to the PPB, and thus potentially regulating diverse functions at PPB (Vanstraelen et al., 2004).

1.7.4 Phragmoplast guidance

The newly formed cell plate is positioned to the region of the cortex, which is formerly occupied by PPB (Lipka et al., 2015) by the directed expansion of phragmoplast. CDZ recognition by expanding phragmoplast is responsible for correct orientation of expanding phragmoplast and thus the precise positioning of the cell plate. How phragmoplast recognizes the division site is not yet clear. Phragmoplast is expanded through the controlled process of depolymerization and polymerization of the lagging edge and the leading edge of the phragmoplast, respectively (Murata et al., 2013; Seguí-Simarro et al., 2007; Smertenko

et al., 2011). Phragmoplast expansion is a plant-specific process that allows rapid recovery of the tubulin subunits and phragmoplast proteins, which further supports the correction of improperly placed cell walls if any. Microtubule turnover is regulated by microtubule-associated and regulatory proteins. The MICROTUBULE-ASSOCIATED PROTEIN65-3 (MAP65-3) is one of such protein known to play roles in phragmoplast expansion. MAP65-3 is phosphorylated by MITOGEN-ACTIVATED PROTEIN KINASE 4 (MPK4) and in turn, regulate the dynamic instability of the phragmoplast lagging strand, which is essential for phragmoplast expansion (Sasabe and Machida, 2012). Radiation of transient microtubules from the expanding phragmoplast towards the cortex suggests its possible roles in the directed lateral expansion of phragmoplasts (Dhonukshe et al., 2005b; Murata et al., 2013). Likewise, astral microtubules in animal cells help to orient the spindle through contact with the cell cortex. This association is mediated by the direct interaction of EB1 associated with astral microtubule plus end and APC (adenomatous polyposis coil) accumulated at the cell cortex (Lu et al., 2001; McCartney et al., 2001; Yamashita et al., 2003). AtTAN, a component of the potential guidance cues for the phragmoplast, is only distantly similar to the basic domain of APC, although it lacks EB1 binding domain (Smith, 2001; Walker et al., 2007). This raises the curiosity about the presence of similar proteins which potentially interact with EB1 at the plus end of exploratory microtubules and subsequently directs the expansion of phragmoplast.

Actin component of phragmoplasts is also known to play role integrity and dynamics of phragmoplasts. Actin filaments act as a bridge between the exploratory microtubule of expanding phragmoplast and the CDS (Dhonukshe et al., 2005b; Dhonukshe and Gadella, 2003; Higaki et al., 2008). The fact is supported by pharmacological treatments of actin filaments with actin-depolymerizing drugs that cause misalignment of cell plates (Granger and Cyr, 2001; (Baluška et al., 2001; Cheryl L. Granger and Cyr, 2001; Palevitz and Hepler, 1974; Reichelt et al., 1999). However, from these experiments, it is not clear which population of microfilaments is important for cell plate positioning. Further, the timely application of actin-depolymerizing drugs reveals little significance of actin filament in phragmoplast expansion (Hoshino et al., 2003; Palevitz and Hepler, 1974; Sano et al., 2005). The study conducted by Wu and Bezanilla (2014) showed myosin VIII localization to the phragmoplast leading edge as a ring and at the cortical division site in the *Physcomitrella* and tobacco BY2 cells. It has been reported that actin filament connects exploratory phragmoplast microtubules from the leading zone to the cell cortex via myosin VIII. Similarly, *Arabidopsis* class VIII myosin *A. thaliana* myosin 1 (ATM1) is localized to the phragmoplasts in BY2 cells (Van Damme et al., 2004). It has been proposed that myosin VIII associated with microtubule ends might help to translocate exploratory microtubules along filaments and thus

guide phragmoplast expansion. This study suggests a coordinated tuning of Myosin VIII and actin-guide expansion of phragmoplast in cells with preprophase band. In addition to the cytoskeletal elements of the cells, a transvacuolar cytoplasmic strand, called phragmosome is also suggested to play a role in phragmoplast guidance (Flanders et al., 1990; Venverloo and Libbenga, 1987). Because phragmosome contains microtubules and microfilaments, which initially coincide with PPB and its persistence throughout the cytokinesis, actin may help to guide phragmoplast.

1.7.5 MAPs and their roles in spatial regulation of cytokinesis

Numerous MAPs are documented in several reviews for their roles in the spatial control of cytokinesis. Here I am describing the specific properties of some of them in detail that are relevant for my thesis work. Organization and positioning of the regulatory proteins at mitotic various microtubular arrays are depicted in schematic representation in Figure 1.6.

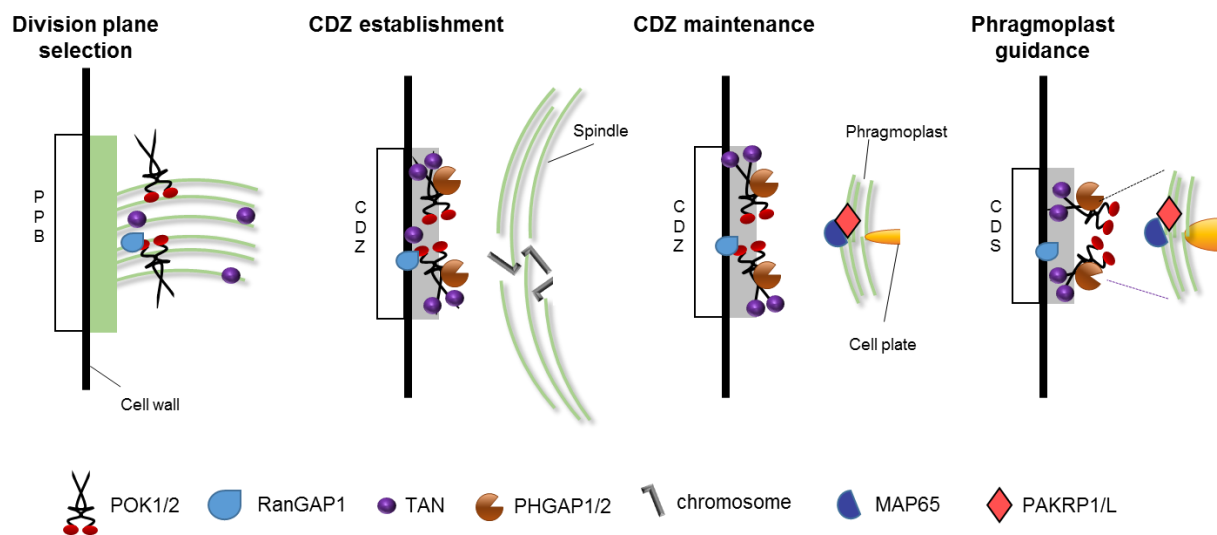


Figure 1.6 Organization and positioning of microtubule-associated regulatory proteins during plant cell division.

Schematic illustration of MAPs throughout the cell division. PPB, preprophase band; CDZ, cortical division zone; CDS, cortical division site; POK1/2, PHRAGMOPLAST ORIENTING KINESIN1/2; RanGAP1, Ran GTPase ACTIVATING PROTEIN1; TAN, TANGLED; MAP65-3, MICROTUBULE-ASSOCIATED PROTEIN65-3, PAKRP1/L, PHRAGMOPLAST ASSOCIATED KINESIN-RELATED PROTEIN1/LIKE. Modified from (Lipka et al., 2014).

1.7.5.1 POKs are the early markers of division plane establishment.

POK1 and POK2 are kinesin-12 proteins known to function in the correct positioning of the cell wall (Müller et al., 2006). Like other kinesins-12 members, they also contain N terminal motor domain, which walks on the microtubules and C-terminal stalk domain, consisting of

the coiled-coil domain for dimerization and tail domain which is responsible for the binding of cargoes. POKs are studied for their roles in the retention of cell division site markers such as PHGAPs (PLECKSTRIN HOMOLOGY GTPase ACTIVATING PROTEIN), TAN, RANGAP1 (Stöckle et al., 2016; Walker et al., 2007; Xu et al., 2008) after PPB disassembly and thus preserving division site information. Impairment of POKs functions leads to phragmoplast guidance defect, resulting in severe mispositioning in *pok12* double mutants. Due to the loss of positional information in the mutant, phragmoplast expands into the unguided pathway, which eventually results in twisted and curved phragmoplast (Herrmann et al., 2018).

1.7.5.2 PAKRP1/PAKRP1L

PAKRP1 (Phragmoplast associated kinesin-related protein1) and PAKRP1L (PAKRP1-like) are another pair of kinesin-12 family proteins which are reported to have remarkable importance during cell wall positioning. GFP translational fusion of protein decorates at phragmoplast midzone. The confined location at the midzone depends on the function of MAP65-3 protein (Lee and Liu, 2000; Pan et al., 2004). Mutation in PAKRP1L leads to cytokinetic failure and aberrant phragmoplast morphology during male gametogenesis (Lee et al., 2007). The two proteins are shown to interact with two in one kinase (TOI) and possibly bring it to midzone to regulate midzone functions and assembly (Oh et al., 2012).

1.7.5.3 RANGAPs

RanGAPs are small GTPase activating protein of Ran-like GTPase. The recruitment of RANGAP at the PPB requires the function of TON2/FASS, which is known to affect the PPB formation (Xu et al., 2008). RANGAP1 are shown to interact with full-length as well as with C-terminal fragments of POK1. Persistence of RANGAP1 at the CDS is dependent on POKs function, but not the initial accumulation at PPB. N-terminal region of the RANGAP is shown to be responsible for the binding of protein at the division site. Unlike POKs, the initial recruitment of RANGAP1 at the division site is microtubule-independent. RANGAP1 signal narrows down progressively from the broad ring at the PPB to further confined and dense signal at CDS (Xu et al., 2008). The pattern of RANGAP1 ring is overlapping with the localization pattern of POKs at the division site. Besides its localization at the division site, it is also reported to be at kinetochore regions, spindle midzone and midline phragmoplast or rising cell plate (Xu et al., 2008). A highly conserved plant-specific WPP (tryptophan proline proline) at the N-terminal region is responsible for mitotic targeting of RANGAP1 (Jeong et al., 2005). Studies conducted on RNAi lines of *rangap12*, revealed its roles in the spatial control of cytokinesis (Xu et al., 2008). Downregulation of the proteins leads to division plane defect like cell wall stubs, misoriented cell plate positioning. The null mutants of RANGAP1 and RANGAP2 are gametophytic lethal (Rodrigo-Peirís et al., 2011).

1.7.5.4 TAN

TAN is a continuous positive marker of the CDS and is recruited to PPB via microtubule and POKs-dependent manner. TAN is a basic protein which binds with microtubules *in vitro* and *in vivo* (Smith et al., 2001). TAN fluorescent fusion proteins from Arabidopsis and Maize localize to the PPB (Walker et al., 2007). TAN recruitment to the PPB is dependent upon the presence of microtubules and POKs. After the PPB disassembly, TAN is further maintained at the CDS in a POKs-dependent manner. Concomitantly with *in vivo* dependency for POK1, TAN interacts with POK1 and POK2 C-terminal fragments (Müller et al., 2006; Rasmussen et al., 2013; Walker et al., 2007). Differential localization of TAN during cell division is mediated by distinct domains of TAN, likely via interaction with different molecular players (Rasmussen et al., 2011b). TAN gene was first identified in maize, where impairment of the gene function leads to a severe defect in cell wall positioning in leaf meristem (Smith et al., 1996). TAN gene from Maize and Arabidopsis was shown to function in maintaining the division plane memory and regulate guided the expansion of the phragmoplast towards the CDS, which is formerly occupied by PPB (Cleary and Smith, 1998; Walker et al., 2007). Impairment of TAN functions leads to a defect in the morphology of spindle and phragmoplast as well as the case of misguided phragmoplast (Martinez et al., 2019).

1.7.5.5 TTP complex

The TTP complex consists of TONNEAU1 (TON1), TON1 RECRUITING MOTIF (TRM) and PROTEIN PHOSPHATASE 2A (PP2A), which regulates the PPB formation. Mutant Impaired in any of the components of the TTP complex produces cells essentially devoid of PPB (Azimzadeh et al., 2008; Drevensek et al., 2012; Schaefer et al., 2017; Spinner et al., 2013; Torres-Ruiz and Jürgens, 1994; Traas et al., 1995; Wright et al., 2009; Zhang et al., 2016). Besides the fact that plant cells lack centrosome, many components of the TTP complex share homology with the centrosomal protein of animal origin. TON1, a regulatory subunit of the TTP complex shares similarities with the human fibroblast growth factor receptor1 (FGFR1), oncogene partner (FOP) and oral-facial digital 1 as well interacts with CENTRIN, a Arabidopsis homolog of human centrosomal protein, (Azimzadeh et al., 2008; reviewed in Rasmussen et al., 2013) and CDK (Van Leene et al., 2007). Impairment of the TON1 function causes the failure of PPB formation. Defects are also seen during organization of interphase cortical arrays as well as several other pleiotropic effects resulting from the loss of TON1. Cytoskeletal defects in the mutants lead to irregular patterns of cell division that eventually result in plants with short root and stunted growth (Azimzadeh et al., 2008).

PP2A complex is a heterotrimeric complex consisting of scaffolding, catalytic and B-type regulatory subunit encoded by FASS/TON2. PP2A possesses phosphatase activity (Camilleri

et al., 2002). TON2 also known as FASS, is the B-regulatory subunit of the PP2A phosphatase complex. Loss of function of TON2 results in the phenotype similar to *ton1* mutants (Camilleri et al., 2002; McClinton and Sung, 1997; Traas et al., 1995). The *fass* mutant shows reduced microtubule density, increased microtubule catastrophe rate and reduced microtubule branching in interphase cells. This suggests that TON2 regulates the formation of PPB likely by altering the phosphorylation status of the microtubule regulatory proteins at PPB (Kirik et al., 2012). Similarly, *pp2aa* mutants produce severely dwarf plants, displaying misshapen cells with randomly oriented cell division patterns (Spinner et al., 2013). TON1 and PP2A complexes are recruited to microtubules via the third member of the TTP complex called TON1 recruitment motif (TRM) (Drevensek et al., 2012; Spinner et al., 2013). TRM binds to microtubules both *in vivo* and *in vitro* and also shares the conserved sequence motifs with human centrosomal proteins, centrosome-associated protein 350 KD (CAP350) (Drevensek et al., 2012). CAP350 interacts with the human centrosomal protein, FOP (Yan et al., 2006). Impairment of the TRM6-8 function leads to complete loss of PPB. However, unlike other components of TTP complex, PPB defects in *trm678* uncouple the PPB loss with the division plane orientation defect, which raises the possibility of PPB-independent alternate mechanism for the correct positioning of cell walls (Schaefer et al., 2017) Similarity of TTP component with centrosomal proteins and its requirement during PPB formation, points to similar nucleation function in plants and animals.

1.7.5.6 MAP65-3

MAP65 protein family is evolutionary conserved and has been studied extensively for their roles in microtubule bundling and crosslinking. The protein crosslink antiparallel microtubules by forming the 30 nm bridge between overlapping plus end of antiparallel microtubules (Gaillard et al., 2008; Smertenko et al., 2004). MAP65 isoforms are functionally divergent (Kosetsu et al., 2013); however, several isoforms are shown to be localized at the midzones of phragmoplasts, where they function to maintain integrity and to provide stability to the structure of phragmoplasts as well as to contribute to the directional expansion of plant cells (Chan et al., 2003b; Li et al., 2017; Müller et al., 2004; Sasabe and Machida, 2012; Smertenko et al., 2018, 2004). Impairment of the MAP65-3 function causes widening of phragmoplast midzone and subsequent defect in cell plate extension resulting in cell wall stubs and multinucleated cells (Caillaud et al., 2008; Ho et al., 2011; Müller et al., 2004). The activity of MAP65-3 is controlled by the action of MAPK. Upon phosphorylation, MAP65-3 reduces its binding affinity to microtubules, leading to the depolymerization of microtubules from the lagging strand of phragmoplasts (Kohoutová et al., 2015; Sasabe and Machida, 2012; Smertenko et al., 2006).

1.7.5.7 PHGAPs

PHGAPs are novel interactors of POK1, comprising the N-terminal (PH) pleckstrin homology domain, a GAP domain and C-terminal coiled-coil domain (Stöckle et al., 2016). The two PHGAPs are structurally similar to each other. The C-terminal coiled-coil domain interacts with the POK1 C-terminal fragment. In interphase cells, both PHGAP1 and PHGAP2 decorate plasma membrane uniformly and to some extent, localize in the cytoplasm. During metaphase, PHGAPs preferentially accumulate at CDZ as bright foci and remains afterwards throughout the cell division. POK1 is essential for recruitment of PHGAPs at CDZ/CDS and their further maintenance at the division site. In the feedback loop, PHGAPs function in the positioning of the division plane, indicated by tilted PPB positioning in *phgap12* double mutants. POK1 cortical rings are co-aligned with PPB positions in *phgap12* double mutants. Consistent with PPB misorientation, further cell division structures, spindles and phragmoplasts also display significant tilting relative to the long axis of the root. *Phap12* double mutant shows moderate cell wall positioning defect compared to *pok12*. The conspicuous accumulation of PHGAPs is proposed to spatially deactivate ROP GTPase targets for local depolymerization of actin (Feiguelman et al., 2018; Stöckle et al., 2016). Clathrin-coated pits and vesicle accumulate at PPB site, which likely causes the deletion of certain proteins from the PPB as well modification of the plasma membrane. The modification of the membrane marks the PPB memory (Karahara et al., 2010, 2009; Stöckle et al., 2016). Such ROP-dependent modification of membrane might help in the division plane selection via the ROP-PHGAP module.

1.8 CaM interacting MAPs in the regulation of microtubule organization and dynamics

A spectrum of CaM binding MAPs is known, such as, ELONGATION FACTOR-1 α (EF1 α) (Browning, 1996), MICROTUBULE DESTABILIZING PROTEIN 25 (MDP25) (Ide et al., 2007), MICROTUBULE-ASSOCIATED PROTEIN 18 (MAP18) (Wang et al., 2007), KINESIN-LIKE CAM BINDING PROTEIN (KCBP) (Reddy et al., 1996) and IQD67 DOMAIN (IQD) (Abel et al., 2005) proteins, which control the microtubule cytoskeleton by transducing Ca²⁺-encoded information. EF1 α , a highly conserved translation factor (Browning, 1996) is identified as one of the CaM binding proteins which is shown to modulate dynamic instability of *in vitro* assembled microtubules by regulating catastrophe frequency as well as shortening velocity of microtubules. Binding of Ca²⁺-CaM influences microtubule bundling activity of EF1 α as well as modulates its effects on dynamic instability of microtubules (Durso and Cyr, 1994; Moore et al., 1998). EF1 α decorates all microtubule arrays and potentially possesses microtubule nucleation activity, depletion of which leads to a defect in mitotic array formation in sea urchin embryo (Ohta et al., 1988).

MDP25 and MAP18, also called PLASMA MEMBRANE ASSOCIATED Ca^{2+} CATION-BINDING PROTEIN1 (PCaP1) and PCaP2, are two paralogous membrane binding proteins (Ide et al., 2007; Kato et al., 2010b), which possess the capacity to bind Ca^{2+} and Ca^{2+} -CaM (Kato et al., 2013; Nagasaki et al., 2008). Both proteins belong to a diverse class of DEVELOPMENTALLY REGULATED PLASMA MEMBRANE PROTEINS (DREPPs), which contain an N-terminal polybasic region, a central conserved region of 110 amino acids and a variable C-terminal region. Structurally, MDP25 shows diversity compared to other members of DREPPs and lacks the central coiled regions (Vosolsobě et al., 2017). PCaP1 and PCaP2 share 28% sequence similarity as well as a range of biochemical and functional properties such as the presence of proline, lysine, glutamate and valine residue, low isoelectric point and a propensity for intrinsic disorder (Kato et al., 2010b). Their plasma membrane association is likely stabilized via myristoylation at Gly2 and by binding to phosphatidylinositol 3,5-bisphosphate and phosphatidylinositol 3,4,5-triphosphate (PtdInsPs) (Kato et al., 2013; Nagasaki et al., 2008), which is mediated via the 23 amino acids N-terminal region. The same N23 region is responsible for binding microtubules and actin in MDP25 (Kato et al., 2010a; Nagasaki et al., 2008; Qin et al., 2014). An increase of Ca^{2+} levels weakens the interaction of MAP18 and MDP25 with PtdInsPs which promotes their interaction with the cytoskeleton as well as well as activates PtdInsPs mediated signaling and thus links Ca^{2+} and PtdIns signaling (Kato et al., 2010a; Qin et al., 2014). MDP25 negatively regulates elongation of etiolated hypocotyl cells likely by destabilizing cortical microtubules, which results in their reorientation (Li et al., 2011). MDP25 also binds directly to actin and causes Ca^{2+} -dependent severing of actin filaments in the subapical region of pollen tubes, which regulates pollen tube growth (Qin et al., 2014).

MAP18 destabilizes microtubules by inhibiting tubulin polymerization. Altered activity of MAP18 leads to disorganized cortical microtubules arrays. MAP18 regulates directional growth of pollen tubes, root hairs and also coordinates lobe formation in pavement cells likely by disorganization of microtubules and actin filaments (Wang et al., 2007; Zhang et al., 2015; Zhu et al., 2013). Overexpression of *MAP18* shows wider and twisted organ, which correlates with an altered organization of cortical microtubules. Attenuation of MAP18 expression in *map18* knockdown mutants causes a defect in the growth directionality of pollen tubes. MAP18 regulates actin organization in the apical region of pollen tubes by providing Ca^{2+} -dependent actin-severing activity and thereby imparts in the directionality of pollen tube growth (Zhu et al., 2013). In addition, MAP18 binds and activates RHO GTPase from plants (ROP2) (Kang et al., 2017), which is a member of GTPase family that control plant growth and polarity via regulation of cytoskeleton dynamics (Craddock et al., 2012; Feiguelman et al., 2018).

One of the well-characterized CaMBPs identified in plants is KCBP/ZWICHEL (Reddy et al., 1996). It is a member of the kinesin-14 family, which contains an N-terminal MyTH4-FERM followed by a central coiled-coil region and a C-terminal conserved motor domain, and known to move progressively towards the minus ends of microtubules (Reddy et al., 1996; Reddy and Day, 2001; Song et al., 1997; Yamada et al., 2017). Similar to myosin VII actin motor, MyTH4-FERM of KCBP mediates coordination between actin and microtubules (Richardson et al., 2006; Tian et al., 2015). KCBP binds to microtubules with its N-terminal MyTH4 and its C-terminal motor domain. The 23 amino acids region adjacent to the C-terminal motor domain mediates Ca²⁺-CaM binding to KCBP. The C-terminal motor domain binds to microtubules in an ATP and Ca²⁺-CaM-dependent manner (Narasimhulu and Reddy, 1998; Reddy et al., 1996). Ca²⁺-CaM binding to KCBP inhibits its association with microtubules, thereby causing destabilization of microtubules. The level of inhibition depends on Ca²⁺ and CaM concentrations (Deavours et al., 1998). It is thus hypothesized that the Ca²⁺ levels in the cell modulate *in vivo* activity of KCBP via regulating its microtubule association.

In addition, KCBP-INTERACTING Ca²⁺ BINDING PROTEIN (KIC) interacts with KCBP via its C-terminal regulatory domain and KIC-KCBP interaction inhibits microtubule binding of KCBP *in vitro* (Deavours et al., 1998; Narasimhulu and Reddy, 1998; Vinogradova et al., 2009). In addition, KIC interacts with Ca²⁺-CML42 (Dobney et al., 2009). These altogether suggest an additional level of regulation of Ca²⁺ on KCBP-mediated microtubule organization and dynamics (Buschmann and Lloyd, 2008). The presence of two microtubule binding domains in KCBP correlates with its *in vitro* microtubule bundling activity (Kao et al., 2000; Tian et al., 2015). KCBP is reported to play roles in trichome development. Loss of KCBP causes the formation of shorter trichomes with fewer branches compared to normal trichomes, by modulating microtubules and actin filaments during trichome formation (Tian et al., 2015). During trichome formation, KCBP labels cortical microtubules attached to the plasma membrane. KCBP accumulates both at the branch point and at the tips of the developing trichome, causing reduced microtubule density and high accumulation of actin filaments at the branch tips (Tian et al., 2015). However, genetic complementation of *kcbp* mutants with CaM binding deleted variants of KCBP indicate a Ca²⁺-CaM-independent regulation of KCBP function during trichome development (Tian et al., 2015). Trichome defects in *kcbp/zwichel* mutants suggest a function of KCBP in cell elongation and thus the organization of cortical microtubules. Besides, KCBP also localizes to the PPB, spindle and phragmoplast and interacts with the CDZ-localized protein AUXIN-INDUCED IN ROOT CULTURES 9 (AIR9) and is proposed to play a role during cytokinesis. At the CDS, it serves as a PPB marker after PPB disassembly, however precise biological function of KCBP during cell division is not known yet (Buschmann et al., 2015; Buschmann and Zachgo, 2016).

1.9 IQD proteins, plant-specific CaM interacting MAPs

The IQD family comprises the largest known class of CaM targets in plants. IQD family is characterized by the presence of a conserved 67 amino acids spanning domain, named IQ67 domain, which contains up to three copies each of the IQ motif, the 1-(8)-14 motif and the 1-(5)-10 motif (Figure 1.7A) (Abel et al., 2005).

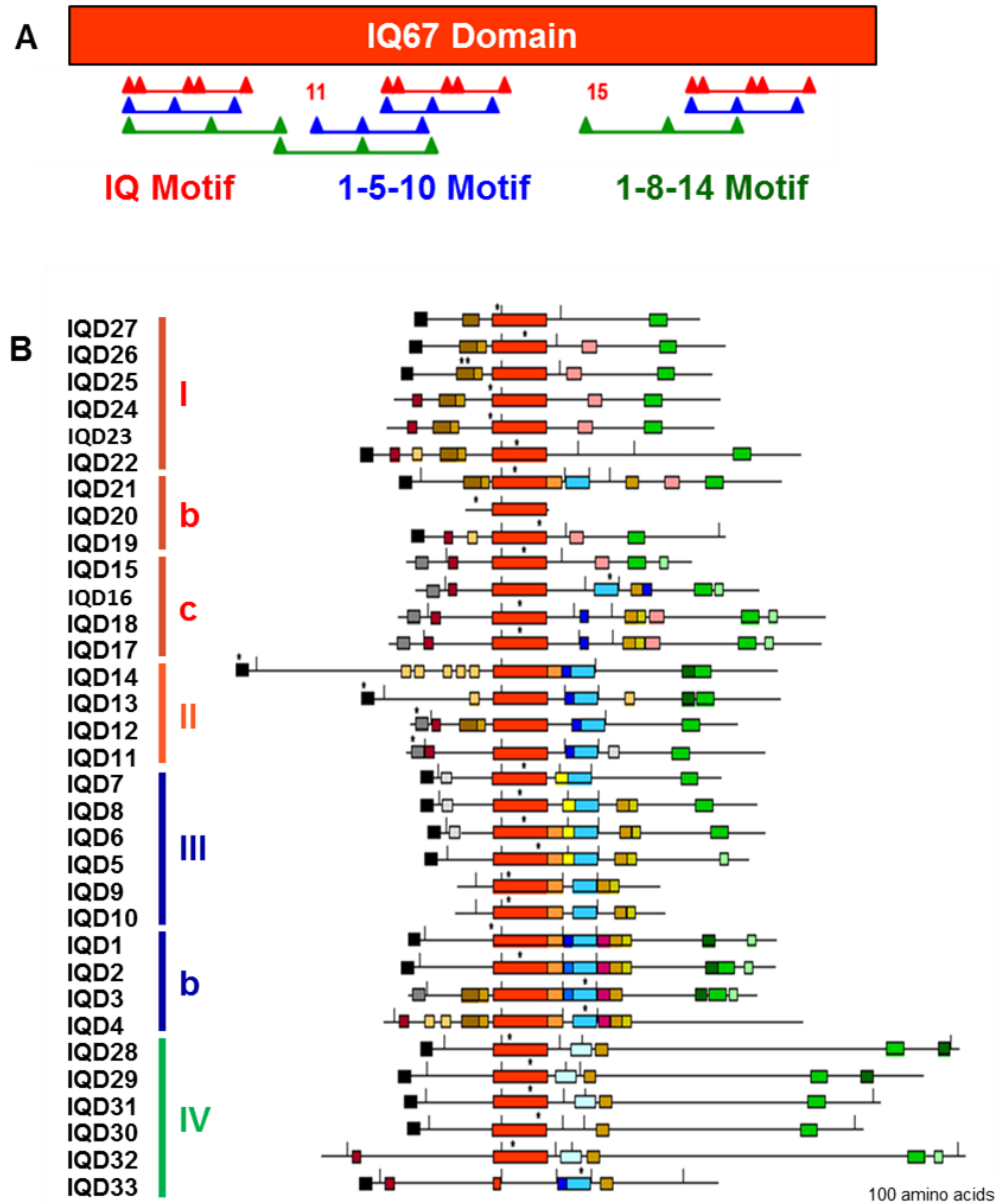


Figure 1.7 Motif organization of Arabidopsis IQDs.

(A) Arrangement of the CaM-binding conserved IQ67 Domain. (B) Domain organization of the 33 Arabidopsis IQDs. Conserved IQ67 domains are represented in red boxes. Structurally diverse domains outside the IQ67 domain are represented in different colored boxes. Modified from (Abel et al., 2005).

The IQ67 domain is required and sufficient for mediating CaM binding (Bürstenbinder et al., 2013). In Arabidopsis, the IQD family comprises 33 members, which are classified into four phylogenetic clades (Figure 1.7B). Members of the IQD protein family share the conserved IQ67 domain but differ in the IQD specific motifs of potentially specialized functions. IQDs are highly diverse in their sizes that vary between 103-794 amino acids and molecular masses ranging between 11 to 86 KD. They, however, share common physicochemical properties. A hallmark of the IQD protein family is the high frequency of basic amino acid residues, resulting in overall high isoelectric points (Abel et al., 2005). IQD families have been annotated in *Solanum lycopersicum* (*S. lycopersicum*) (34 members), *Glycine max* (*G. max*) (67 members), *O. sativa* (29 members), *Brachypodium distachyon* (*B. distachyon*) (23 members), *P. trichocarpa* (40 members), *Phyllostachys edulis* (*P. edulis*) (29 members), *A. thaliana* (33 members) (Abel et al., 2005; Cai et al., 2016; Feng et al., 2014; Filiz et al., 2013; Huang et al., 2013; Ma et al., 2014; Wu et al., 2016).

IQD families in Arabidopsis and rice consist of a high fraction of sister pairs which arises from segmental genome duplication events. Arabidopsis IQDs consists 8 sister pairs, which are 45% of the total paralogous gene set (Abel et al., 2005). IQD proteins are one of the largest classes of CaMBPs in plants. The founding member of the IQD family, Arabidopsis IQD1 is shown to recruit CaM to microtubules and nucleolus when both proteins are co-expressed together in *Nicotiana benthamiana* (*N. benthamiana*) (Bürstenbinder et al., 2013). IQD1 was characterized by screening of activation tagged T-DNA lines for mutants with altered glucosinolate content and composition (Levy et al., 2005). Glucosinolate-derived products, isothiocyanates, act in plant defense against herbivores as well as in the prevention of mammalian cancer (Grubb and Abel, 2006; Halkier and Gershenzon, 2006). In this context, IQD1 may links Ca²⁺-CaM signals to defense responses by transcriptional activation of defense-related genes (Levy et al., 2005). Extensive analysis of the subcellular localization of the entire Arabidopsis IQD family revealed that most IQDs are associated with microtubules and membranes, and are often localized in the nucleus (Bürstenbinder et al., 2017). Most IQD family members interact *in vitro* with apoCaM (Ca²⁺ free) and holoCaM (Ca²⁺ bound), which is consistent with the presence of multiple motifs engaged in binding to both states of CaM (Abel et al., 2005).

Arabidopsis IQDs are shown to sequester CaM/CML to distinct subcellular sites, possibly to restrict Ca²⁺ signaling to the specific domains for precise biological function (Figure 1.8A). IQDs preferentially accumulate in dividing tissues and are expressed at relatively low levels (Bürstenbinder et al., 2017). Expression of IQDs is shown to be controlled by phytohormones (Bi et al., 2018; Feng et al., 2014; Möller et al., 2017; Rashotte et al., 2003; Zentella et al.,

2007). A recent report showed that expression of *AtIQD15-18*, as well as *OsIQD14*, are regulated by AUXIN RESPONSE FACTOR 5/MONOPTEROS (ARF5/MP) (Möller et al., 2017), suggesting that several IQDs function downstream of auxin.

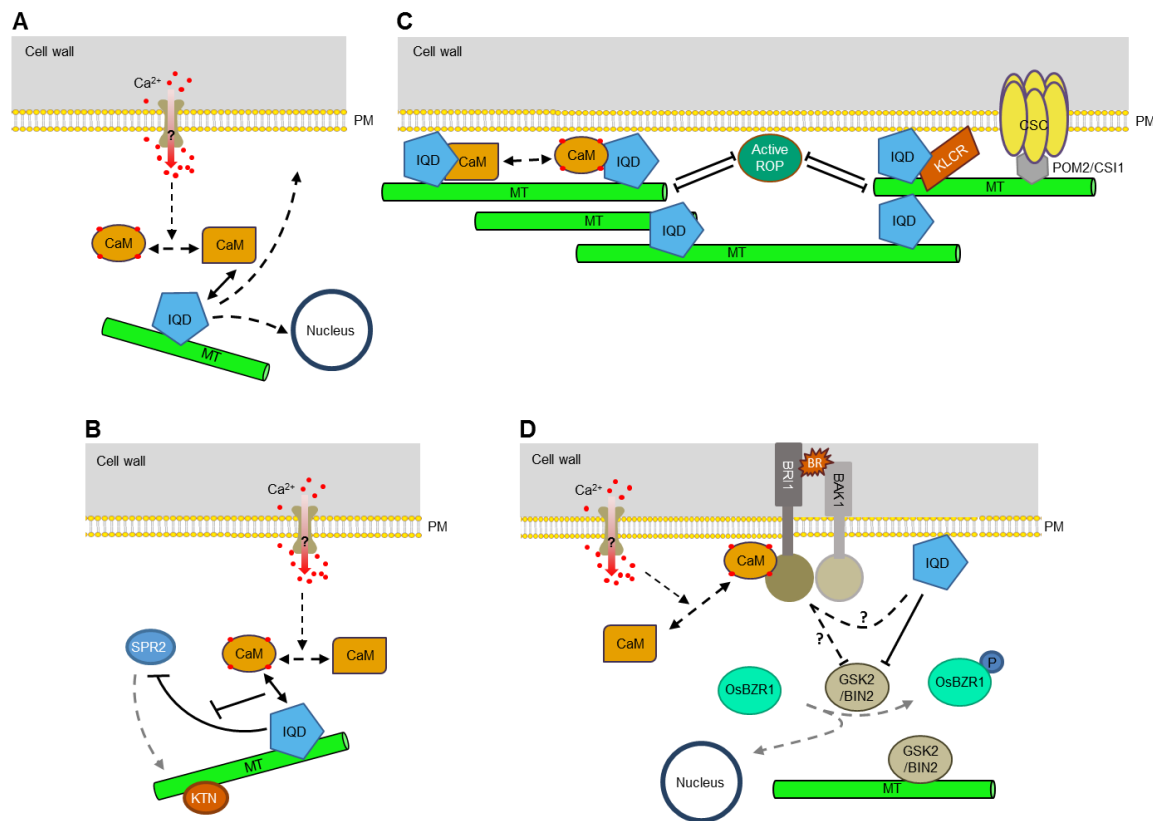


Figure 1.8 Proposed function of IQD proteins at the plasma membrane-microtubule nexus.

(A) IQDs interaction with apo and holo CaM at distinct subcellular sites. (B) IQD mediated regulation ROP GTPase domain at the plasma membrane. (C) Ca^{2+} -CaM-IQD-SPR2 mediated regulation of microtubule dynamics. (D) Function of IQD in brassinosteroid signaling. PM, plasma membrane; MT, microtubule; IQD, IQ67 DOMAIN; CaM, calmodulin; ROP, RHO GTPase from plants; CSC, CELLULOSE SYNTHASE COMPLEX; CSI1/POM2, CELLULOSE SYNTHASEINTERACTING 1; BRI1, BRASSINOSTEROIDINSENSITIVE1; BAK1, BRI1 ASSOCIATED RECEPTOR KINASE1; BZR1, BRASSINAZOLE RESISTANT1; GSK2, GLYCOGEN SYNTHASE KINASE2; BIN2, BRASSINOSTEROID INSENSITIVE2. Modified from (Kölling et al., 2019).

Localization of IQDs along the microtubule lattice is similar to those of microtubule-associated regulatory proteins. Interestingly, over-expression of GFP-tagged IQD fusion proteins is shown to exert differential effects on microtubule organization and bundling, which suggest the potential function of IQDs in microtubule crosslinking and bundling (Bürstenbinder et al., 2017). This view is also supported by the truncation analysis of IQD13, which showed the presence of several microtubule binding domains, and thereby likely providing microtubule crosslinking and bundling (Sugiyama et al., 2017). Interestingly a very recent report showed the effect of IQD in the regulation of microtubule activity in a Ca^{2+} -CaM-dependent manner. In the presence of elevated Ca^{2+} -CaM level, SPR2 gets separated from

IQD18 and promotes microtubule dynamics (Figure 1.8B) (Wendrich et al., 2018). SPR2 promotes KTN1-dependent severing of microtubules and thereby influences the dynamic properties of microtubules (Nakamura et al., 2018). The biological significance of IQD-CaM interaction has been evident in recent research, where OsIQD14 activity is shown to be inhibited by OsCaM. Hence, reorientation of microtubules in a Ca^{2+} -CaM-IQD-dependent manner potentially provides a mechanism to transduce Ca^{2+} signals generated in response to environmental and developmental stimuli (Yang et al., 2019). Auxin induces a rapid increase in Ca^{2+} levels and is shown to induce rapid reorganization of microtubules (Chen et al., 2014; Monshausen et al., 2011). Other studies have also shown the ARF-dependent transcriptional regulation of *IQDs* (Möller et al., 2017; Yang et al., 2019). Altogether, this suggests that IQDs might act as mediators of auxin and Ca^{2+} signals. Further information about this module will solve the potential signal transduction mechanism of IQD.

Overexpression of *IQDs* exerts different effects on the general organization of microtubules, which further suggest individual IQD-specific regulatory activities on the organization of the microtubule network. Distinct roles in microtubule regulation are supported by analysis of over-expression lines in Arabidopsis, in which IQD11 and IQD14 or IQD16 differentially affect microtubule organization and altered growth properties like twisting of organs and elongation of leaves (Bürstenbinder et al., 2017). Such effects are also observed in mutants of proteins known for regulatory functions on microtubules (Buschmann et al., 2004; Lee et al., 2006), which further suggests the involvement of IQDs in microtubule-dependent functions. In another example, Arabidopsis IQD13 is shown to promote microtubule rescue events and supports assembly, thereby providing microtubule stability (Sugiyama et al., 2017). Increased sensitivity of *iqd5* loss of function lines to oryzalin, a microtubule depolymerizing drug, further supports the role of IQD in controlling microtubule stability (Yang et al., 2019).

Several lines of evidence suggest a possible function of IQDs in regulating plant growth via controlling cell shape and division (Bürstenbinder et al., 2017; Liu et al., 2017), as part of an elaborate microtubule network that mediates cell expansion and directional growth (Sedbrook and Kaloriti, 2008). Consistently, elongated fruit shape in cucumber, watermelon, tomato and rice is caused by mutations in Arabidopsis *IQDs* homologs *CsSUN*, *CIFS1*, *SISUN* and *GSE5*, respectively (Dou et al., 2018; Duan et al., 2017; Liu et al., 2017; Pan et al., 2017; Xiao et al., 2008). However, the precise molecular mechanisms in these processes are not known. IQD-mediated reorientation of microtubules is reported to play a role in improving agronomic traits of crop plants. Altered expression of *OsQD14*, a rice homolog of *AtIQD16*, causes changes in shape and size of seeds via realignment of microtubules. Overexpression of *OsIQD14* leads to decreased microtubule dynamics caused by an

increase in catastrophe events, which in turn leads to a reorientation of microtubules (Yang et al., 2019).

Additionally, important functions of membrane-localized IQDs have been reported. Overexpression of plasma membrane-localized *IQD25* in Arabidopsis and *OsIQD21/GW5/GRAIN SIZE CHROMOSOME5 (GSE5)* in rice is shown to alter cell shape and size (Bürstenbinder et al., 2017; Liu et al., 2017). The spikelet hulls of *gse5-cr* produce more cells in the direction of grain width, whereas *proActin:GSE5* produces fewer cells towards grain width and more cells towards grain length. Alteration in cell numbers corresponds to wider and heavier grains of *gse5-cr*, and narrower and longer grain size of *GSE5* overexpressing plants. It is concluded that *GSE5* controls grain shape and size by limiting cell proliferation in spikelet hull cells. *GSE5* inhibits GLYCOGEN SYNTHASE KINASE 2 (*GSK2*) activity via its direct interaction (Figure 1.8D) (Liu et al., 2017). *GSK2* is the rice homolog of Arabidopsis BRASSINOSTEROID INSENSITIVE2 (*BIN2*), which is a negative regulator of BRASSINOSTEROID (BR) responsive genes (He et al., 2002). By inhibition of *GSK2* activity, *GSE5/OsIQD21* may thus promote BR-dependent growth regulation and potentially link BR to the Ca^{2+} signaling (Liu et al., 2017). Interestingly dual localization of several IQDs further suggests a possible function at the plasma membrane-microtubule continuum (Bürstenbinder et al., 2017). The indirect support for roles of IQDs at microtubules and/or plasma membrane has been provided by studies conducted in tomato. Overexpression of tomato *SUN*, a homolog of Arabidopsis *IQD12*, causes elongated fruit shapes possibly via its regulatory function at the plasma membrane-microtubule continuum similar to membrane-localized scaffold proteins (Wu et al., 2011; Xiao et al., 2008).

Other known components of IQD signaling modules are KINESIN LIGHT CHAIN-RELATED (KLCR)/CELLULOSE-MICROTUBULE UNCOUPLING PROTEINS (CMU), which provide lateral stability to cortical microtubule against the pushing forces of CSCs (Liu et al., 2016). IQD facilitate microtubule binding of KLCR protein (Bürstenbinder et al., 2013) and thus may function in KLCR mediated lateral stability of cortical microtubules. Additionally, *IQD13* is reported to function at the plasma membrane-microtubule junction to locally restrict ROP GTPase function and helps in the formation of oval secondary cell wall pits (Figure 1.8C) (Sugiyama et al., 2017). ROPs are major regulators of cellular polarity, known to control cell polarity via effector proteins at the actin and microtubule cytoskeleton (Feiguelman et al., 2018). Thus, IQDs may provide a link between Ca^{2+} signaling and ROP signaling. Dual localization of IQDs at the microtubule-plasma membrane junction provide physical connection of cortical microtubules to the plasma membrane which may suggest potential roles in the delivery and deposition of cellulosic and noncellulosic wall materials (Oda, 2018).

Consistently, *iqd5* knockout mutant shows reduced deposition of cellulose in anticlinal walls of pavement cells (Mitra et al., 2019).

Outside of their CaM and KLCR binding domain, IQDs are predicted to be intrinsically disordered, and structurally resemble scaffold proteins (Bürstenbinder et al., 2017). Multiple domains mediate subcellular localization, as indicated by at least two distinct microtubule-binding domains and a plasma membrane-localized domain, pointing to roles of IQDs in membrane tethering and bundling or crosslinking of microtubules. Altogether, the prospect arises that IQDs act as hubs for the integration of different signaling modules at the plasma membrane-microtubule and transduce information into microtubule organization and dynamics to control cell division and cell expansion.

1.10 KLCRs as IQD interactors

IQD1, IQD2 and IQD23 interact with KLCR proteins both in yeast two-hybrid (Y2H) and in transient expression assay in *N. benthamiana*, where IQD proteins recruit KLCRs to their distinct subcellular sites (Bürstenbinder et al., 2013; Mukhtar et al., 2011). KLCRs belong to a family of TETRATRIPEPTIDE REPEAT (TPR) domain-containing proteins that share structural similarity to mammalian KLCs (Bürstenbinder et al., 2013). KLCs are functional subunits of type-1 kinesin complexes, which are heterotetramers of two motor activity containing KINESIN HEAVY CHAINS (KHCs) and two cargo binding KLCs. In mammals, KHC and KLC of the heterotetramer complex are encoded by *Kif5A-C* and *KLC1-4*, respectively. Distinct cells and tissue-specific expression profiles of *KHCs* and *KLCs* (Hackney, 2007), suggest the possible diversity of the complex. Heterotetrameric kinesin-1 complexes have been reported to play roles in the transport of ribonucleic acids, vesicles, organelles and protein complexes (Vale, 2003; Vale et al., 1985). Cargo binding and movement of the kinesin complex on microtubules is mediated by KLCs and KHC, respectively. However, several other studies document the cargo binding domain directly in the stalk and/or tail domains of KHC (Skoufias et al., 1994).

The Arabidopsis genome encodes 3 KLCRs, which are localized to microtubules and play roles in anchoring microtubules at the plasma membrane. It is not known yet whether KLCRs interact with plant kinesins. The Arabidopsis genome encodes 61 kinesins, 58 of which fall into 10 out of 14 kinesins families, while the remaining three are not grouped into any of the 14 families and represent a plant-specific family (Reddy, 2001; Reddy and Day, 2001; Richardson et al., 2006). Besides large number of kinesins, Arabidopsis lacks bonafide type-1 kinesins. The only predicted type-1 kinesin contains a very short stalk and coiled-coil domain with little or no similarity to animal kinesins, but lacks stalk and tail regions that are

essential to mediate interaction with KLCs in animal type-1 kinesin (Reddy and Day, 2001). Arabidopsis type-1 Kinesin is more closely related to fungal kinesins in terms of structural similarity (Reddy and Day, 2001), suggesting a similar mechanism of action. However, the fungal genome does not encode for KLC-like proteins (Steinberg et al., 1998; Steinberg and Schliwa, 1995). Similar to Arabidopsis, rice also encodes a single type-1 kinesin, termed PSS1 POLLEN SEMI STERILITY 1 (PSS1), which also lacks a typical KLC binding region (Zhou et al., 2011). A search against the gene database further identifies another type-1 kinesin from a third plant species, *Vitis vinifera* (*V. vinifera*) (Jaillon et al., 2007) although its function remains elusive. The data from flowering plants suggest the diversification of higher plant type-1 kinesins compared to their animal counterpart (Jaillon et al., 2007; Wang et al., 2014; Zhou et al., 2011).

1.11 Thesis aims

The first aim of my thesis was to characterize the roles of IQDs in plants by reverse genetics approach. Considering the potentially conserved function of group III IQDs, we particularly focused on this group for our analysis. From previous studies in our group, it was shown that over-expression of *IQDs* causes defects in plant growth as well as altered microtubule organization (Bürstenbinder et al., 2017). Most of the IQD related phenotypes reported so far are due to the effects of ectopic over-expression of *IQDs*, and therefore precise biological functions could not be revealed. In my thesis, I focused on T-DNA lines for functional characterization of members of the IQD family, with a focus on group III IQDs. In this part of my dissertation work, we used following approaches:

1. Establishment of double and triple mutant combinations and their detailed phenotypic analysis.
2. Generation of complementation lines and subsequent phenotypic analysis.
3. Analysis of subcellular localization of IQDs using confocal laser scanning microscopy.
4. Investigation of potential interactors.
5. Generation of higher-order mutants of IQDs and identified interactors to deduce their *in planta* and genetic interaction.

In frame of the second aim of my thesis, we investigated KLCR functions in terms of their predicted role as a subunit of kinesin complexes. For this, we focused on identifying KLCR-interacting KHCs from Arabidopsis. We studied the interaction of KLCRs with a set of selected kinesins. Both full-length as well as motor domain deleted (Δ MD) variants of kinesins were used for this analysis. We used a combinations of targeted interaction studies in yeast and transient expression assays in *N. benthamiana*. Subcellular localization studies were done initially by using cell biological assays. Different experimental approaches were used to test KLCRs-kinesins interactions, including Y2H assay, bimolecular fluorescence complementation (BiFC) assay, co-recruitment assays and *in vitro* pull-down assays. Candidate kinesins used in the study were:

1. The predicted type-1 kinesin: KIN1.
2. Kinesins with structural similarity to type-1 kinesins from animals.
3. Kinesins which are closely related to type-1 kinesins in the phylogenetic tree.

2 Functional characterization of Arabidopsis IQD6 to IQD8

2.1 Introduction:

2.1.1 IQD: A novel class of microtubule-associated, Ca²⁺-CaM interacting protein

IQD proteins plant-specific CaM targets that contain large regions of predicted intrinsic disorder flanking the conserved CaM binding IQD67 domain. Regions of intrinsic disorder are hallmarks of scaffold proteins. Disorder proteins either function directly or via molecular recognition upon binding with their interaction partner. The latter is called molecular recognition where binding with interacting proteins leads to conformational changes from disorder to order. Short peptides of intrinsic disorder interspersed by regions of known function often mediate molecular recognition. These short peptides of low complexity provide flexibility and mediate protein-protein interactions. These interactions are often transient and context-dependent, suggesting versatility of the complexes and thus potentially serve multifunctional roles. It also serves a site for posttranslational modifications, thereby fine-tuning and regulating the complex formation. (Tompa, 2014). Both bound and free disordered regions are accessible to post-translational modifications. The intrinsic flexibility of the disordered region provides promiscuous binding with various cellular partners. To prevent this, scaffold proteins are usually expressed at a low level in their steady-state (Berlow et al., 2015). Similarly, IQD proteins are also expressed in low protein abundance. Low levels of *IQD* expression might prevent promiscuous complex formation, as reported in the case of scaffold proteins. These all together bring IQD as a potential regulator of microtubule structure and function as well as play various role in plasma membrane-microtubule continuum, which acts as a scaffold during the process of plant growth and development (Abel et al., 2005; Bürstenbinder et al., 2017).

Overexpression of *IQDs* leads to phenotypes such as twisting of organs and tissues as well as changes in cell shape and alteration of cell division, reminiscent of proteins with regulatory functions of microtubule growth and dynamics. Most IQDs are located on microtubules in a uniform fashion, in contrast to preferential binding of microtubule plus and minus end binding proteins, suggesting microtubule-stabilizing functions of IQDs. In addition, recent studies suggested roles of IQD in the regulation of microtubules dynamics via Ca²⁺-CaM-dependent manner (Duan et al., 2017; Mitra et al., 2019; Wendrich et al., 2018; Yang et al., 2019). Besides its potential functions at microtubules, several plasma membrane-localized IQDs also show distinct patterns, suggesting specific regulatory functions, which is also reflected in specific morphological defects of these specific *iqds* mutants (Bürstenbinder et al., 2017;

Duan et al., 2017; Wu et al., 2011; Xiao et al., 2008). Altogether these observations suggest that IQD proteins play an important role in plant growth.

Previous studies conducted in our group suggested an evolutionarily conserved function of clade III IQDs, which motivated us to focus our phenotypic analysis on this particular group. Quantitative analysis of the microtubule patterns labeled by GFP-IQDs, expressed under the control of 35S promoter in *N. benthamiana* shows similar effects of over-expression of *IQD6*, *IQD7* and *IQD8*, on microtubule organization (Bürstenbinder et al., 2017), which outgroups *IQD7*, *IQD8* (encoded by sister pair) and *IQD6* (the most closely related member of this group). They share high similarity at the sequence level and their motif organization. Analysis of GFP-GUS reporter expressions driven under endogenous promoter revealed that *IQD6*, *IQD7* and *IQD8* are expressed in dividing tissues (shoot apical meristem, apical root meristem, cotyledons), suggesting a potential function in cell division.

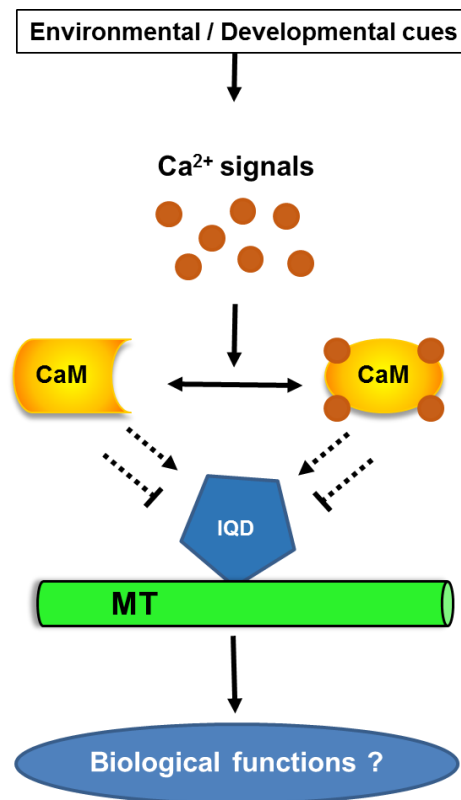


Figure 2.1. Proposed model of IQD function.

IQD proteins decorate microtubules and recruit KLCRs/CMUs as well as CaM2 to its various subcellular sites, indicating a potential scaffolding function. IQDs play various roles during plant development, from microtubule organization to maintenance of plant cell shape. All together IQDs may work as a potential candidate to provide scaffolding activity in organization and regulation of mitotic microtubule arrays during spatial control of cytokinesis. MT, microtubule; IQD, IQD67 DOMAIN; CaM, calmodulin.

Interestingly, in the root meristem, *IQD6*, *IQD7* and *IQD8* show unique and up to some extent, overlapping expression pattern at the tissue level, suggesting a tissue-specific function of corresponding IQDs. Further, RNA seq analysis and promoter-GFP reporter study showed the gradual expression profile of *IQD6* and *IQD8* with very strong expression in the proximal region of roots relative to QC that gradually decreases towards the distal region, hence showing a downward expression gradient (P>M>D) (Wendrich et al., 2017). Such expression patterns are shown for genes involved in root meristem development and cell division, such as *ARF6*, *ARF8*, *KINESIN-12B*, *LONELY GUY3LOG3*, *PIN-FORMED1 (PIN1)*, *PIN4*, *PLETHORA1 (PLT1)*, *PLT2*, *SHORT-ROOT (SHR)*, *ZWILLE*, and several *CYCLIN* and *CDK* (Wendrich et al., 2017 and references therein) Perturbance of normal expression gradients of *IQD6* leads to disturbed root growth. Hence, the expression gradient is important for normal growth and development. In addition, *arf5/mp* knockout mutant lines showed reduced expression of *IQD6-IQD8*. Similar to this, *IQDs* from the other clades are also shown to be transcriptionally regulated via auxin signaling (Möller et al., 2017). Transcript analysis of *OsIQD14* upon auxin treatment further suggests auxin-dependent transcriptional regulation of IQD (Yang et al., 2019). Altogether suggest the conserved mechanism of Auxin-dependent transcriptional regulation among IQDs. Here, we thus embarked on a comprehensive reverse genetics characterization of *IQD6*, *IQD7*, and *IQD8* with a focus on their potential role in root growth and development.

2.2 Results

2.2.1 Phenotypic characterization of *iqd6*, *iqd7*, and *iqd8* mutants

In previous work of our group, T-DNA insertion lines of *IQD6*, *IQD7*, and *IQD8* had been established for functional analyses. Homozygous lines of *iqd6-1*, *iqd7-1* and *iqd8-1* single mutants were available in the laboratory prior to the start of this project, which carry insertions in exons (*iqd6-1*, *iqd7-1*) and in the second intron (*iqd8-1*) of the coding sequence (Figure S 1A) and which cause gene knock out in *iqd6-1* and *iqd7-3*, and strong gene knock down to approximately 10% of wild type levels in *iqd8-1* (Figure S 1B). Because single mutants were macroscopically indistinguishable from wild type (WT) plants, generation of double and triple mutants was initiated to reduce potential functional redundancies. First macroscopic phenotypic analysis indicated that the growth was unaffected by the loss of *IQD6*, *IQD7*, and *IQD8*.

Previous work in the group, however, pointed to unique and overlapping expression domains of these three genes in root and shoot meristems, as indicated by analysis of transgenic *pIQD:GFP-GUS* lines. These findings motivated us to investigate root meristems at the microscopic level. Root meristems were analyzed in 7-day-old seedlings grown under long-day conditions. Cell walls were visualized by propidium iodide (PI) staining and seedlings were analyzed by confocal laser scanning microscopy. Our analysis revealed that root meristem organization and cell wall patterning was comparable to WT in *iqd6-1* and *iqd7-1* single mutants (Figure 2.2A). Interestingly, we noticed increased frequencies of mispositioned cell walls in *iqd8-1* single mutants when compared to WT (Figure 2.2A, upper row). We defined three categories of deviation angle (0° - 5° , $>5^{\circ}\leq 15^{\circ}$ and $<15^{\circ}$) to determine whether the cell wall is transverse or deviated. The 0° - 5° degree deviation angle is considered as the normal transverse orientation of the cell wall positioning. While cell walls in WT were inserted in a transverse orientation (0° - 5°), some of the cells in *iqd8-1* mutants displayed oblique orientation of cell walls that deviated by average of greater than 7° from the transverse orientation (Figure 2.2B). Phenotypic analysis of double mutant combinations revealed that frequencies of mispositioned cell walls were enhanced when *iqd8-1* was combined with *iqd7-1* or *iqd6-1* in *iqd68* and *iqd78*, while *iqd67* double mutants were indistinguishable from WT (Figure 2.2A, B). The phenotype was further enhanced in *iqd678* triple mutants, in which larger number of the cells showed improper cell wall positioning with average of greater than 25° deviation from the transverse orientation of cells (Figure 2.2A, B). Enhancement of phenotype in the triple mutant suggests a partially redundant but also additive function of *IQD6*, *IQD7* and *IQD8*.

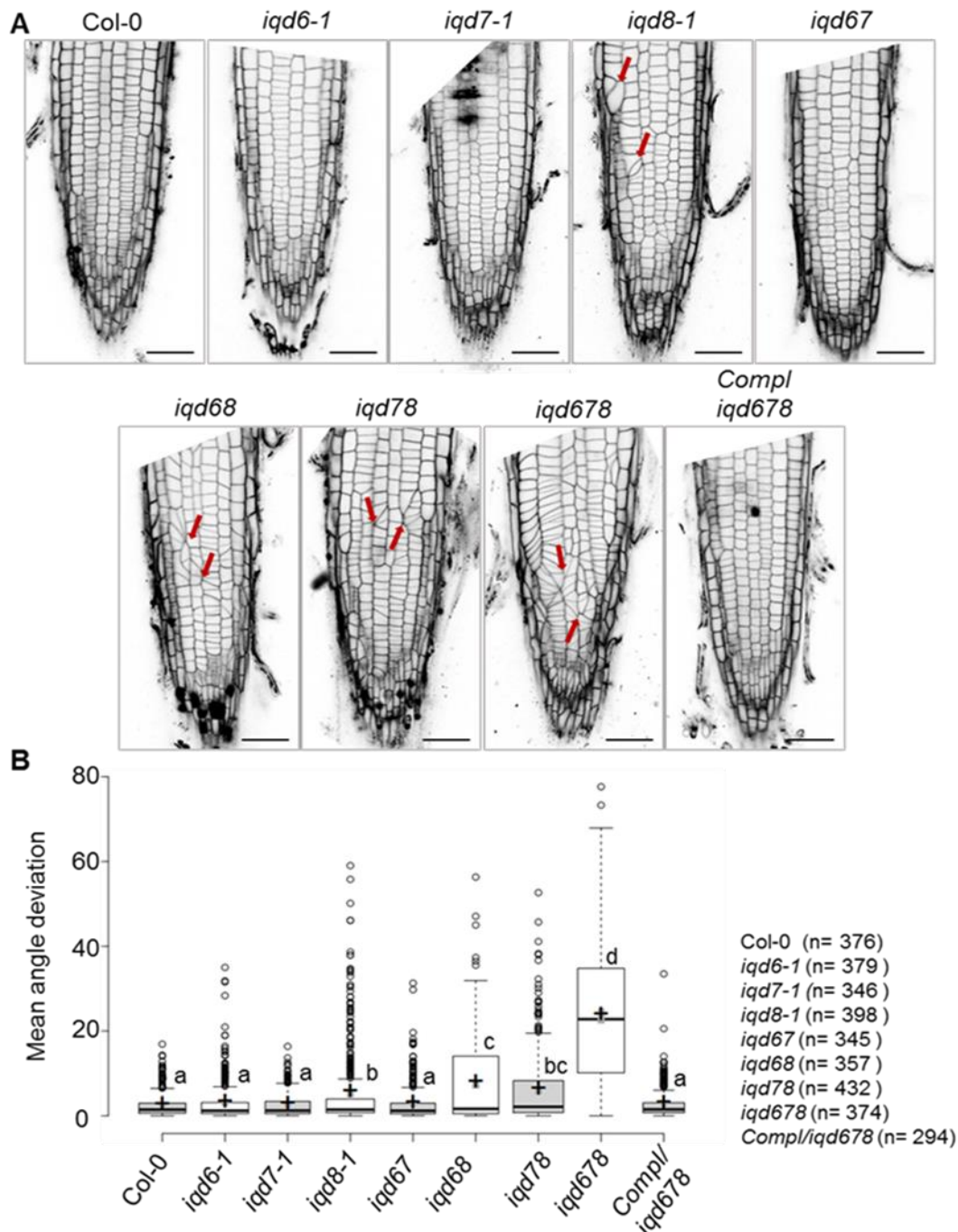


Figure 2.2 Phenotype of combinations of *iqd6*, *iqd7* and *iqd8* mutants.

(A) PI stained Arabidopsis root meristem cells of 7-day-old seedlings showing the patterns of cell wall positioning in single mutants, higher-order mutants and complementation line (*Compl/iqd678*) grown under long-day conditions. Red arrows indicate the irregularly positioned cell walls. The images are representative of 8-10 seedlings per genotype. Experiments were repeated at least 6 times with two different seed batches. PI was used to stain cell walls. Scale bars, 50 μ m. (B) Cell wall deviation angles were measured using ImageJ. Box limits indicate the 25th to 75th percentiles, center lines represent the medians, crosses indicate mean points, and dots represent outliers. Whiskers extend 1.5 times the IQR from the 25th and 75th percentiles. Individual letters denote statistically significant differences calculated by one-way ANOVA and post hoc HSD ($p < 0.001$). (n) = the number of cells analyzed per genotype. Quantification was performed ones using data from 8-10 independent seedlings per genotype. IQR, Interquartile range.

Additionally, the defects observed in the *iqd8-1* single mutant line indicates a major role of IQD8 in cell wall positioning. Because of the severe phenotype in the *iqd678* triple mutants, complementation was easier to access in the triple mutant background. Therefore we introgressed *pIQD8:IQD8-GFP* in *iqd678* triple mutants. Complementation of phenotype suggested that the phenotype is caused by loss of *IQD8* and also proved the functionality of the GFP-fusion construct (Figure 2.2A, B).

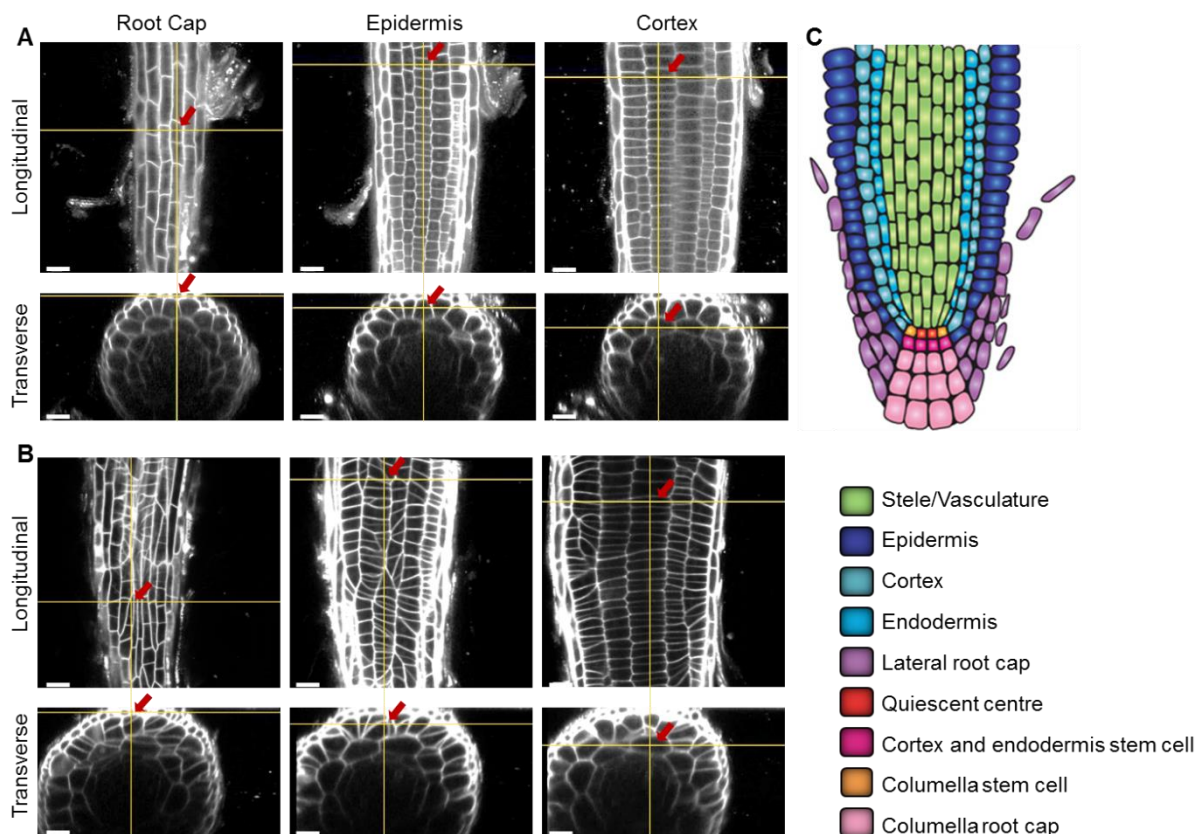


Figure 2.3 Patterns of cell wall positioning in the epidermis, cortex and root cap cells of WT and *iqd678* triple mutants.

Orthogonal views of 7-day-old *Arabidopsis* root meristem, showing pattern of cell wall positioning in different tissue layers of WT (A) and *iqd678* triple mutants (B). Red arrows indicate cells in the longitudinal section and the corresponding transverse section. Cell walls were visualized by PI staining. Scale bars, 20 μ m. (C) Schematic representation of median longitudinal section of a root showing the different tissue layers. Modified from (Marquès-Bueno et al., 2016).

Mutations primarily affected division plane orientation in the epidermis, while underlying tissue layers appeared to be unaffected with very rare event of division plane defect (Figure 2.3A, B). In *iqd678*, very few cases of division plane defect were detected in the endodermis and the tissue subtending the cortex. The restriction of the phenotype to a single tissue layer might suggest a redundant function of other IQDs or similar proteins in other tissue layers. We were wondering whether IQD8 and related proteins specifically affect division plane orientation in the root meristem or also function in other tissues. During octant stage of embryo development, cell walls are positioned in a regular pattern in WT. In contrast, during

embryo development in *iqd678* triple mutants, we observed few instances of oblique cell wall positioning (Figure S 2).

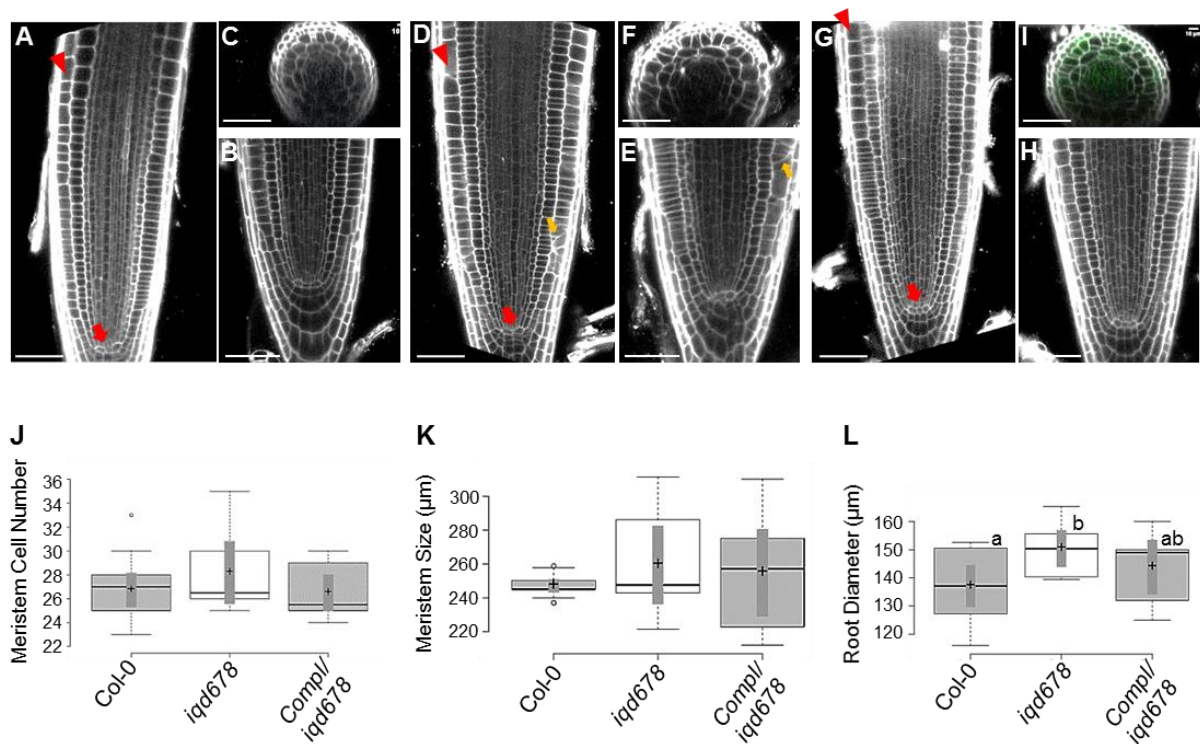


Figure 2.4 Effect of *iqd678* mutations on root morphology.

(A-H) Longitudinal view of 7-day-old *Arabidopsis* root meristem showing single-cell files of different cell types and the QC. Single optical sections were used for analyzing cell number, meristem size and root diameter (A, D, G) and the arrangement of cell layers in the root tissue of WT (B), *iqd678* (E) and *Compl/iqd678* (H). The transverse optical sections of root meristems were used as a visual representation of root diameter (C, F, I). Red arrowheads indicate the start of the transition zone, where the meristematic zone ends. Red arrows indicate the position of the QC, and yellow arrows indicate the extra epidermal cell layer in *iqd678* triple mutants. Cell walls were visualized using PI staining. Scale bars, 50 μm. (J-L) Quantification of measured values for root meristem size, meristem cell number and root diameter. Data obtained from the analysis using ImageJ was exported in MS Excel to create boxplots using BoxplotR. Box limits indicate the 25th to 75th percentiles, center lines represent the medians, crosses indicate the mean points and dots represent outliers. Whiskers extend 1.5 times the IQR from the 25th and 75th percentiles. Individual letters denote statistically significant differences calculated by one-way ANOVA and post hoc HSD ($p < 0.05$). More than 8 independent seedlings per genotype were used in all analyses. IQR, Interquartile range.

Following the observations, our next obvious question was whether cell wall positioning defect in *iqd678* causes any secondary effect on root morphology. For this, we analyzed meristem size, cell number and root diameter in the *iqd678* triple mutants in comparison to WT roots of 7-day-old seedlings grown under long-day conditions. Single epidermal cell layers of median longitudinal section of root were used for all analyses. The region from the QC up to the first cell of the transition zone (TZ) in the epidermis was used to analyze cell number and meristem size. The orientation of cell division planes determines the direction in which new cells will form. Often the mutations affecting the orientation of cell division causes an increase in cell numbers (Zhang et al., 2016). In contrast, the increase in cell number was

not significant in the *iqd678* triple mutants compared to the WT and complementation line (Figure 2.4A, D,G,J). This showed that cell division in general was not affected in *iqd678* triple mutants compared to WT. Consistently, meristem size along the proximodistal axis of the *iqd678* triple mutant roots was comparable to that of WT (Figure 2.4K), indicating general root growth is not affected in the mutant. However *iqd678* mutations lead to additional epidermal layers through extra periclinal division in the root epidermal layer (Figure 2.4D, E), such as alteration in normal pattern of division correlated with wider roots in *iqd678* triple mutants. A fixed distance (180 μm) from quiescent center (QC), in root meristem, was used to measure the root width of all genotypes (Figure 2.4A, D, G). Lateral root cap cells were excluded from the measurements. Optical transverse-sections of roots is used to visualize the root width in Col-0 (Figure 2.4C), *iqd678* (Figure 2.4F) and complementation lines (Figure 2.4I). Data analysis showed significant widening of root diameter in triple mutant compared to WT. The defect was partially complemented to WT level in the complementation line (Figure 2.4L). In addition, we did not observe any obvious defects in the concentric organization of root tissue, as well as organization of stem cell niche (Figure 2.4B, E, and H). This indicates the ability of the mutant to give rise different tissue types as the WT roots. Thus, our data indicates that IQDs play a role in symmetrical division plane control in the Arabidopsis root epidermis.

To test whether the loss of *IQD6*, *IQD7*, and *IQD8* affects plant growth, we initiated the systematic phenotyping, in which we monitored growth macroscopically throughout the entire life cycle of Arabidopsis. Seedling morphology and root length were comparable between *iqd6-1*, *iqd7-1*, and *iqd8-1* single, double and triple mutants, the complementation line and wild type (Figure 2.5A, D). In some cases, we observed a moderate reduction in root length in *iqd68* double and *iqd678* triple mutants, but quantification data did not show any statistical differences when compared to WT. Our observation is in accordance with other milder mutants such as *phgap12*, and *tancsh*, where mispositioning of cell wall does not cause any noticeable effects on root growth (Stöckle et al., 2016; Walker et al., 2007). Similarly, plant growth and rosette leaf area did not differ significantly between *iqd* mutants and the wild type (Figure 2.5B, E), and overall plant morphology was comparable at later stages of development, when flowers and siliques were fully developed (Figure 2.5C).

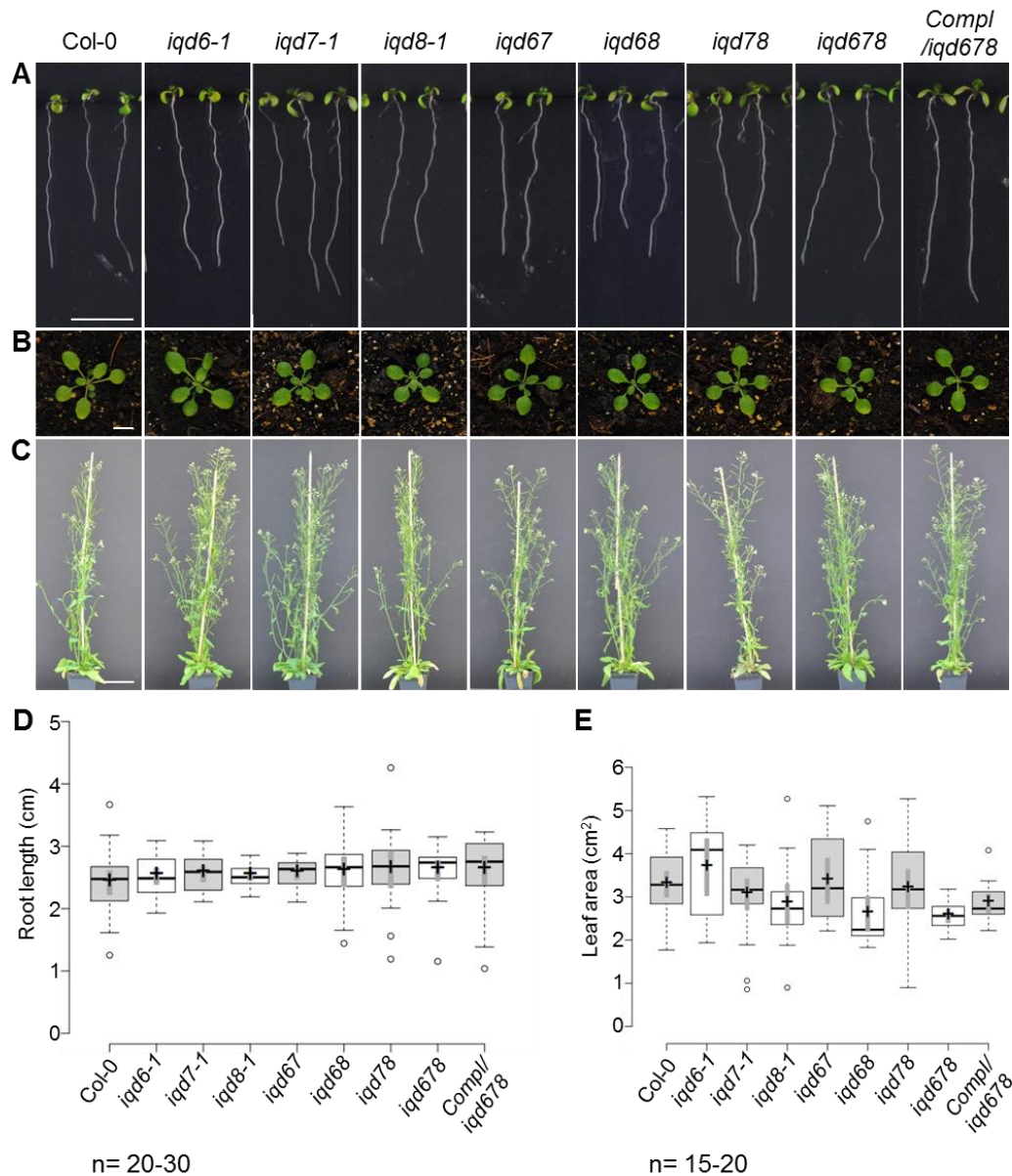


Figure 2.5 Growth phenotypes throughout development.

Morphology of 7-8-day-old *in vitro* grown seedlings (A), 18-day-old rosette leaves (B) and 49-day-old mature plants (C) of Col-0 and combination of *iqd6-1*, *iqd7-1* and *iqd8-1* mutants. Scale bars, 1 cm. (A, B) and 5 cm (C). (D, E) Root lengths and leaf areas were determined by using ImageJ. Data obtained from the analysis was exported in MS Excel to create boxplots using BoxplotR. Box limits indicate the 25th to 75th percentiles, center lines represent the medians, crosses indicate the mean points and dots represent outliers. Whiskers extend 1.5 times the IQR from the 25th and 75th percentiles. The statistically significant differences were calculated by one-way ANOVA and Tukey post hoc HSD ($p < 0.05$). (n)= number of analyzed roots (D) and number of analyzed plants (E). All experiments were repeated twice and results were consistent. IQR, Interquartile range.

However, we noticed appreciable difference in the silique morphology of mutants compared to WT (Figure 2.6). Slightly pale colored and mature siliques were used for quantification of silique phenotypes (silique area and length). Silique area was comparable between *iqd678* triple mutants and WT (data not shown). However, silique length was noticeably different in

iqd678 triple mutants compared to WT (Figure 2.6A, B, D). Mutant plants showed comparatively wider and shorter siliques compared to the WT. The phenotype was reverted to WT in the complementation line (Figure 2.6C, D). In conclusion, we did not notice any major developmental defects in single as well as higher-order mutants of *iqd6-1*, *iqd7-1* and *iqd8-1*. Our analysis revealed that loss of IQDs did not affect vegetative growth.

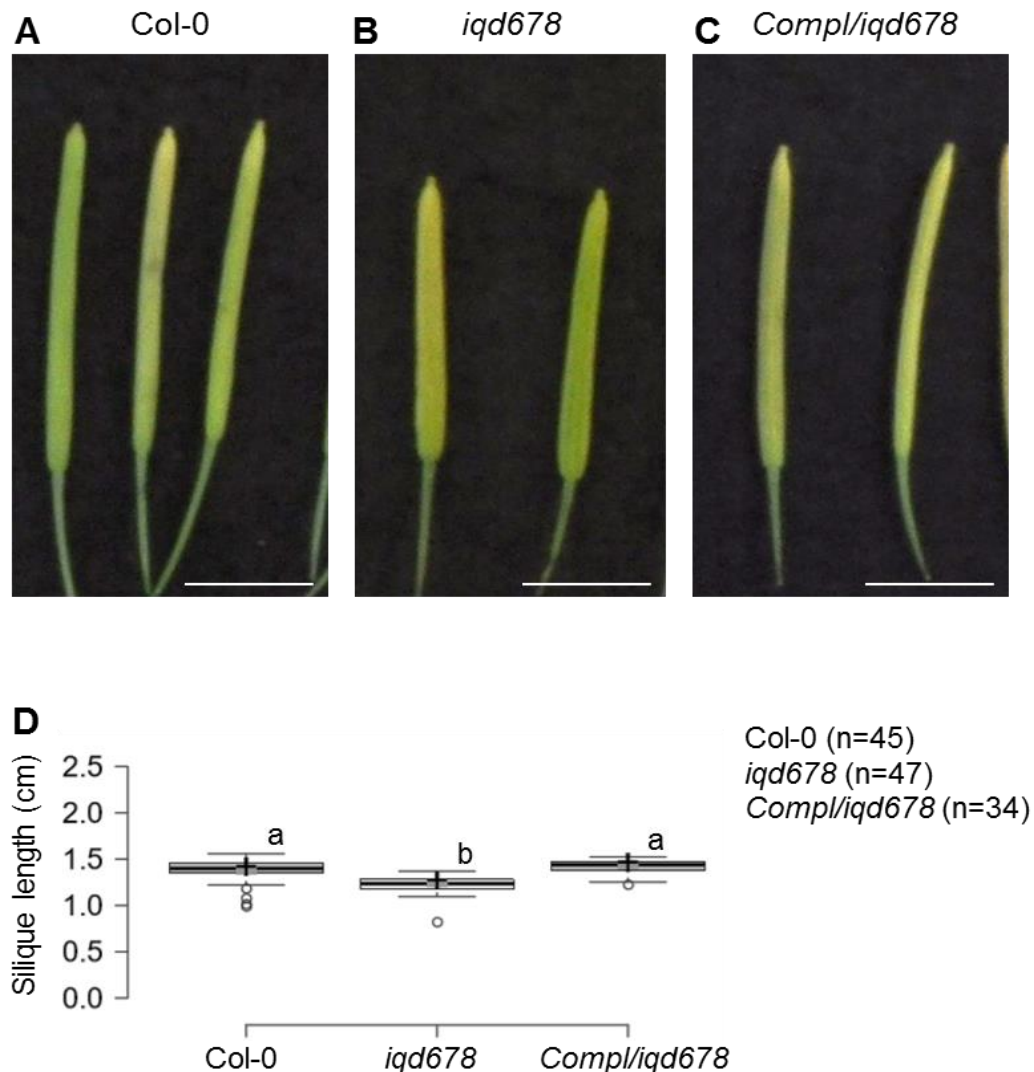


Figure 2.6 Comparison of silique phenotype.

Comparative analysis of silique morphology of WT (A), *iqd678* (B) and *Compl/iqd678* (C). Scale bars, 0.5 cm. (D) Quantitative analysis of silique length. Polygon tool of ImageJ was used to measure silique length. Box plots were generated using BoxPlotR. Statistically significant differences denoted by different letters, and were determined between different genotypes using one-way ANOVA and Tukey post hoc HSD ($p < 0.05$). Box limits indicate the 25th to 75th percentiles, center lines represent the medians, crosses indicate the mean points and dots represent outliers. Whiskers extend 1.5 times the IQR from the 25th and 75th percentiles. (n) = number of siliques measured per genotype. Siliques used for the quantification were collected from more than 5 independent plants (49-day-old). IQR, Interquartile range.

Our result so far suggested the possibility of different mechanisms of spatial control of cytokinesis in different tissues. The phenotypic resemblance of *iqd678* triple mutants to cytokinetic mutants, such as *pok12* and *phgap12* double mutants (Buschmann and Lloyd, 2008; Müller et al., 2006; Stöckle et al., 2016; Walker et al., 2007; Xu et al., 2008) prompted us to investigate the requirement of IQD6, IQD7 and IQD8 during cytokinesis.

2.2.2 Subcellular localization of IQD8 and related proteins during cell division and their expression domains

To understand the molecular mechanisms underlying the *iqd678* phenotype, we analyzed subcellular localization of IQD8. Promoter-GFP-GUS analysis performed previously in our group showed that *IQD8* is expressed in dividing cells (unpublished; Figure 2.7A, B). As a means to determine whether IQD8 acts cell-autonomously, we compared *pIQD8:GFP-GUS* expression domain with IQD8-GFP protein expression domain in transgenic *pIQD8:IQD8-GFP/iqd678* lines. Our analysis revealed that promoter activity and protein abundance is in the same tissue layers (Figure 2.7B, C). This suggests that IQD8 acts cell-autonomously.

To study the localization of IQD8 at subcellular resolution, we used transgenic Arabidopsis lines co-expressing IQD8-GFP with the microtubule marker RFP-MBD (Lipka et al., 2014). In prophase cells, IQD8 decorated microtubules of the PPB (Figure 2.7D) and remained localized with CDZ/CDS throughout mitosis until the completion of cell division. (Figure 2.7E, F; Figure S 3A, B). Unlike other CDZ resident proteins, IQD8-GFP signals did not further narrow down at CDZ as the cell progress through mitosis. Broader labeling of IQD8-GFP at the CDZ might set the platform for assembly of signaling modules such as Ca²⁺ signaling, in addition to its role as CDZ marker protein in the cell division. In cytokinetic cells, IQD8-GFP localized along the entire length of phragmoplast microtubule (Figure 2.7F) and remained associated throughout the radial phragmoplast expansion and ultimately merged to the division site. Uniform labeling of IQD8-GFP at the phragmoplast microtubules suggests its potential role in phragmoplast stability. IQD8-GFP signals also labeled emanating microtubules of radially expanding phragmoplast (Figure S 3C). Exploratory microtubules of radially expanding phragmoplast are assumed to contribute to the phragmoplast-guidance towards division site. Localization of IQD8 to the exploratory microtubules of phragmoplast may suggest the potential function of IQD8 in the guidance of the phragmoplast towards the CDS. Besides this, we also observed IQD8-GFP at the cell plate (membrane structure) (Figure 2.7F, G; Figure S 3A).

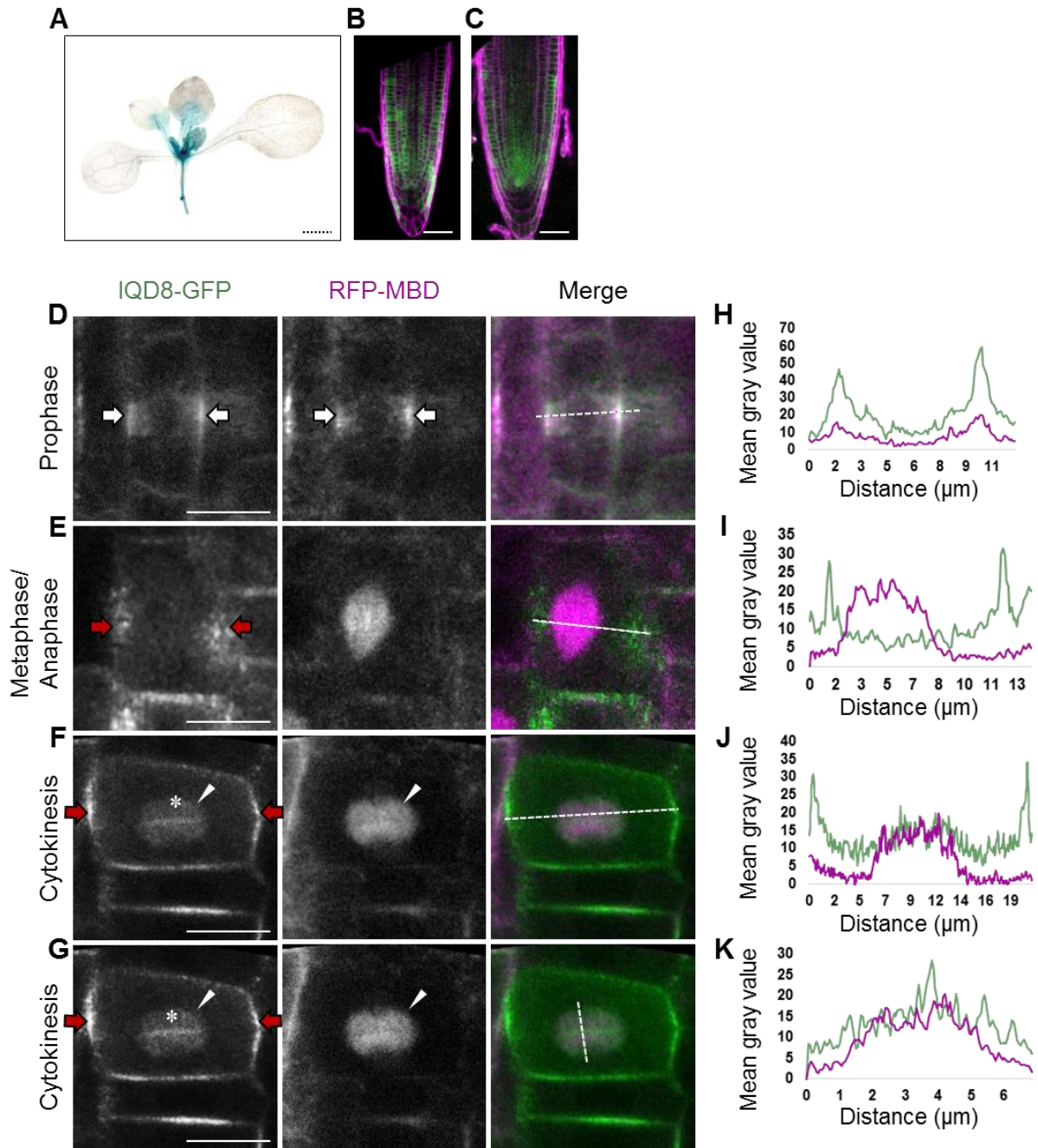


Figure 2.7 Subcellular localization of IQD8 and related proteins during cell division.

(A-B) Plants expressing *pIQD8:GFP-GUS* reporter, showing GUS staining indicative of GUS reporter expression in shoot tips (A), and GFP fluorescence in root tips (B) of 4-day-old seedlings. (C-G) show localization of IQD8-GFP in *pIQD8:IQD8-GFP/iqd678* lines. Localization of IQD8-GFP in overview of a root tip (C) and in single-cell resolution at the PPB (white arrows) in prophase cell (D), at cortical division zone (red arrows) in metaphase/anaphase cell (E), at phragmoplast (white arrowheads), CDZ/CDS (red arrows) and cell plate (asterisk) during cytokinesis (F, G). Scale bars, 0.5 mm (A), 50 μm (B, C) and 10 μm (D-G). Left column shows GFP signals, center column represents RFP signals and right column shows merged signals. RFP-MBD was used to visualize microtubules. (H-K) Plot profiles showing co-localization of RFP-MBD and IQD8-GFP signal distribution along the dashed line shown in the merge channel. The confocal images and plot profile are representative of 8-10 roots and experiments were repeated at least three times.

Localization of IQD8 to the microtubules of PPB and phragmoplast are also confirmed by fluorescence intensity plot profile along a line drawn over the merged and composite image using ImageJ (Figure 2.7H, J). Similar distribution patterns of GFP and RFP signals indicated co-localization of IQD8-GFP with RFP-MBD-labeled microtubules of PPB and phragmoplast. In addition, GFP signals showed maximum peaks at CDZ and cell plate, which further confirm localization of IQD8 at CDZ and cell plate (Figure 2.7I, J, K). In metaphase/anaphase, IQD8-GFP decorated the CDZ and was only rarely dispersed on spindle microtubules (Figure 2.7E).

Consistently, fluorescence intensity plot profile showed the intensity peak of GFP signal at the CDZ, and absence of intensity peak from the spindle, which is in contrast to RFP signal distribution that showed the signal maxima only at the spindle microtubule (Figure 2.7I). Fluorescence intensity patterns further suggested that in metaphase, IQD8-GFP is mainly present at the CDZ and largely absent from spindle microtubules. Upon proceeding to telophase, IQD8-GFP progressively associated with phragmoplast microtubules and the cell plates, and additionally remained at CDZ. Absence of IQD8-GFP signal from spindle microtubules and its progressive reappearance at microtubules of the spindle suggested the involvement of distinct mechanisms in directing IQD8 at PPB microtubules and phragmoplast microtubules.

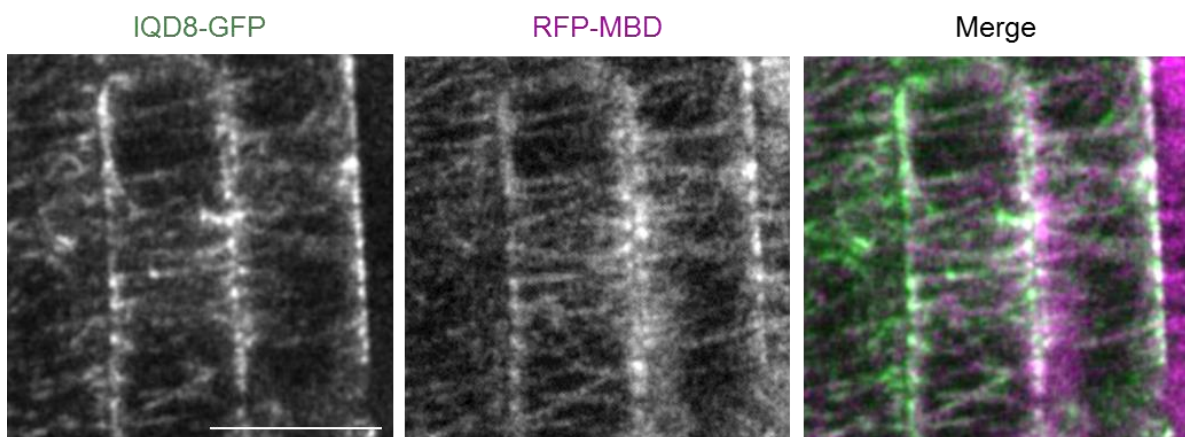


Figure 2.8 Localization of IQD8 during interphase.

Single-cell resolution of 7-day-old Arabidopsis root tip cells showing IQD8-GFP signal at interphase microtubules. RFP-MBD was used as a microtubule marker. Left, center and right image showing GFP, RFP and merge signals, respectively. The merged image shows co-localization of IQD8-GFP signal and RFP-MBD signal. The images are representative of 8-10 seedlings from at least three independent experiments. Scale bar, 50 μm .

In addition, an entirely different mechanism could be involved in IQD8 localization at the cell plate and CDZ/CDS. These results suggest the existence of a regulatory mechanism underlying cell stage-specific accumulation of IQD8. Due to variance in the localization

pattern of IQD8, we quantified distinct localization patterns of IQD8 during cell division. Quantification was done using data from 15-20 roots from cell imaging (Table 2-1). As per our data, 100% of cells at the prophase stage of cell division, showed localization of IQD8-GFP to the microtubules of PPB and in 81% of cells IQD8-GFP decorated the perinuclear microtubules. During metaphase/anaphase, only 39% of cells showed IQD8-GFP signal to microtubules of spindles; in contrast, a larger percentage of cells (93%) showed IQD8-GFP signal at CDZ. In most cases, IQD8-GFP showed very weak labeling of spindle microtubules. In cytokinetic cells, 95.2%, 92% and 86% of cells, showed IQD8-GFP signals to the phragmoplast microtubules, at the cell plate and at the CDZ/CDS, respectively. In conclusion, IQD8 mainly localized to the microtubules of PPB and phragmoplast as well as membrane-based structure, CDZ/CDS and cell plate.

Besides, IQD8 presence during mitotic stage of cell division, IQD8-GFP also localized with cortical microtubules in interphase cells, indicated by co-localization with RFP-MBD. (Figure 2.8). Localization of IQD8 during cell division was also confirmed via immunolocalization studies using GFP and tubulin specific antibodies (Figure S 5). Immunolocalization was performed to confirm the subcellular localization of IQD8 by an independent experimental approach as well as to rule out an effect of the microtubule marker on the localization pattern of IQD8.

Table 2-1 Subcellular distribution of IQD8-GFP

Differential subcellular localization of IQD8-GFP fusion protein scored during cell division. RFP-MBD was used to visualize different cell division stages. Experiments were repeated twice.

	IQD8-GFP/RFP-MBD full-length (n=15-20 roots)						
	Prophase (n=46 cells)		Meta-/Anaphase (n=41 cells)		Cytokinesis (n=63 cells)		
	PPB	Perinuclear microtubule	Spindle	CDZ	Phragmoplast	Cell Plate	CDZ
IQD8-GFP	(n=46 cells)100%	(n=9 cells)81%	(n=16 cells)44%	(n= 38 cells)93%	(n=60 cells)95.2%	(n=57 cells)92%	(n=54 cells)86%
RFP-MBD	(n=46 cells)100%	(n=11 cells)100%	(n=41 cells)100%	0%	(n=63 cells)100%	0%	0%

Because phenotypic analysis of *iqd678* triple mutants indicated partially redundant or additive roles of IQD6, IQD7 and IQD8, we aimed at monitoring their subcellular localization during cell division. For this purpose, we cloned the translational fusion of IQD6 and IQD7 with a C-terminal GFP tag under the control of their endogenous promoter and generated stable transgenic Arabidopsis lines. Comparison of the expression domain of *pIQD6:GFP-GUS* reporter (Figure S 8) and *pIQD6:IQD6-GFP/iqd6-1* lines (Figure 2.9A) showed the IQD6

promoter activity in the same tissues where the IQD6-GFP fusion protein was detected. This suggests a cell-autonomous function of IQD6 similar to IQD8. Reminiscent of IQD8, IQD6 also decorated microtubules of PPB and phragmoplast as well as localized on the cell plate (Figure 2.9B, C; Figure S 6). However, unlike IQD8, IQD6 either showed very weak appearance at CDZ or was absent in most of the cases. Promoter expression patterns and localization of IQD6 and IQD8 during cell cycle suggest potential redundancy in their functions. Information about IQD7 localization is missing because of failure to detect IQD7-GFP signals (data not shown). However, the same construct which was used for stable transformation, when expressed transiently, showed accumulation of IQD7-GFP signals sparsely at microtubules (Figure S 7A,B), which may suggest its microtubule-based functions.

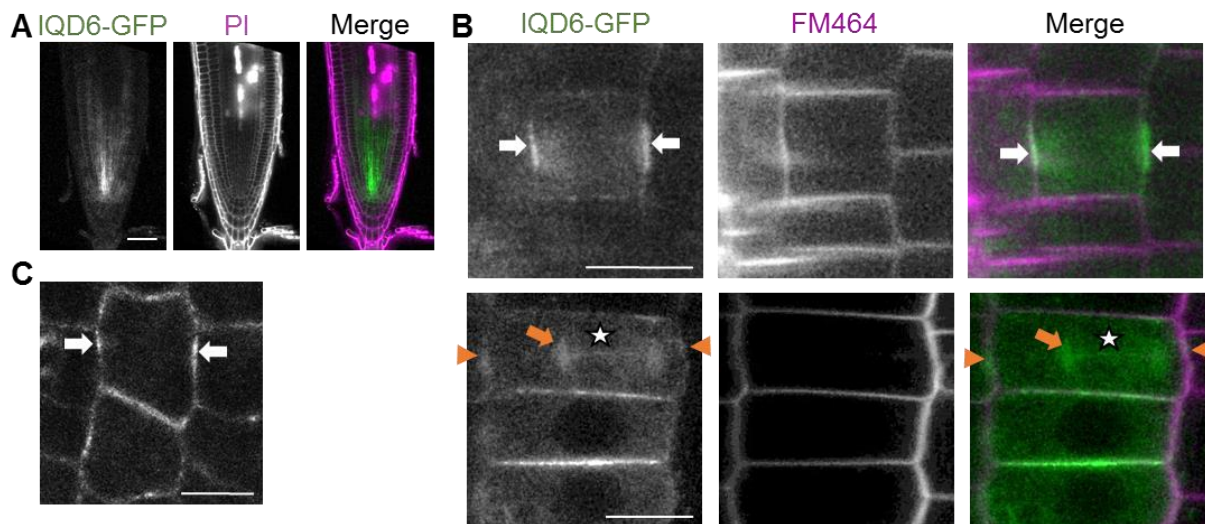


Figure 2.9. Localization of IQD6 in dividing tissues.

(A) Longitudinal median section of 7-day-old Arabidopsis root tip cells showing overview for the expression of IQD6-GFP under the control of its endogenous promoter and in the *iqd6-1* mutant background. (B) Single-cell resolution displaying IQD6-GFP signal at PPB (white arrows), CDZ/CDS (brown arrowheads), phragmoplast (brown arrows) and cell plate (asterisks). (C) Shoot apical meristem cells showing IQD6-GFP signal at PPB (white arrows). PI and FM464 were used to stain cell wall (A) and plasma membrane (B, C), respectively. Images are representative of 6-10 seedlings from at least three independent experiments. Scale bars, 50 μ m (A), 10 μ m (B, C).

Analysis of promoter-GFP-GUS expressions revealed that *IQD6*, *IQD7* and *IQD8* are expressed in dividing tissues of the shoot apical meristem and root meristem. In the root meristem, the *IQD8* promoter showed wider expression patterns compared to those of the *IQD6* and *IQD7* promoters (Figure S 8). Within the root meristem, *IQD8* showed patchy expression patterns reminiscent of cell cycle-related genes throughout the root tissue which was strongest in the epidermis. In contrast, *IQD6* and *IQD7* promoters showed strongest activity in the inner root tissue layers (Figure S 8). Thus, expression patterns of *IQD6*, *IQD7*

and *IQD8* promoters overlapped partially, which further point to the partial redundancy in their functions. In addition, *IQD6*, *IQD7*, and *IQD8* also showed some unique expression patterns, potentially reflecting tissue-specific functions. Data from our phenotypic analysis as well as broader localization pattern of *IQD8* throughout out the cell-cycle, suggest its prominent role towards the phenotype.

In conclusion, our results revealed dual localization of *IQD8*-GFP at membranes (division site, cell plate) as well as at PPB and phragmoplast. We thus presumed that *IQD8* at the plasma membrane plays a role in maintenance and organization of the division site, and when present at the phragmoplast, stabilizes phragmoplast microtubule and subsequently direct its expansion towards the division site.

2.2.3 Impairment in *IQD8* function leads to defects in microtubule array orientation and formation

To test whether loss of *IQD6*, *IQD7* and *IQD8* affect microtubule functions during cell division, we investigated microtubule patterns in 7-day-old Arabidopsis seedlings of *iqd8-1* single and *iqd678* triple mutants compared to WT via live-cell imaging (Figure 2.10). To avoid any artefacts of microtubule marker proteins on the general organization of microtubules as well as to study the microtubule array organization via the second independent system, we additionally performed tubulin immunolabeling in *iqd8-1* single, *iqd678* triple mutants and compared to WT and *pIQD8:IQD8-GFP/iqd678* line (Figure 2.11). Due to unavailability of microtubule marker in *pIQD8:IQD8-GFP/iqd678*, we only used data from tubulin immunolabeling to quantify microtubule pattern in the *iqd* mutant lines compared to WT and complementation line (Figure 2.12).

WT cells showed a concentric ring of PPB microtubules at the cellular periphery and appeared as the bright foci on the lateral wall of cells in median longitudinal sections (Figure 2.10A, Figure 2.11A). Except for a few cases, nearly 82% of the analyzed WT cells in prophase stage of cell division showed a normal arrangement of PPB microtubules (Figure 2.12A). In contrast, around 48% of *iqd678* triple mutant cells showed pronounced accumulation of microtubules around the nuclear periphery and a loss of PPB formation (Figure 2.10A, Figure 2.11B, Figure 2.12A). In *iqd8-1* single mutants, approximately 11% of the analyzed cells were impaired in the PPB formation (Figure 2.10A, Figure 2.12A). Even if PPB was present in other cases of *iqd678* triple mutants, they either showed abnormal accumulation with sparse, unequal microtubule at the cortex or showed tilted orientation (Figure 2.10A, Figure 2.11B). We also quantified the percentage of cells with tilted orientation.

The degree of rotation was categorized into three groups; namely, 0° - 5° , $>5^{\circ}$ ≤ 15° and greater than 15° . The orientation of 0° - 5° was considered as the ideal orientation of PPB. 96% of analyzed prophase cells in WT showed ideal transverse orientation of PPB (Figure 2.12B). In contrast, the percentage of cells in ideal orientation was reduced to 62% and 73% of the analyzed cells in *iqd678* triple and *iqd8-1* single mutants, respectively (Figure 2.12B).

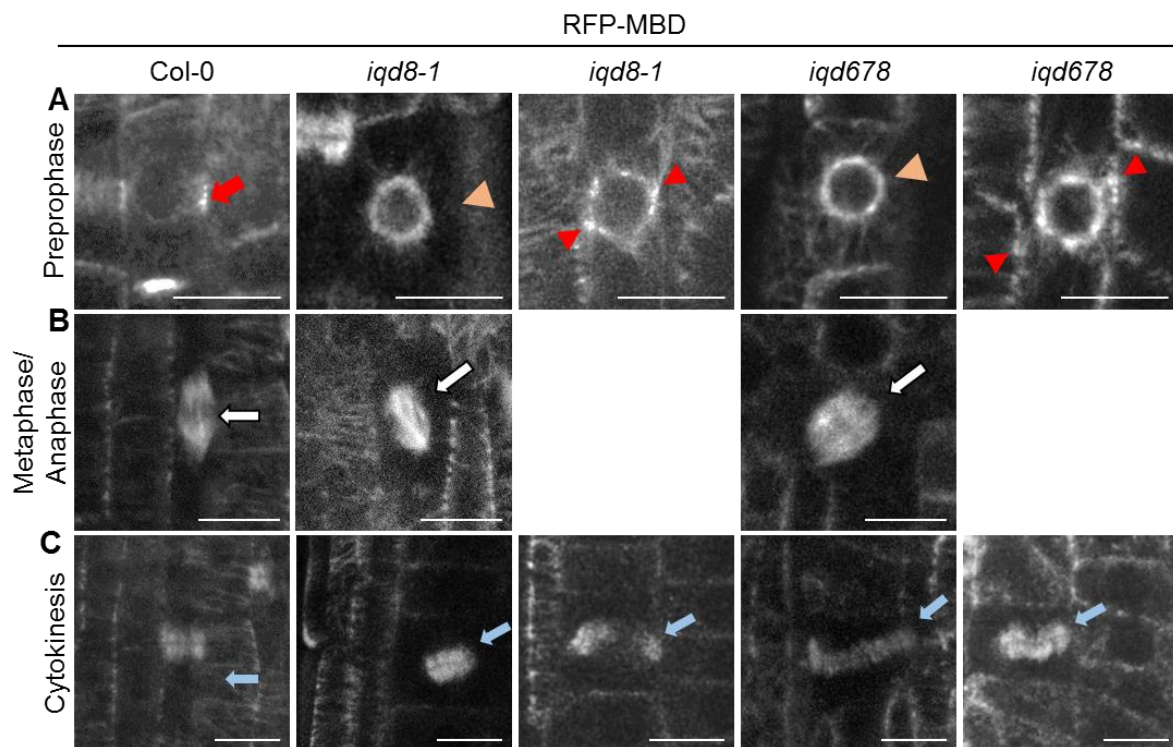


Figure 2.10 Microtubule pattern analysis.

Analysis of microtubule arrays labeled with RFP-MBD in 7-day-old seedlings of *iqd8-1* single, *iqd678* triple mutants and Col-0. Microtubules organization during preprophase (A), metaphase/anaphase (B), and cytokinesis (C) stages of cell division in *iqd8-1* single (second and third columns) and *iqd678* triple mutants (fourth and fifth columns) compared to the Col-0 (first column). Red arrow indicates the position of PPB, red arrowheads indicate PPB orientation, brown arrowheads depict the PPB loss. White and blue arrows indicate the orientation of spindle and phragmoplast, respectively. The images are representative of 8-10 seedlings from at least three independent experiments. Scale bars, 10 μ m.

The PPB defects were considerably complemented by introgression of *pIQD8:IQD8-GFP* into the *iqd678* triple mutant background (Figure 2.11D, Figure 2.12A, B). Our data showed that PPB defects in *iqd678* triple mutants are more severe compared to *iqd8-1* single mutant and WT (Figure 2.12A, B). Although milder, the presence of phenotype in *iqd8-1* single mutant itself as well as phenotypic reversion in the complementation line point to the role of IQD8 primarily in positioning and formation of PPB microtubules for regulating the spatial control of cytokinesis. The loss of PPBs in *iqd678* triple mutants is analogous to previously characterized cell division mutants like *ton1*, *fass/ton2*, *pp2a*, *trm678* (Azimzadeh et al.,

2008; Camilleri et al., 2002; Schaefer et al., 2017; Zhang et al., 2016). These factors are known for their roles in PPB organization and formation, mutation in any of these factors results in severe loss of PPB. In addition, misorientation of PPBs in *iqd678* triple mutants closely resemble the PPB orientation defect of *phgap12* double mutants. Proper PPB formation and its orientation in these mutants influence orientation of spindle and concomitantly, phragmoplast positioning for timely progression of mitosis (Ambrose and Cyr, 2008; Chan et al., 2005). This prompted us to further analyze microtubule organization in later division structures, the spindle and cytokinetic phragmoplast.

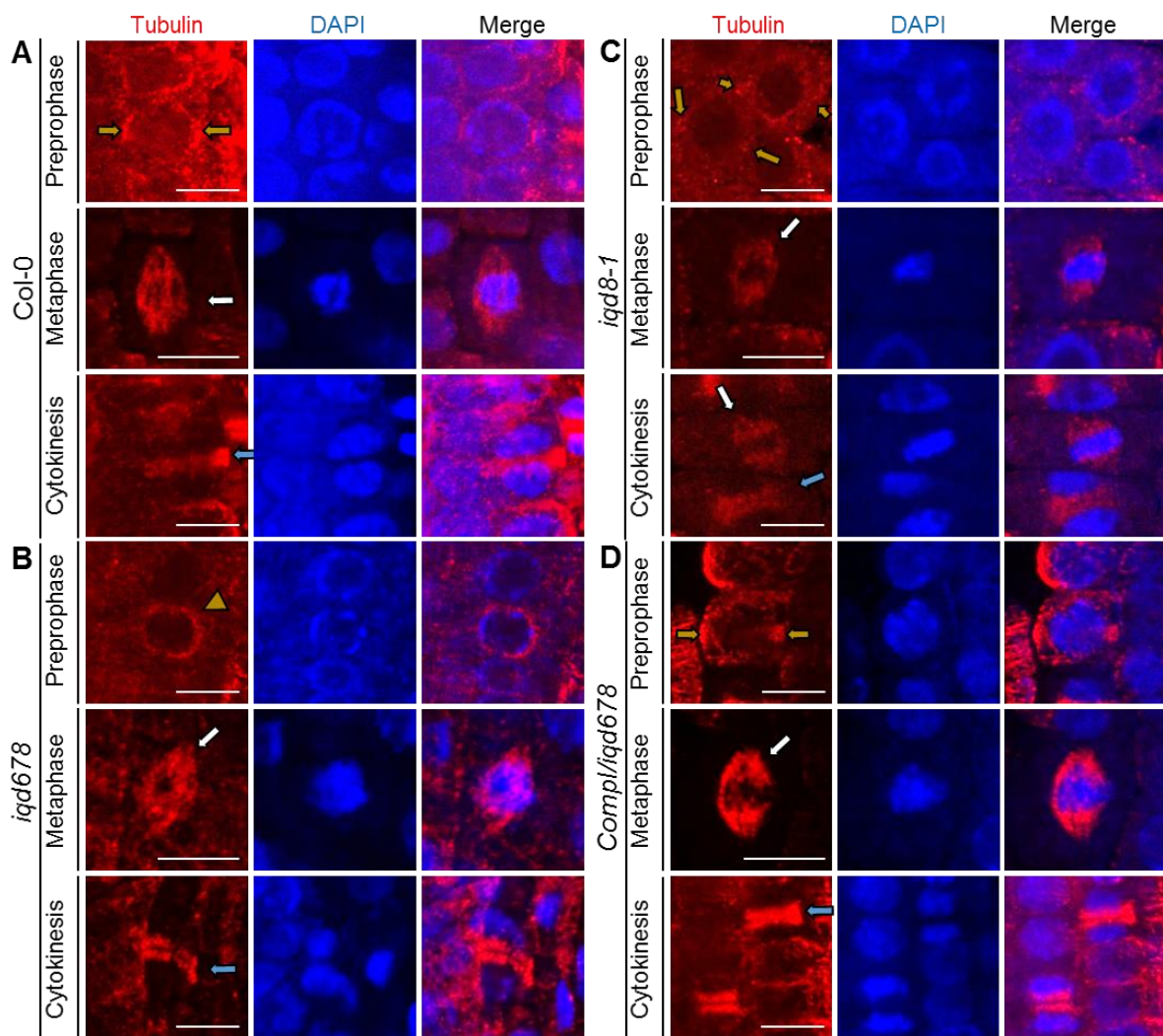


Figure 2.11 Immunolabeling showing microtubule patterns in *iqd678* and *iqd8-1* mutants compared to WT and complementation line.

Single-cell resolution of 7-day-old seedlings showing coimmunolocalization using tubulin-specific antibody. Nuclei were counterstained with 4', 6-diamidino-2-phenylindole (DAPI). Immunolabeling of tubulin was used to visualize microtubules in Col-0 (A), *iqd8-1* (B) *iqd678* (C) and *pIQD8:IQD8-GFP/iqd678* complementation line (D). Images are single optical sections of Z-stacks images and represent results of at least two independent experiments. Arrows indicate the orientation of PPBs (yellow arrows), the position of spindles (white arrows) and position of phragmoplast (blue arrows). Arrowheads depict the loss of PPB. Scale bars, 50 μ m.

In general, organization of microtubules appeared to be normal in *iqd678* triple mutants with occasional disturbance of spindle microtubule assembly. In *iqd678*, spindle microtubule occasionally appeared to be disorganized and collapsed. In very few cases, similar events also happened in WT but were more pronounced in *iqd678* triple mutant (data not shown). This suggests a potential role of IQD8 in bundling and crosslinking or bundling of spindle microtubules. However, this occasional disturbance of spindle reflects the presence of a redundant mechanism of spindle assembly. Unlike the Arabidopsis *tan* mutant, where the similar spindle defect causes a delay in metaphase progression (Martinez et al., 2019), in *iqd678*, metaphase progression appeared to be normal in most of the cases (Figure S 9). In most cases, spindle organization in *iqd678* triple mutant was comparable to that of the WT, which is in turn reflected in normal metaphase progression in the *iqd678* triple mutants.

During metaphase, the most obvious difference that we observed in the *iqd678* and *iqd8-1* mutants was the positioning of spindles (Figure 2.10B, Figure 2.11B, C). Approximately 44% and 16% of cells in *iqd678* triple and *iqd8-1* single mutants, respectively, showed oblique orientation of spindles (Figure 2.12C). In contrast, 90% of the WT spindles, oriented in transverse orientation of 0° - 5° (Figure 2.12C). However, around 3% of WT spindle also showed tilted orientations, which is consistent with results reported in the literature. Altogether the data suggest that spindles misorientation in *iqd678* triple and *iqd8-1* single mutants are likely caused by defects in the formation and orientation of PPBs. A similar defect in spindle rotation has been observed in Arabidopsis mutants lacking TRM6-8, EB1C, AKT1 or AKT5 (Ambrose and Cyr, 2008, 2007; Komaki et al., 2010; Marcus et al., 2005). Besides spindle defects in all these cytokinetic mutants, some produce severe defects in cell wall positioning while others have no apparent defects. The spindle rotation is a normal event that has also been reported in WT cells, which is corrected to the right plane during phragmoplast formation and orientation. However, the significant degree of orientation may not be corrected back to normal orientation during phragmoplast stage (reviewed in Rasmussen et al., 2013). Similar to cell wall positioning and PPB orientation, angles of spindles orientation were categorized into three different categories (0° - 5° , $>5^{\circ}$ ≤ 15° and $>15^{\circ}$). 0° - 5° rotation of spindle was considered as ideal orientation. Our results showed that the loss of PPB *iqd678* triple mutants leads to a major defect in the spindle orientation which potentially causes aberrant phragmoplast orientation.

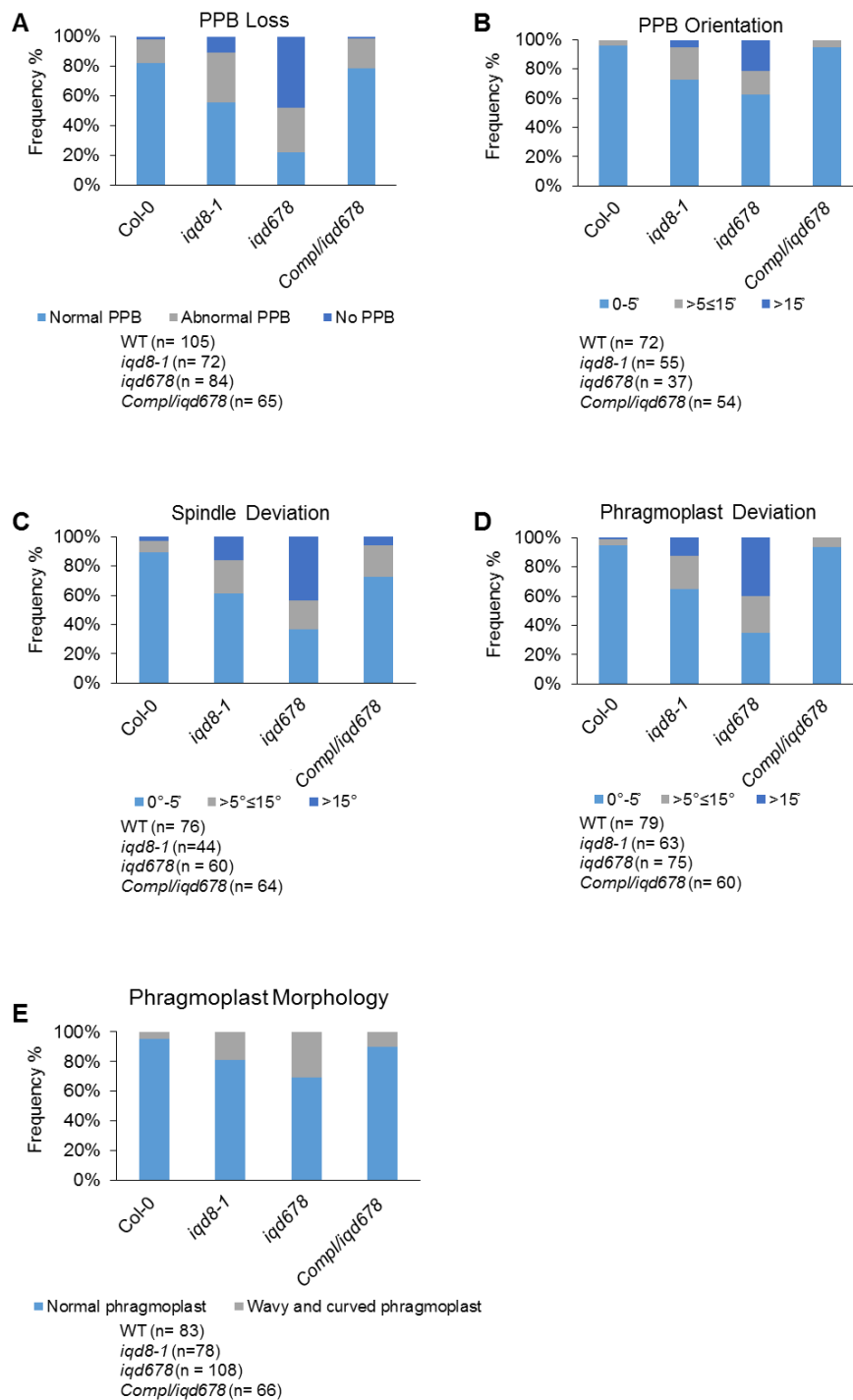


Figure 2.12 Quantification of microtubule patterns.

Frequency distribution of microtubule orientation and organization in *iqd8-1* single and *iqd678* triple mutants compared to the WT and complementation line. Percentage frequency of cells showing loss of PPB (A), misorientation of PPBs (B), misorientation of spindles (C), misorientation of phragmoplasts (D) and altered phragmoplasts morphology (E) in respective genotypes. (n)= total number of cells analyzed per genotype. Total of 20-25 roots were used for the analysis. Data is representative of two independent experiments. Different colors represent the frequency of cells showing a specific pattern of microtubules which is indicated below each image.

Corroborated with the altered orientation of spindle, majority of cytokinetic cells in the *iqd678* triple mutant showed oblique positioning of early and late phragmoplast (Figure 2.10C, Figure 2.11B,C). 12% and 40% of the total analyzed phragmoplasts in the *iqd8-1* single and *iqd678* triple mutants, respectively showed oblique orientation (Figure 2.12D) which was consistent with PPB loss in these mutants. This indicates that the phragmoplasts misorientation in the *iqd* mutants are most likely caused by a loss of phragmoplast guidance resulting from the loss of positional information of the PPB. Beside oblique orientation of phragmoplasts, *iqd678* triple mutants and to some extent *iqd8-1* single mutants also showed profound undulation of the phragmoplast microtubules (Figure 2.10C, Figure 2.11B, C), which is likely due to the lack of stability as well as hampered guidance mechanisms of phragmoplasts. During cytokinesis, we noticed both curved and straight phragmoplast in *iqd678* and *iqd8-1* mutants. However, curved phragmoplasts have never been reported in WT cells. In contrast to WT phragmoplasts, in the *iqd678* triple mutants, 31% of analyzed phragmoplasts were curved (Figure 2.12E). The effect occurred less frequently in *iqd8-1* single mutants (11% of the total phragmoplast), albeit more often than in the WT (Figure 2.12E). The effect of *iqd678* impairment on mitotic microtubule organization raised the question, whether the organization of microtubule during interphase is also affected or not. Our analysis revealed that as in the epidermis of WT, the vast majority of interphase cortical microtubules in *iqd8-1* single and *iqd678* triple mutants, aligned in transverse orientations to the elongation axis of cells (Figure 2.13).

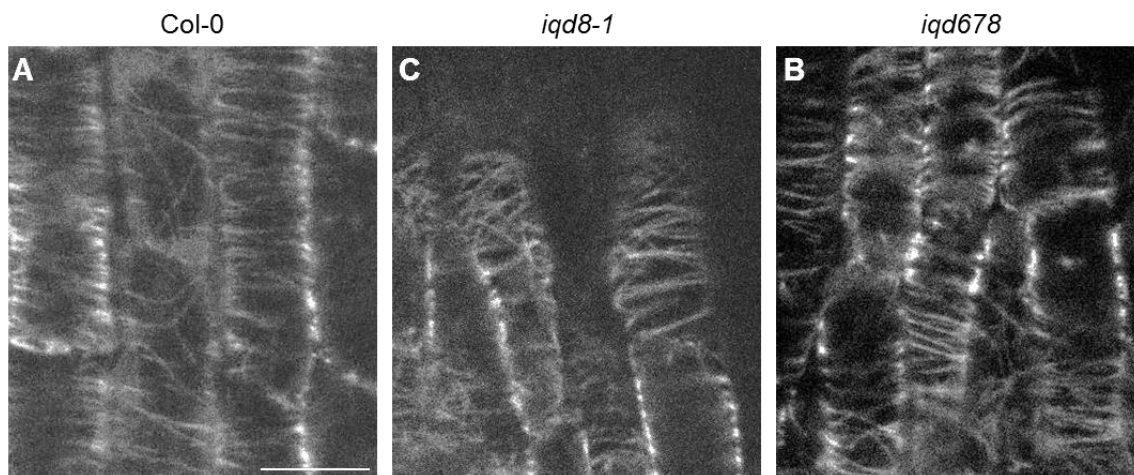


Figure 2.13 Organization of interphasic microtubule arrays in the *iqd8-1*, *iqd678* and Col-0. (A-C) Analysis of interphasic cortical microtubule arrays in root epidermal cells of 7-day-old seedlings. Microtubules are visualized by introducing RFP-MBD marker in Col-0 (A), *iqd8-1* (B) and *iqd678* triple mutants (C). Images are single optical section and represent two independent experiments from 8-10 roots per genotype. Scale bars, 10 μ m.

Our results are similar to reports on other cell division mutants that show loss of PPB without any noticeable effects on the organization of interphasic cortical microtubule arrays (Schaefer et al., 2017; Zhang et al., 2016). Together, these observations suggest that IQD8 is only required for the formation of PPBs but not for the overall organization of interphasic microtubule arrays.

To monitor the duration of cell division pattern in Col-0, and *iqd678* triple mutants, we additionally performed time-lapse microscopy of the RFP-MBD marker in the living root tips of the plants (Figure S 9). We observed the tendency of faster progression from preprophase to metaphase stage of cell division in *iqd678* triple mutant compared to WT. However, we noticed variations in other cases in the *iqd678* triple mutant. Therefore, at this point, any conclusion could not be drawn concerning the effects of mutations in *iqd678* triple mutants on the duration of the cell cycle.

Microtubule pattern analysis revealed that in contrast to PPB loss, all subsequent mitotic microtubule arrays were present in the *iqd8-1* and *iqd678* mutants. Moreover, microtubule pattern analysis of *iqd678* triple and *iqd8-1* single mutants revealed that IQD8 is primarily required for organization and formation and positioning of PPB, and IQD6 and IQD7 additionally facilitate the function. Our result demonstrates multifunction of IQD8, and its impairment leads to a defect during several stages of cell wall positioning, which is consistent with the observed differential localization pattern of IQD8.

2.2.4 IQDs interact with key players of cytokinesis

Because IQDs share hallmarks of scaffold proteins, we hypothesized that their function might involve interactions with additional proteins. We thus tested the interaction of IQD8 with key players of cytokinesis via a targeted interaction screen using a GAL4 based Y2H approach. For this, we selected the candidates such as POKs, PHGAPs, RANGAP, TAN, ROPGEF6, KCBP and MAP65-3. These factors are known to play important roles during spatial control of cytokinesis at the PPB, CDZ/CDS, phragmoplast and cell plate. In addition, we included KINESIN4A (KIN4A), KINESIN13A (K13A) in our assay, KIN4A and K13A are known to play important roles in microtubule related processes, such as transport of cargoes as well as regulating organization and dynamics of microtubules (Zhu and Dixit, 2012) (discussed in detail in chapter 3). Candidate interaction partners were fused to the GAL4 activation domain (AD) and tested for interaction with GAL4 DNA binding domain (DBD) fusions of IQD8 (Figure 2.14, Figure S 11, Figure S 12). Yeast cells transformed with both empty vectors (AD and DBD) were used as the negative control of interactions. Growth of yeast cells on vector selective media was used as a growth control of yeast cells which were transformed with

binary combinations of plasmids (Figure 2.14A). The interaction was analyzed on interaction selective media (Figure 2.14B).

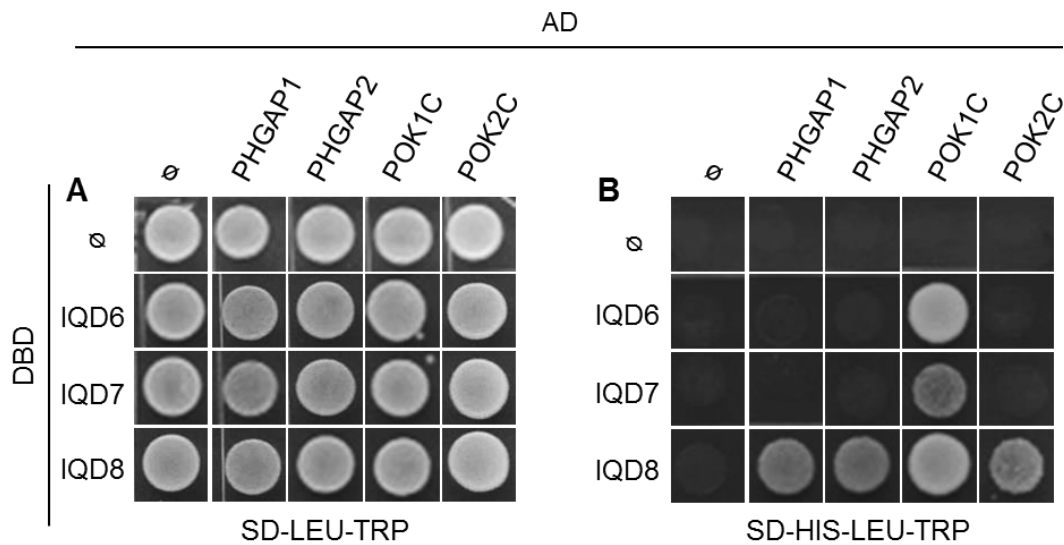


Figure 2.14 Interaction of IQD6-8 with key players of cytokinesis.

Y2H experiment testing for the physical interaction between IQD6, IQD7, and IQD8 and PHGAP1, PHGAP2, POK1C and POK2C. DBD fusion of IQDs and AD fusion POKs, PHGAPs were co-expressed in yeast cells. Growth of yeast colonies on vector selective media (SD-LEU-TRP) (A) and on interaction selective media (SD-LEU-TRP-HIS) (B). Interaction pattern was analyzed 3 days after spotting. Images are representative of at least three independent experiments. SD-LEU-TRP-HIS, yeast media lacking leucine, tryptophan and histidine. POK1C and POK2C indicate C-terminal fragments of POK1 and POK2, respectively.

Our result revealed that IQD6, IQD7 and IQD8 interacted with C-terminal fragment of POK1 (1213-2066). IQD8 additionally interacted with C-terminal fragment of POK2 (2083-2771) (Figure 2.14B). C-terminal POKs fragments were reported to be sufficient for mediating interaction with most of the interaction partners like TAN, RANGAP and PHGAPs (Stöckle et al., 2016; Walker et al., 2007; Xu et al., 2008). POK1 and POK2 are the two closely related kinesins of the kinesin-12 family. POK1 is an early and continuous marker of the division site and required for recruitment as well as maintenance of CDZ resident proteins (Lipka et al., 2014; Walker et al., 2007; Xu et al., 2008). The two PHGAPs (PHGAP1, PHGAP2) interacted exclusively with IQD8 (Figure 2.14B). PHGAPs, a class of putative ROP-GAPs with pleckstrin homology (PH) domains, are reported to act in PPB positioning, and loss of PHGAPs in *phgap12* mutant lines leads to moderate defects in cell wall orientation (Stöckle et al., 2016). PHGAPs interact physically with POKs and are recruited to the division site in a POK-dependent manner (Stöckle et al., 2016). Absence of interaction for the negative control combinations showed specificity of the assays.

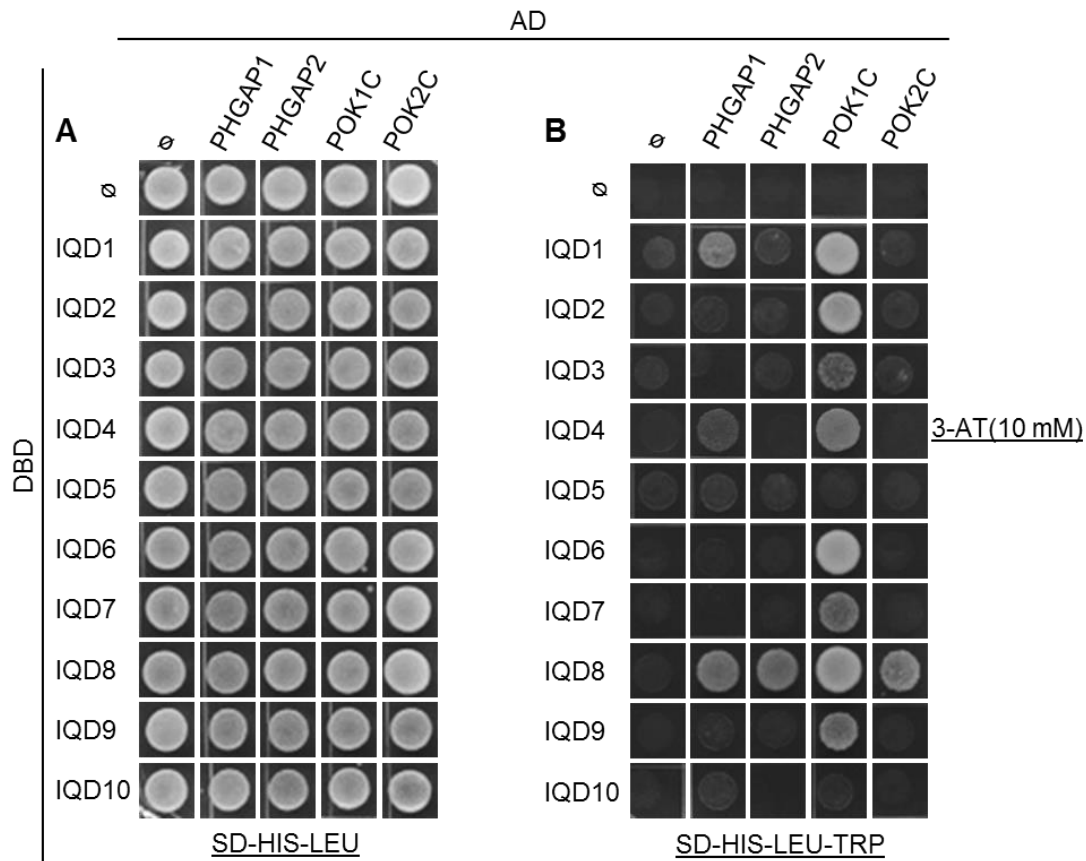


Figure 2.15 POKs and PHGAPs interaction with group III IQDs.

(A-B) Y2H assay showing interaction of IQD1-10 with POKs and PHGAPs. GAL4-DBD and -AD were fused to IQDs and POKs or PHGAPs, respectively. Growth of yeast cells on control plate (SD-LEU-TRP) (A) and on interaction selective media (SD-HIS-LEU-TRP) (B). Yeast cell growth on the latter indicating physical interaction of tested proteins. Interaction pattern was analyzed 3 days after spotting. Images are representative of two independent experiments. SD-HIS-LEU-TRP, yeast media lacking leucine, tryptophan and histidine. 3-AT (3-amino-1-2-4- triazole) was used to prevent autoactivation. POK1C and POK2C indicate C-terminal fragments of POK1 and POK2, respectively.

We extended our analysis to other members of group III IQDs, IQD1-IQD10 (Figure 2.15). Group III IQDs are conserved structurally and functionally (unpublished data). Growth of yeast cells on vector selective media was used as growth control of the experiment (Figure 2.15A), and interaction was analyzed on nutrient deficient SD-HIS-LEU-TRP triple drop out plates (Figure 2.15B). Indeed, POK1C interacted throughout with group III IQDs except for IQD5 and IQD10 (Figure 2.15B). The absence of interaction might be due to the insufficient expression of IQD5 and IQD10 in the yeast system. Also, PHGAP1 interacted with IQD1, IQD8 and showed weak interaction with IQD4 (Figure 2.15B). In addition, as shown in Figure 2.14, PHGAP2 and POK2C interacted exclusively with IQD8 (Figure 2.15B). Interactions of POKs and PHGAPs with IQDs group III suggest a conserved interaction of IQDs-POKs, PHGAPs and possibly indicating a conserved function of IQDs along with POKs and PHGAPs.

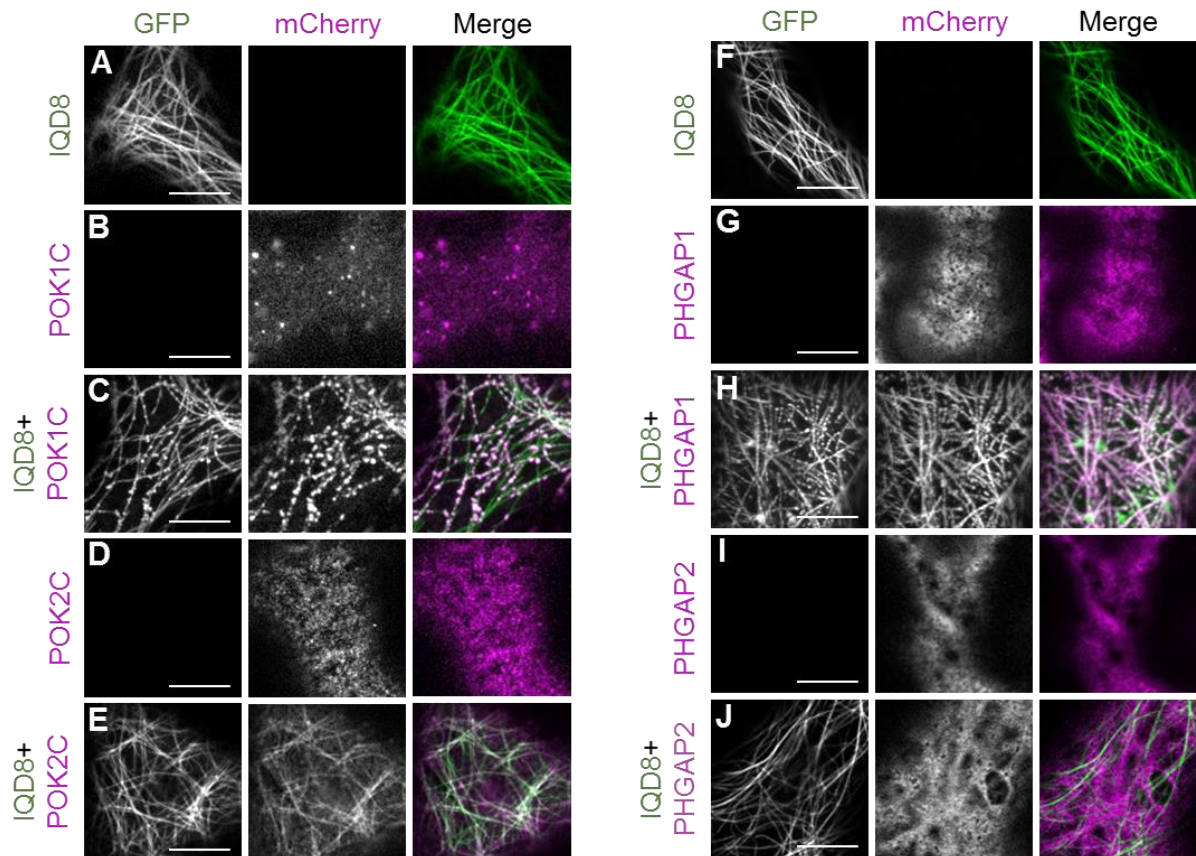


Figure 2.16 Co-expression assay of GFP-IQD8 with mCherry-POKs and mCherry-PHGAPs.

Confocal images of transiently transformed *N. benthamiana* leaf epidermal cells showing single expression of GFP-IQD8 (A), mCherry-POK1 (B), mCherry-POK2 (D) and co-expression of GFP-IQD8 with mCherry-POK1 and mCherry-POK2 C-terminal fragments (C, E, respectively). (F-J) Co-expression of GFP-IQD8 with mCherry-PHGAPs. *N. benthamiana* leaf epidermal cells showing single expression of GFP-IQD8 (F), mCherry-PHGAP1 (G) and mCherry-PHGAP2 (I) and co-expression of GFP-IQD8 with mCherry-PHGAP1 (H) and mCherry-PHGAP2 (J). Left rows show expression of IQD8-GFP, middle rows show expression of mCherry-POKs and mCherry-PHGAPs, and merged channels show co-expression of IQD8-GFP with mCherry-POKs or mCherry-PHGAPs. All constructs were expressed under the control of 35S promoter. Images were acquired 2 days after infiltration. The result represent at least three independent experiments. Images are single optical sections. Scale bars, 10 μ m.

We further extended our analysis *in planta* using transient co-expression assay in *N. benthamiana*. GFP-IQD8 decorated microtubules in *N. benthamiana* interphase cells which is consistent with earlier results of our group (Bürstenbinder et al., 2017) (Figure 2.16A). Similar to localization of POK1 fragments in Arabidopsis protoplast (Lipka et al., 2014), mCherry-POK1C (1213-2066) and POK2C (2083-2771) decorated punctate structures reminiscent of membrane microdomains in *N. benthamiana* interphase cells (Figure 2.16B, D). Upon co-expression of mCherry-POK1C with GFP-IQD8, we observed co-localization of mCherry-POK1C along microtubules (Figure 2.16C), indicating IQD8-mediated recruitment of POK1C from punctate-like structures to linear microtubule strands. Similarly, the patterns of GFP-

IQD8-labeled microtubules also changed when co-expressed with mCherry-POK1C in comparison to the single expression of GFP-IQD8 (Figure 2.16A, C). The appearance of punctate-like structures in addition to GFP-IQD8-labeled microtubule strands, indicated the partial shift of IQD8 towards membranes in a POK-dependent manner. Hence, both proteins were mutually affecting each other's localization. Similarly, we observed recruitment of mCherry-POK2C-terminal fragments to linear microtubule strands upon co-expression with GFP-IQD8 (Figure 2.16E). Substantial overlap of GFP-IQD8 and mCherry-POK2C (2083-2771) signals, indicated their co-localization and interaction. However, GFP-IQD8 recruitment to membrane domain was not as prominent as in the case of mCherry-POK1C (Figure 2.16A, E). This might be the result of weak interaction of POK2C with IQD8 compared to that of POK1C-IQD8.

As with POKs, we investigated IQD8 interaction with PHGAPs via transient expression in *N. benthamiana* leaf epidermal cells (Figure 2.16F-J). PHGAP1 and PHGAP2 were tagged with mCherry at N-terminus and co-expressed with GFP-IQD8. During interphase, PHGAPs are shown to display cytoplasmic and membrane-associated signals (Stöckle et al., 2016). Likewise, what has been reported, we also detected mCherry-PHGAPs signals in the cytoplasm and at the plasma membrane (Figure 2.16G, I). Upon co-expression of mCherry-PHGAP1 with GFP-IQD8, PHGAP1 fusion protein co-localized with IQD8 along microtubules (Figure 2.16H), suggesting the ability of IQD8 to recruit PHGAP1 at the microtubule filaments. The interaction was not evident in the case of PHGAP2. This might result from the over-expression of the protein, which potentially masked the microtubule filaments (Figure 2.16J). The interaction between GFP-IQD8 and mCherry-PHGAP1 was also noticed to some extent on the membrane which was visualized by appearance of more membrane microdomain-like structures in GFP-IQD8-labeled microtubule strands compared to a single expression of GFP-IQD8 (Figure 2.16F, H). Similar to IQD8-POK1C interaction, PHGAP1 and IQD8 also exerted a mutual effect on each other's localizations. N- and C-terminally GFP-tagged IQD8 fusion proteins showed partially different localization patterns. N-terminal GFP-tagged IQD8 localized more towards the membrane, while localization of C-terminally GFP-tagged IQD8 shifted more towards the membrane.

This prompted us to test whether the addition of GFP at the N or C-terminal of IQD8 affect the protein interaction. For this, we performed interaction assays using untagged and C-terminally GFP-tagged IQD8 translational fusion expressed under the control of 35S promoter (Figure S 10). We did not observe noticeable differences in interaction, suggesting that addition of GFP to the C-terminal of IQD8 does not hamper its interaction capability, and thus, functionality. Like N-terminally tagged IQD8, IQD8-GFP recruited POKs to linear

filaments that co-localized with microtubules (Figure S 10C, E). However, interaction appeared to be more shifted toward the membrane, consistent with stronger plasma membrane localization of IQD8-GFP when compared to GFP-IQD8 (Figure S 10A, C, E). In addition, untagged variants of IQD8 also recruited POKs from membrane microdomains to microtubules (Figure S 10F-I).

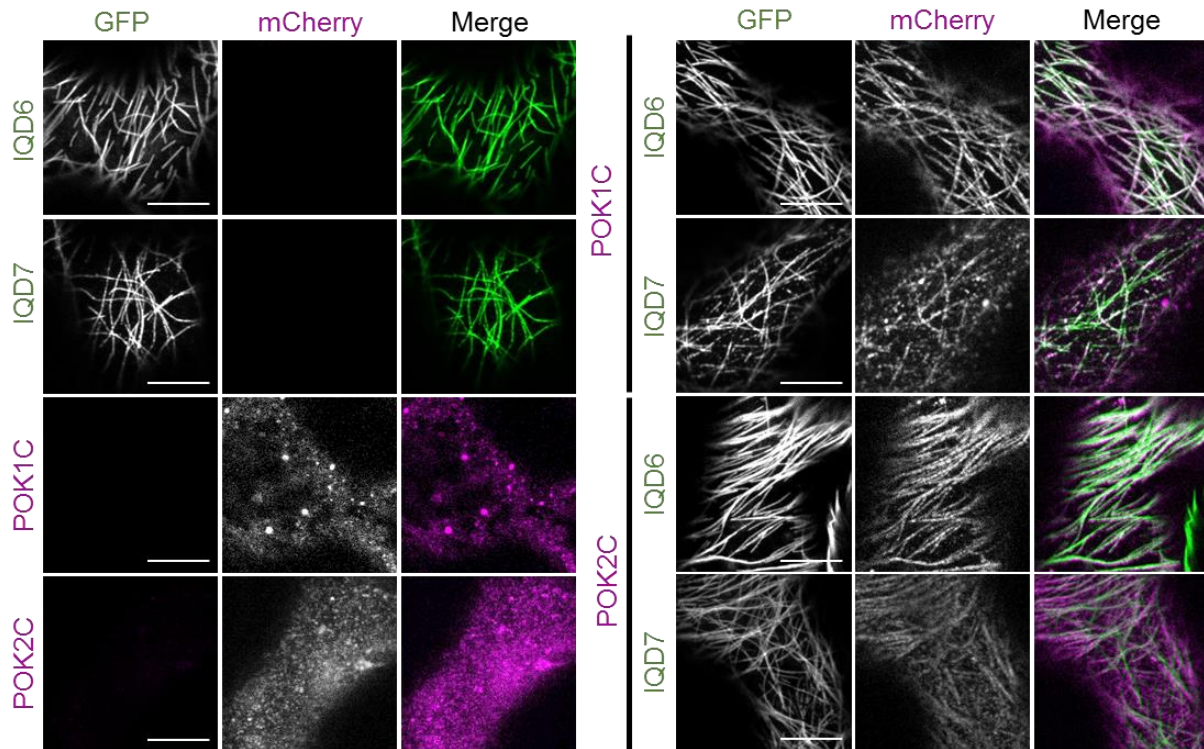


Figure 2.17 Co-expression assays of GFP-IQD6 and GFP-IQD7 with mCherry-POKs.

(A-D) Single expression of GFP-IQD6 (A), GFP-IQD7 (B), mCherry-POK1C (C) and mCherry-POK2C (D). (E-H) Co-expression of GFP-IQD6 with mCherry-POK1C (E) and mCherry-POK2C (F), GFP-IQD7 with mCherry-POK1C (G) and mCherry-POK2C (H). Left columns display GFP signals, center columns display mCherry signals, and right columns display merged images from both channels. POK1C, POK2C indicate C-terminal fragment of POK1 and POK2, respectively. All constructs were expressed under the control of 35S promoter. The result represents at least three independent experiments. Images are single optical sections and were acquired 2 days after infiltration in *N. benthamiana*. Scale bars, 10 μ m.

Likewise, IQD8, both IQD6 and IQD7 also showed *in planta* interaction with POKs fragments in transient expression assays in *N. benthamiana* (Figure 2.17). As reported before, GFP-IQD6 and GFP-IQD7 individually decorated microtubules (Figure 2.17A, B) (Bürstenbinder et al., 2017) and mCherry-POKs accumulated in punctate clusters (Figure 2.17C, D). Upon co-expression of GFP-IQD6 with mCherry-POK1C and mCherry-POK2C, POK1 and POK2C-terminal fragments were recruited from their microdomain localization to linear strand reminiscent of microtubules (Figure 2.17E, G). Similarly, upon co-expression of GFP-IQD7 with mCherry-POK1 and mCherry-POK2 C-terminal fragments, mCherry-POKs fragments are recruited to linear microtubule strands in a GFP-IQD7-dependent manner (Figure 2.17 F,

H). Although, the result contradicts our Y2H data, the absence of interaction in yeast might be explained by the requirement of a plant-specific factor to mediate IQD6 and IQD7 interaction with POK1 and POK2 fragments. Alternatively, weak expression of POKs or IQDs in yeast might result in no detectable interaction. These observations suggested that IQDs can mediate microtubule recruitment of POKs.

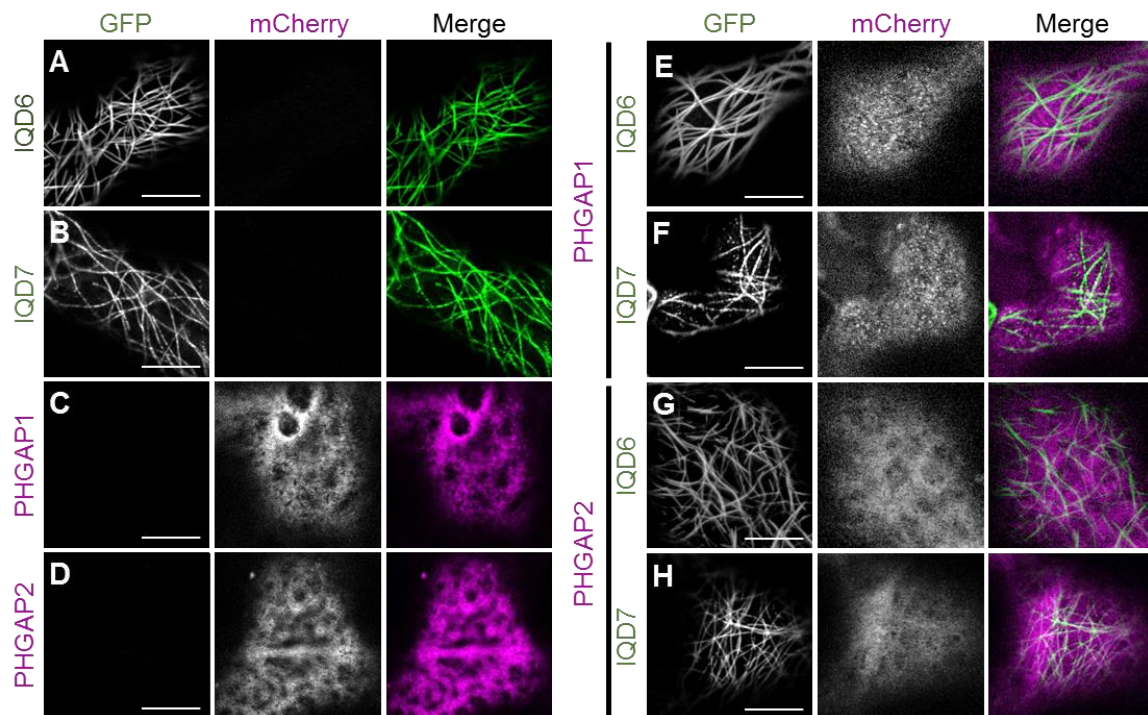


Figure 2.18 Co-expression assays of GFP-IQD6 and GFP-IQD7 with mCherry-PHGAPs.

Confocal laser scanning images showing single expressions of GFP-IQD6 (A), GFP-IQD7(B), mCherry-PHGAP1 (C) and mCherry-PHGAP2 (D). (E-H) Co-expression of GFP-IQD6 with mCherry-PHGAP1 (E) and PHGAP2 (F), and co-expression of GFP-IQD7 with mCherry-PHGAP1 (G) and mCherry-PHGAP2 (H) in *N. benthamiana* leaf epidermal cells. Left columns represent the expression pattern of fusion proteins in GFP channel, center columns indicate the expression pattern of fusion proteins in mCherry channel and right columns show merged images from both channels. All constructs were expressed under the control of 35S promoter. One representative experiment out of at least three independent experiments is shown. Images were acquired 2 days after infiltration. Scale bars, 10 μ m.

Further, we also tested *in planta* interaction of IQD6 and IQD7 with PHGAPs (Figure 2.18A-H). Consistent with previous experiments, GFP-IQD6 and GFP-IQD7 localized to the microtubules (Figure 2.18A, B) and mCherry-PHGAPs (mCherry-PHGAP1 and mCherry-PHGAP2) showed cytosolic and membrane-associated signals (Figure 2.18C, D). Unlike POKs, when mCherry-PHGAPs are co-expressed with GFP-IQD6 or GFP-IQD7, PHGAPs remained cytosolic or accumulated in punctate pattern, similar to their localization pattern when expressed individually (Figure 2.18E-H). This indicates a lack of interaction between

IQD6 and IQD7 with PHGAPs, which is consistent with our Y2H results. However, effects of over-expression on proteins function and localization should be considered while interpreting the results. Interaction results will be confirmed via other independent assays like protein biochemistry methods and Co-IP.

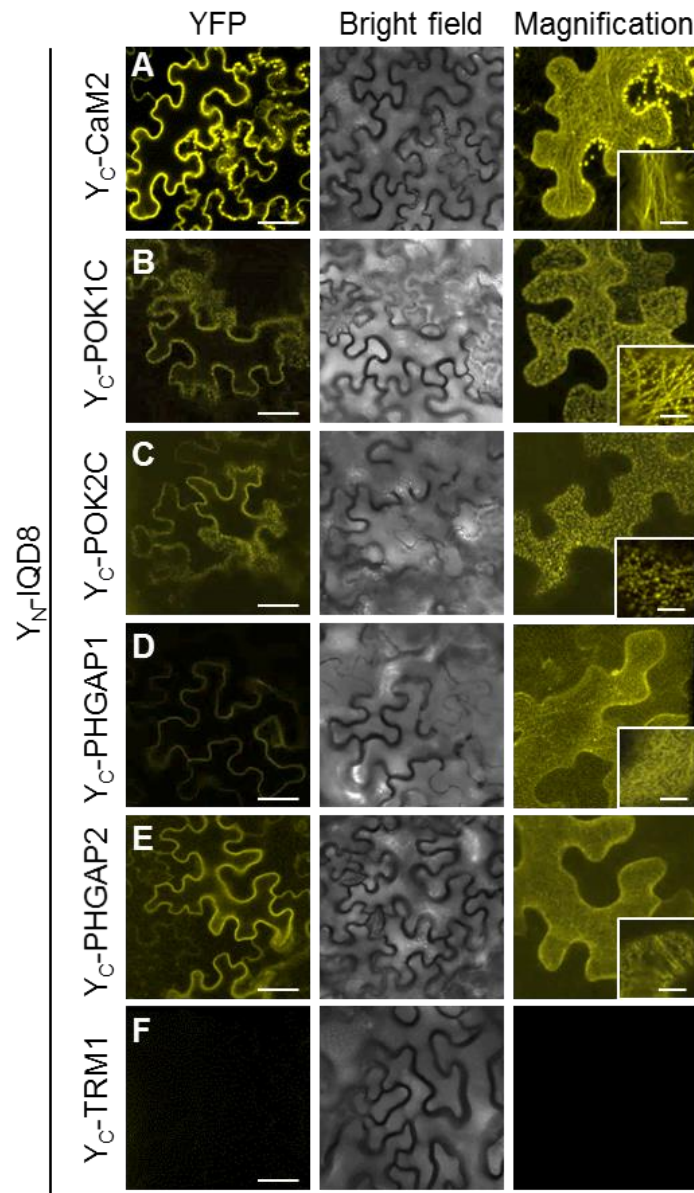


Figure 2.19 BiFC interaction assay between IQD8 and POKs or PHGAPs.

BiFC analysis of the interaction between IQD8 fused to the N-terminal half of YFP and PHGAP1, PHGAP2, POK1 C-terminal fragment or POK2 C-terminal fragment, which are fused to the C-terminal half of YFP. Single optical section of YFP signal (left column) and corresponding bright-field (center column) as well as Z projection of image stacks (right column) and magnified view (right column, inset view). IQD8-TON1 recruitment motif (TRM) interaction was used as biological negative control. Representative result out of two independent experiments is shown. Images were acquired 2 days after infiltration in *N. benthamiana*. Scale bars, 10 μ m.

Out of all interactions the most iterative and strong interaction observed was between IQD8 and those of POKs and PHGAPs, which are essential components of PPB memory and positioning. Therefore, I next focused on the functional relationship of IQD8 with division site resident proteins POKs and PHGAPs. BiFC assays were performed to corroborate direct interaction of IQD8 with POKs and PHGAPs *in vivo* in the cellular context of plant cells (Figure 2.19). For this purpose, POK and PHGAP constructs were fused to the C-terminal half of YFP (Y_C -POKs/PHGAPs) and IQD8 was fused to the N-terminal half of YFP (Y_N -IQD8). Constructs were transformed into *Agrobacterium tumefaciens* (*A. tumefaciens*) strain GV3101 and were used for co-transformation in *N. benthamiana*. A combination of Y_N -IQD8 and Y_C -TRM1 was used as a negative control, and interaction of Y_N -IQD8 with Y_C -CaM2 was used as a positive control. Recovery of fluorescence was observed upon co-expression of Y_N -IQD8 with Y_C -POKs/PHGAPs as well with Y_C -CaM2. No interaction was observed in case of negative control, indicating the specificity of the BiFC assays and interaction between IQD8 with POKs and PHGAPs. Collectively, our interaction assays in yeast and *in planta* confirmed the IQD8 interaction with POKs and PHGAPs. The observations together indicate that IQD8 is a realistic candidate for a potential scaffold that helps in organizing and assembling factors to regulate proper cell wall positioning. In addition, the interaction pattern of IQD6-8 with key players of cytokinesis further supports partially redundant but also different functions of IQD6, IQD7, and IQD8.

2.2.5 IQD8 plays roles in the efficient recruitment of POKs and PHGAPs to the division site

POKs are reported as an initial marker of division sites that are recruited to the PPB during prophase in a microtubule-dependent manner. After disassembly of microtubules of the PPB, POKs remain at the CDZ throughout cell division and help in retention of other division site resident proteins. POKs also help in the recruitment of CDZ resident proteins such as PHGAPs during metaphase and later stages cell division (Stöckle et al., 2016). The pair of division site markers, PHGAP1 and PHGAP2, is reported to play a role in PPB positioning as indicated by tilting of the PPB in *phgap12* double mutants. POKs and PHGAPs are proposed to work in a feedback loop to position the PPB and for further recruitment of positional markers to eventually guide the phragmoplast towards the CDS. Our results showed that IQD8 localized at the PPB, CDZ/CDS, as well as interacted with POKs and PHGAPs. This raised the questions whether IQD8 localization depends on presence of POKs or PHGAPs or vice versa, and whether IQD8 is required for localization of POKs and PHGAPs. To the answer the first question, the localization of IQD8-GFP expressed under the control of the endogenous promoter, was analyzed in the *pok12* and *phgap12* double mutants background.

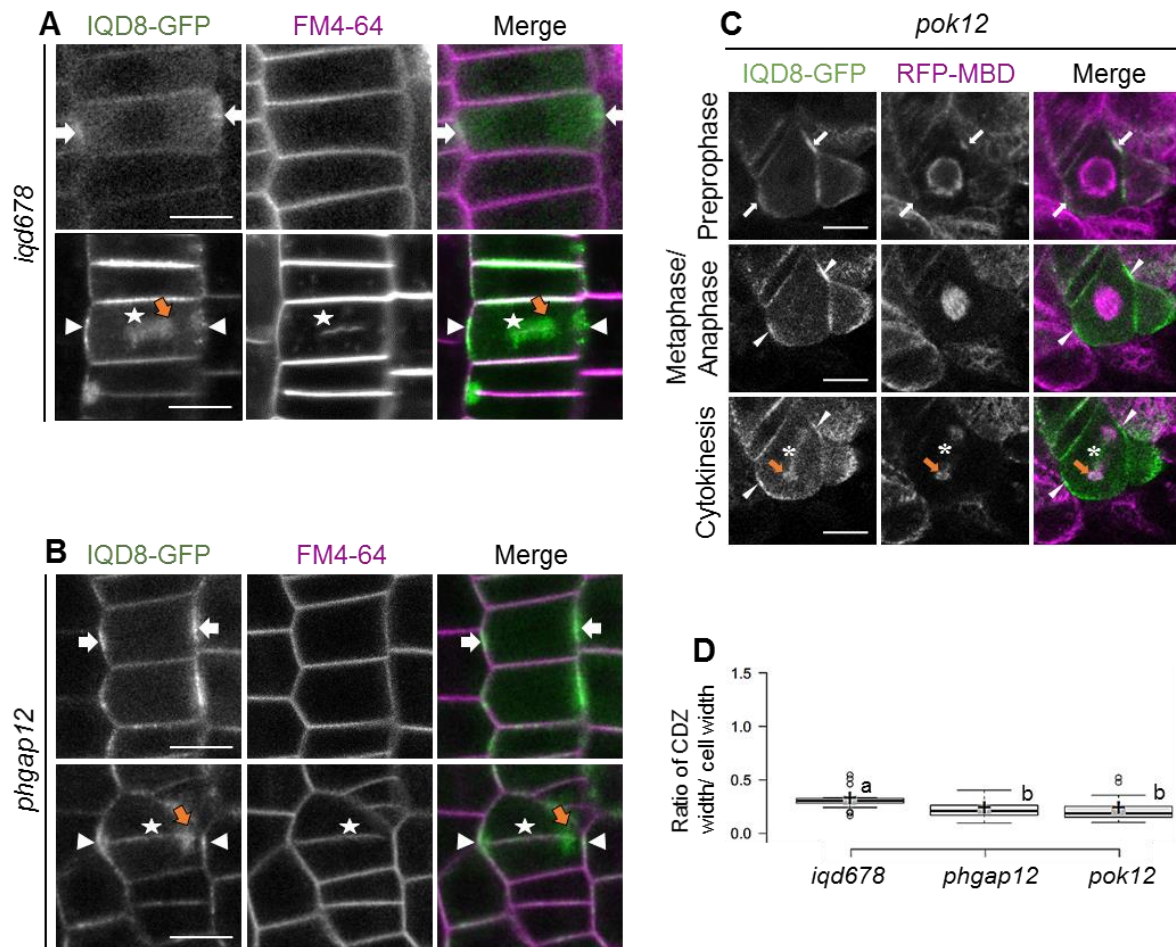


Figure 2.20 IQD8 localization during cell division in *pok12* and *phgap12* mutants.

(A) Arabidopsis root meristem cells expressing *pIQD8:IQD8-GFP* in the background of *iqd678* triple mutants, showing localization pattern of IQD8-GFP at PPB (white arrows), CDZ (arrowheads), phragmoplast (brown arrows) and cell plate (asterisks). Cytokinetic cells are visualized by staining of growing cell plates with FM4-64 dye. Images are representative of 8-10 roots from at least three independent experiments. Scale bars, 10 μ m. (B) Arabidopsis root meristem cells expressing *pIQD8:IQD8-GFP* in *phgap12* double mutant background. Single-cell resolution images showing localization pattern of IQD8-GFP at PPB (white arrows), CDZ (white arrowheads), phragmoplast (brown arrows) and cell plates (asterisks). Growing cell plates in cytokinetic cells are visualized by FM4-64 staining. Images are representative of 6 roots from two independent experiments. Scale bars, 10 μ m. (C) Confocal images showing co-expression of *pIQD8:IQD8-GFP* and *pUBQ10:RFP-MBD* in *pok12* double mutants background. RFP-MBD was used to visualize microtubules. PPB, CDZ, phragmoplast are marked by white arrows, white arrowheads and brown arrows, respectively. Asterisks represent the developing cell plate. Images are representative of 10-15 roots from three independent experiments. Scale bars, 10 μ m. (D) Quantification analysis showing the width of IQD8-GFP signal at CDZ relative to the lateral width of the cell in *phgap12* and *pok12* compared to *iqd678* triple mutants. 12 cells from 6 roots were used for the quantification.

We did not observe any obvious differences in native localization pattern of IQD8 (Figure 2.20). Similar to WT, *pok12* and *phgap12* double mutants showed accumulation of IQD8-GFP signals at PPB and phragmoplast. IQD8-GFP presence at division site and cell plate also remained consistent (Figure 2.20A, B, C). However, the width of IQD8-GFP at CDZ

often appeared narrower in *pok12* and *phgap12* double mutants compared to its native localization pattern. Therefore, to quantitatively assess the CDZ localization, we measured the average full width half maximum (FWHM) of IQD8 signals at CDZ relative to the lateral width of the cell in *iqd678* triple mutants and compared with corresponding signal pattern in the background of *pok12* and *phgap12* double mutants (Figure 2.20D). Data showed significant narrowing of IQD8 signals at CDZ in both *pok12* and *phgap12* double mutants compared to *iqd678* triple mutants (Figure 2.20D). However, IQD8 localization defects were comparable between *pok12* and *phgap12*, which may suggest that POKs and PHGAPs functions together at the cortex to set the wider localization pattern of IQD8 at CDZ. Altogether this analysis suggests that IQD8 localization is largely independent of POKs and PHGAPs. However, POKs and PHGAPs are required to set wider platform of IQD8 at CDZ.

Further, in order to study the requirement of IQDs for POKs recruitment and maintenance at the division site, we introduced *pPOK1:YFP-POK1* in the *iqd678* triple mutant background. In contrast to YFP-POK1 localization in WT background (Figure 2.21A), *iqd678* triple mutants showed reduced accumulation of YFP-POK1 to the cell cortex (Figure 2.21B). In *iqd678* mutants, we observed less frequent appearance of an YFP-POK1 ring compared to WT. YFP-POK1 recruitment to the division site was reduced from 67% in WT to 29% in *iqd678* triple mutant cells during preprophase stage (Figure 2.21C, D). During anaphase/metaphase stage of cell division only 22% of analyzed cells in mutants showed YFP-POK1 signal at CDZ, compared to 95% in WT (Figure 2.21C, D).

Similar to other two cases, at telophase stage, we also observed reduction in the accumulation YFP-POK1 at the division site, with 40% of mutant cells showing cortical rings of YFP-POK1 compared to normal 92% in case of WT (Figure 2.21C, D). Notably, we also observed partial reduction in the efficient recruitment of YFP-POK1 to the cell cortex in *iqd8-1* single mutants (Figure S 13). More pronounced effects on YFP-POK1 localization in the *iqd678* triple mutant compared to *iqd8-1* single mutants suggest additional roles of IQD6 and IQD7 in CDZ recruitment. Reduced frequency of POK1 recruitment correlates with a gradual frequency of PPB defects in the triple mutant. Since POK1 is an early marker of the division plane, which maintains the positional information of the PPB and helps to recruit and/or tether CDZ resident protein to the division site, its loss in *iqd678* might point to the loss of positional information in the *iqd678* triple mutants. Taken together, we propose that IQD8 acts upstream of POKs and promotes association of POKs at division sites for proper orientation of the division plane. Notably, the overall expression of YFP-POK1 in *iqd678* appears weaker compared to WT. However, both the control lines (*pPOK1:YFP-POK1/Col-0*)

and *pPOK1:YFP-POK1/iqd678* were recovered from same cross. Hence the reduction in the signal is likely not caused by any difference in growth condition and effect on YFP-POK1 signal might be the result of *iqd678* mutations. Similar to *iqd678* triple mutants, POK1 recruitment is also delayed in *trm678* mutants that fail to form PPB, indicating that a functional PPB may be required for efficient CDZ recruitment (Schaefer et al., 2017). However, the effect is much more severe in the *trm678* triple mutants compared to *iqd678* triple mutants. Additionally, IQD8 interacted with a CDZ resident POK interactor, PHGAPs in yeast as well as *in planta*. This motivated us to analyze the localization of PHGAPs in *iqd678* triple and *iqd8-1* single mutants.

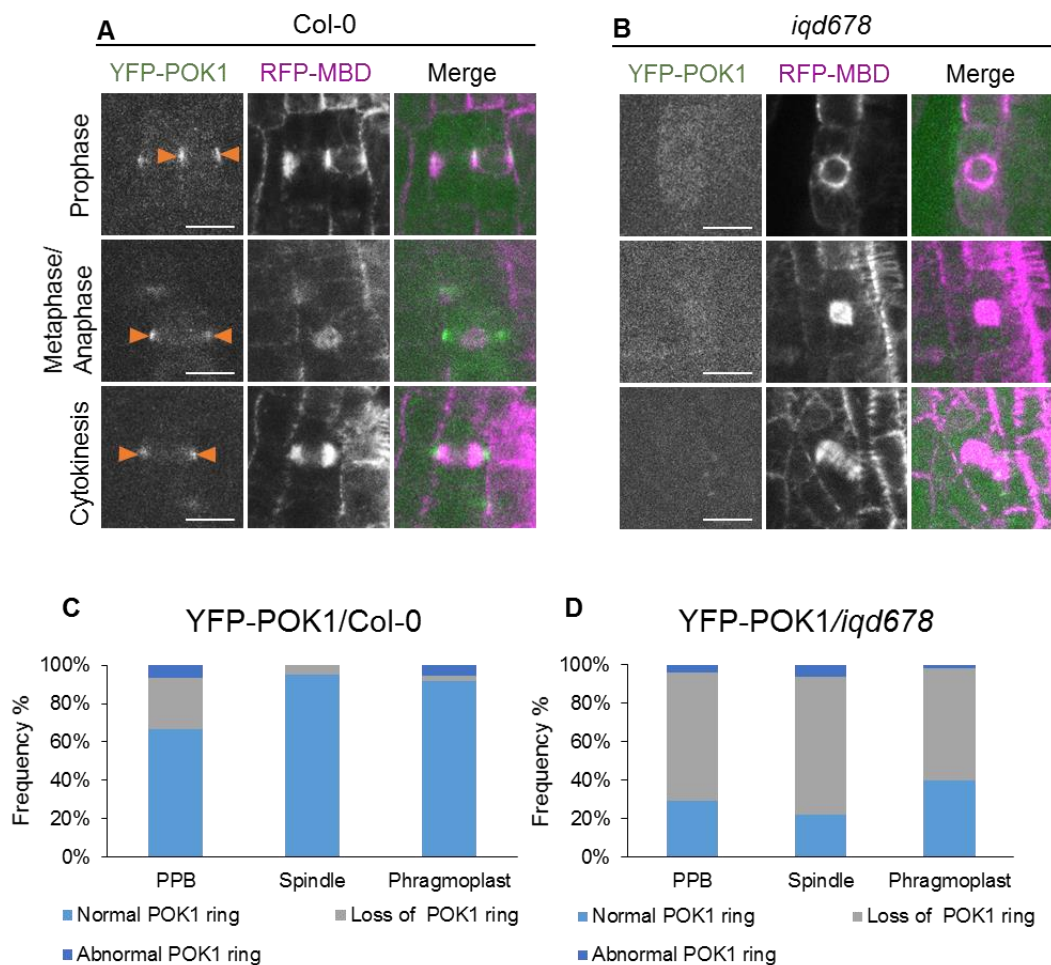


Figure 2.21 Efficiency of POK1 ring accumulation at cortical division site is reduced in *iqd678* triple mutants.

(A-B) YFP-POK1 localization pattern in Arabidopsis root meristem of 7-day-old seedlings of Col-0 (A) and *iqd678* triple mutants (B) in prophase, metaphase/anaphase and in cytokinetic cells. Scale bars, 10 μ m. (C, D) Distribution of YFP-POK1 in Col-0 and *iqd678* triple mutants in cells showing PPB, spindle and phragmoplast microtubules. RFP-MBD was used to visualize microtubules. Dark blue, light blue and gray color represent three categories of cells depending upon localization pattern of YFP-POK1 at division site. Confocal images and quantification data represent 20-25 roots from two independent experiments.

For this we introduced *pPHGAP2:GFP-PHGAP2/phgap12* in the *iqd678* triple mutant background via crossing. In contrast to WT scenario, we observed reduced recruitment of PHGAP2 to the CDZ in *iqd678* triple mutants (Figure 2.22). In the *phgap12* background, GFP-PHGAP2 decorated as bright foci on lateral wall of dividing cells (Figure 2.22, upper row) which is consistent with earlier reports (Stöckle, et al., 2016). In contrast to WT, we did not observe frequent accumulation of GFP-PHGAP2 signal at the cell cortex of *iqd678* triple mutant (Figure 2.22, lower row).

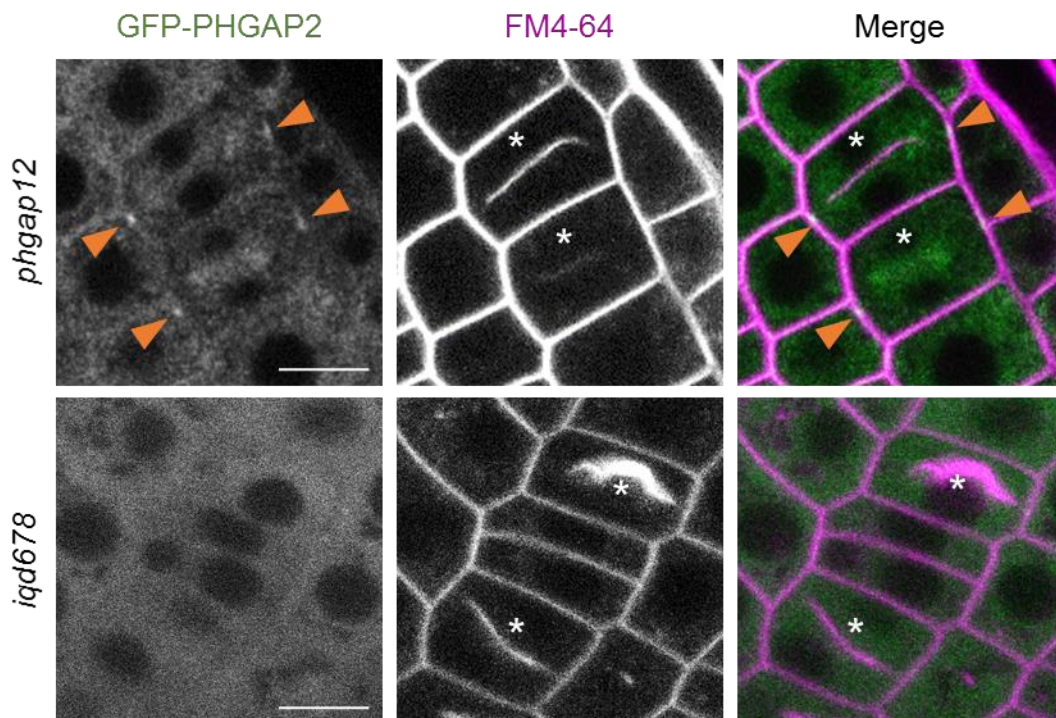


Figure 2.22 IQD proteins help in efficient recruitment of GFP-PHGAP2.

Arabidopsis root meristem cells of 7-day-old seedlings showing expression of *pPHGAP2:GFP-PHGAP2* in the background of *phgap12* (first row) and *iqd678* (second row) mutants. Root cells were stained with FM4-64 dye to visualize cell plates (asterisks) and membranes. Developing cell plates are indicative of cytokinetic cells. Accumulation of GFP-PHGAP2 signals at the cell cortex (First row, arrow heads). Images are representative of 6-10 roots from three independent experiments. Scale bars, 10 μ m.

Because PHGAPs interacted exclusively with IQD8 in our experimental approaches, we wondered whether reduced efficiency of PHGAP2 recruitment already could be detected in *iqd8-1* single mutants. To investigate this, we analyzed the localization pattern of *pPHGAP2:GFP-gPHGAP2/phgap12* in the *iqd8-1* mutant. Although we did not notice any profound alteration in localization patterns of GFP-PHGAP2 in *iqd8-1* single mutants, small but insignificant numbers of cells showed aberrant recruitment of PHGAP2 (data not shown). The threshold of IQD6, IQD7 interaction with PHGAP2 might be beyond the detection level, which likely explains the collective effect in the triple mutant. Physical interaction data as well as the dependency of POK1 and PHGAP2 localization on IQD functions, together indicate

that IQD8 potentially works upstream of POKs and PHGAPs and helps in their efficient recruitment at the division site, but in a feedback loop, POKs and PHGAPs are required to maintain unique broad localization pattern of IQD8 at CDZ.

2.2.6 IQDs interact genetically with POKs and PHGAPs

Interaction of IQD6-IQD8 with POKs and PHGAPs, alteration in the localization pattern of IQD8 and POKs/PHGAPs and vice versa in reciprocal genetic background, as well as phenotypic similarity of *iqd678* with *pok12* and *phgap12* mutants, prompted us to investigate the genetic relation of *IQD8* with *POKs* and *PHGAPs*. To study this, we generated quintuple mutants of *iqd678pok12* and *iqd678phgap12*.

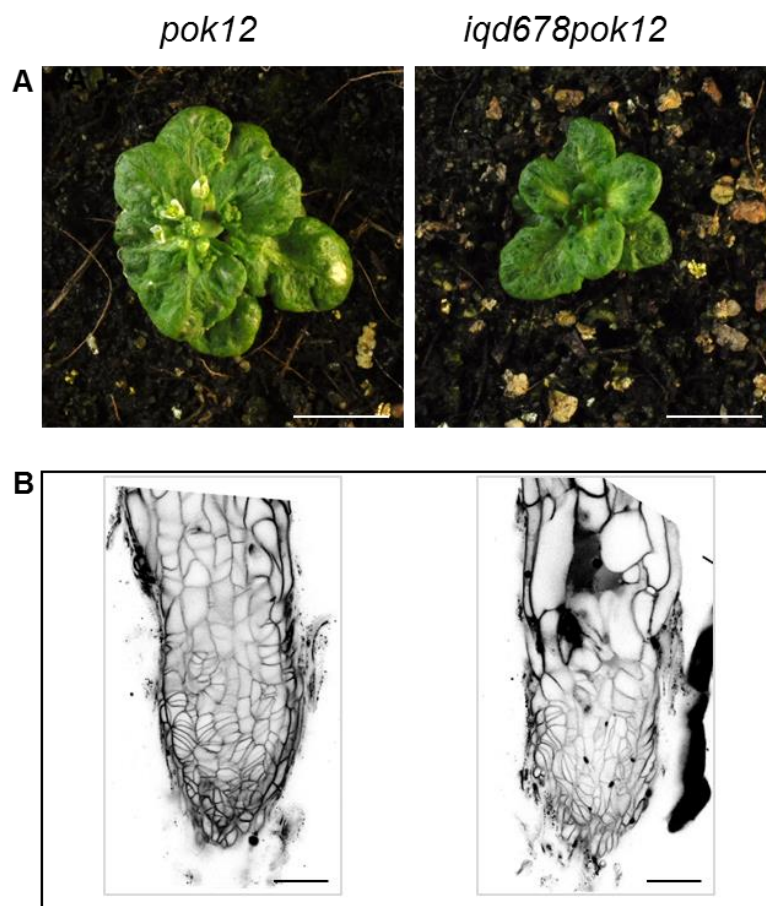


Figure 2.23 Genetic interaction of *IQD6*, *IQD7* and *IQD8* with *POKs*.

Comparative growth morphology of 5-week-old plants of *pok12* double (left) and *pok12iqd678* quintuple (right) mutants. Images are representative of 10 plants per genotype from two independent experiments using two different seed batches. (B) Confocal longitudinal section of 7-day-old PI-stained Arabidopsis root meristem cells from *pok12* and *pok12iqd678* mutants. PI was used to stain the cell walls. Scale bars, 1 cm (A) and 50 μ m (B).

Loss of *pok12* results in severe defects in cell wall positioning in all tissues, and leads to a dwarf plant, yet the mutant is able to produce progeny (Lipka et al., 2014). The quintuple

mutant of *iqd678pok12* showed enhanced growth defects of aerial tissues, indicated by a more severe dwarf stature of *iqd678pok12* compared to *pok12* double mutants (Figure 2.23A). Although *iqd678pok12* still produced viable seeds, mutants tend to produce fewer seeds (data not analyzed in detail). Because of the severe cell wall mispositioning in *pok12* double mutant, it is hard to distinguish *pok12* double mutants from *iqd678pok12* quintuple mutants at the cellular level (Figure 2.23B). These observations suggest that IQD6-8 and POKs act synergistically to regulate spatial control of cytokinesis.

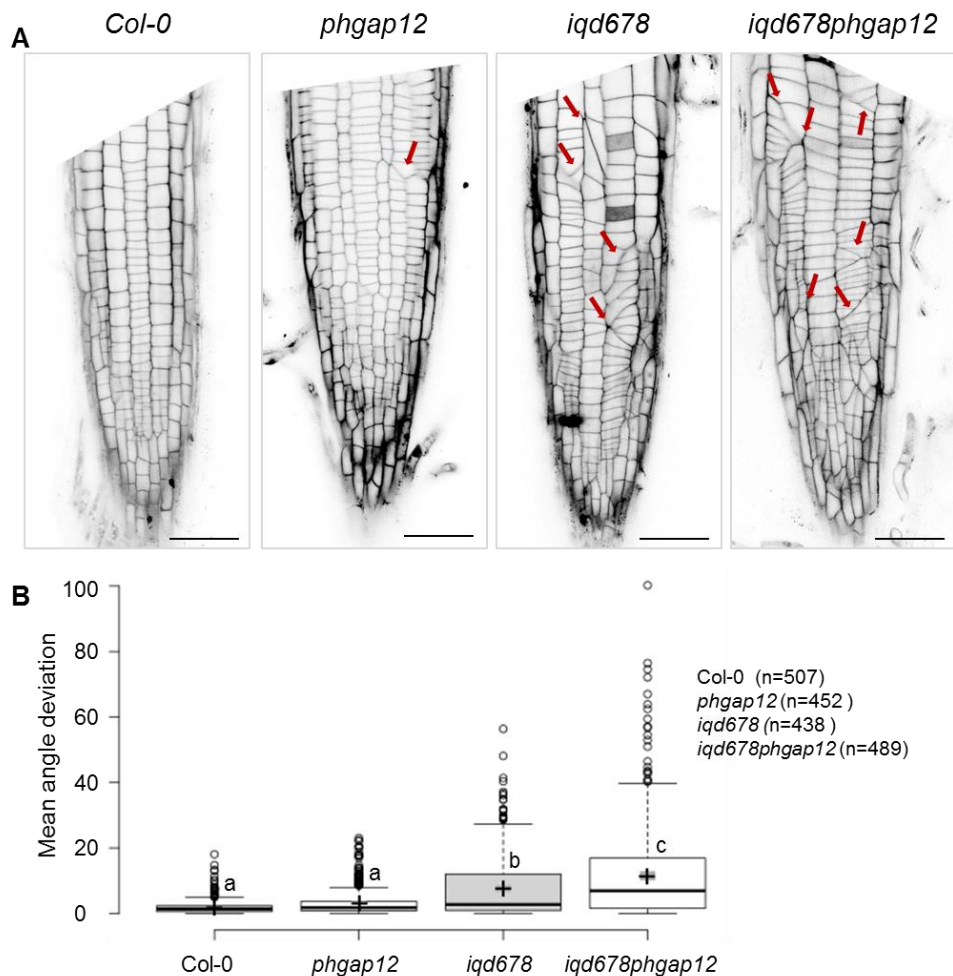


Figure 2.24 Genetic interaction of IQD6, IQD7 and IQD8 with PHGAPs.

(A) Single longitudinal section of 7-day-old root meristem of Col-0, *phgap12* double mutants, *iqd678* triple mutants and *phgap12iqd678* quintuple mutants showing comparative analysis of cell wall patterning in corresponding genotypes. Arrows point to misoriented cell wall in mutants. PI was used to stain cell wall. Images are representative of 6-10 roots from two independent experiments using two different seed batches. Scale bars, 50 μ m. (B) Angles were measured using ImageJ. Boxplots represent quantitative analysis of cell wall misorientation in Col-0, *phgap12*, *iqd678* and *iqd678phgap12*. Boxplots were generated using BoxPlotR. Box limits indicate the 25th to 75th percentiles, center lines represent the medians, crosses indicate mean points, and dots represent outliers. Whiskers extend 1.5 times the IQR from the 25th and 75th percentiles. Individual letters denote statistically significant differences calculated by one-way ANOVA and post hoc HSD ($p < 0.01$). (n) = number of cells analyzed per genotype. Quantification was performed using data from 6-10 seedlings per genotype.

In addition to POKs, IQD8 also showed robust interaction with PHGAPs in our interaction assays. Afterthat, as a means of identifying functional relation between *IQDs* and *PHGAPs*, we also explored the microscopic and macroscopic phenotype of the *iqd678phgap12* quintuple mutant. Macroscopically the phenotype of *iqd678phgap12* did differ from that of WT (data not shown). However, analysis of the microscopic phenotype of the mutants, revealed enhanced events of misplaced cell wall mispositioning in *iqd678phgap12* compared to *phgap12* and that of *iqd678* (Figure 2.24A, B). In *phgap12* double mutants, the phenotype was more visible in inner tissue layers and columella cells, however, in contrast to *iqd678*, *phgap12* showed comparatively weaker phenotype in the root epidermal layer (Figure 2.24A).

Intriguingly, *iqd678phgap12* quintuple mutants showed phenotypes in all tissue layers. The severity of misoriented cell walls enhanced even in the same tissue layer compared to *iqd678* triple mutant (Figure 2.24A). Also, the altered arrangement of columella cells was evident in the quintuple mutant, which is potentially caused by impairments in *phgap12* double mutants. Both *phgap12* and *iqd678* mutants, showed occurrence of tilted PPB (Stöckle et al., 2016 and our data), indicating a role in division plane positioning. Together with the enhanced phenotypes observed in *phgap12iqd678* compared to *phgap12* and *iqd678*, we propose that IQD8 might function together with PHGAPs in division plane orientation, potentially by regulating ROP signaling. Taken together, our results indicate that IQD8 acts as a novel scaffold which helps in recruitment of PPB memory factors during various stages of cell division as well as play a credential role in organization and positioning of mitotic microtubule arrays, to eventually regulate proper cell wall placement.

2.3 Discussion

In this study, we showed for the first time a role of IQDs in cell division related processes. Our interaction studies identified POKs and PHGAPs as novel interactors of IQD8. Functional significance of their interaction is indicated by similar phenotypes of *phgap12* and *pok12* to that of *iqd678* mutant as well as the dependency of POKs and PHGAPs localization on IQD8 function. Here, we discovered the role of IQDs in organization and formation of mitotic microtubule arrays. Thus, loss of IQD6 to IQD8, primarily IQD8, affects PPB formation and causes aberrant phragmoplast morphology. Our research identifies IQD8 as a potential scaffold acting upstream of POKs and PHGAPs and playing multiple roles starting from the early event such as division plane formation, positioning as well as maintenance and up to phragmoplast guidance.

2.3.1 Impairment of IQD function affects cell wall positioning primarily in the epidermis

In WT cells, newly developed cell walls are positioned transversely or longitudinally to the long axis of root cells depending upon the type of cell division. However, in *iqd678* triple mutants, cell walls are positioned in a variety of abnormal orientations (Figure 2.2) similar to what has been observed in other mutants like *pok12*, *tan*, *phgap12*, and *rangap12*, that are essential during spatial control of cytokinesis (Lipka et al., 2014; Stöckle et al., 2016; Walker et al., 2007; Xu et al., 2008). Presence of a mild phenotype in *iqd8-1* and normal cell wall patterning in *iqd6-1* and *iqd7-1* single mutants suggested that IQD8 acts as a major contributor in the directed cell wall insertion. However, severe phenotypes of *iqd678* triple mutants compared to *iqd8-1* single mutants could be explained by functional redundancy with IQD6, and IQD7 to some extent. The partial redundancy is supported by partially overlapping expression patterns of the 3 genes (Figure S 8). *IQD6* and *IQD7* expressed more strongly in inner tissues of the root, while *IQD8* showed expression patterns in all tissue layers with strongest expression in the epidermis. In addition, the patchy expression pattern of *IQD8* is reminiscent of cell cycle-regulated genes (BursSENS et al., 1998; Ferreira et al., 1994). These facts suggest that IQD8 plays a primary role in the process of cell wall positioning. The primary importance of IQD8 in cell wall positioning is further confirmed by its ability to complement the *iqd678* triple mutant phenotypes (Figure 2.2).

Impairment of IQD6, IQD7 and IQD8, primarily affects cell wall orientation in the epidermis. Cell wall positioning in the cortex and underlying tissues appeared mostly normal (Figure 2.3). In contrast, PPB defects were observed both in the epidermis as well as in the cortex. This suggests that IQD8 is required to form PPB both in the root epidermis and cortex, which

is also consistent with the broad expression pattern of IQD8 (Figure 2.7C). However, restriction of the cell wall misorientation in the *iqd678* triple mutants only to the epidermis might indicate the tissue-specific requirement of PPB for the correct positioning of the cell wall. Alternatively, PPB-independent mechanism in the cortex might compensate for the loss of PPB. This view is further supported by the study of Zhang et al. (2016), where the impaired function of TON1a leads to loss of PPB in the root epidermis and cortex, however, events of cell wall misorientation are only visible in the epidermal layer of roots. The PPB-independent mechanism is described in more detail in section 2.3.2 below. The similar phenotypes of *iqd678* and *ton1a-1*, suggest a similar mechanism of IQD8 and TON1a in regulating spatial control of cytokinesis. Interestingly, defects in the division plane orientation were not visible in all epidermal cells of *iqd678* triple mutants. The lack of severe cell wall positioning defects in *iqd678* triple mutants may point toward the existence of an IQD-independent mechanism for accurate positioning of the cell wall. Alternatively, other IQDs might act partially redundant to IQD6-8 and likely replace their function in the *iqd678* triple mutants to some extent. Likewise, myosin triple knockout mutant *xi-k xi-1 xi-2* (3KO) plants display moderate cell wall positioning defects only in the stele cells. It is hypothesized that the function of other myosin XI isoform might compensate for the elimination of myosins XI-K, XI-1 and XI-2 (Abu-Abied et al., 2018).

Despite the defects in cell wall positioning, *iqd678* triple mutant did not show any obvious defects in cellular differentiation (Figure 2.4). Identity of cell types could be visualized by cellular morphology. Similarly, even in the case of severe mutants like *ton2/fass* and *pok12*, cellular fates are still recognizable (Camilleri et al., 2002; Müller et al., 2006). This indicates that mutations in these genes only affects symmetrical cell divisions in roots, which contribute to overall growth of plants, however, asymmetric divisions responsible for the generation of new tissue layers remain intact. This points to additional roles of external cues in determining cellular fates during asymmetric cell divisions (Rasmussen et al., 2011a). Until now, studies revealed that the extent of altered growth morphology is correlated with the severity of cell wall positioning defects. In most of the mutants with severely misoriented cell walls, normal physiological processes are not affected. However, depending upon the phenotypic severity, growth-related processes might be delayed which results in slow growth of plants as reported in the case of *pok12* double mutants (Lipka et al., 2014; Müller et al., 2006). A milder defect in cell wall orientation of *iqd678* compared to severe mutants like *pok12*, explains the absence of growth-related defects.

2.3.2 Requirement of IQD8 during cell division

Our data revealed the localization of IQD8 along the entire length of microtubules at all stages of the cell cycle (Figure 2.7, Figure 2.8), suggesting a role in microtubule organization through out the cell cycle. In correlation with our hypothesis, *iqd678* triple mutants showed defects in PPB formation as well as morphology of phragmoplasts (Figure 2.10, Figure 2.11). During prophase stage of cell division *iqd8-1* single and *iqd678* triple mutants showed loss of PPB in nearly 11% and 48% of the analyzed cells (Figure 2.12A), respectively, indicated by strong accumulation of perinuclear microtubules around the nucleus and absence of microtubules from the cell cortex (Figure 2.10A, Figure 2.11B,C). IQD5, a member of the same clade, has been shown to affect the stability of microtubules in an *in vivo* assay (Liang et al., 2018). The role of IQD5 in microtubule stability is also supported by microtubule depolymerizing drug treatment (Liang et al., 2018). Because of the similarity between IQD5 and IQD8, we propose that IQD8 may also function to provide stability of microtubules during PPB formation. In addition, IQD13 possess two microtubule binding domains and helps in the bundling of microtubules (Sugiyama et al., 2017). IQD8 may function in a similar mechanism to promote microtubule bundling/crosslinking and thereby helping in organization of microtubules of PPB. IQD8 also showed dual localization pattern, i.e., it interacted with both plasma membrane as well as microtubules (Figure 2.7). Similarly, IQD13 is also shown to bind both with microtubules as well as with plasma membrane and to help in tethering of cortical microtubules to the plasma membrane (Sugiyama et al., 2017). In a similar way, IQD8 may also function in targeting of PPB microtubules to the cell cortex.

Localization of IQD8 at PPB resembles other protein factors such as MOR1, components of TTP complex as well as POKs. These proteins are reported to play a role in organization and formation of PPB microtubules as well as maintenance of division sites via recruitment and retention of division site marker proteins (Kawamura et al., 2006; Livanos and Müller, 2019). However, unlike other division site-localized proteins, IQD8-GFP labeled a relatively broad region at the cell cortex throughout division (Figure 2.7E-G). This suggests a possible role of IQD8 in general stability and organization of PPB microtubules. Mispositioning of cell walls in *iqd678* triple and *iqd8-1* single mutants suggest an additional role in maintaining positional information of the PPB, similar to what has been observed for POK1 and POK2. Similar to *pok12* double mutants, *iqd678* triple mutants also showed 3-way junctions of cell walls, as well as tilted and curved positioning of the cell walls (Figure 2.2A, Figure 2.23A). Based on available data for POKs and IQDs interactions and their phenotypes, we can envision that IQDs and POKs may function in the same or different pathways regulating the different mechanism of establishment and maintenance of PPB memory.

Some of the *iqd678* mutant cells did show the PPB, however, very often with sparse microtubules, and frequent tilting of PPBs was observed (Figure 2.10A, Figure 2.11B, Figure 2.12B). Similarly, *phgap12* double mutants display frequent misorientation of PPB (Stöckle et al., 2016). PHGAPs are putative ROPGAPs which are shown to play role in division plane selection possibly by localized modification of plasma membrane via spatio-temporal regulation of ROP activities (Stöckle et al., 2016). Interaction of IQD8 with PHGAP1 and PHGAP2 as well oblique orientation of PPB in *iqd678* and *phgap12*, suggest a possible role of IQD8 in division plane selection via association of PHGAPs mediated ROP signaling. *ton1*, *ton2/fass* and *trm* are the only known mutants which completely suppress PPB formation. TON1, TON2 and TTP are the components of TTP complex and are credential for the formation of PPB microtubules. Developmental and cellular defects arise in these mutants and are more or less direct effect of PPB loss (Azimzadeh et al., 2008; Camilleri et al., 2002; Spinner et al., 2013; Zhang et al., 2016). In all other mutants such as Arabidopsis *phgap12*, Arabidopsis *mor1* and maize *tan* are only known to affect the PPB structure specifically as partial suppression and/or positioning defect (Kawamura et al., 2006; Stöckle et al., 2016). Proteins such as POK1 and POK2 act downstream of division plane determination and accomplish establishment and maintenance of the division plane.

Despite the loss of PPB in the cortex of *iqd678* triple mutants, cells of the cortex divide in the regular orientations, suggesting the presence of PPB-independent mechanism in the cortical tissues. This is consistent with the studies in the cell cultures showing proper cell wall orientation besides the absence of PPB (Ambrose and Cyr, 2008; Chan et al., 2005; Marcus et al., 2005; reviewed in Rasmussen et al., 2013). In addition, endosperms (Sabelli and Larkins, 2009) and gametophytes (Otegui and Staehelin, 2000) of higher plants also lack PPB, however, cells divide normally. PPB emerged first in bryophytes, but not all the cell types form the PPB (reviewed in Buschmann and Müller, 2019). The leafy gametophyte of mosses form PPB, however, the moss protonema cells (chloronema and caulonema) are devoid of a PPB, yet cell walls are oriented in the anticipated direction, indicated by cell wall orientations in neighboring cells relative to the growth axis (Doonan et al., 1987; Schmiedel et al., 1981; Spinner et al., 2010). A recent discovery regarding the functional investigation of *trm678* also uncoupled the necessity of PPB for spatial control of cytokinesis. Despite a massive loss of PPB, *trm678* mutants did not display apparent defects in division plane orientation, indicating that the PPB is dispensable for division plane orientation but required for its robustness (Schaefer et al., 2017). These findings altogether indicate the existence of alternative mechanisms of tracking positional memory to properly orient cell division plane. It is possible that various factors work independently and redundantly in various aspects of division plane determination. Taken together, PPB requirement for division plane

establishment is still in debate. An alternative mechanism that might maintain division site information in the absence of a PPB is still unknown. Localized thickening of the cell wall as in the case of early land plants or remaining actin filaments might instead provide the division plane information. In addition, increased endocytic activity is reported at PPB and could lead to modifications of the plasma membrane in the vicinity of the PPB to establishing a cortical mark (reviewed in Rasmussen et al., 2011a).

Several lines of evidence point to the roles of interphase cortical microtubule arrays in the formation and positioning of the PPB. For example, mutants which are impaired in subunits of the TTP complex (except *trm*) (Azimzadeh et al., 2008; Camilleri et al., 2002; Schaefer et al., 2017; Zhang et al., 2016), show defect in organization of interphase cortical microtubule arrays together with PPB defects. Unlike these mutants, the arrangement of interphase microtubules in *iqd678* was comparable to WT (Figure 2.13). Our results were in close resemblance to *trm678* triple mutants, where the loss of PPB microtubules is uncoupled from defects in interphase cortical microtubules. Likewise, *ton1a-1* also showed substantial loss of PPB without affecting interphase microtubules. Altogether any decisive relation could not be set within the cortical microtubule arrangement and its effect on PPB fate.

Our data showed the persistence of IQD8 at CDZ after PPB assembly, where it remained till the completion of cytokinesis. However, compared to other CDZ/CDS-resident proteins, IQD8 showed a broader localization pattern at the CDZ. The exceptionally broader localization pattern of IQD8 at the division site might provide a local platform for the assembly of factors regulating cell wall orientation and/or tethering the components of signaling such as Ca²⁺ signaling. In metaphase, IQD8 scantily labeled spindle microtubules (data not shown). Consistent with the localization of IQD8, we did not observe any obvious defect in general organization of spindle microtubules. However, during anaphase to metaphase stage of cell division, around 16% and 43% of *iqd8-1* single and *iqd678* triple mutant cells, respectively, showed tilted spindles with a rotation greater than 15° (Figure 2.12C). PPB is proposed to promote bipolarity of spindle via polar accumulation of microtubules onto the nucleus, in a perpendicular direction to the PPB. Thereby, PPB prevents the rotation of spindle (Ambrose and Cyr, 2008). Similarly, spindle rotation in *iqd678* might be the direct consequence of PPB loss. The PPB loss in *iqd678* triple mutants may have further effects on the polar accumulation of microtubules on to the nucleus poles, which directs the polarity of the spindle. However, spindle rotation is a common phenomenon also reported even in WT cells (Panteris et al., 2011; Rasmussen et al., 2013). Spindle axis rotation is corrected at the end of division. In case of extreme rotation from its original axis, a new division plane may be chosen, which leads to the orientation defect (Rasmussen et al.,

2013). In *iqd8-1* and *iqd678* mutants, substantial amounts of cells showed spindle axis rotation to the extent that it could not be corrected at a later stage of cell division. Therefore, spindle rotation in *iqd* mutants is likely caused by PPB loss. In addition, misorientation of PPB observed in *iqd678* and *iqd8-1* might also lead to the tilted orientation of spindles.

In addition to PPB microtubules and CDZ/CDS, IQD8 also labeled phragmoplast microtubules uniformly along the entire lengths (Figure 2.7F, G), which suggests a potential role of IQD8 in guidance of phragmoplast and/or phragmoplast stability and organization. Consistently, around 13% and 40% cytokinetic cells in *iqd8-1* single, *iqd678* triple mutants, respectively, showed the oblique orientation of phragmoplast, unlike WT cells where the majority of phragmoplasts aligned transversely along the growth axis of cells (Figure 2.12D). Frequency of cells showing the tilted orientation of phragmoplast is correlated with PPB loss observed in the *iqd678* triple mutants. This further suggests the potential loss of phragmoplast guidance in *iqd678* triple mutants, as indicated by tilted phragmoplast orientation, which is likely due to loss of positional information of PPB. We also found instances of twisted/wavy or curved phragmoplasts in *iqd8-1* single and *iqd678* triple mutants (Figure 2.10C; Figure 2.11B,C; Figure 2.12E), which might also be the consequence of defects in phragmoplast guidance mechanisms.

Absence of phragmoplast guidance mechanism may cause frequent changes in the direction of expanding phragmoplasts, which may eventually result in wavy phragmoplasts as well as delayed expansion of phragmoplast. Consistently, *iqd678* triple mutants also showed tendencies of extended duration of phragmoplast expansion compared to WT phragmoplast (data not shown). The undulation of phragmoplasts has also been observed in *tan1* in Maize and *mor1*, *pok12* in Arabidopsis (Cleary and Smith, 1998; Herrmann et al., 2018). TAN is the positive marker of division site and serves as a PPB memory after disintegration of PPB microtubules (Cleary and Smith, 1998; Walker et al., 2007). It is proposed that loss of phragmoplast guidance leads to wavy phragmoplast in the *tan1* mutant. Similarly, POKs are the early and continuous markers of division site. POK1 localizes to the division site (Lipka et al., 2014) and additionally, POK2 is present at both the division site as well as at the phragmoplast midzone (Herrmann et al., 2018). POKs are shown to function in the division plane establishment and in phragmoplast guidance towards the CDZ. Loss of phragmoplast guidance in *pok12* double mutants results in wavy and twisted phragmoplast (Herrmann et al., 2018). Likewise, IQD8 also decorated division sites throughout the cell division as well as labeled phragmoplast microtubules. This suggests potentially similar functions of IQD8 and POKs, and wavy as well as curved phragmoplast in *iqd8-1* and *iqd678* mutants might be caused by defects in phragmoplast guidance.

Intriguingly, like POK2, IQD8 also localizes to peripheral microtubules emanating from the leading edge of phragmoplasts and at the division site. POK2 is known to guide phragmoplast by the virtue of its dual localization via bridging phragmoplast and the cortical division site (Herrmann et al., 2018). Based on the similarity of *pok12* and *iqd678* phenotypes, we hypothesized that IQD8 may also act to guide the expansion of the phragmoplast via mediating the association of the leading edge of phragmoplast microtubules to the division site via its dual localization pattern. Corroborated with this, an earlier report by Sugiyama et al., 2017 also showed IQD13-mediated plasma membrane-microtubule association via its dual localization at both plasma membrane as well as to the microtubules. Additionally, IQD8 localized at emanating phragmoplast microtubules might interact with CDZ-resident proteins to guide the directed expansion of the phragmoplast.

Although most of the abnormally structured cells attributed to a defect in phragmoplast morphology, in few instances even cells with normal morphology also possessed aberrant phragmoplasts (wavy and tilted). Because of this variation, no conclusion could be drawn for relation between structural feature of cells and phragmoplast abnormality. It is not yet clear whether undulation in phragmoplasts results from loss of division site information in cells which are impaired in PPB formation. Time-lapse imaging showed that wavy phragmoplasts do not always occur in cells lacking PPB. Besides, defects in phragmoplast morphology, we did not observe any abnormalities related to cell wall biosynthesis, defined by cell wall stubs and multinucleated cells. Curved and wavy phragmoplasts also led to the formation of steeply oblique angles of cell walls. This possibly contributes towards cell wall positioning defects independently of cell wall orientation defects resulting from PPB loss and misorientation. Besides proteins which play a role in phragmoplast guidance, impaired function of MOR1 also leads to phragmoplast morphology defects (wavy and twisted phragmoplast). MOR1 uniformly labels the phragmoplast microtubules and plays roles in the organization and stability of microtubules (Kawamura et al., 2006). Similar localization patterns of IQD8 and that of MOR1 might suggest similar function of IQD8 at phragmoplast, and defects in organization and stability of phragmoplast, which is consistent with the uniform localization of IQD8 along the phragmoplast microtubules.

Our data also showed the interaction of IQD8 with one of the well-established microtubule crosslinking/bundling proteins, MAP65-3 (Figure S 11). Although IQD8 localizes uniformly throughout the entire length of phragmoplast microtubules, association with MAP65-3 might suggest its function in bundling of phragmoplast midzone. In addition, IQD8 at phragmoplast might help in delivery and fusion of membrane-bound Golgi-derived vesicles at cell plate and

thus the formation of cell plate. Our hypothesis is consistent with localization of IQD8 at cell plate. However, as stated earlier, we did not notice any defects in crosslinking of phragmoplast midzone as well as cell plate biosynthesis. Unidentified redundant function of other IQDs at phragmoplast midzone and cell plate might explain the absence of cell plate-related phenotypes in *iqd678* triple mutants. *iqd678* showed cell plate positioning defects as well as undulation of phragmoplast reminiscent of what is shown for *pok12* (Lipka et al., 2014; Müller et al., 2006). In addition, PPB misorientation in *iqd678* triple mutants is similar to *phgap12* double mutants. Furthermore, IQD8 interacts with POKs and PHGAPs, which are shown to interact with each other (Stöckle et al., 2016). Altogether, these findings suggest a possible analogy of IQDs with POKs and PHGAPs and a potential function of a trimeric complex during spatial control of cytokinesis.

IQD8 diverse localization patterns during cell division, and its proposed microtubule bundling and scaffolding activity, might explain the cytoskeletal defect observed in *iqd678*, likely mediated via IQD8 in most cases. The exact mechanism is still under investigation. N-terminally GFP-tagged IQD8 localizes more towards microtubules while C-terminally GFP-tagged IQD8 localizes more towards the membrane, suggesting that the N-terminal of IQD8 likely mediates membrane binding and the C-terminal of IQD8 mediates microtubule binding. This differential localization pattern of IQD8 might be mediated via its domain-dependent interaction with various factors regulating spatial control of cytokinesis or possibly via post-translational modification such as phosphorylation, lipid modifications. IQDs in general contain basic amino acid-rich domains responsible for mediating its microtubule association (section 1.9). However, IQD8 does not contain any transmembrane binding domain, which is known to mediate membrane association. It would be interesting in future to know how IQD8 associated with the membrane. Potential post-translational modifications such as lipid modifications (myristoylation and palmitoylation) or phosphoregulation might serve this function.

2.3.3 IQDs interaction with division site markers and its requirement for proper localization

Interactions of POKs and PHGAPs with IQD8 *in planta* and yeast and their phenotypic similarities to *iqd678* triple mutants further support joint functions of POKs, PHGAPs and IQD8 in the spatial control of cytokinesis. The requirement of IQDs for efficient recruitment of POKs and PHGAPs at the division site suggests a scaffolding function of IQD8 to sustain CDZ/CDS resident protein by their efficient retention. While the majority of cells in the *iqd678* triple mutants are impaired in PPB formation, still some cells form normal PPB. This explains

why YFP-POK1 recruitment is not completely abolished in *iqd678* triple mutants, but efficiency is reduced. Alternatively, such an event could be explained by the general affinity of IQDs to POKs, indicated by POKs interaction with all members of clade III. Similar to *iqd678*, *trm678* mutants also showed loss of PPB as well as reduced accumulation of POKs at the division site, suggesting that TRMs and IQDs function upstream of POKs and PHGAPs and likely function in a similar mechanism.

Reduced accumulation of PHGAPs at the division site of *iqd678* triple mutants is most likely due to loss of positional information (Figure 2.22). PHGAP accumulation at the CDZ/CDS also depends on functional POKs (Stöckle et al., 2016). This suggests a likely interplay of POKs and IQDs for the recruitment of division site markers such as PHGAPs. Phenotypic severity of *pok12iqd678* quintuple mutant compared to *pok12* further supports their synergistic action towards the positioning of cell walls (Figure 2.23). POKs and PHGAPs on the other hand tend to function in a feedback loop to maintain the broader localization pattern of IQD8 at CDZ/CDS (Figure 2.20), although corroborating evidence is still missing. PHGAPs might promote this by modification of the plasma membrane via regulation of ROP signaling (Feiguelman et al., 2018; Karahara et al., 2009; Stöckle et al., 2016). Furthermore, our result showed the tilted orientation of PPB in *iqd678* and *iqd8-1* same as *phgap12* double mutants, suggests a common function of IQDs and PHGAPs in division plane selection. The synergistic function of IQDs and PHGAPs is further supported by the enhancement of cell wall deviations in *iqd678phgap12* quintuple mutants compared to *iqd678* (Figure 2.24). Functional interdependency of IQDs and PHGAPs in mitotic cells is consistent with their mutual effects on the localization of each other in tobacco pavement cells (Figure 2.16F-J).

2.3.4 Conclusion and outlook

Persistent localization throughout cell division indicates multi-functionality of IQD8 during spatial control of cytokinesis. Our research indicated the potential function of IQD8 in division plane selection likely via association of PHGAP mediated ROP signaling. Together, IQD8 via its interaction with POKs potentially functions in the establishment of division planes when present at the division site. IQD8 via its dual localization at the plasma membrane and microtubules might also help in attachment of PPB microtubules at the division site. In addition, our research also suggests the potential function of IQD8 in timely, directed expansion of phragmoplast when it localizes to both phragmoplast microtubules and CDS, likely via microtubule-protein or protein-protein interactions. Various studies showed the mechanism of PPB formation, its establishment and maintenance. However, until now, the exact mechanisms of division plane selection and phragmoplast guidance are still largely

elusive. Pleiotropic effects of *iqd678* triple mutants together with persistent localization of IQD8 throughout the cell cycle suggests IQD8 as a potential candidate to answer open questions of spatial control of cytokinesis. Previous studies in our group established IQDs as the largest class of CaM target (Abel et al., 2005; Bürstenbinder et al., 2017). However, the direct roles of Ca²⁺ on *iqd678* phenotypes are not evident yet. It would be fascinating to uncover the role of Ca²⁺ in the regulation of cell wall position via IQDs. In conclusion, our results suggest that IQD8 may act as a scaffold to provide spatial information for PPB and CDZ components as well as for the timely and directed expansion of the phragmoplast towards the CDS via coordinating ROP and Ca²⁺ signaling at plasma membrane-microtubule continuum.

3 Characterization of KLCR interacting Arabidopsis kinesins

3.1 Introduction

Plants lack bonafide components of kinesin-1 complexes. Arabidopsis encode 61 kinesins and 3 KLCRs, but their function towards conventional kinesin-1 complex is unknown. Based on this information and the fact that IQDs recruits KLCRs/CMUs to microtubules, IQDs are proposed to assist in formation of KLCR-Kinesin complex and thus transport of cargoes.

3.1.1 KLCR as kinesin subunit

KLCR1, also called CMU1 interact with IQD1 in yeast as well as *in planta* (Bürstenbinder et al., 2013; Mukhtar et al., 2011). The Arabidopsis KLCR family consists of 3 members, which localize to microtubules (Liu et al., 2015). KLCRs are distantly related to human KLCs (Bürstenbinder et al., 2013; Liu et al., 2016). KLCs consist of an N-terminal heptad repeat domain which mediates dimerization and KHC binding, and a central to C-terminal domain with six TPR domains that facilitate cargo binding via protein-protein interaction (Grummt et al., 1998). The TPR domain consists of a 34 amino acid long minimally conserved domain that contains consensus motifs of W4 L7 G8 Y11 A20 F24 A27 P32. The positions of hydrophobic residues are conserved. Analysis of 3D structural data revealed that the consensus motif of TPR is often arranged in tandem arrays and forms 2 antiparallel α helices (Cervený et al., 2013; Das et al., 1998; Lamb et al., 1995). Three to sixteen tandem arrangements of TPR domains form a super helical structure with an amphipathic channel, which is associated with complementary region of the target proteins. The mouse KLC2 TPR domain interacts W-acidic domain of cargoes adapter (Yip et al., 2016). Based on the structural similarity to KLC subunits, KLCRs are predicted to function as potential subunits of plant kinesins (Bürstenbinder et al., 2013). KLCs exist in a dynamic conformational state via self-interaction and cargo binding. N-terminal to the TPR region of KLC2 from mouse contains a conserved Leucine-Phenylalanine-Proline (LFP) motif, which regulates its conformational change. The LFP motif is present in the highly divergent linker regions of all annotated KLCs from HomoloGene database. This short motif (residue167-169) is followed by Asn/Ser (N/S) and flanked by Asp/Glu (A/G). Structural analysis using intrinsic-disorder prediction tools, revealed that this region of the KLC2 is likely unstructured (Yip et al., 2016).

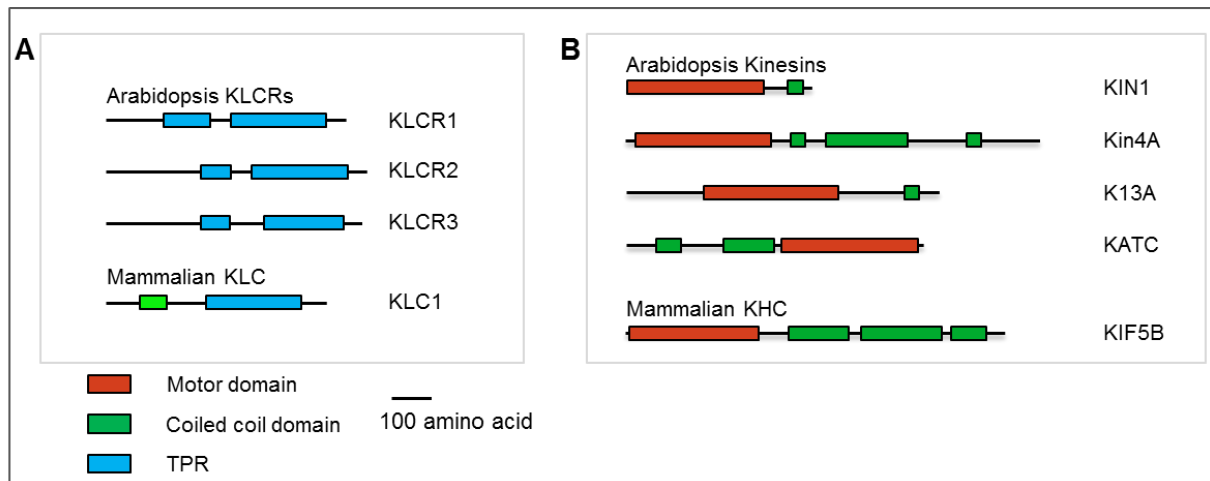


Figure 3.1 Comparison of Arabidopsis KLCRs and kinesins with KLCs and KHCs of mammalian kinesin-1 complex, respectively.

(A) Schematic diagrams showing domain arrangement of Arabidopsis KLCRs in comparison to mammalian KLCs. (B) Schematic representation of KHC of mammalian kinesin-1 complex. KIN represent the only type-1 kinesin from Arabidopsis. KIN4A, K13A and KATC represent N-terminal, internal and C-terminal motor domain containing kinesin, respectively. Red, Green and blue boxes represent motor domain, coiled-coil domain and TPR domain, respectively. KLC(R), KINESIN LIGHT CHAIN (RELATED); KHC, KINESIN HEAVY CHAIN; TPR, TETRATRICOPEPTIDE REPEAT.

Impairment of KLCR1 function leads to left-handed twisting of epidermal cell files in etiolated seedlings and changes in cell shape, as well as skewed roots (Liu et al., 2016), reminiscent of proteins with regulatory functions on microtubules such as *spr2* and *eb1b* (Bisgrove et al., 2008; Buschmann et al., 2004). Consistent with the phenotype, KLCR1, KLCR2 and KLCR3 localize to cortical microtubules at stable punctate structures. Microtubule localization was corroborated with *In vitro* binding assays which show direct binding of KLCR1 to microtubule subunits. In addition, microsomal membrane enrichment experiment showed enriched KLCR1 in the microsomal fraction (Liu et al., 2016). Consistent with this finding, proteomic study also showed the association of KLCR1 with the plasma membrane fractions (de Michele et al., 2016). During cell division, KLCR1 is associated with the PPB in a diffused manner and labels the cell plate. Localization studies of KLCR1 suggest a potential function at the plasma membrane-microtubule continuum. Consistently, a recent discovery showed that KLCRs/CMU help in lateral stabilization of microtubules at the plasma membrane and prevent the lateral drafting of microtubules, thereby providing stability to microtubules against pushing forces of cellulose synthase complexes. *k1cr1k1cr2* double mutants show a lateral displacement of cortical microtubules against the driving forces of CSCs and thus compromised the guidance of CSCs along microtubules. The increased sensitivity of *k1cr1k1cr2* double mutants to oryzalin treatment further indicates microtubule stabilizing functions of KLCRs (Liu et al., 2016).

3.1.2 Kinesins: microtubule localized motor proteins for trafficking of cargoes along microtubules.

Kinesins are microtubule-based motor proteins which are reported to function in unidirectional transport of cargoes along microtubules. Cargoes mainly include vesicles and proteins. Besides its function as molecular motor, kinesins also play roles in signals transduction, cell division and microtubule organization (Hirokawa et al., 2009; Pan et al., 2004; Reddy and Day, 2001). Kinesins were first identified in squid axoplasm (Amaratungas et al., 1993). Each heavy chain contains a conserved motor domain of 350 amino acids that is also termed as head, and a stalk region consisting of coiled-coil domains and a globular tail domain. The motor domain binds to microtubule and adenosine triphosphate (ATP). Hydrolysis of ATP leads to conformational changes which generate forces to mediate movement along microtubules (Vale and Fletterick, 1997; Zhu and Dixit, 2012). The stalk region is reported to mediate protein-protein interaction via its coiled-coil TPR domain and is involved in dimerization of two KHC polypeptides (Amaratungas et al., 1993; Reddy and Day, 2001). Both the stalk domain and the globular tail domain have been implicated in cargo binding. Most kinesins possess motor domains at their N-terminal region and C-terminal coiled-coil cargo binding domains (Reddy and Day, 2001). Between the head and stalk domain is a flexible neck region, which provides flexibility for conformational changes. The directionality of kinesin movement along microtubules, is primarily determined by the position of its motor domain. In general, N-terminal motor domain contributes to plus-end directed motility and C-terminal motor domains provide the minus end-directed movement along microtubules (Endow, 1999). The directionality of kinesin minus end directed motors is also provided by a consensus Gly/Asn (G/N) residue in the neck/motor core junction (Endow, 1999; Reddy and Day, 2001). Kinesins share 35 to 45% similarity in their motor domains but have little or no homology outside this domain (Vale and Fletterick, 1997).

In the absence of cargoes, kinesin-1 exists in a folded and inactive conformation, this state is called autoinhibition, which prevents unnecessary cycles of ATP hydrolysis. Autoinhibition is achieved via the intramolecular interaction, in which an Isoleucine-Alanine-Lysine (IAK) motif in the tail region of KHC combines with the motor dimer interface and thereby reduces the flexibility of the neck linker region. This conformational change prevents ATP hydrolysis (Dietrich et al., 2008; Friedman and Vale, 1999; Hackney et al., 2009; Hackney and Stock, 2000; Kaan et al., 2011; Wong et al., 2009). Binding of cargoes relieves the tail-mediated autoinhibition, which results in a fully extended conformation that allows ATP hydrolysis to accomplish (Blasius et al., 2007; Cai et al., 2007; Friedman and Vale, 1999; Hackney et al., 1992; Kawano et al., 2012). In addition, binding of KLCs to KHCs also contributes to the

regulation of autoinhibition, which has been corroborated in studies where disruption of the LFP motif from KLCs are shown to enhance ATPase activity of purified type1 Kinesin. In contrary, several studies delineate the direct role of KLCs in mediating auto inhibition (Kaan et al., 2011). *In vitro* pull-down experiments using recombinantly expressed proteins, revealed that C-terminal stalk domain of human kinesin-1 heavy chain is necessary and sufficient for the interaction with KLCs (Diefenbach et al., 1998). Kinesin-1 family members from animals and fungi are reported to play a role in long-distance transport of organelles and vesicles. Kinesin-1 interacting cargoes share a conserved W-acidic domain. Based on the similarity of the motor domain, only one type-1 kinesin has been annotated in Arabidopsis, the Arabidopsis KIN1, however, lacks the typical C-terminus involved in KLC interaction (Reddy and Day, 2001). AtKIN1 plays an important role in gametophyte development and nuclear division cycle (Wang et al., 2014). In addition, type-1 kinesin from rice has recently been reported to play a role in pollen fertility (Zhou et al., 2011).

In contrast to animals, plant kinesins are encoded by multiple genes, indicating diversity in kinesin functions during evolution. Multiple copies of kinesins in plants suggest other functions of kinesins besides its conventional function of microtubule-based transport of cargoes. This view is further supported by the fact that the plant lacks minus end-directed motors like dyneins. Concomitantly, plants possess some minus end-directed kinesins, possibly replacing the minus end-directed functions of animal dyneins in the plant kingdom (Richardson et al., 2006). There are 61 kinesin genes *A. thaliana* and 52 kinesin genes in *O. sativa* (Reddy and Day, 2001; Richardson et al., 2006). In *P. patens* 78 genes encode for kinesins (Shen et al., 2012). Based on sequence similarity and conservation of the motor domain, the kinesin superfamily has been divided into 14 subfamilies (Reddy and Day, 2001).

Discrepancies can be found within the plant kingdom when the predicted kinesin proteomes of ancient plants are compared. For example, kinesin-2, which is a key motor for intraflagellar transport, is present in *P. patens* but absent in angiosperms, consistent with the fact that mosses produce flagellated cells at the gametophytic stage of their life cycles. Besides, plants also lack most of the kinesins of kinesin-1 and kinesin-3 families (Hamada et al., 2014; Richardson et al., 2006). Kinesin-6 and Kinesin-10 are present in angiosperms but absent in the moss. But their functions are largely unknown in plants. In contrast, the kinesin-14 class is greatly expanded in plants with 21 members in *A. thaliana*, 19 in *O. sativa*, and 15 in *P. patens*. Besides, kinesin-14, kinesin-7, kinesin-2 families and ARMADILLO REPEAT-CONTAINING KINESINS (ARK) are more prominent in plants (Hamada et al., 2014; Richardson et al., 2006).

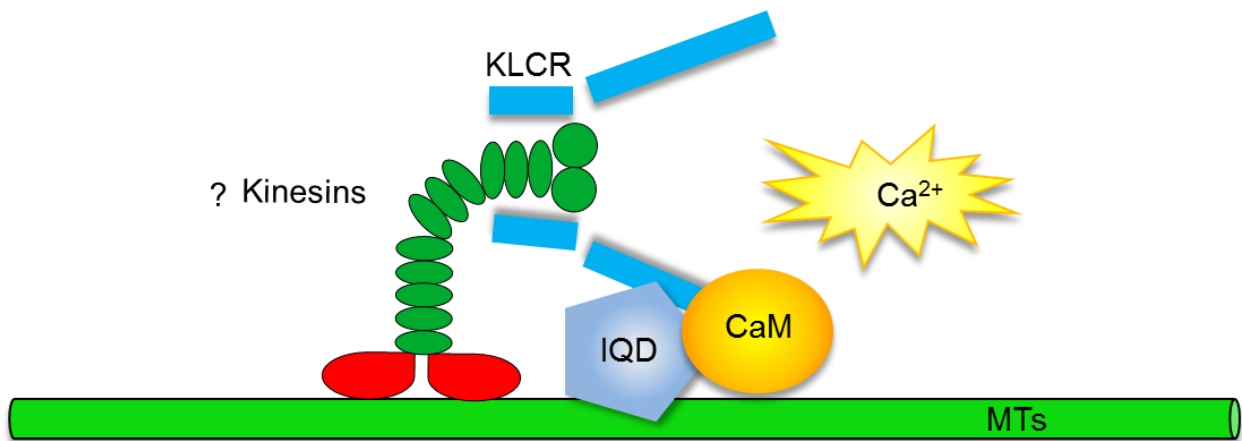


Figure 3.2 Working Model.

IQD proteins localize on microtubules and recruit KLCRs and CaM to various subcellular sites of IQDs. IQDs interact with CaM both in presence as well as in absence of Ca²⁺-CaM and thus modulate IQDs function via trasducing Ca²⁺ signaling information. Putative KHCs that may interact with KLCRs yet remain to determined. MT, microtubule; CaM, calmodulin; IQD, IQD67 DOMAIN; KLCR, KINESIN LIGHT CHAIN-RELATED. Modified from (Bürstenbinder et al., 2013).

3.2 Results

Since the discovery of plant kinesins in tobacco (Tiezzi et al., 1992), several genes encoding kinesin-like motor proteins have been annotated. Extended kinesins in plants possess a variety of microtubule-based cellular functions, such as cell division (Lee and Liu, 2000; Liu et al., 1996; Nishihama et al., 2002; Tanaka et al., 2004), deposition of cell wall materials (Oda and Fukuda, 2013; Zhong et al., 2002), morphogenesis (Reddy and Day, 2000) and organelles movements (Cai and Cresti, 2012). Many of the plant kinesins have evolved to perform plant-specific functions that is correlated with the evolution of plant-specific unique microtubule arrays and cell walls. However, nothing is known about conventional kinesins from plants. Genome-wide analyses have shown that there is only one possible KHC type kinesin member in Arabidopsis, named MAA21.110 encoded by the At3g63480 locus (Reddy and Day, 2001). Based on amino acid sequence similarity of motor domain, MAA21.110 is grouped into kinesin-1 family (Richardson et al., 2006), and we termed it here as KINESIN1 (KIN1). KIN1 is similar to animal KHCs only in their motor domains but lacks the binding domain for light chain (Reddy and Day, 2000). Nevertheless, the Arabidopsis genome encodes three KLC-related proteins with similarity to mammalian KLCs only in their C-terminal TPR domains (Bürstenbinder et al., 2013). To test whether Arabidopsis KLCRs also form type-1 complexes, we investigated the interaction between the Arabidopsis KLCRs and the selected kinesin candidates.

3.2.1 Selection of candidate kinesins

Because, of the only one type-1 kinesin in Arabidopsis, for the targeted interaction screen with KLCRs, we selected several candidate kinesins based on the structural similarity to mammalian KHCs, i.e., an N-terminal motor domain followed by a long stalk with coiled-coil and globular tail domains at the C-terminus (Figure 3.3). Additionally, we selected representative kinesins from each Arabidopsis kinesin family (Figure 3.3). These selected kinesins represent kinesin-4 [KIN4A, KINESIN4B (KIN4B), KINESIN4C (KIN4C)], kinesin-5 [*N. tabacum* KINESIN-RELATED PROTEIN (NtKRP)-like Arabidopsis kinesin (KRP125a)], kinesin-7 (ZCF125a), kinesin-12 (PAKRP1/PAKRP1L, T15B3, MAL21), kinesin-13 (K13A) and kinesin-14 family (KATC, KATD) of the phylogenetic tree (Lawrence et al., 2004; Zhu and Dixit, 2012) (Figure 3.3A). Based on the kinesin-related studies from the animal field (Stock et al., 1999) and our hypothesis, we assumed that the coiled-coil region of kinesins would be necessary and sufficient for the interaction assay with KLCRs. Also, most of the kinesins are encoded by big genes (12.5 kb-10.6 kb). Keeping these facts in mind, we cloned deleted motor domain (Δ MD) variants of kinesins to test their interaction with KLCRs (Figure 3.3A). Additionally, we cloned the full-length variants of the candidate kinesins and compared

their functions with Δ MD variants. For some of the selected candidates, the sets of full-length and its Δ MD variants are incomplete (Figure 3.3A, two columns on the right).

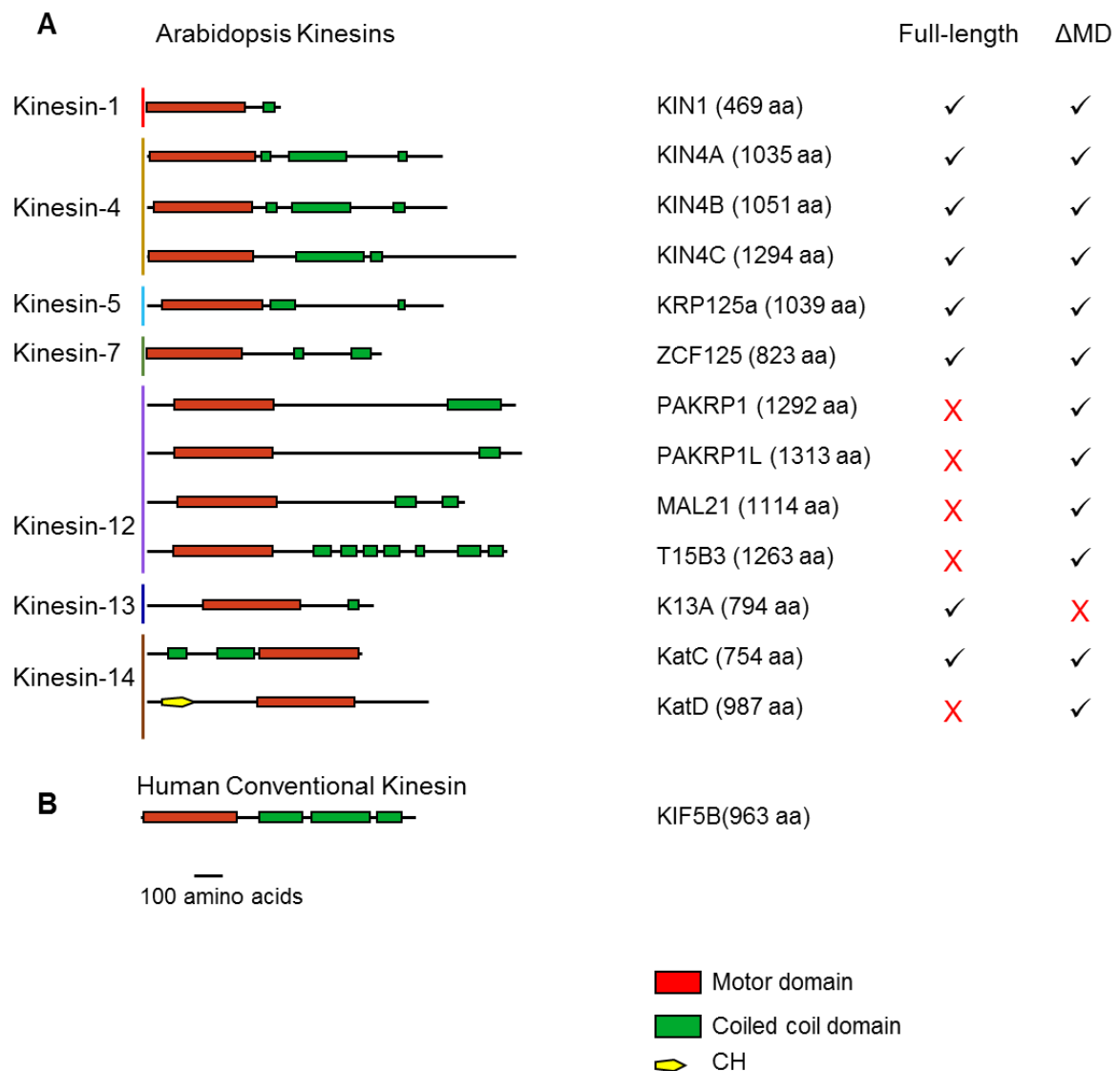


Figure 3.3 Domain architecture of Arabidopsis kinesins and their cloning status.

(A) Schematic representation showing the domain organization of selected Arabidopsis kinesin candidates. Motor and coiled coil domains are indicated in red and green color, respectively. Outside the motor domain, kinesins are diverse. Cloning status of selected kinesins are indicated in two rightmost columns. (B) Domain arrangement of mammalian kinesin, KIF5B. Second column indicates the sizes of kinesins. Vertical colored lines indicate the individual kinesin family included in the targeted interaction screen. CH, calponin homology domain.

3.2.2 Localization and interaction analysis of kinesin-1 protein

To gain insight into the cellular site of KIN1 function, we analyzed the subcellular localization of both the full-length protein as well as its Δ MD variants. For this, KIN1 variants were transiently transformed in the abaxial surface of *N. benthamiana* leaves. Detection was facilitated by expressing N-terminal YFP-tagged fusion of KIN1 variants under the control of

35S promoter. Both YFP-KIN1 as well as KIN1 Δ MD decorated network-like and punctate structures which are reminiscent of the Golgi network (Figure 3.4). To support this, we further co-expressed YFP-KIN1 with a mCherry-Golgi-specific marker protein (Figure 3.5). Upon co-expression, we indeed noticed a substantial overlap of YFP-KIN1 and mCherry-Golgi maker signals, indicating their co-localization. This suggests that KIN1 might be related to the motor functions involving the Golgi complex and likely helps in the correct spatial and temporal positioning of the Golgi complex. Kymograph analysis of YFP-KIN1-labeled punctate structures showed the movement of some of these structures, while others remained static (Figure S 14). In addition, YFP-KIN1 full-length and YFP-KIN1 Δ MD signals were also decorated nuclear membrane.

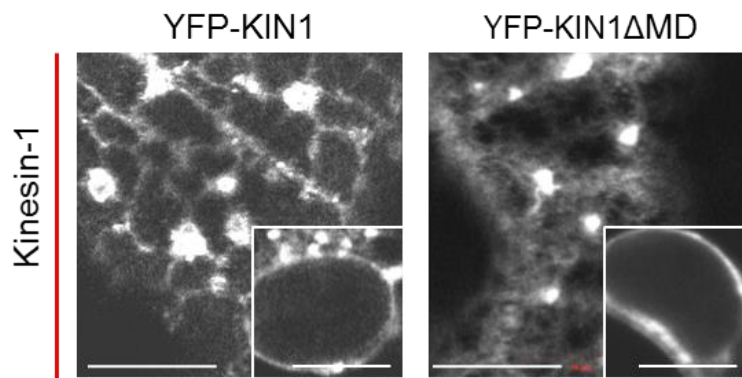


Figure 3.4 Subcellular localization of KIN1.

Confocal images of *N. benthamiana* leaves transiently expressing YFP-KIN1 and YFP-KIN1 Δ MD under the control of 35S promoter. Images are maximum projection of stacks (larger views) and single optical section (insets). Images were acquired 2 days after transient transformation. Images represent the results of two independent experiments. Scale bars, 10 μ m.

To further investigate whether KIN1 forms complexes with KLCRs, similar to what has been reported for kinesin-1 members from animals, we performed interaction assays of KIN1 with three KLCR isoforms via different experimental approaches. At first, we performed BiFC assays to test the interaction (Figure 3.6A). Constructs were generated using the vector series of Gehl et al. (2009). All constructs were N-terminal fusions of the N-terminal (Y_N) or C-terminal (Y_C) half of YFP. Y_N -KIN1 Δ MD was transiently co-expressed in *N. benthamiana* by infiltration with *A. tumefaciens* harboring the respective plasmids. The combination of Y_N -IQD1 and Y_C -KLCR1 was included as the positive control (Figure 3.6A; first row, first column) while the Y_N -WRKY21 and Y_C -KLCR1 combination served as the negative control (Figure 3.6A; first row, second column). Y_N -IQD1 and Y_C -KLCR1, the positive control, showed recovery of YFP fluorescence at microtubule lattices. Further fluorescence recovery was detected when Y_N -KIN1 Δ MD combined with Y_C -KLCR1 or Y_C -KLCR2, indicating the interaction of KIN1 Δ MD with KLCR1 and KLCR2 (Figure 3.6A; second row). No fluorescence

was detected in case of the negative control, demonstrating the specificity of the assay. All images were acquired with identical laser settings.

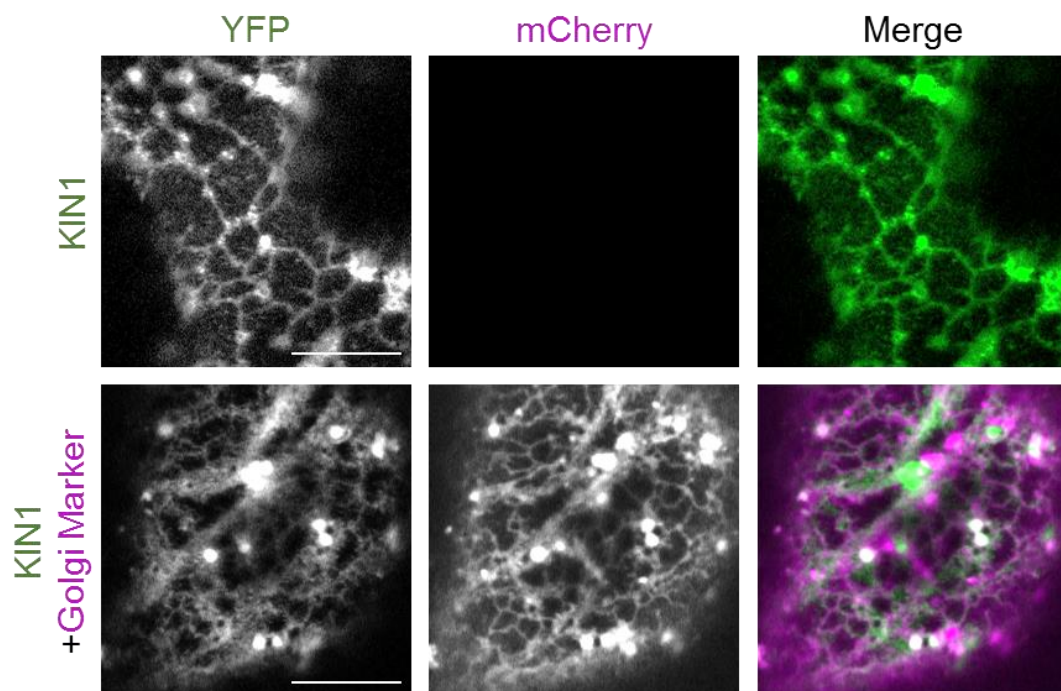


Figure 3.5 Co-localization of YFP-KIN1 with mCherry-Golgi marker.

Confocal image of *N. benthamiana* leaves transiently expressing YFP-KIN1 and mCherry-Golgi specific marker protein. First row shows localization pattern of YFP-KIN1 alone. Co-expression of YFP-KIN1 and mCherry-Golgi is visualized in the last row. YFP, mCherry and merge signals are shown in left, center and right column, respectively. Images are single optical sections and taken 2 days after transient transformation *N. benthamiana* leaves. Constructs were expressed under the control of 35S promoter. The representative experiment out of two independent experiments is shown. Scale bars, 10 μ m.

To further confirm the interaction via an independent experimental approach, we conducted Y2H assays of KIN1 Δ MD with KLCRs (Figure 3.6B). This analysis was performed by Anshu Khatri, a former master student at our lab. Kinesins were fused to the DNA binding domain (DBD) of GAL4 and tested against the activation domain (AD)-fusions of the three KLCRs. All constructs were generated as N-terminal fusions. Growth of yeast cells co-expressing particular combination of plasmids on vector selective (SD-TRP-LEU) and interaction selective (SD-HIS-TRP-LEU) media plates were used as the growth control and to assess the interaction of respective proteins, respectively. DBD-IQD1 and AD-KLCR1 combination was used as the positive control of the assay. Yeast cells co-expressing DBD-KIN1 Δ MD and AD-KLCRs did not show growth on interaction selective media, indicating the absence of interaction (Figure 3.6B). However, we did not further analyze the expression of DBD-KIN1 Δ MD and AD-KLCRs in yeast, this might explain the absence of detectable interactions.

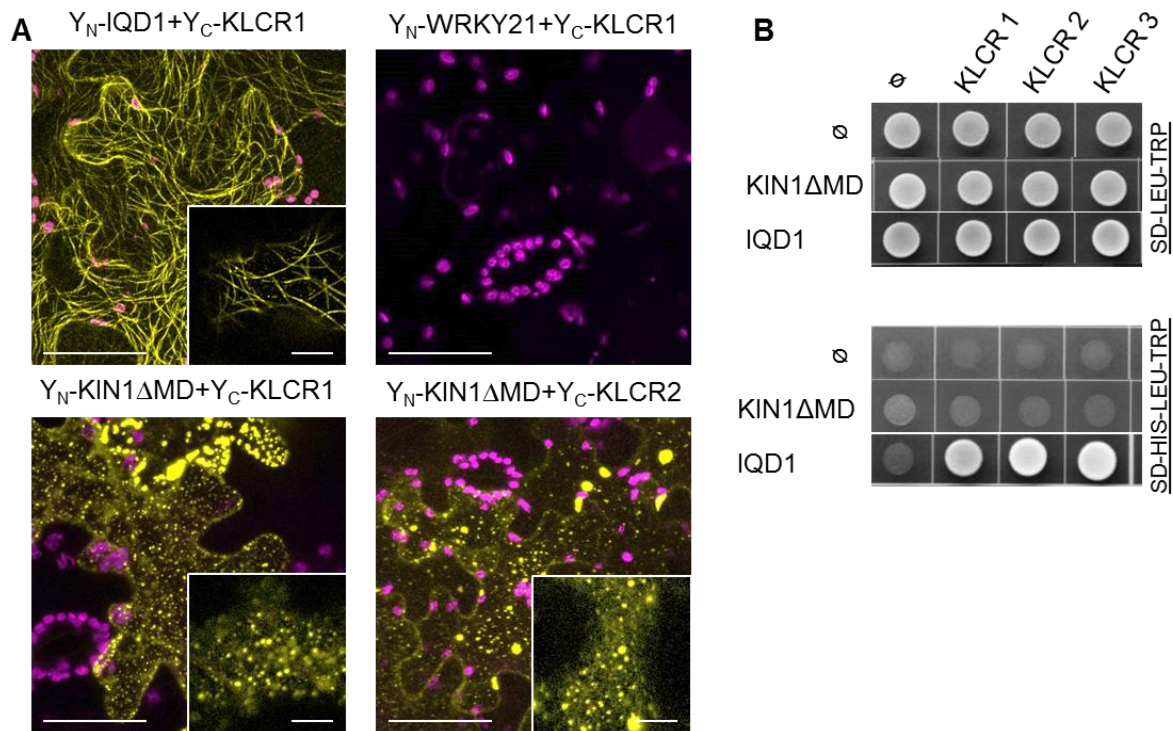


Figure 3.6 Interaction assays between KIN1 and KLCRs.

(A) BiFC assay showing interaction of AtKIN1 and Arabidopsis KLCRs. Analysis were done 2 days after transient transformation of *N. benthamiana* leaves. Scale bars, 50 μ m (Overview) and 10 μ m (inset). Analysis was performed only ones. (B) AtKIN1-KLCRs interaction assay in Y2H system. Top: 3-day-old control plate showing growth of transformed yeast cells on vector selective media (SD-LEU-TRP); Bottom: growth of transformed yeast cells on 3-day-old interaction selective media (SD-HIS-LEU-TRP). The representative experiment out of two independent experiments is shown.

Additionally, the interaction was tested in a transient co-expression assay in *N. benthamiana* leaves via infiltration with *Agrobacterium* harboring the respective plasmids. We co-expressed YFP-KIN1 Δ MD along with only RFP-KLCR1 as well as in combination with untagged IQD1 (Figure 3.7). When KLCR1 was expressed under the 35S promoter, it accumulated in the cytosol (data not shown), consistent with what has been shown previously (Bürstenbinder et al., 2013). Upon co-expression with YFP-KIN1 Δ MD, which localized on Golgi bodies and network-like structures (Figure 3.7, upper row), we did not observe re-localization of RFP-KLCR1 (Figure 3.7, middle row). In the third combination, we also included untagged IQD1 expressed under the control of 35S promoter along with 35S:YFP-KIN1 Δ MD and 35S:RFP-KLCR1. As described previously, RFP-KLCR1 was recruited to microtubules and the nucleolus via untagged IQD1 (Bürstenbinder et al., 2013), which indicated the presence of IQD1 in the experimental system. Because YFP-KIN1 Δ MD alone localized to the Golgi, in the ideal case of kinesin-KLCR interaction, we expected the relocalization of KIN Δ MD to microtubules along with KLCR1.

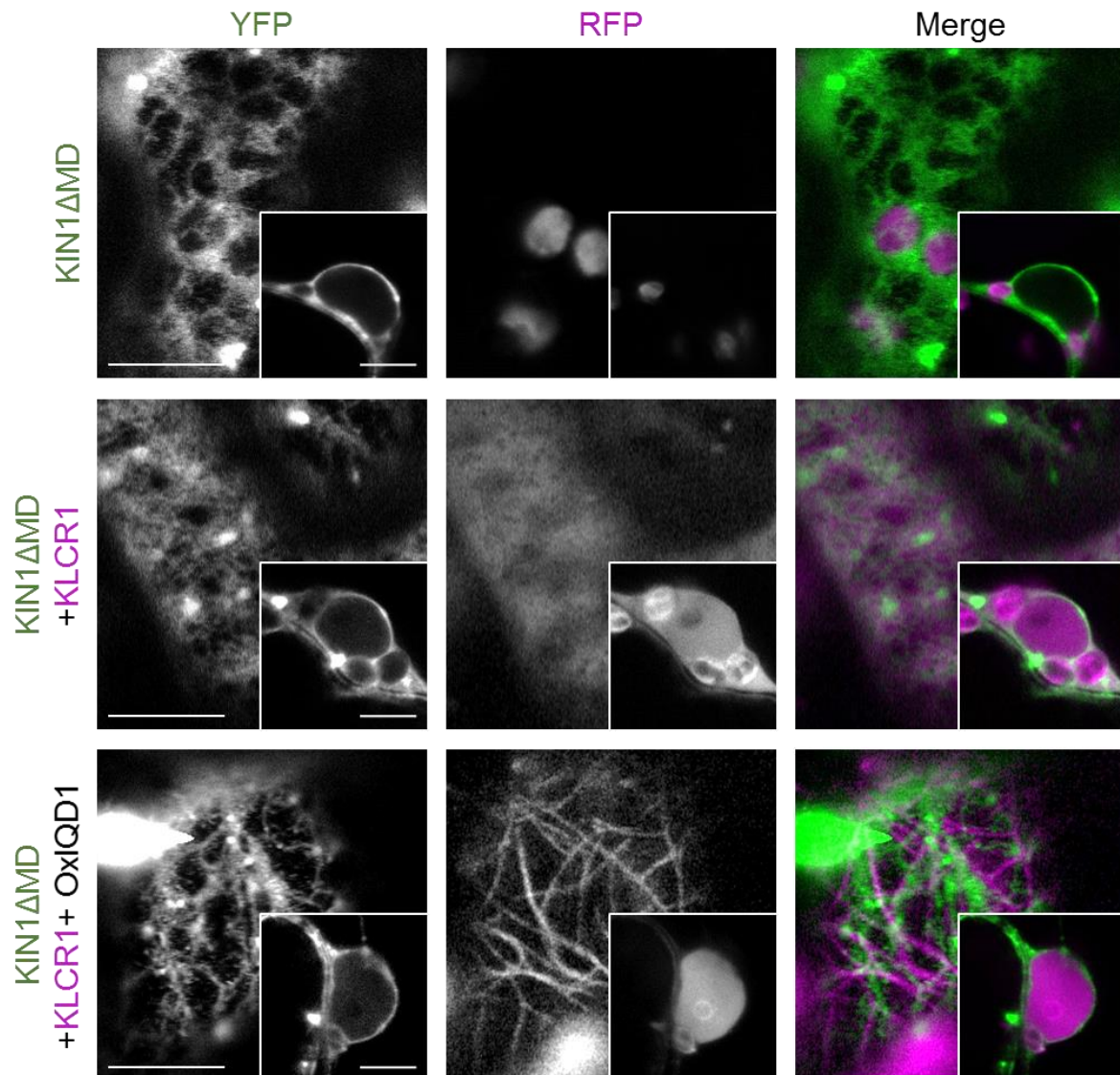


Figure 3.7 Co-localization of YFP-KIN1 with RFP-KLCR1 and untagged IQD1.

Confocal images of *N. benthamiana* leaf epidermal cells expressing YFP-KIN1 Δ MD alone (upper row), YFP-KIN1 Δ MD co-expressed only with RFP-KLCR1 (middle row) and together with untagged IQD1 (lower row). YFP, RFP, and merged signals are shown in left, center, and right column, respectively. Constructs were expressed under the control of 35S promoter and images were acquired 2 days after transformation. The representative experiment out of two independent experiments is shown. Scale bars, 10 μ m.

Contrary to what we anticipated, we did not observe the change in localization pattern of KIN1 Δ MD (Figure 3.7, lower row). Altogether, we did not notice KLCR1 interactions with KIN1 in co-expression assays. However, we could not exclude the influence of the over-expression of proteins on their original functions and localization. In addition to KIN1, we extended our analysis to a few other selected kinesins that represent other families of the kinesin superfamily. All further localization analysis and interaction assays were performed with similar experimental approaches as described in this section.

3.2.3 Localization and interaction analysis of kinesin-4 proteins

The second kinesin family included in our assay was the kinesin-4 family. Structurally, KIN4 proteins contain an N-terminal motor domain, followed by a long stalk domain consisting of coiled coils, and a C-terminal cargo-binding globular tail domain (Reddy and Day, 2001). In terms of structure and function, it is one of the well-characterized kinesin families. To investigate the potential function of kinesin-4 proteins as a subunit of hypothetical kinesins-KLCRs heterotetramer complexes, we first studied their subcellular localization by expressing the N-terminal YFP fusion of KIN4A/FRAGILE FIBER1(FRA1), KIN4B and KIN4C under the control of 35S promoter in *N. benthamiana* leaf epidermal cells (Figure 3.8).

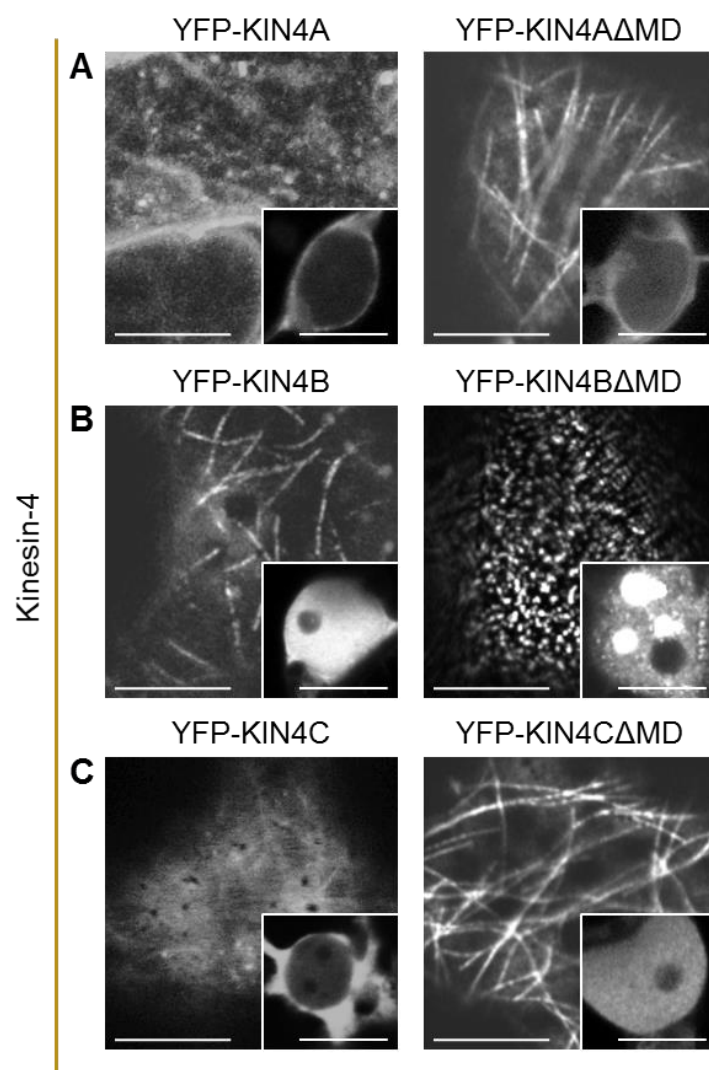


Figure 3.8 Localization of kinesin-4 proteins.

Confocal images of *N. benthamiana* leaf epidermal cells showing subcellular localization of YFP-KIN4 proteins. (A) localization of KIN4A variants; (B) localization of KIN4B variants; (C) Localization KIN4C variants. Images are maximum projection of Z-stacks (largerviews) and single optical sections (insets). All constructs were expressed under the control of 35S promoter. Images were acquired 2 days after transient transformation. The representative images out of three independent experiments were shown. Scale bars, 10 μ m.

YFP-KIN4A labeled punctate structures, resembling vesicles-like structures to the cortical microtubules (Figure 3.8A), which is consistent with what has been reported previously (Kong et al., 2015; Zhong et al., 2002; Zhu and Dixit, 2012). Similar to YFP-KIN4A, YFP-KIN4C also showed punctate labeling of cortical microtubule (Figure 3.8C), which further explains the functional redundancy of KIN4A and KIN4C in cortical microtubule mediated trafficking of non-cellulosic cell wall components (Kong et al., 2015; Zhu et al., 2015). Interestingly, YFP-KIN4A Δ MMD and YFP-KIN4C Δ MMD variants co-localized to microtubule strands (Figure 3.8A, C; right column), indicating the presence of second microtubule binding domain at the C-terminus of both KIN4A and KIN4C. The presence of two microtubule binding domains in KIN4A and KIN4C suggests their potential function in the crosslinking/bundling of microtubules. Besides microtubule bundling, the second microtubule binding domain in KIN4A and KIN4C, might help in their non-processive movement via microtubule sliding, in the absence of cargoes.

Intriguingly, Δ MMD of YFP-KIN4A and YFP-KIN4C showed uniform microtubule labeling pattern compared to its full-length variants. This may point to their domain-dependent differential regulatory function on microtubules. YFP fusion of the KIN4A and its Δ MMD variants also labeled the nuclear envelope (Figure 3.8A, insets). Upon co-expression with CFP-IQD1, YFP-KIN4A is recruited to the nucleolus (Figure S 15). IQD1 may assist the transcription factor activity of KIN4A, similar to what has been reported for rice and its animal homologue AtKIN4 proteins, which are known to regulate transcription in the nucleus (J. Li et al., 2011; Mazumdar and Misteli, 2005; Zhang et al., 2010). Similarly, YFP-KIN4C also localized to the nuclear membrane, however, YFP-KIN4C Δ MMD localized to the nucleus (Figure 3.8C, insets). Arabidopsis KIN4 proteins do not contain nuclear localization signals. Nuclear localization of KIN4C Δ MMD might be mediated via a cryptic nuclear localization signal or accumulation of YFP alone due to truncation of YFP-KIN4C Δ MMD.

In contrast to YFP-KIN4A and YFP-KIN4C, YFP-KIN4B decorated microtubule strands uniformly (Figure 3.8B), which might point to its unique and distinct function. Our data is in agreement with the previous report which demonstrates the structural and functional similarity of KIN4A and KIN4C but not KIN4B (Kong et al., 2015) Interestingly, YFP-KIN4B Δ MMD localized to punctate structures reminiscent of plasma membrane subdomains (Figure 3.8B, right column). Domain-dependent localization of KIN4B to microtubules and the plasma membrane, suggesting a potential function at the microtubule-plasma membrane junction. Consistently, *in silico* analysis using ATTED (Obayashi et al., 2018) revealed the co-expression of *KIN4B* and *REMORIN6.1* (*REM6.1*) (Figure 3.9), which is a plant-specific protein that accumulates in membrane microdomains (Jarsch et al., 2014). Co-expression is

frequently observed for the genes encoding proteins of functionally connected complexes (Spira et al., 2012). *In silico* expression data was further corroborated with transient co-expression analysis of YFP-KIN4BΔMD with mCherry-REM6.1 via transient transformation in *N. benthamiana* leaves.



Figure 3.9 Co-expression network.

In silico analysis using ATTED showing co-expression network for *KIN4B* (At3g50240) The thickness of lines connecting the circles refer to the relative strength of co-expression. Circle representing *KIN4B* (At3g50240) is marked with yellow color and circle representing *REM6.1* (At2g02170) is outlined by red color.

When KIN4BΔMD was expressed alone, it showed the anticipated punctate labeling pattern (Figure 3.10, upper row). Similarly, transient expression of mCherry-REM6.1 also showed the punctate labeling pattern, which is consistent with the previous report (Jarsch et al., 2014) (Figure 3.10, middle row). However, when both proteins were co-transfected, we observed a clear overlap of KIN4BΔMD and mCherry-REM6.1-labeled membrane microdomains (Figure 3.10, lower row). REM6.1-labeled microdomains are proposed to serve as the signaling platform (Jarsch et al., 2014; Malinsky et al., 2013; Raffaele et al., 2007). In most of the cases, proteins of the same membrane compartments perform similar functions (Spira et al., 2012). In the same way, co-existence of KIN4BΔMD and REM6.1-labeled microdomains might suggest the function KIN4B and REM6.1 together in the same signaling pathway.

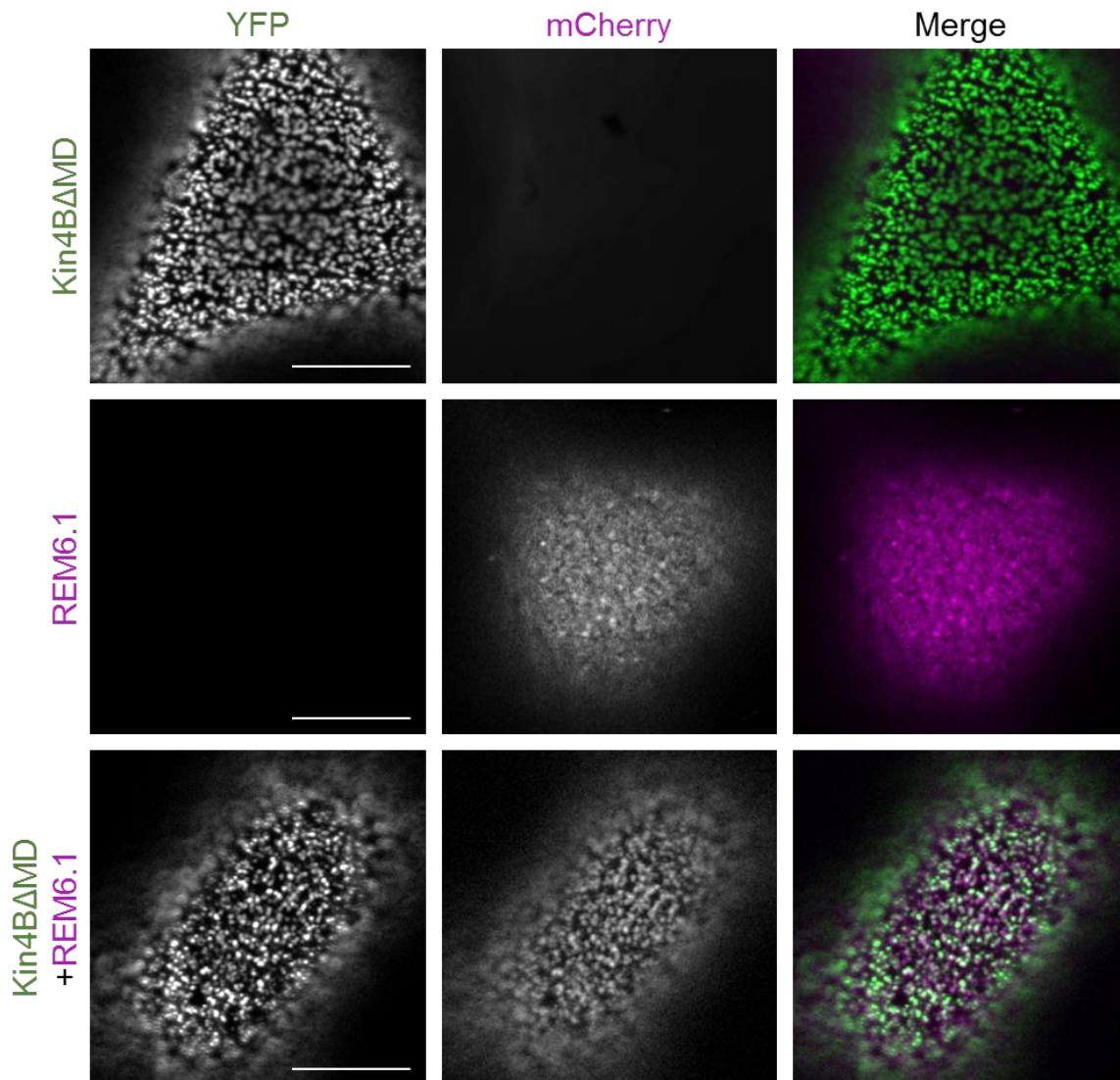


Figure 3.10 Co-localization of YFP-KIN4 Δ MD and plasma membrane localized mCherry-REM6.1.

Confocal laser scanning images showing single expressions of YFP-KIN4 Δ MD (upper row) and mCherry-REM6.1 (middle row) as well as their co-expression (Lower row) in *N. benthamiana* leaf epidermal cells. Images are single optical sections, representing the closeup views. Left column shows YFP signal, center column shows mCherry signal and right column shows merged images from both channels. Constructs were transformed transiently under the control of 35S promoter. Images were acquired 2 days after transient transformation. The representative experiment out of two independent experiments is shown. Scale bars, 10 μ m.

In addition, full-length YFP-KIN4B and YFP-KIN4B Δ MD localized to the nucleus and nuclear bodies, respectively. KIF4s of animals and rice BRITTLE CULM (OsBC12) also localize to the nucleus (Wang and Adler, 1995) and contain a bZIP motif, which is identified to have transcription factor activity (Aikin et al., 2008; Cheung et al., 2009). However, Arabidopsis KIN4 proteins do not contain any bZIP motif. Thereafter, we tested the interaction of KIN4

proteins with KLCRs via BiFC assays (Figure 3.11). All three members of the kinesin-4 family, KIN4A, KIN4B and KIN4C were tested against three Arabidopsis KLCRs. Y_N -KIN4A, Y_N -KIN4B and Y_N -KIN4C, each were co-transformed with Y_C -KLCRs in *N. benthamiana* leaves. Y_C -KLCR1 in combination with Y_N -IQD1 or Y_N -WRKY21 was used as the positive or negative control of the experiment, respectively.

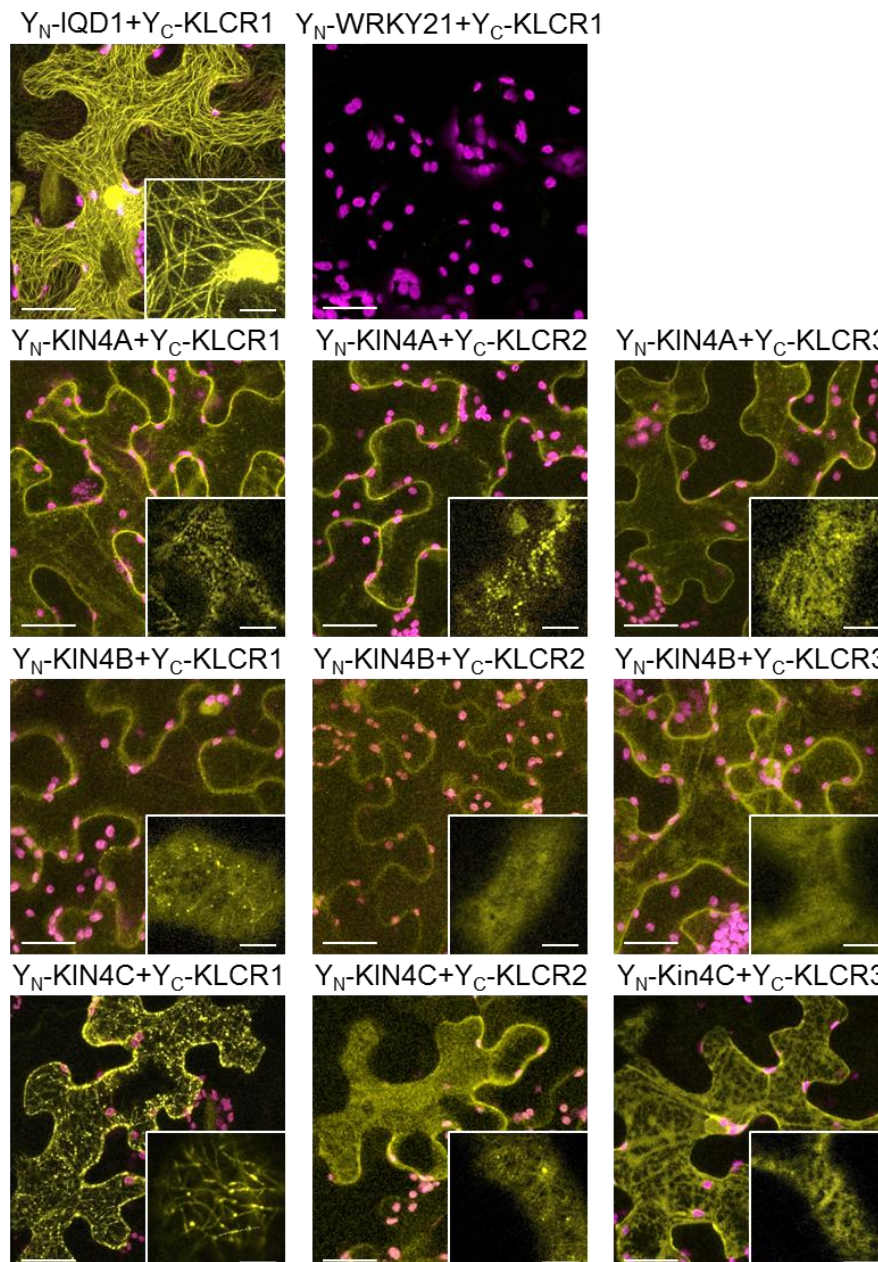


Figure 3.11 interaction analysis of kinesin-4 proteins with KLCRs via BiFC.

Confocal images of *N. benthamiana* leaves co-expressing constructs fused to N- and C-terminal halves of YFP. Recovery of fluorescence signal indicate interaction. Overviews, maximum projections of Z- stacks; insets, single optical sections. Images were acquired two days after transient co-transformation of the constructs. The representative experiment out of four independent experiments is shown. Scale bars, 50 μ m (overview image) and 10 μ m (inset images).

Recovery of YFP fluorescence was visible along microtubule lattice for the positive control (Y_N -IQD1 combination with Y_C -KLCR1) (Figure 3.11; first row, first column), suggesting the accuracy of the experimental setup. Similar to the positive control, fluorescence complementation was also observed upon co-expression of Y_N -KIN4A, Y_N -KIN4B and Y_N -KIN4C with Y_C -KLCRs (Y_C -KLCR1, Y_C -KLCR2 and Y_C -KLCR3), indicating interactions of KIN4A-C with KLCRs (Figure 3.11; inset images of second, third and fourth rows). Interactions were primarily observed on microtubules, and the pattern of interactions closely resembled the localization of corresponding KIN4 proteins. (Figure 3.11; inset images of the second, third and fourth row), which may suggest kinesins mediated recruitment of KLCRs to microtubules for the regulating potential functions of the KIN4s-KLCRs complexes. KIN4A and KIN4C interacted strongly with KLCR1, KLCR2 and KLCR3 compared to KIN4B interactions with KLCRs. Recovery of YFP fluorescence was not detectable in case of the negative control (Y_N -WRKY21 combination with Y_C -KLCR1), suggesting the specificity of the interactions (Figure 3.11; first row, second column).

We further verified this interaction in Y2H assays (Figure 3.12). For this assay, we used Δ MD variants of KIN4A, KIN4B and KIN4C. Kinesin and KLCRs were fused to DBD and AD of GAL4 transcription factor, respectively, and further transformed into competent yeast cells. Growth of yeast cells on vector-selective media (SD-LEU-TRP) was used to access the successful transformation of yeast cells (Figure 3.12A). Growth of yeast cells co-transformed with respective plasmids on interaction selective media (SD-HIS-LEU-TRP) was used to

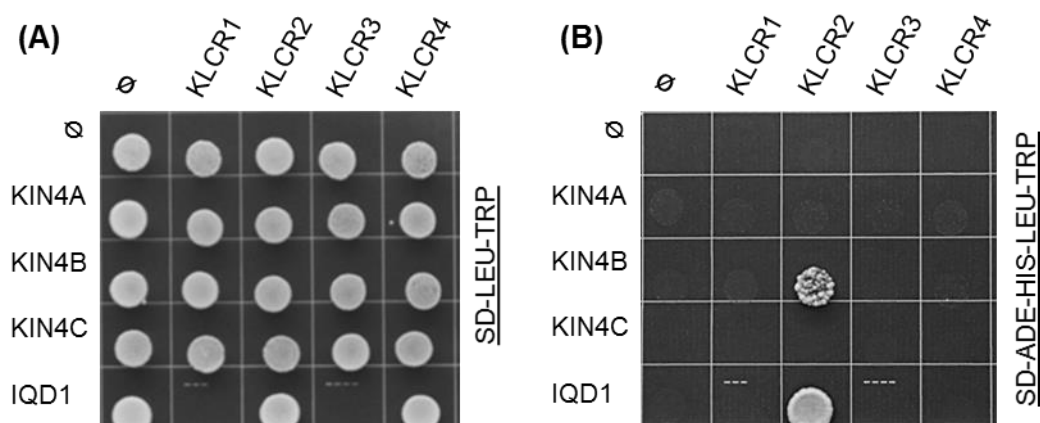


Figure 3.12 Y2H Interaction matrices of KIN4A-4C with KLCR1-3.

Y2H experiment testing for the physical interaction between KIN4A, KIN4B, and KIN4C and KLCR1, KLCR2 and KLCR3. DBD fusion of IQDs and AD fusion KLCRs were co-expressed in yeast cells. (A) Growth of yeast cells on vector selective media (SD-LEU-TRP) and (B) on high stringent media (SD-ADE-HIS-LEU-TRP). Interaction pattern was analyzed 6 days after spotting. SD-ADE-HIS-LEU-TRP, yeast media lacking adenine, leucine, tryptophan and histidine. The representative experiment out of two independent experiments is shown.

determine the protein-protein interaction. DBD-IQD1 interaction against AD-KLCRs was used as the positive controls of the Y2H assay. We did not observe the growth of yeast cells when transformed with DBD-KIN4A Δ MD or DBD-KIN4C Δ MD and AD-KLCRs. Only for DBD-KIN4B Δ MD and AD-KLCR2, we noticed weak growth of yeast, suggesting an interaction (Figure 3.12B). We observed unspecific growth of yeast cells on (SD-HIS-LEU-TRP) interaction selective triple drop out media, therefore we used high stringent (SD-ADE-HIS-LEU-TRP) quadruple drop out media to test for interactions. Absence of growth of yeast cells, when transformed with empty vectors, suggest the specificity of the interaction. The lack of interaction between KIN4A and KIN4C with KLCRs in yeast may suggest inefficient expression, and hence no conclusions can be drawn from the Y2H experiment for those two kinesins.

3.2.4 Localization and interaction analysis of kinesin-5 proteins

Kinesin-5 members from animal, yeast and plants are structurally conserved, suggesting their conserved function throughout the eukaryotes (Bannigan et al., 2007; Reddy and Day, 2001; Vanstraelen et al., 2006). This motivated us to include kinesin-5 members from Arabidopsis in our analysis. Kinesin-5 members possess an N-terminal motor domain followed by a long C-terminal domain consisting of a stalk domain and tail domain (Reddy and Day, 2001). We included Arabidopsis kinesin-5 member, KRP125a for the identification of KLCRs interacting kinesins.

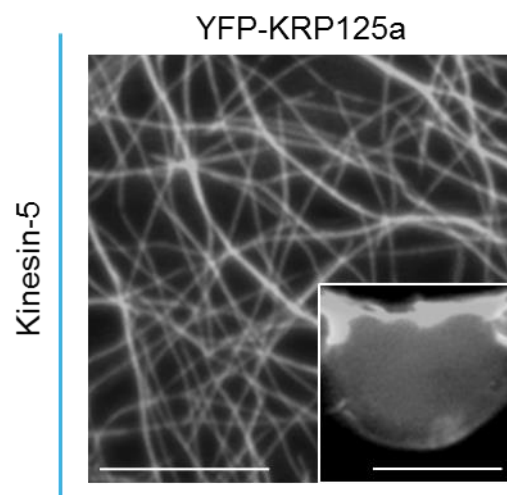


Figure 3.13 Subcellular localization of KRP125a.

Single optical section of *N. benthamiana* leaf epidermal cell showing localization of YFP-KRP125a. Constructs were expressed under the control of 35S promoter. Analysis was done 2 days after transient transformation. Large view, maximum projection of Z-stacks; inset, single optical section. The representative image out of three independent experiments is shown. Scale bars, 10 μ m.

We first studied the localization of KRP125a using *Agrobacterium*-mediated transient transformation of *N. benthamiana* leaf epidermal cells. An N-terminal YFP fusion of KRP125a

expressed under the control of 35S promoter was used to analyze subcellular localization. YFP-KRP125a decorated highly bundled microtubules in *N. benthamiana* interphase cells (Figure 3.13, largerview), suggesting its potential function in microtubule stability. In addition, YFP-KRP125a also showed weak accumulation in the nucleus as well as labeling of the nuclear membrane (Figure 3.13, inset). KRP125a is a homologue of tobacco-phragmoplast localized KRP protein and grouped into the BimC family along with three Arabidopsis kinesin-5 members, KRP125b, KRP125c and F16L2.60 as well as the tobacco and carrot homologues. Some of the BimC family members bind uniformly along the microtubules and are reported to play roles in crosslinking and sliding of antiparallel microtubules and thereby contribute to spindle pole separation and spindle assembly (Goldstein and Philp, 1999; Reddy and Day, 2001). In order to investigate its potential role as KHC of hypotheticalKHC-KLCR complex, we tested the interaction of KRP125a with KLCRs via different experimental approaches. First, we performed BiFC assay of Y_N -KRP125a with Y_C -KLCR1 and Y_C -KLCR2 (Figure 3.14). Combination of Y_C -KLCR1 and Y_N -IQD1 was used as a positive control of the assays. Fluorescence recovery was observed for the positive control, indicating the accuracy of the experimental setup. Similarly, YFP fluorescence recovery suggested the interaction of Y_N -KRP125a with Y_C -KLCR1 or Y_C -KLCR2 at microtubules lattices (Figure 3.14). The interaction pattern of KRP125a with KLCR1 and KLCR2 resembled more closely the localization of KRP125a.

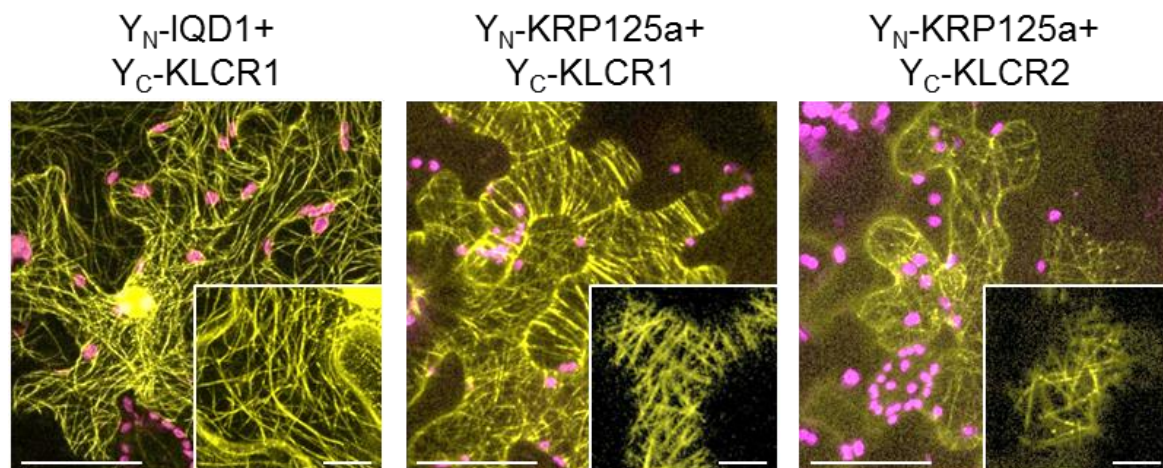


Figure 3.14 BiFC analysis of KRP125a with KLCR1 and KLCR2.

BiFC assay in *N. benthamiana* leaf epidermal cells transiently co-expressing KRP125a and KLCRs isoforms fused to N and C-terminal halves of YFP, respectively. Images are maximum projection of Z-stacks (overview) and single optical section (closeup view, inset). Images were acquired 2 days after transient co-transformation. Experiment was performed only once. Scale bars, 10 μ m (insets), 50 μ m (overviews).

To further confirm *in planta* interaction of KRP125a and KLCRs via BiFC assay, we performed co-recruitment assays of YFP-KRP125a with RFP-KLCR1 and RFP-KLCR2 using a transient expression system in *N. benthamiana* (Figure 3.15). Intriguingly, in the co-

recruitment assay, we noticed recruitment of KLCR2 from cytosol to microtubules along with YFP-KRP125a, suggesting the interaction between YFP-KRP125a and RFP-KLCR2 (Figure 3.15, second row). However, RFP-KLCR1 localization was unaffected upon co-expression with KRP125a (Figure 3.15, middle row), suggesting the specificity of the KRP125a and KLCR2 interaction.

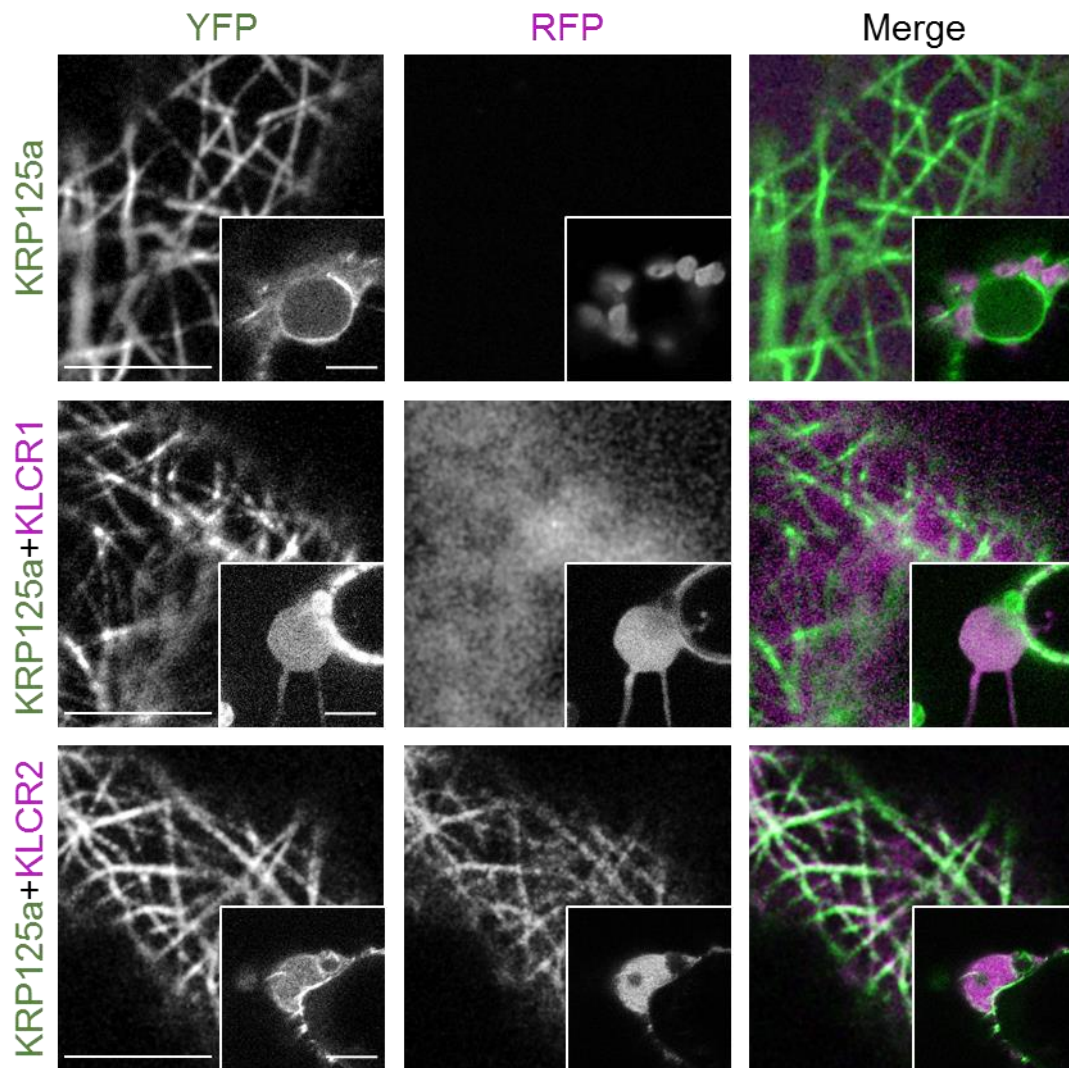


Figure 3.15 Co-expression of YFP-KRP125a with RFP-KLCRs *in planta*.

Confocal images of *N. benthamiana* leaf epidermal cells showing co-expression of YFP-KRP125a and RFP-KLCRs. Upper row represents the cells showing single expression of KRP125a, middle and lower rows represent the cells co-expressing KRP125a with KLCR1 or KLCR2, respectively. YFP, RFP merge signals are shown in left, center, and right column, respectively. Constructs were expressed under the control of 35S promoter and images were acquired 2 days after transient transformation. Experiment was performed only ones. Scale bars, 10 μ m.

3.2.5 Localization and interaction analysis of kinesin-7 proteins

Structurally kinesin-7 contains an N-terminal motor domain and a C-terminal coiled-coil domain including a long stalk and tail domain. The kinesin-7 family expanded extensively in plants and is anticipated to carry out the plant-specific functions (Reddy and Day, 2001).

Indeed HINKEL/NACK1 which is a member of kinesin-7 family functions during phragmoplast expansion via activation of MAPK signaling pathway at the phragmoplast (Komis et al., 2011; Nishihama et al., 2002; Strompen et al., 2002; Takahashi et al., 2010; Tanaka et al., 2004). However, some of the plants kinesin-7 members function in the processes that are normally attributed to this family, such as attachment of chromosomes to the spindle microtubules (Walczak and Heald, 2008).

We included ZCF125 as a representative member of the kinesin-7 family in our search for KLCRs-interacting candidate kinesins. Because the function of a protein depends on its localization in cells, we first analyzed the subcellular localization of ZCF125. We transiently expressed the N-terminal YFP fusion of ZCF125 under the control of 35S promoter in *N. benthamiana* leaves. ZCF125 labeled curved and fragmented microtubules (Figure 3.16, largerview). Such microtubule patterns have been reported in the case of microtubule depolymerizing proteins such as K13A (Moores and Milligan, 2006), suggesting a role of ZCF125 in microtubule depolymerization and thus may regulate the dynamics of microtubules. In addition, ZCF125 also localized to the nucleus (Figure 3.16, inset view). Functions of ZCF125 has not been reported until now.

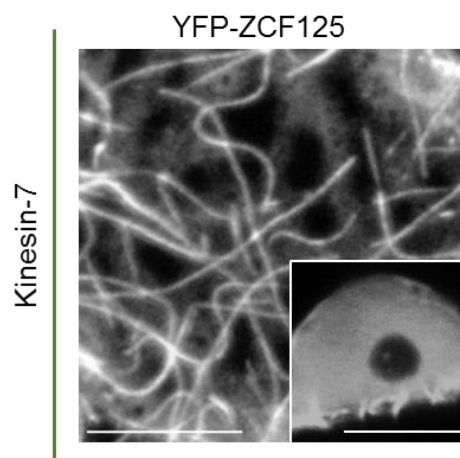


Figure 3.16 Subcellular localization of ZCF125.

Single optical section of *N. benthamiana* leaves transiently expressing ZCF125 under the control of 35S promoter. Images are maximum projection of Z-stacks (largerview) and single optical section (inset). Image was acquired 2 days after transient transformation, and represents result of at least three independent experiments. Scale bars, 10 μ m.

To investigate whether ZCF125 potentially serves as a heavy chain of Arabidopsis KLCRs, we tested the interaction of ZCF125 against KLCRs via BiFC assay, Y2H and co-recruitment assay. We first studied ZCF125 interaction with KLCR isoforms via BiFC assay (Figure 3.17A). The constructs fused to the N- and C-terminal halves of YFP were co-expressed using Agrobacterium-mediated transient transformation of *N. benthamiana* leaves. Fluorescence recovery of YFP signals was observed at microtubule lattices when Y_N-IQD1

was combined with Y_C-KLCR1 (Figure 3.17, first row) as well as for Y_N-ZCF125 and Y_C-KLCRs (Figure 3.17A, second and third row), indicating the interaction of the respective proteins. Combination of Y_N-IQD1 and Y_C-KLCR1 was used as the positive control. Further absence of fluorescence in case of the negative control combination (Y_N-WRKY21 combined with Y_C-KLCR1) (Figure 3.17, first row), suggesting the specificity of the assay. We also observed noticeable differences in the interaction pattern of ZCF125 with KLCR1 or KLCR2 or KLCR3 (Figure 3.17A; second and third row, inset views), which might suggest distinct functions of ZCF125 with different isoforms of KLCRs.

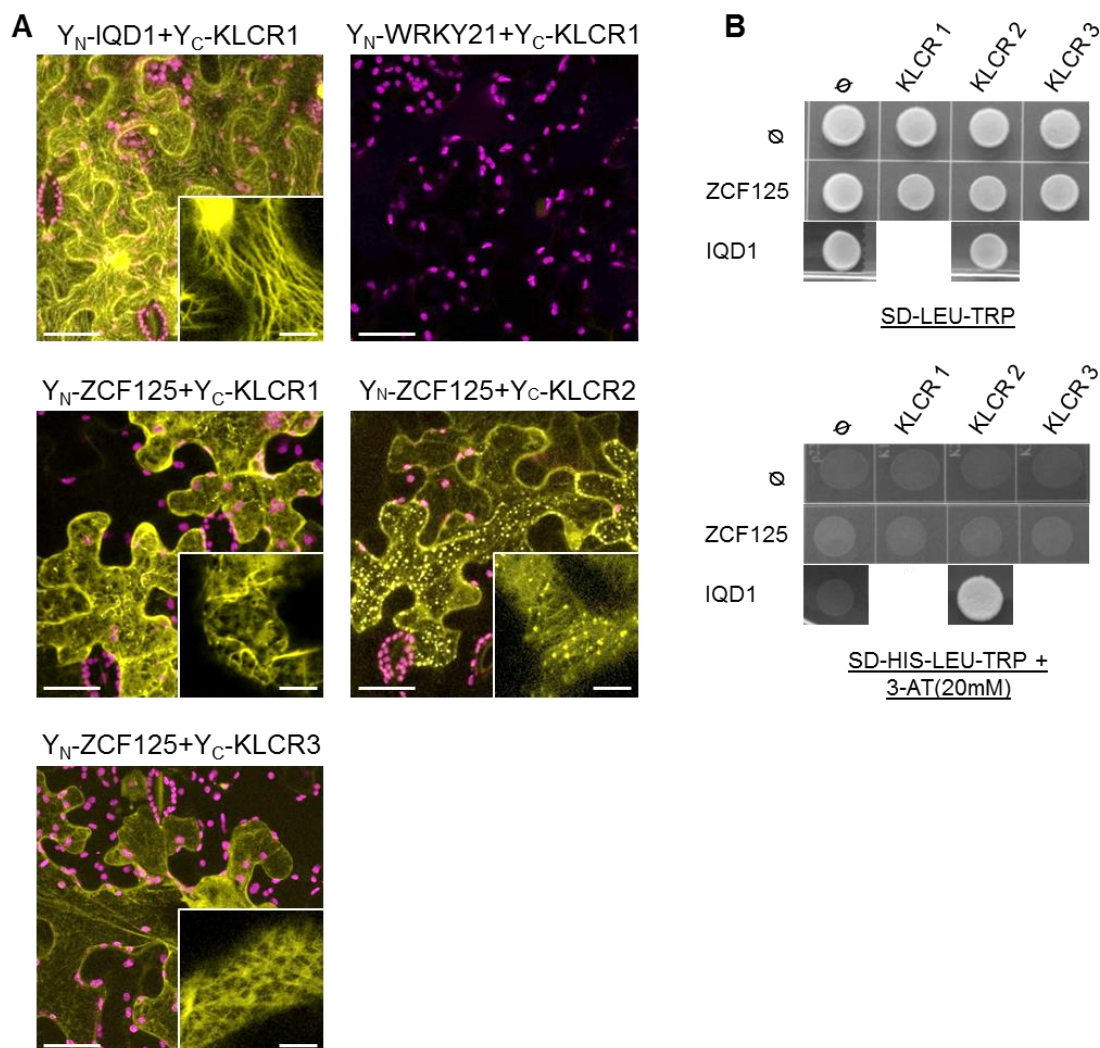


Figure 3.17 Interaction analysis of ZCF125 and KLCRs.

(A) Confocal images of *N. benthamiana* leaves co-expressing constructs fused to the N- and C-terminal halves of YFP. Overviews, maximum projections of Z-stacks; insets, single optical sections. Scale bars, 10 μ m (inset), 50 μ m (overview). Fluorescence signals were analyzed 2 days after transient transformation. The representative experiment out of three independent experiments is shown. (B) Y2H assays to show interaction of ZCF125 with KLCRs. Interaction was analyzed 3 days after spotting. Upper image: control plate showing growth of yeast cells on vector selective media (SD-LEU-TRP); lower images: growth of yeast cells on interaction selective media (SD-HIS-LEU-TRP). The representative experiment out of two independent experiments is shown. 3-AT, 3-amino-1, 2, 4-triazol.

To further validate the interaction via an independent experimental approach we performed Y2H assays (Figure 3.17). This analysis was performed by Anshu Khatri, a former master student in our lab. For this assay, ZCF125 was fused to DBD domain of GAL4 promoter and tested against KLCRs fused to AD (Figure 3.17B). DBD-ZCF125 was auto-activated and hence, we used 20 mM 3-AT in combination with selective media to observe the interaction. DBD-IQD1 interaction against AD-KLCRs was used as the positive controls of the Y2H assay. We did not observe the growth of the yeast cells when transformed with DBD-ZCF125 and AD-KLCRs on the interaction selective media (SD-HIS-LEU-TRP+ 20mM 3-AT) (Figure 3.17B), indicating the absence of detectable interaction. ZCF125 belongs to the plant-specific kinesins-7 family, and likely needs some plant-specific factors to perform its native function.

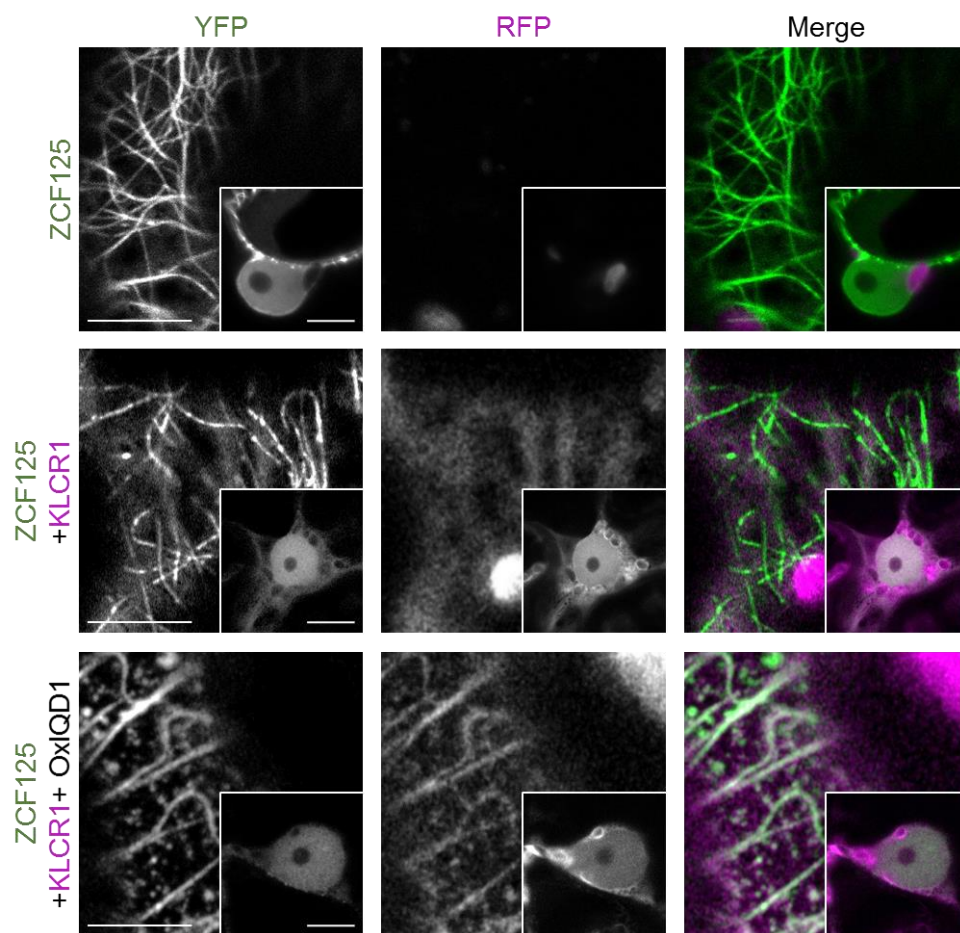


Figure 3.18 Co-localization study of YFP-ZCF125 with RFP-KLCR1 and untagged IQD1. Confocal images of *N. benthamiana* leaf epidermal cells expressing YFP-ZCF125, RFP-KLCR1 and untagged IQD1. Presence of untagged IQD1 was monitored via KLCR1 recruitment to microtubule strands. Upper row shows single expression of YFP-ZCF125, middle row represents co-expression of YFP-ZCF125 with RFP-KLCR1, and lower row represents co-expression of YFP-ZCF125 with RFP-KLCR1 in combination with untagged IQD1. YFP, RFP, and merge signals are shown in left, center, and right column, respectively. Constructs were expressed under the control of 35S promoter and images were acquired 2 days after transformation. Images are representative of at least three independent experiments. Scale bars, 10 μ m.

expression of RFP-KLCR1 with YFP-ZCF125, we did not notice any alteration in the localization of both proteins, RFP-KLCR1 remained cytosolic and ZCF125 remained associated with microtubules (Figure 3.18, middle row). When YFP-ZCF125 was co-expressed with RFP-KLCR1 in the presence of untagged IQD1, we observed re-localization of RFP-KLCR1 to microtubules which is likely mediated via IQD1 as has been described before (Bürstenbinder et al., 2013) (Figure 3.18, lower row). Nevertheless, we observed a noticeable difference in microtubule labeling pattern of ZCF125 compared to when it was expressed alone as well as along with KLCR1 (Figure 3.18, lower row). From the previous report, we know KLCR1 localizes to the nucleus, which upon co-expression with IQD1, recruited to the nucleolus (Bürstenbinder et al., 2013).

To test this, we further extended ZCF125 interaction with KLCR1 via co-recruitment assays (Figure 3.18). As described earlier, YFP-ZCF125 alone decorated microtubules (Figure 3.18, upper row). From previous research, it is known that KLCR1, when expressed under the control of 35S promoter, localizes to the cytoplasm (data not shown). However, when RFP-KLCR1 was co-expressed with untagged IQD1 along with YFP-ZCF125, we did not observe any further recruitment of RFP-KLCR1 to the nucleolus (Figure 3.18, inset images of lower row), which might suggest the possible interplay of ZCF125-IQD1-KLCR1 complex. The second possibility is that IQD1 may mediate the ZCF125 and KLCR1 interaction, which may plausibly interfere with IQD1-mediated nucleolar relocalization of KLCR1.

3.2.6 Localization and interaction analyses of kinesin-12, kinesin-13 and kinesin-14 proteins

Next, we included kinesin-12 members for our analysis. The kinesin-12 family is positioned near to kinesin-1 in the phylogenetic group and structurally resembles KHC of animal kinesin1 complex (Dagenbach, 2004; Reddy and Day, 2001), potentially suggesting their similar function. Kinesin-12 proteins contain an N-terminal motor domain which is followed by a C-terminal coiled-coil containing a stalk and a tail domain. Members of kinesin-12 are large in size and thus difficult to clone as full-length variants. Also, from the previous research, it is known that the C-terminal stalk and tail domain of KHC are sufficient to mediate interaction with KLC. Therefore, we only included PAKRP1 Δ MD, PAKRP1L Δ MD, T15B3 Δ MD and MAL21 Δ MD of kinesin-12 family for this analysis. With a similar approach as described above, we investigated the subcellular localization of kinesin-12 members as well as their interaction with KLCRs.

In the transient expression system of *N. benthamiana*, YFP-PAKRP1L Δ MD, YFP-T15B3 Δ MD, and YFP-MAL21 Δ MD showed predominant cytosolic localization. However, YFP-PAKRP1 Δ MD localized to microtubules which suggests the presence of a second microtubule binding domain (Figure 3.19A, largerviews), which possibly mediate the ATP-independent association to microtubule strands. The presence of a second microtubule binding domain may point to the roles of PAKRP1 in crosslinking, bundling or sliding of antiparallel microtubules. In addition, the selected kinesin-12 proteins localized to the nucleus (PAKRP1 Δ MD, PAKRP1L Δ MD), nucleolus (PAKRP1) and nuclear membrane (T15B3 Δ MD and MAL21 Δ MD) (Figure 3.19, inset images). However, their potential function in the nucleus yet needs to be determined. Out of our selected candidates from the kinesin-12 family, PAKRP1 and PAKRP1L are the most studied candidates. Both proteins decorate the plus ends of microtubules and are reported to maintain the length of the overlapping region in the phragmoplast midzone possibly by controlling microtubule dynamics at plus ends (Lee et al., 2007). Besides, N-terminal motor domain-containing kinesins, we also examined the localization and potential interaction of a few structurally distinct kinesins with KLCRs.

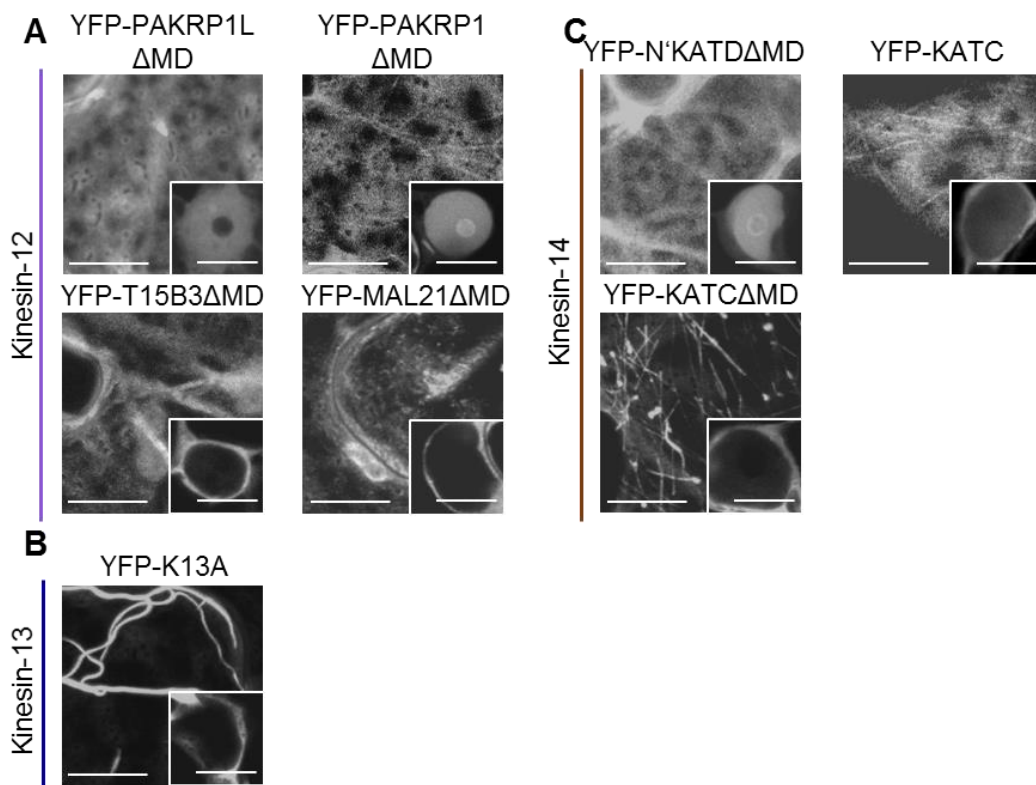


Figure 3.19 Distinct subcellular localization of kinesin-12, kinesin-13 and kinesin-14 proteins. (A) Confocal images of *N. benthamiana* leaves transiently expressing kinesin-12, (B) kinesin-13 protein and (C) kinesin-14 family proteins. Vertical colored lines indicate different phylogenetic clades. Constructs were expressed under the control of 35S promoter and images were acquired 2 days after transformation. Images are maximum projections of Z-stacks (largerviews) and single optical sections (insets). The representative images out of three independent experiments are shown. Scale bars, 10 μ m.

The K13A from kinesin-13 family (Lawrence et al., 2004; Reddy and Day, 2001) and KATC and KATD from kinesin-14 family (Frey et al., 2010; Lawrence et al., 2004; Reddy and Day, 2001) were used for the analysis. K13A and KATD are internal motor kinesins while KATC is the C-terminal motor domain-containing kinesin. C-terminal motor kinesins move along minus ends of the microtubules while internal motor domain-containing kinesins are primarily static (Reddy and Day, 2001). In transiently transfected *N. benthamiana* leaf epidermal cells, YFP-K13A labeled distorted and curved cortical microtubules (Figure 3.19B), suggesting a microtubule depolymerizing activity of K13A. The observed localization pattern of YFP-K13A is consistent with the previous report (Mucha et al., 2010). We used N-terminal KATD (N'KATD) Δ MD and both full-length as well as Δ MD KATC variants for the localization and interaction assays. For localization studies, N-terminal YFP-tagged fusion constructs were expressed under the control of 35S promoter in *N. benthamiana* leaf epidermal cells. YFP-N'KATD Δ MD showed a diffused expression pattern that is indicative of cytosolic localization (Figure 3.19C). Interestingly, YFP-KATC as well as YFP-KATC Δ MD variants, both localized to microtubules (Figure 3.19C), indicating the presence of second microtubule binding, which may also help in ATP-independent sliding along microtubules as well as bundling or crosslinking of microtubules.

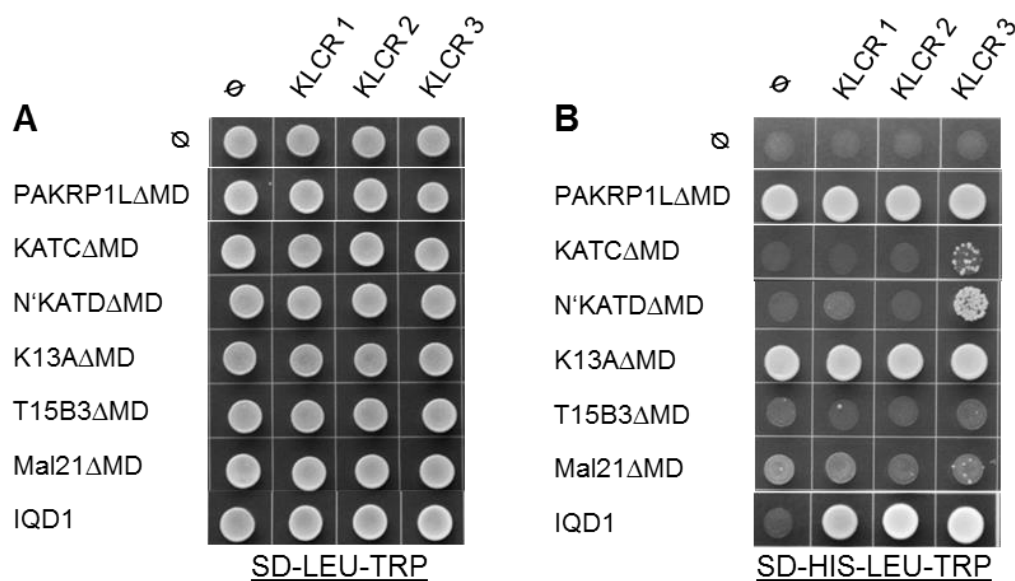


Figure 3.20 interaction matrices of kinesin-12, kinesin-13 and kinesin-14 proteins with KLCRs. Y2H assays to show interaction of DBD-Kinesins and AD-KLCRs. (A) Control plate showing growth of yeast cells co-transformed with plasmids of interests on vector selective media (SD-LEU-TRP). (B) Growth of yeast cell on interaction selective media (SD-HIS-LEU-TRP). Interaction was analyzed 3 days after spotting. SD-HIS-LEU-TRP, yeast media lacking histidine, leucine, and tryptophan. The representative experiment out of two independent experiments is shown.

We next, examined the interaction of selected kinesin candidates from kinesin-12, kinesin-13 and kinesin-14 family with KLCRs isoforms in Y2H assays (Figure 3.20). Kinesins and KLCRs were fused with DBD and AD domain of the GAL4 transcription factor. Yeast cells were grown on vector selective media (SD-LEU-TRP) and interaction selective media (SD-HIS-LEU-TRP) to access the growth control and to determine protein-protein interactions, respectively. DBD-IQD1 interaction against AD-KLCRs was used as the positive control. Except for the weak interaction for DBD-KATC Δ MD and DBD-N'KATDMD with AD-KLCR3, we did not observe the interaction of KLCRs with any other selected kinesins candidates of kinesin-12, kinesin-13 and kinesin-14 family (Figure 3.20). Other independent experimental approaches will be performed to confirm the interactions.

In summary, we could not verify the iterative interaction of KLCRs and kinesins in BiFC, Y2H and co-recruitment assays. In future, promising candidate kinesins will be cloned and expressed under the control of endogenous promoter to rule out the effect of ectopic expression on protein functions. Additionally, other potential candidates may be cloned in the future to test the possible interactions with KLCRs. Alternatively, we hypothesize that KLCRs might have different functions than being part of kinesin-KLCR complexes. This could be addressed with Co-IP followed by MS-MS to identify KLCRs interacting partners or other kinesins candidates via an untargeted approach.

3.3 Discussion

3.3.1 Regulation of kinesin-KLCR complex formation in Arabidopsis

In a targeted approach, we investigated the interaction of selected kinesin candidates with Arabidopsis KLCRs. Out of all interactions, KIN4s showed the most robust interaction with KLCRs isoforms both *in planta* and in yeast (Figure 3.11, Figure 3.12). Interaction sites of KIN4 proteins and KLCRs via BiFC resemble the native localization of KIN4 proteins, suggesting the recruitments of KLCRs to their native subcellular sites. KRP125a is the second kinesin candidate which showed promising interactions with KLCRs (Figure 3.14, Figure 3.15). When co-expressed in BiFC assays, KRP125a interacted strongly with KLCR1 and KLCR2. Similar to KIN4 proteins, KRP125a and KLCRs interaction patterns resembled their native localization, suggesting a KRP125a-mediated recruitment of KLCRs to its native localization site. Further *in planta* and *in vitro* experiments will be performed to prove these interactions.

In addition, ZCF125 also showed strong interaction with KLCR1, KLCR2 and KLCR3 in BiFC assays (Figure 3.17). The interaction of ZCF125a was stronger with KLCR1 compared to KLCR2 and KLCR3. Interestingly, we noticed a unique interaction pattern of different KLCRs isoforms with ZCF125, suggesting the differential function of ZCF125 and KLCRs complexes. The localization pattern of ZCF125 suggests its potential function as the depolymerizing kinesin. Upon co-expression of ZCF125 with KLCR1 in BiFC assay, we observed increased incidences of fragmented microtubules, suggesting that KLCR1 may help in the enhancement of ZCF125 functions. Nonetheless, to verify this, a microtubule marker protein must be included as an additional control in the co-expression experiment. Similarly, the pattern of interaction between ZCF125 and KLCR2 appeared noticeably different compared to that of KLCR1 and KLCR3.

Upon interaction of ZCF125 and KLCR2, YFP fluorescence signals were recovered on punctate-like structures, which resemble membrane microdomains. Membrane microdomains are reported to set the platforms for signal transduction (Lingwood and Simons, 2010; Malinsky et al., 2013). The similar localization pattern of ZCF125-KLCR2 complex suggests a potential function of the complex in signal transduction. In addition, the complex may function at the plasma membrane for the fusion of the cell wall material containing vesicles and/or may provide the lateral stability of the cortical microtubule against the pushing forces of CSCs, similar to what has been reported for KIN4A-KLCR1 complex (Ganguly et al., 2019). The Data from BiFC assay also revealed differential interaction patterns between ZCF125 and KLCR3 relative to KLCR1 and KLCR2. ZCF125-KLCR3

complex labeled microtubule uniformly, which may suggest the potential function of the complex in the stabilization, bundling or crosslinking of microtubules.

In addition, we also observed a tendency for ZCF125 to interact with KLCR1 in co-expression assay (Figure 3.18). In a few cells expressing YFP-ZCF125 and RFP-KLCR1, we found the co-recruitment of RFP-KLCRs from the cytosol to microtubules (data not shown). However, in the most of the cells, we observed a tendency towards slightly increased cytosolic accumulation of ZCF125 when interacting with KLCRs. This may be the result of KLCRs-mediated inactivation of kinesins and subsequent recruitment to the cytosol in the absence of cargoes. This further suggests the interaction of YFP-ZCF125 and RFP-KLCR1. The lack of strong and iterative KLCRs-kinesins interactions in our assays might be explained by a masking effect of overexpressed kinesins on their native localizations and functions. Secondly, it is possible that the kinesins we have selected may not be suitable candidates for interaction with KLCRs. Native KLCR-kinesin interaction might be affected by post-translational modifications of either of the proteins or both as has been described for KIN4A interactions with KLCR1 and KLCR2 (Ganguly et al., 2019), and similar factors might be missing in our experimental system.

In addition, MAPs crowding on microtubules might also explain the failure of co-recruitment of the complex to the microtubule (reviewed in Sabharwal and Koushika, 2019). In our assays, we only used kinesins expressed under the control of 35S promoter. The over-expression of kinesins may pose a roadblock for KLCR-kinesin co-recruitment. The absence and presence of cargoes control kinesin motility in plants. In the absence of cargoes, kinesins are inactivated by various mechanisms. One of the best described mechanisms is autoinhibition (reviewed in Adio et al., 2006; Verhey et al., 2011; Verhey and Hammond, 2009). This action prevents the loss of futile adenosine triphosphate. In the absence of cargoes, tail domains interact with the head domain in a folded conformation to make the kinesin inactive (Coy et al., 1999; Dietrich et al., 2008; Hackney et al., 2009; Wong et al., 2009). Hinge regions in the coiled-coil regions help in autoinhibition, probably by providing flexibility to the stalk domain (Verhey et al., 2011). Research have shown that the conserved QIAKPIRP motif in mouse kinesin-1 tail directly interacts with the motor domain and prevents release of ADP from the nucleotide pocket (Dietrich et al., 2008; Hackney and Stock, 2008). Another intramolecular mechanism of inactivation of kinesins includes the action of KLCs (Cai et al., 2007). According to one hypothesis, KLCs interact with the motor dimer interface and physically separate motor domains of kinesin complexes and thus interfere with their motor activity. It has been hypothesized that in the absence of cargoes, kinesin-1 holoenzyme (KHCs+KLCs) adopts an inactive state and is retained in the cytosol (Cai et al.,

2007). In contrast, another study showed that KLCs enhance the kinesin-1 activity via inhibiting the binding of kinesin tail to its head as well as to microtubules (Wong and Rice, 2010).

Also, it is challenging to detect motors by live-cell imaging, mainly when they are not concentrated at a particular site. Such deficiency is often compensated by expressing the proteins under the control of the constitutively active promoters. Caution should be taken when the results of such experiments are used to interpret the localization and function of a kinesin motors, as the over-expression may alter the general behavior of proteins (Hamada, 2014; Lee et al., 2015). Perhaps future technological advancements may help to detect plant kinesins when they are expressed under the control of native promoter or expressed at low but physiologically relevant expression levels. Although kinesin-1 heavy chains are generally considered to exist in a heterotetrameric complex with KLCs, it has been shown that KHC could function even in the absence of KLC. AtKIN1 is more closely related to fungal type 1 kinesins than to the animal counterpart (Reddy and Day, 2001). Further experimental data suggest that fungal kinesins do not have KLCs (Steinberg and Schliwa, 1995). The similarity in structure with fungal type-1 kinesins and the lack of KLCs may suggest a similar mode of action for Arabidopsis kinesins.

Besides these facts, we also observed direct or indirect interaction of KIN4A with IQD1 and IQD8 in the *N. benthamiana* and in the yeast system, respectively (Figure S 15, Figure S 12). Also, from previous research, we know that IQD1 recruits KLCR1 to microtubules in *N. benthamiana* leaf epidermal cells (Bürstenbinder et al., 2013). These observations suggest that IQDs may serve as scaffolds to bring together the KLCRs and the kinesins, where the complex may interact transiently for their regulation and function. This potential transient interaction may be below the level of detection, which may explain the failure to detect KLCRs-interacting kinesins in our experimental approaches. The role of Ca^{2+} in the regulation of kinesin activity and cargo binding has been evident in several studies (Vinogradova et al., 2009; Wang and Schwarz, 2009). Kinesin-1 activity is shown to be regulated by Ca^{2+} -binding protein MIRO, which interacts with kinesins via association with an adapter named Milton. Likewise, the intracellular motility of KCBP, a member of kinesin-14, is regulated by calcium signaling (Wang and Schwarz, 2009). Ca^{2+} -binding protein, CaM and KLC regulate the ATPase activity as well as microtubule binding affinity of KCBP (Deavours et al., 1998; Reddy et al., 2004; Vinogradova et al., 2009). These observations suggest that IQD might help to bring kinesin and KLCRs in the proximity of Ca^{2+} influx site, to promote the interaction and activity of the kinesin-KLCRs complexes. (Bürstenbinder et al., 2013).

3.3.2 Alternative functions of Arabidopsis KLCRs

Alternatively, KLCRs may have different functions than being part of kinesin complexes. The following observations support this view: First, the N-termini of KLCRs, which are supposed to mediate interaction with kinesins, lack coiled-coil domains that are essential for KHC binding in animal KLCs, and the N-termini have no significant sequence similarity. Second, analysis of GFP-KLCR dynamics in Arabidopsis and tobacco showed that KLCRs are not moving along microtubule tracks, but rather label microtubules stationary (Liu et al., 2016). Consistently, KLCR1 protein is reported to function in providing lateral stability of cortical microtubules against the counter balancing force of CSCs. Microtubule-related phenotypes such as organ twisting and pavement cell shape defect in *klcr1klcr2* double mutant suggest its function on microtubules to regulate plant growth (Liu et al., 2016). However, the precise mechanism has not been deciphered. In addition, Mukhtar et al. (2011) proposed the role of KLCR2 in plant defense. It has been experimentally shown that the impairment of KLCR2 functions leads to increased susceptibility to pathogen infection. This suggests the potential role of KLCR2 as a target of effector proteins and thus is required for immune system function, potentially via regulation of microtubule-based functions.

3.3.3 Potential novel functions of kinesin motor proteins in plants

Most of the kinesins, which we included in our studies, were found to be associated with microtubules, suggesting the microtubule-based motor function of these kinesins. However, microtubule localization patterns are highly diverse ranging from dot-like structures on cortical microtubules such as KIN4 family members, to uniform labeling of microtubule as in the case of ZCF125, K13A, KRP125a, PAKRP1 Δ MD and KATC. Diverse localization of these kinesins is consistent with heterogeneity in the proposed functions of plant kinesins. The function of some of our candidate kinesins is unknown. Kinesins are known to play roles in the regulation of microtubule polymer dynamics and crosslinking and bundling of microtubules. Kinesins also regulate directional transport of cargoes or coordination of other cellular components such as actin or attachment to chromosomes.

Data from our localization studies suggested the presence of two microtubule binding domains in KIN4A and KIN4C (Figure 3.8A, C), suggesting their potential function in crosslinking/bundling or sliding of antiparallel microtubules. Similarly, kinesins like *A. thaliana* plants lacking a kinesin-14 (ATK5), KCBP also possess a second ATP-independent microtubule binding domain and are reported to play a role in microtubule bundling (Kao et al., 2000). However, the *fra1/kin4a* mutant shows normal cortical microtubule organization (Zhong et al., 2002). This could be explained in the two possible ways: First, Arabidopsis

KIN4A proteins do not play essential roles in the organization of cortical microtubules; second, microtubule organization function of KIN4A is taken over by other functionally redundant kinesins.

We observed that PAKRP1L Δ MD localized to microtubules and conclude that PAKRP1L might possess an ATP-independent second microtubule binding domain (Figure 3.19B). The presence of a second microtubule binding domain in PAKRP1L suggests its potential role in microtubule crosslinking/bundling. It has been shown that PAKRP1L together with its closest homolog PAKRP1, plays a pivotal role in the formation of phragmoplast overlap during cytokinesis (Lee et al., 2007; Lee and Liu, 2000). However, the precise mechanism is not known. It is likely possible that PAKRP1L and PAKRP1 together help in the formation of phragmoplast midzone by crosslinking of antiparallel microtubule at the phragmoplast midzone via their second microtubule binding site outside the motor domain.

We also showed that both full-length as well as KATC Δ MD, localized to microtubules (Figure 3.19C). KATC belongs to the kinesin-14 family, which contains a C-terminal motor domain and possesses minus end-directed motility along microtubules (Reddy and Day, 2001). Our finding is consistent with the previous report (Jiang et al., 2007), which identified a second microtubule binding domain at the N-terminal tail domain of KATB and KATC. The presence of a second microtubule binding domain in KATC may suggest its possible roles in crosslinking as well as sliding of antiparallel microtubules. Our localization study also demonstrated the existence of a second microtubule binding domain in KATD (Figure 3.19C). KATD also belongs to the kinesin-14 family; however, unlike other members of the family, KATD contains an internal motor domain (Tamura et al., 1999). Although the function of KATD is unknown, the presence of second microtubule binding domain in KATD may suggest a potential function in crosslinking and bundling of microtubules. Kinesin-14 proteins are reported to play roles in the formation and functioning of spindle and PPB most likely via sliding of adjacent microtubules (reviewed in Zhu and Dixit, 2012).

In addition, KRP125a uniformly labeled highly bundled microtubules in interphase cells of *N. benthamiana* (Figure 3.13), which suggests the potential role of KRP125a in the bundling of microtubules, consistent with the proposed function of BimC family/kinesin-5 members to which it belongs (Goldstein and Philp, 1999). KRP125c, another member of the kinesin-5 family from *Arabidopsis*, also decorates interphase microtubules. In addition, AtKRP125c decorates mitotic microtubules and thus functions throughout the cell cycle (Bannigan et al., 2007; Li et al., 2015). Mutation in KRP125c causes disorganization of cortical microtubules at restrictive temperature, suggesting its role in microtubule stability (Bannigan et al., 2007).

Microtubule depolymerization experiments further confirm to the microtubule-based function of KRP125c in interphase cells (Bannigan et al., 2007). In addition, *KRP125a, b, c* all are upgraded during mitosis (Vanstraelen et al., 2006), suggesting their function during cell division. Impaired function of KRP125c leads to a massive disruption of the mitotic spindle. A similar function has been assigned to animal and fungal kinesin-5, suggesting the conserved function of the kinesin-5 families in the spindle assembly and dynamics throughout eukaryotes (Bannigan et al., 2007; Endow, 1999; Sawin and Mitchison, 1995). AtKRP125c activity is controlled via phosphorylation (Blangy et al., 1995). Because KRP125c is 69.7% identical to KRP125a in their motor domain, this may suggest the similar regulation of KRP125a function. Likewise, human kinesin-5, Eg5 is also regulated via cdc2-dependent phosphorylation of the motor domain during mitosis and possibly helps in specific locations to the spindle. These observations suggest the common regulatory mechanism for regulation of kinesin-5 members via posttranslational modifications.

Despite the similarity to KRP125c, loss of function analysis of *AtKRP125a*, *AtKRP125b* reveals normal interphase and mitotic structure, suggesting their independent function compared to KRP125c as well as their potential functional redundancy. Additionally, the microtubule patterns of KRP125a shows similarity to IQD5 (Mitra et al., 2019), which is shown to function in maintaining the jigsaw puzzle shape of Arabidopsis leaf epidermis cells. The similar localization pattern of KRP125a might suggest a potential function in controlling the cell shape. However, the precise biological function of KRP125a remains elusive.

Our research also revealed the potential depolymerizing activity of plant kinesins. Upon transient expression of ZCF125 in *N. benthamiana*, it decorated curved and fragmented microtubules (Figure 3.16), suggesting its potential function as depolymerizing kinesins. Similar to ZCF125, K13A also decorated curved and fragmented microtubules (Figure 3.19B), which is consistent with the earlier report (Mucha et al., 2010). K13A is shown to have depolymerizing activity both *in vivo* and *in vitro*, and might eventually determine the shape and function of plant cells (Mucha et al., 2010; Oda and Fukuda, 2013). K13A from animals has been shown to mediate depolymerization at both ends of microtubules, thereby regulating microtubule dynamics to control assembly of spindle and microtubule attachment to the kinetochore (Desai et al., 1999; Ems-McClung and Walczak, 2010; Moores and Milligan, 2006). In similarity to the animal system, Arabidopsis K13A upon co-expression with MICROTUBULE DEPLETION DOMAIN1 (MDD1) causes depolymerization of cortical microtubules in xylem cells, which suggest microtubule depolymerizing activity of K13A in plants. In addition, K13A also induces ATP-dependent depolymerization of *in vitro* synthesized microtubules (Oda and Fukuda, 2013). Another pair of kinesins proposed to

have such activities is ARK1 and ARK2. It has been shown that the defects in microtubule organization and root hairs and root cell file twisting in *ark1 and ark2* loss of function mutants, respectively, are recovered by the use of microtubule depolymerizing drug, suggesting microtubule depolymerizing activity of ARK kinesins (Jones et al., 2006; Sakai et al., 2008; Yang et al., 2007). ZCF125 might promote depolymerization of microtubule via similar mechanisms, however, nothing is known yet.

3.3.4 Roles of kinesins in organelles transport

Movement and positioning of organelles are essential to plant cell growth and regulation. The process requires the combined function of the cytoskeletal system and their associated proteins. Kinesin-1 from animalis known to play a role in long-distance transport of organelles (Goldstein and Philp, 1999; Verhey et al., 2011). Correct positioning of organelles is very important for cellular function. In plants, this function known for animal kinesin is primarily taken over by actin-myosin (Cai and Cresti, 2012; Peremyslov et al., 2008; Williamson, 1993, 1986). Plant kinesins have been hypothesized to mediate only local positioning of organelles and molecules. However, it is still possible that kinesins help in long-distance transport of organelles. Indeed, recent research accumulates the evidence for the possible function of these kinesins in long-distance transport of organelles such as nucleus, mitochondria, and chloroplast etc. Association of kinesins with various organelles, suggesting specialization of kinesins for cargo transport (reviewed in Cai and Cresti, 2012).

We found that the predicted type-1 kinesin from Arabidopsis localized to Golgi network-like structure which was further validated by the substantial overlap of YFP-KIN1 with mCherry-Golgi marker protein upon transient co-expression in *N. benthamiana* (Figure 3.5). Analysis of both full-length, as well as Δ MD variants of KIN1 indicated that the C-terminal fragment of KIN1 is sufficient for its Golgi localization (Figure 3.4). Golgi association of KIN1 suggests a potential role of KIN1 in linking microtubule motor function to Golgi. The Golgi apparatus is a vital organelle in the process of cellular secretion and thus uniform dispersal of Golgi-derived vesicles during early anaphase stage of cell division provides a simple way to ensure equal distribution of Golgi membranes into daughter cells (Herrington et al., 2017; Puthenveedu et al., 2006). Localization studies of KIN1 also suggest functions of KIN1 distinct from its animal homolog (Wang et al., 2014). Mutant analysis of *kin1* showed that KIN1 functions in the nuclear division during female gametogenesis (Wang et al., 2014), potentially via a targeted delivery of cargoes and signaling molecules to the plasma membrane.

Based on localization data and available information from the previous research, we postulate two possible roles of KIN1. First, KIN1 may act as a motor that functions in the distribution of Golgi apparatus in the cell cortex. Second, Myosin may play a role in long-distance transport of vesicles, and KIN1 only helps in the local distribution and positioning of Golgi. KIN1 is expressed throughout the tissue in the ovule and young anthers (Wang et al., 2014). The expression pattern correlates with the observed defect in *kin1-1* mutant during female gametogenesis. The reason why other tissues are not affected might be because the function of KIN1 could be shared by other kinesins in other cells. In point of fact, K13A, from kinesin-13 family also associated with the Golgi. Lu et al. (2005) showed that K13A decorates Golgi in various cells of Arabidopsis. K13A localizes on the margin of Golgi vesicles in root cap cells. Increase in the number of secretory vesicles in root cap peripheral cells is associated with increased secretory activity in these cells, which is needed for root growth in soil (Wei et al., 2009). Also, K13A has been reported to play an important role in the dispersion of Golgi stacks and budding Golgi-associated vesicles via interaction of K13A with RIP (Mucha et al., 2010). Impairment of K13A from cotton and Arabidopsis leads to the aggregation of Golgi stacks, which results in altered trichome morphology (Lu et al., 2005).

In addition to Golgi, plant kinesins are also associated with other organelles. Rice kinesin with a CAPOLIN HOMOLOGUE DOMAIN (OsKCH1) localizes to both poles of the nucleus and to filamentous structures that connect the nucleus to the cell periphery (Frey et al., 2010). Overexpression of OsKCH1 leads to delay in nuclear migration (Frey et al., 2010), suggesting its role in nuclear transport. Another kinesin-14 member, *Arabidopsis thaliana* KINESIN-LIKE PROTEIN (KP1) is associated with mitochondrial outer membrane protein, voltage-dependent anion channel-3 (VDAC3) (Ni et al., 2005), suggesting the role of AtKP1 in mitochondrial function. In addition, kinesins have also been reported in chloroplast movement and chloroplast-based activities (Suetsugu et al., 2010). KCA1, and KCA2 from the kinesin-14 family localize to chloroplasts and help in light-induced chloroplast movement as well as the attachment of chloroplast to the plasma membrane (Suetsugu et al., 2010), however, the precise mechanism is not known yet. Association of plant kinesins with various organelles suggests specialization of plant kinesins for cargo transport.

3.3.5 Roles of kinesins in plasma membrane-microtubule continuum.

Our data provide evidence for the plasma membrane localization of KIN4B Δ MD (Figure 3.8B). Punctate-like labeling of KIN4B Δ MD resembles membrane microdomain-like structure. Membrane microdomains are primarily the immobile compartment in the plasma membrane. Co-localization of YFP-KIN4B Δ MD with another membrane microdomain-localized protein,

mCherry-REM6.1, further confirmed localization of KIN4B Δ MD to plasma membrane microdomains (Figure 3.10). These microdomains are mainly immobile, and their stability depends upon cortical cytoskeletal elements (Kusumi et al., 2012; Malinsky et al., 2013). Interestingly, full-length variants of KIN4B localized to microtubules (Figure 3.8B), suggesting domain-specific regulation and a possible function of KIN4B at the plasma membrane-microtubule continuum for the formation of specific membrane microdomain. Each microdomains represent distinct compartments within the plasma membrane, constitute the specific composition, and perform a particular function. Microdomains are primarily reported to provide a signaling platform for the signal transduction during abiotic, biotic response and polarized growth (Jarsch et al., 2014; Malinsky et al., 2013). REM6.1 has been reported to function during pathogen infection as well as during various types of stresses such as cold stress and osmotic stress (Raffaele et al., 2007). Some reports also claim the function of REM6.1 as targets of bacterial effector proteins Extensive co-localization studies in yeast demonstrated that proteins of the same membrane likely perform similar functions (Spira et al., 2012). Based on this fact and data from our study, we hypothesize that KIN4B may function together with REM6.1 in the signaling process in response to pathogen infections, and abiotic stresses.

KIN4A/FRA1 decorates punctate like structures to cortical microtubules in the leaf epidermal cells of *N. benthamiana* (Figure 3.8A). Previous research has shown a role of KIN4A in transport non-cellulosic materials along the cortical microtubules and has also demonstrated that impaired function of which affects the orientation of cellulosic microfibrils without altering cortical microtubules organization (Kong et al., 2015; Zhong et al., 2002; Zhu et al., 2015). Similar to AtKIN4A, its rice homolog OsBC12, has been reported to function in the organization of cellulose microfibrils, suggesting the conserved function of kinesin-4 proteins from plants (J. Li et al., 2011; Zhang et al., 2010). Recent reports show the role of KIN4A in providing lateral stability of cortical microtubules against backwards pushing force of CSCs via promoting the association of KLCR1/CMU1 to cortical microtubules (Ganguly et al., 2019). The closely related member of this group, KIN4C is reported to function along with KIN4C in the transport of non-cellulosic material to the PM, indicated by the severe phenotype of *kin4akin4c* double mutant (Kong et al., 2015). However, until now, the molecular mechanism of only KIN4A function has been studied extensively. Consistent with the reported function, KIN4C also labeled the punctate structure to cortical microtubules, which resembled vesicle-like structures (Figure 3.8C). The similarity in the localization patterns of KIN4C and KIN4A suggests their similar functions in the regulation of cell wall composition. Localization information on KIN4B and KIN4C had not been reported yet in any of the previous studies, and nothing is known about the precise mechanism of KIN4B and

KIN4C functions. Our data might help to reveal the precise mechanism of cell wall material deposition by kinesin-4 family proteins in Arabidopsis.

3.3.6 The potential functions of kinesins in the nucleus

Kinesins are motor proteins, which possess the ability to bind microtubules and primarily function in microtubule-related processes (Miki et al., 2005; Zhu and Dixit, 2012). However, several reports have shown functions of kinesins at other subcellular sites such as the nucleus (Aikin et al., 2008; Cheung et al., 2009; Li et al., 2011; Wang and Adler, 1995; Zhang et al., 2010). In subcellular localization studies, we observed localization of several candidate kinesins in the nucleus, nucleolus and nuclear bodies. In parallel to their nuclear-specific localization, some of the kinesins also possess specific domains, indicating their potential nucleus-specific functions in the nucleus. ZCF125 localized in the nucleus (Figure 3.16), and its coiled-coil domains have been reported to overlap with basic leucine zipper domains (bZIP) (Reddy and Day, 2001). Leucine zipper domains are known to mediate dimerization (Hu and Sauer, 1992), and thus are likely involved in oligomerization of these kinesins. bZIP domains are also present in transcription factors (Hu and Sauer, 1992). Similarly, OsBC12, a homolog of Arabidopsis kinesin-4, also localizes to the nucleus and contains the bZIP motif. Consistently, OsBC12 also possesses transcription activity for the synthesis of the phytohormone Gibberellin (Li et al., 2011). Characterization of the transcription function of ZCF125 needs further investigations.

Arabidopsis KIN4A and KIN4C are recruited to the nucleolus via IQD1 (Figure S 15). IQD1 may promote transcription factor activity to KIN4A and KIN4C, similar to the transcription factor-like functions of OsBC12 and animal kinesins. In addition, KIN4B full-length and its Δ MD variant localized in the nucleus and nuclear speckles (Figure 3.8B), which further suggests a potential function of KIN4 family proteins in the nucleus. Nuclear speckles are interchromatin granules cluster, which is located in the nucleoplasm and contain mRNA splicing factors. Several studies have reported that transcription sites are often found at the periphery of the speckles and that the disassembly of speckles often affects coordination between transcription and pre-mRNA splicing (Spector and Lamond, 2011). The direct or indirect localization of KIN4 proteins and ZCF125, together with their localization on microtubules, may suggest their possible function in nuclear positioning. Similar to OsKCH1 and GhKCH2, which localize to the nucleus and nucleolus as well as in cytoplasmic microtubules and microfilaments (Frey et al., 2010; Xu et al., 2009) and through the coordinated activity of microtubules and microfilaments regulate positioning of the nucleus (Frey et al., 2010). However, nothing is known yet, and further experiments will be done to validate these hypotheses.

4 Materials and methods

4.1 Chemicals and other supplies

All chemicals were obtained from the following suppliers: BD Difco, Carl Roth, Clontech Laboratories, Duchefa Biochemie, Merck, Sigma-Aldrich and Serva Electrophoresis. Molecular biology supplies including RNA/DNA purification kits and kits for cloning, including Gateway cloning reactions, were obtained from Thermo Scientific and Qiagen. Primer synthesis and sequencing of vectors and PCR products were carried out by Eurofins Genomics.

Table 4-1 Bacterial strains used for the study

Bacterial strain	Genotype	Purpose
<i>Escherichia. Coli</i> (Top10)	F- <i>mcrA</i> Δ (<i>mrr-hsdRMS-mcrBC</i>) Φ80 <i>lacZ</i> ΔM15 Δ <i>lacX74 recA1 araD139</i> Δ (<i>araI</i>) 7697 <i>galU galK rpsL</i> (StrR) <i>endA1 nupG</i>	Cloning
GV3101	C58 (rif r) pMP90 (pTiC58DT-DNA)	BiFC assay
GV3101pK	C58 (rif r) pMP90RK (pTiC58DT-DNA)	Co-expression assay
PJ69-4a	<i>MATa leu2-3,112 ura3-52 trp1-901 his3 200gal4_gal80_GAL-ADE 2lys2::GAL1-HIS3 met2::GAL7-LacZ</i>	Y2H assays

Table 4-2 Vectors

Vector	Property	Resistance
pENTR/D-TOPO	ENTRY Vector	50 µg/mL Kanamycin
pDONR207	ENTRY Vector	25 µg/mL Gentamycin
pDONR221	ENTRY Vector	50 µg/mL Kanamycin
pENTR3C	ENTRY Vector	50 µg/mL Kanamycin
pDEST22	GAL4 AD	50 µg/mL Carbenicillin
pDEST32	GAL4 DBD	25 µg/mL Gentamycin
pB7WGF2	35S:GFP-GW	75 µg/mL Spectinomycin
pB7FWG2	35S:GW-GFP	75 µg/mL Spectinomycin
pB7WGC2	35S:CFP-GW	75 µg/mL Spectinomycin
pB7WGY2	35S-YFP-GW	75 µg/mL Spectinomycin
pB7WG2	35S-GW	75 µg/mL Spectinomycin
pJOG393	35S:mCherry-GW	75 µg/mL Spectinomycin
pB7FWG,O	no promoter GW-GFP	75 µg/mL Spectinomycin

pDEST VYNE (R)-GW	N-YFP BiFC vector	50 µg/mL Kanamycin
pDEST VYCE (R)-GW	C-YFP BiFC vector	50 µg/mL Kanamycin

Table 4-3 Primers used for cloning

Gene	Locus	Size in bp	Source of Cloning	Primer	5'→3' sequence
ZCF125	At1g59540	2472	cDNA	FWD	GGGGACAAGTTTGTACAAAAAAGCAGGCTT CATGGAAAAGATCTGTGTCGCA
				REV	GGGGACCACTTTGTACAAGAAAGCTGGGT CCTAAGGAGCTTTTGAGTTTGA
KRP125a	At2g37420	3120	cDNA	FWD	GGGGACAAGTTTGTACAAAAAAGCAGGCTT CATGTCGTTTACGCCAGAGGT
				REV	GGGGACCACTTTGTACAAGAAAGCTGGGT CTCATTGTTTACTTCCAAGAAT
KIN4A	At5g47820.1	5725	Genomic DNA	FWD	GGGGACAAGTTTGTACAAAAAAGCAGGCTT CATGGAATCTACGCCGCCA
				REV	GGGGACCACTTTGTACAAGAAAGCTGGGT CTTACATGATCTTATTAGGTAGA
KIN4A ΔMD		1977	cDNA	FWD	GGGGACAAGTTTGTACAAAAAAGCAGGCTT CATGGATCCTGTGTCTAG TGAG
KIN4B	At3g50240	5405	Genomic DNA	FWD	GGGGACAAGTTTGTACAAAAAAGCAGGCTT CATGGAATCACATTCTTCCTTAT
				REV	GGGGACCACTTTGTACAAGAAAGCTGGGT CTTAAGCACCTTGAACATTGA
Kn4B ΔMD		1995		FWD	GGGGACAAGTTTGTACAAAAAAGCAGGCTT CATGGACTTAATATGTTCTGAG
KIN4C	At5G60930.1	7114	Genomic DNA	FWD	GGGGACAAGTTTGTACAAAAAAGCAGGCTT CATGGAGAGCACAGAGTGCG
				REV	GGGGACCACTTTGTACAAGAAAGCTGGGT CTCAAACCTCAAACCTTAACT
Kin4C ΔMD		2976	cDNA	FWD	GGGGACAAGTTTGTACAAAAAAGCAGGCTT CATGGACCCAGCAACCGCAC
KIN1	At3g63480	2745	Genomic DNA	FWD	GGGGACAAGTTTGTACAAAAAAGCAGGCTT CATGTCTAACGTAACCGTCTG
				REV	GGGGACCACTTTGTACAAGAAAGCTGGGT CTTAGGACGTAAAGAACGATG
KATD	At5g27000	2964	cDNA	FWD	GGGGACAAGTTTGTACAAAAAAGCAGGCTT CATGGCGACGACATCGGAG
				REV	GGGGACCACTTTGTACAAGAAAGCTGGGT CTCATGTGCCTAACTCAGTC

Table 4-4 Primers used for genotyping

Locus	T-DNA/EMS lines	Primer	5'→3' sequence	Annealing temperature	Amplicon length (bp)	Reference
<i>IQD6</i> (At2g26180)	SALK_107689 .47.80.X (<i>iqd6-1</i>)	FWD (IQD015)	GGGTCAAGTCCA TTATCGGTC	55°C; 55°C	960; 580- 790	Preestablished in the lab
		REV (IQD014)	AAACAAGATTCC CGATTCCAGC			
		SALK_LP (REV) (A004)	ATTTTGCCGATTT CGGAAC			
<i>IQD7</i> (At1g17480)	SALK_025224 (<i>iqd7-1</i>)	FWD (IQD017)	CTTCAACAAGAAT CCAGGCTG	55°C;55°C	695; 650- 850	Preestablished in the lab
		REV (IQD014)	TACCAGTTCCAA CCAGGACTG			
		SALK_LP (REV) (A004)	ATTTTGCCGATTT CGGAAC			
<i>IQD8</i> (At1g72670)	SALK_137365 .54.75.X (<i>iqd8-1</i>)	FWD (IQD019)	TTTCAAATTTGAG CAAATGGG	55°C;55°C	860; 454- 654	Preestablished in the lab
		REV (IQD020)	TGATCAGATGGC TTCTCCAAC			
		SALK_LP (FWD) (A004)	ATTTTGCCGATTT CGGAAC			
<i>POK1</i> (At3g17360)	SALK_067862 (<i>pok1-1</i>)	FWD (IQD1738)	GTCACTGTCAGG TGCATAATTC	55°C;55°C	1791; 941	(Stöckle et al., 2016)
		REV (IQD1739)	TCACTAGTGAC CTCTATCATAG			
		LBa1 (REV) (IQD1740)	TGGTTCACGTAG TGGGCCATCG			
<i>POK2</i> (At3G19050)	<i>pok2-3</i> (F126)	FWD (IQD1741)	AAGTTTTGTTATT ATGGTACTTGCA GATAT	55°C	(28+122) EcoRI digestion of WT POK2 fragments	(Stöckle et al., 2016)
		REV (IQD 1742)	GTACCTGGTTTC GCAGAT			
<i>PHGAP1</i> (At5g12150)	WISCDXSLOX Hs135_04D (<i>phgap1-1</i>)	FWD (IQD1621)	TGGAATGGGAG TTGAACAAG	55°C;55°C	977; 300- 500	(Müller et al., 2006)
		REV (IQD1622)	GCCTCCAAGGGT CAAATTTAC			
		L4 (FWD) (IQD1757)	TGATCCATGTAG ATTTCCCGGACA TGAAG			
<i>PHGAP2</i> (At5g19390)	SALK_083351 (<i>phgap2-1</i>)	FWD (IQD1623)	AGAGAGTCGTAG CTCGGATCC	53.5°C;55°C	1171; 545-845	(Müller et al., 2006)
		REV (IQD1624)	TGGACCACTCTT GAAAACCTG			
		SALK_LP (FWD) (A004)	ATTTTGCCGATTT CGGAAC			

Table 4-5 Other primers used for confirmation of transgene

Constructs	Primer	Annealing temperature	Amplicon length
<i>pPHGAP2:GFP-PHGAP2</i>	GFP specific primer FWD (IQD551) REV (IQD552)	62°C	762
	GFP and gene specific primer FWD (IQDA038) REV (IQD1624)	62°C	187
<i>pPOK1:YFP-POK1</i>	YFP specific primer FWD (IQD551) REV (IQD552)	62°C	187
<i>pUB10:RFP-MBD</i>	MBD specific primer FWD (A017) REV (A018)	62°C	1254

Table 4-6 Expression clones used for this thesis work

Construct	Vector	Purpose	Reference
mCherry-POK1C	pJOG393	Localization and interaction study	Generated via LR reaction
mCherry-POK2C	pJOG393	Localization and interaction study	Generated via LR reaction
mCherry-PHGAP1C	pJOG393	Localization and interaction study	Generated via LR reaction
mCherry-PHGAP2	pJOG393	Localization and interaction study	Generated via LR reaction
mCherry-MAP65-3	pJOG393	Localization and interaction study	Generated via LR reaction
pIQD6:gIQD6-GFP	pB7FWG,0	<i>In planta</i> localization study	Available in the lab
pIQD7:gIQD7-GFP	pB7FWG,0	<i>In planta</i> localization study	Available in the lab
pIQD8:gIQD8-GFP	pB7FWG,0	<i>In planta</i> localization study	Available in the lab
pIQD8-gIQD8-mCherry	pJOG565	<i>In planta</i> localization study	Generated via LR reaction
p22-POK1C	pDEST22	Y2H	Generated via LR reaction
p22-POK1C	pDEST22	Y2H	Generated via LR reaction
p22-POK1C	pDEST22	Y2H	Generated via LR reaction
p22-POK1C	pDEST22	Y2H	Generated via LR reaction
P32-IQD6	pDEST32	Y2H	Available in the lab
P32-IQD7C	pDEST32	Y2H	Available in the lab
P32-IQD8C	pDEST32	Y2H	Available in the lab

Y _C -POK1	pDEST VYCE	BiFC	Generated via LR reaction
Y _N -POK2	pDEST VYCE	BiFC	Generated via LR reaction
Y _C -PHGAP1	pDEST VYCE	BiFC	Generated via LR reaction
Y _C -PHGAP2	pDEST VYCE	BiFC	Generated via LR reaction
Y _C -CaM2	pDEST VYCE	BiFC	Available in the lab
Y _N -IQD8	pDEST VYNE	BiFC	Available in the lab
GFP-IQD8	pB7WGF2	Localization and interaction study	Available in the lab
IQD8-GFP	pB7FWG2	Localization and interaction study	Available in the lab
GFP-IQD6	pB7WGF2	Localization and interaction study	Available in the lab
GFP-IQD7	pB7WGF2	Localization and interaction study	Available in the lab
YFP-KIN1	pB7WGY2	Localization and interaction study	Generated via LR reaction
YFP-KIN1ΔMD	pB7WGY2	Localization and interaction study	Generated via LR reaction
YFP-KIN4A	pB7WGY2	Localization and interaction study	Generated via LR reaction
YFP-KIN4BΔMD	pB7WGY2	Localization and interaction study	Generated via LR reaction
YFP-KIN4B	pB7WGY2	Localization and interaction study	Generated via LR reaction
YFP-KIN4C	pB7WGY2	Localization and interaction study	Generated via LR reaction
YFP-KIN4C	pB7WGY2	Localization and interaction study	Generated via LR reaction
YFP-KRP125a	pB7WGY2	Localization and interaction study	Generated via LR reaction
YFP-ZCF125	pB7WGY2	Localization and interaction study	Generated via LR reaction
YFP-PAKRP1	pB7WGY2	Localization and interaction study	Generated via LR reaction
YFP-PAKRP1L	pB7WGY2	Localization and interaction study	Generated via LR reaction
YFP-K13A	pB7WGY2	Localization and interaction study	Generated via LR reaction
YFP-KATC	pB7WGY2	Localization and interaction study	Generated via LR reaction
YFP-KATCΔMD	pB7WGY2	Localization and interaction study	Generated via LR reaction
YFP-KATD	pB7WGY2	Localization and interaction study	Generated via LR reaction
Y _N -KIN1ΔMD	pDEST VYNE	BiFC assay	Generated via LR reaction
Y _N -KIN4A	pDEST VYNE	BiFC assay	Generated via LR reaction
Y _N -KIN4B	pDEST VYNE	BiFC assay	Generated via LR reaction
Y _N -KIN4C	pDEST VYNE	BiFC assay	Generated via LR reaction
Y _N -KRP125a	pDEST VYNE	BiFC assay	Generated via LR reaction
Y _N -ZCF125	pDEST VYNE	BiFC assay	Generated via LR reaction
Y _N -WRKY21	pDEST VYNE	BiFC assay	Available in the lab
Y _C -KLCR1	pDEST VYCE	BiFC assay	Available in the lab
p22-KIN1ΔMD	pDEST22	Y2H	Available in the lab
p22-KIN4AΔMD	pDEST22	Y2H	Generated via LR reaction
p22-KIN4BΔMD	pDEST22	Y2H	Generated via LR reaction
p22-KIN4CΔMD	pDEST22	Y2H	Generated via LR reaction
p22-KRP125a	pDEST22	Y2H	Available in the lab
p22-ZCF125	pDEST22	Y2H	Available in the lab
p22-PAKRP1	pDEST22	Y2H	Available in the lab
p22-PAKRP1L	pDEST22	Y2H	Available in the lab
p22-KATC	pDEST22	Y2H	Available in the lab
p22- KATCΔMD	pDEST22	Y2H	Available in the lab

p22- N'KATDΔMD	pDEST22	Y2H	Available in the lab
p22- K13A	pDEST22	Y2H	Available in the lab

Table 4-7 List of transgenic and mutant lines generated for the study

Lines	Purpose
<i>iqd67</i>	Phenotypic analysis
<i>iqd68</i>	Phenotypic analysis
RFP-MBD	Microtubule pattern analysis
<i>iqd678x</i> RFP-MBD	Microtubule pattern analysis
<i>iqd8-1X</i> RFP-MBD	Microtubule pattern analysis
<i>pPOK1:YFP-POK1,RFP-MBD</i> (recovered from the cross)	<i>In planta</i> localization study
<i>iqd678x pPOK1:YFP-POK1, RFP-MBD</i>	<i>In planta</i> localization study
<i>iqd8-1X pPOK1:YFP-POK1, RFP-MBD</i>	<i>In planta</i> localization study
<i>pok12</i> (recovered from the cross)	Genetic interaction
<i>pok12xiqd678</i>	Genetic interaction
<i>pok12xiqd8-1</i>	Genetic interaction
<i>pPHGAP2:GFP-GAP2</i> (recovered from the cross)	<i>In planta</i> localization study
<i>pPHGAP2:GFP-GAP2/iqd678</i>	<i>In planta</i> localization study
<i>pPHGAP2:GFP-GAP2/iqd8-1</i>	<i>In planta</i> localization study
<i>Phgap12</i> (recovered from the cross)	Genetic interaction
<i>phgap12xiqd678</i>	Genetic interaction
<i>phgap12xiqd8-1</i>	Genetic interaction
<i>pIQD8:IQD8-GFP/iqd678</i>	Localization of IQD8 in <i>iqd678</i>
<i>pIQD8:IQD8-GFP/iqd8-1</i>	Localization of IQD8 in <i>iqd8-1</i>
<i>pIQD8:IQD8-GFP/col-o</i>	Localization of IQD8 in Col-0
<i>pIQD8:IQD8-GFP/phgap12</i>	Localization of IQD8 in <i>phgap12</i>

4.2 Media

All media were autoclaved at 121 °C and 15 psi for 20 min after preparation. Supplements were filter sterilized and added to the media after autoclaving.

4.2.1 Solid medium (SM) for sterile growth of Arabidopsis seedlings

For the sterile growth of Arabidopsis seedlings on agar plates, Solid Medium (SM) of the following composition was used.

Table 4-8 ATS medium (Wilson et al., 1990)

D-Sucrose	0.5 % (w/v)
Agargel	0.5 % (w/v)
KNO ₃	5 mM
KH ₂ PO ₄	2.5 mM
Fe-EDTA	0.05 mM
MgSO ₄	2 mM
Ca(NO ₃) ₂	2 mM
MES-KOH (pH 5.6)	2.5 mM

4.2.2 Lysogeny broth (LB) medium

For cultivation of bacterial cells LB medium was used.

Table 4-9. LB medium (Bertani, 1951)

Tryptone	1 % (w/v)
Yeast extract	0.5 %
NaCl	1 %

The preparation of LB agar plates was carried out by addition of Agar-agar to a total of 1.5 %. For selective growth, the corresponding antibiotics were added after autoclaving.

4.2.3 Super optimal broth with catabolite repression (SOC) medium, pH 7.0

For the transformation of bacterial cells, SOC medium was used.

Table 4-10 SOC medium (Hanahan, 1983)

Tryptone	2 % (w/v)
Yeast extract	5 % (w/v)
NaCl	10 mM
KCl	2.5 mM
MgCl ₂	10 mM
MgSO ₄	10 mM
Glucose	2 % (w/v)

4.2.4 Preparation of YPD medium for cultivation of yeast cells, pH 6.5

For the preparation of YPD medium, YPD broth (Roth) was used according to the manual. Agar-agar was added to a total of 1.5 % for preparation of YPD agar plates.

Table 4-11. YPD medium

Bacto peptone	2 % (w/v)
Yeast extract (Applichem)	1 % (w/v)
Adenine hemisulphate (Sigma)	0.1% (w/v)
Glucose (add after autoclaving)	2 % (w/v)

4.2.5 Preparation of synthetic defined (SD) medium

For the preparation of SD medium for selective growth of yeast cells, Yeast Nitrogen Base without amino acids (MP-Biomedical) was used according to the instruction manuals. If not described otherwise. Glucose (2 % [w/v]) served as a carbon source. To prepare SD plates, 8.5 g Agar-agar (Bacto-Agar, AppliChem) was dissolved in 500 ml of media and autoclaved. In case of auto-activation, filter-sterilized 3-amino-1, 2, 4-triazole (3-AT), was added to the media, prior to casting the SD plates. The concentration of 3-AT varied as per strength of auto-activation. All ingredients and additional supplements were filter sterilized with filter of pore size 0.1 μm , prior to addition to the medium.

4.3 Plant cultivation and growth conditions

4.3.1 Sterile growth of Arabidopsis seedlings on agar plates

Before seeding, Arabidopsis seeds were surface-sterilized with chlorine gas. Therefore, sodium hypochlorite (12% w/v NaClO) was mixed with fuming hydrochloric acid (37% v/v HCl) and the seeds incubated in the generated chlorine gas for 35 – 45 min. After removal of the gas, the seeds were placed on the *A. thaliana* salt medium (ATS) with 0.5% agar gel. Alternately, seeds were surface-sterilized in Eppendorf tubes using 6% (v/v) NaClO. After usual stratification for 2-3 days at 8°C in the dark, they were moved to light chambers or cabinets where they grew vertically under continuous light or long-day conditions (16 h light and 8 h dark) at 20 - 22°C with $\sim 130 \mu\text{mol} / (\text{m}^2/\text{s})$ light fluency and $\sim 55 \%$ humidity. As WT ecotype, Col-0 was used for all analyses. 7-day-old seedlings were used for mutant analysis. For comparing the *pIQD8:GUS-GFP* expression to *pIQD8:IQD8-GFP*, 4-day-old seedlings were used. Root lengths analysis was done using 7 to 8-day-old seedlings. To investigate the morphological difference in mutants, rosettes of 18-day-old plants were used, while for the phenotype analysis of adult plants, 49-day-old, mature plants were used.

4.3.2 Cultivation of *A. thaliana* and *N. benthamiana* on soil

Unless stated otherwise, the cultivation of Arabidopsis and Nicotiana took place in the greenhouse under long-day conditions at 18 – 20°C and $\sim 55 - 60 \%$ relative humidity.

“Einheitserde Typ GS 90” mixed with vermiculite (1 – 2 mm) in a 4:3 ratio served as a substrate.

4.3.3 Stable transformation of *A. thaliana* via the floral dip method.

For the generation of stable transgenic Arabidopsis lines, flowering Arabidopsis plants were transformed via the *A. tumefaciens*-mediated floral dip method (Clough and Bent, 1998). *A. tumefaciens* carrying the gene of interest on a binary vector were cultivated for 2 days on LB medium containing appropriate antibiotics. The bacteria were resuspended in 60 ml LB medium to an OD₆₀₀ of 2.0. Freshly prepared 5% (w/v) sucrose solution was added to the bacterial suspension in a ratio of 4:1. Silwet L-77 at a concentration of 0.03 % was added to the total solution. Flowering Arabidopsis plants were then dipped into the bacterial solution for 15–30 s and shaken gently. The plants were placed horizontally in a tray and covered with saran wrap allowing them to dry for 1–3 days. The saran wrap was then discarded and the plants were moved to upright position and continued to be cultivated in the greenhouse for setting seeds. T1 seeds from transformed plants were sown densely on soil and after germination, Basta (80 mg/L) was sprayed to select plants transformed with the gene of interest. Several independent T2 lines were further selected for segregation ratio of 3:1 on ATS medium plates supplemented with Basta (10 µg/ml) and further genotyped to check background mutations of the parent plants. 10-15 transgenic T2 lines were selected and propagated for T3 seeds, which were again grown on Basta (10 µg/ml) containing ATS medium plates to select for homozygous lines.

4.3.4 Transient transformation of *N. benthamiana* leaves.

The transient transformation of *N. benthamiana* leaves was carried out using *A. tumefaciens* strains that carried the gene of interest and the gene silencing inhibitor p19 (Voinnet et al., 2003). Bacteria were grown overnight in 4 ml LB medium containing the corresponding antibiotics to an OD₆₀₀ = 0.5 – 0.8. The cells were harvested at 10.000 g for 4 min. The pellet was washed two times with 2 ml transformation buffer and subsequently dissolved in transformation buffer to an OD₆₀₀ of 0.5. The bacteria carrying the expression construct were mixed in ratio of 1:1 with the ones harboring the p19 plasmid and incubated for 1 h at 18 ° C. Afterwards, the bacteria were injected at the abaxial side of leaves of 5–7-week-old plants via a syringe. The plants were then placed in the greenhouse until further experiments were carried out. In most cases, transformed plants were analyzed 2-3 days after transformation under the microscope.

Table 4-12. Transformation buffer

MES-KOH pH 5.5	10 mM
MgCl ₂	10 mM
Acetosyringone	150 µg / ml (w/v)

4.3.5 Generation of mutant lines

iqd6-1 (SALK_107689.47.80.), *iqd7-1* (SALK_025224) and *iqd8-1* (SALK_137365.54.75.) single mutants were first verified for homozygosity via genotyping and then crossed to generate higher-order mutants. All mutants were in Col-0 background. All transgenic lines used for analysis were generated by transfection of respective genotypes mediated by *A. tumefaciens* harboring the transgene of interest. *pIQD8:IQD8-GFP* was introduced via Agrobacterium-mediated floral dip transformation into Col-0, *iqd8-1* and *iqd678* triple mutants. YFP-POK1, GFP-PHGAP2 were introduced into *iqd678* via crossing of *pPOK1:YFP-POK1*, *RFP-MBD* (Lipka et al., 2014) and *pPHGAP2:GFP-gPHGAP2/gap12* (Stöckle et al., 2016) with *iqd678* triple mutants. *pIQD8:IQD8-GFP* was introduced into *pok12* via crossing of *pIQD8:IQD8-GFP/Col-0* with line segregating for *pok12* and harboring RFP-MBD (kindly provided by Dr. Sabine Müller, ZMBP Tübingen). For the generation of *pIQD8:IQD8-GFP/phgap12*, the IQD8 translational fusion construct was transformed into *phgap12* double mutants. All mutant lines were genotyped for homozygosity of the construct. Localization study was performed with T2 and/or T3 lines.

4.4 Cultivation of bacteria and yeast

4.4.1 Cultivation of *Escherichia coli* (*E. coli*)

E. coli cells were grown overnight at 37°C in liquid LB medium or on LB agar plates containing the selective marker antibiotics. Liquid cultures were grown overnight in a shaker incubator at 120–160 rpm. For long term storage, liquid cultures were mixed with glycerol to a final concentration of 20 to 40 % (v/v) and stored at -80°C.

4.4.2 Cultivation of *A. tumefaciens*

The *A. tumefaciens* cells were grown in liquid LB medium or on LB agar plates containing the appropriate antibiotics (antibiotic selecting for the harbored plasmid plus Agrobacterium strain-specific antibiotic) for 2 days at 28°C. Liquid cultures were incubated overnight at 120–160 rpm. For long term storage, liquid cultures were mixed with glycerol to a final concentration of 20 to 40 % (v/v) and subsequently stored at -80°C.

4.4.3 Growth and transformation of *S. cerevisiae* cultures for Y2H assays

For 12 transformation reactions, an inoculum of the required yeast strain was added to 50 ml of YPDA media supplemented with glucose and grown overnight at 28°C shaking at 160 rpm. The OD₆₀₀ of all pre-cultures was determined and adjusted to OD of 0.5–0.8. Competent yeast cells were prepared immediately before transformation.

4.5 Transformation of bacteria and yeast

4.5.1 Transformation of chemical competent *E. coli* cells

100–500 ng of plasmids were added to 50 µl chemically competent *E. coli* cells and incubated on ice for 30 min. The mixture was heat shocked for 45 s at 42°C and immediately placed on ice. After addition of 250 µl of S.O.C. medium, the cells were incubated at 37°C for 60 min at 800 rpm. For selection of transformed plasmids, cells were plated on LB Agar plates containing the appropriate antibiotic and incubated overnight at 37°C. 3-4 individual positive colonies were picked and resuspended in a culture tube with LB liquid medium and the corresponding antibiotic and allowed to grow overnight in a 37°C shaker incubator at 140 rpm. After confirmation of plasmids via restriction digestion and colony PCR, a glycerol stock was made from the corresponding culture.

4.5.2 Transformation of chemical competent *A. tumefaciens*

For the transformation of chemically competent *Agrobacterium* (GV3101pk) cells, 100–500 ng of plasmids were added to 50 µl chemically competent *A. tumefaciens* cells and incubated on ice for 30 min. The transformation was carried out by cold shock for 3 min in liquid nitrogen and a subsequent heat shock for 5 min at 37°C. Thereafter, 250 µl S.O.C. medium was added, and the culture was shaken for 1–2 h at 28°C and 800 rpm. The complete solution was plated on a plate with LB medium containing appropriate antibiotic and incubated for 2 days at 28°C. After that, 3 to four individual colonies were checked via colony PCR for the presence of the plasmid of interest. Positively tested colonies were resuspended in culture tubes with LB liquid medium and the corresponding antibiotic. Overnight cultivation at 28°C with shaking at 140 rpm followed. A glycerol stock was made for permanent preservation. For transformation of electro-competent *Agrobacterium* (GV3101) cells, 2–5 µl of plasmid of interest were mixed into 50 µl of *Agrobacterium* cells thawed on ice. The mixture was then incubated for 30 min on ice and subsequently subject to electroporation. Subsequently, 450 µl of SOC media was added and mixed carefully by pipetting. The culture was transferred to an Eppendorf tube and incubated in a shaker incubator at 28°C for 1 h at 120–150 rpm. The mixture was then plated on LB medium plate

containing appropriate antibiotics and incubated for 2 days at 28°C. Positive plasmids were isolated from positive colonies and further verified via PCR.

4.5.3 Transformation of *Saccharomyces cerevisiae* (*S. cerevisiae*)

The Lithium acetate (LiOAc) method was used for the transformation of yeast (*S. cerevisiae*). A single colony of PJ69-4a (*S. cerevisiae*) was inoculated in 200 ml YPD medium and incubated overnight at 30°C at 120–160 rpm to an OD₆₀₀ of 0.8–1.0. The cells were harvested by centrifugation of 50 ml cell suspension at 5,000 rpm for 5 min, and the supernatant was discarded. The pellet was then washed with 10 ml sterile autoclaved MilliQ water and centrifuged again as described above. The pellet was then washed in 1 ml MilliQ water. After the third centrifugation, the pellet was resuspended in 1 ml 1X TE/LiOAc. After the last centrifugation step, the pellet was dissolved in 250 µl 1X TE/LiOAc. Salmon sperm DNA (ssDNA [Sigma]) was diluted in TE buffer (5 mg/ml [w/v]) and incubated at 95°C for 20 min, placed on ice and used immediately for the next transformation step. 4 µl of the ssDNA was mixed with 20 µl cell suspension (competent yeast cells). The transformation reaction was performed in a 96-well plate. In each well, 24 µl of master mix containing ssDNA and competent cells was added to 100 ng of plasmid DNA for expression of each interacting partner resulting in 200 ng of plasmid DNA in total. Next, 100 µl polyethylene glycol (PEG) solution was added to each well and mixed carefully. The mixture was incubated for 1 h at 29°C with shaking at 120 rpm. Subsequently, a heat shock was carried out for 15 min at 42°C and the reaction samples were centrifuged for 5 min at 1800 rpm. After carefully removing 100 µl of the supernatant, the cells were washed by adding 180 µl 1X TE buffer, of which 130 µl buffer were removed immediately. The cells were finally resuspended in the remaining 50 µl 1x TE buffer and 10 µl were plated on SD-LEU-TRP double drop out agar plates (vector selective media). After 2–4 days of growth at 30°C, positive colonies were picked and inoculated into 200 µl of 1X TE buffer. Yeast cultures were incubated overnight at 30°C and 120-150 rpm shaking. 10 µl of the yeast cultures were then transferred to SD-HIS-LEU-TRP triple dropout (interaction selective media) medium and high stringency SD-ADE-HIS-LEU-TRP quadruple drop out medium plates and incubated for 3–4 days at 29°C. The presence and strength of the interactions were estimated based on growth of the yeast colonies under selective conditions.

Table 4-13. 10X TE_buffer

Tris-HCl	0.1 M
EDTA	0.01 M
pH	7.5

Table 4-14. 10X LiOAC

Lithiumacetate	1 M
pH	7.5

Table 4-15. PEG Solution

PEG 4000	40 % (w/v)
Lithiumacetate	100 mM
Tris-HCl	10 mM
EDTA	1 mM
pH	7.5

4.6 Molecular biological methods

4.6.1 DNA-based methods

4.6.1.1 Isolation of plant DNA

Approximately 100 mg of plant material (leaves, roots or whole seedlings) were put into a 1.5 ml reaction tube and 400 μ l of plant DNA extraction buffer was added. The material was then crushed using a mini pestle until a homogenized solution was obtained. The samples were vortexed, centrifuged at 13,000 rpm for 5 min and approximately 300 μ l of supernatant was transferred in to a new tube. After the addition of 300 μ l Isopropanol the tubes were inverted several times, incubated for 2 min and centrifuged again at 13,000 rpm for 5 min. After the supernatant was removed, the pellet was washed with 70 % ethanol, air-dried for 10–30 min and dissolved in 50 μ l sterilized MilliQ water. The DNA concentration was measured at a NanoQuant Infinite M200 (Tecan). The isolated DNA was stored at -20°C.

Table 4-16. Plant DNA extraction buffer

Final concentration	stock	<u>50ml</u>	<u>100ml</u>
200mM Tris-HCL (pH 7.5)	1M	10ml	20ml
250mM NaCl	4M	3.125ml	6.25ml
25mM EDTA (pH 8.0)	0.5M	2.5ml	5ml
0.5% SDS	20%	1.25ml	2.5ml

4.6.1.2 Isolation of plasmid DNA

For the isolation of plasmid DNA from bacteria, the GeneJET plasmid Mini-Prep Kit (Thermo Fisher Scientific) was used according to the manufacturer's instruction. The isolated plasmid was eluted in 50 µl ddH₂O and stored at -20°C. The concentration of isolated plasmid DNA was measured using a NanoQuant Infinite M200 (Tecan).

4.6.1.3 Polymerase chain reaction (PCR)

PCR was carried out for amplification of DNA fragments. Based on the requirements, different setups were used. In general, for analytical PCR reactions, i.e. Colony PCR or genotyping of plant material, homemade Taq Polymerase and 10 x Taq Buffer was used. For amplification of DNA fragments for cloning purposes, High Fidelity Phusion Polymerase and 5 x Phusion Green Buffer (Thermo Fisher Scientific) was used. The PCR reactions were carried out either in 8 well PCR stripes or in 96 well plates in a Veriti 96 well thermal cycler (Applied Biosystems). As a template either plasmid DNA or DNA isolated from plant material was used. PCR mix and reaction condition used for Taq Polymerase and Phusion Polymerase are as follows:

Table 4-17. PCR mixture

Taq polymerase	
10x PCR Puffer	2 µl
dNTPs (10 mM total)	1 µl
Primer (FWD)	1 µl
Primer (REV)	1 µl
Taq-Polymerase (5 U/µL)	0.7 µl
DNA-Template	2 µl
MilliQ	12.3 µl
5x Phusion polymerase	
HF Green buffer	10 µl
dNTPs (10 mM total)	1.5 µl
Primer (fwd)	2 µl
Primer (rev)	2 µl
Phusion-Polymerase (2 U/µl)	0.5 µl
DNA-Template	2 µl
MilliQ water	32 µl

Reaction Conditions

	Taq-Polymerase			Phusion-Polymerase		
Initial Denaturation	95°C	2 min		98°C	30 s	
Denaturation	95°C	1 min	} 40 Cycle	98°C	10 s	} 35 Cycle
Annealing	55°C	45 s		58°C	30 s	
Extension	72°C	1 min / kb		72°C	40 s / kb	
Final Extension	72°C	10 min		72°C	5 min	

4.6.1.4 Restriction digestion

For the verification of plasmids, restriction digestion was performed with the following setup:

Plasmid	2 µl
FastDigest Buffer (10X)	2 µl
Enzyme	1 µl
H ₂ O	10 µl

Mixture was incubated at 37°C for 30 min. The digestion was checked by gel electrophoresis on a 1% (w/v) agarose gel.

4.6.1.5 Preparation of agarose gels for separation of DNA fragments

To separate DNA fragments, agarose gel electrophoresis was used. Agarose (Roth) was added at 0.8 – 1.5 % (w/v) to 1X TAE buffer and dissolved under heating in a microwave oven. After 30 s, 0.001% (v/v) of stain G (Serva) was added to the solution. The solution was then cast into a gel chamber and allowed to solidify. The samples were mixed with DNA loading buffers and loaded into wells of the agarose gel. After loading, the gel was subject to 70 V of voltage for about 30 – 45 min to separate the DNA fragments. As a size standard, 5 µl "GeneRuler 1kb and 100 bp DNA Ladder" provided by Thermo Scientific was used. To visualize and document the separation pattern of the DNA fragments a Gene Genius (Syngene) UV table was used.

4.6.1.6 Purification of DNA fragments from agarose gels

Separated DNA fragments were purified from agarose gels via GeneJET Gel extraction Kit (Thermo Fisher Scientific) according to the manufacturer's instructions. The purified DNA was stored at -20°C.

4.6.1.7 Gateway Cloning

All clones were generated using the Gateway cloning (Invitrogen) system. pDONR constructs were generated using BP reaction. Primers were designed with attB1 and attB2 sites, and PCR was performed using specially designed primers and template DNA. The reaction mixture was prepared with purified PCR product (150 ng), DONR vector (150 ng), BP clonase (2 µl) and 1x TE buffer in total volume of 10 µl. The mixture was incubated for 2 h at room temperature (RT). The reaction was stopped by addition of 1 µl of proteinase K and subsequent incubation at 37°C for 10 min. The whole reaction mixture was used to transform *E.coli*. After transformation, colonies were cultured in liquid media, and subsequently plasmids were isolated. Plasmids were checked with PCR and restriction digestion for the presence of construct of interest. Further LR reaction was used to generate DEST constructs. For this, a reaction mixture of 5 µl consisting of DONR entry clone (110 ng), DEST vector (110 ng), LR clonase (1 µl) and TE buffer, was incubated for at least 2 h at RT. The reaction was terminated using 0.5 µl proteinase K and further incubation at for 10 min at 37°C. Subsequently, the complete mixture was transformed into *E.coli*. After successful transformation, plasmids were isolated and verified using PCR and restriction digestion.

4.6.2 RNA-based methods

4.6.2.1 Isolation of plant RNA

RNA was isolated using TRI-Reagent (Sigma Aldrich). In brief, 100 mg of plant material was harvested into a 2 ml reaction tube and frozen in liquid nitrogen. Plant material was homogenized using steel beads and a "Tissue Lyser II" (Retsch). After removing the beads, 500 µl of TRI-Reagent was added to the ground material. Tubes were vortexed to obtain a homogenous solution. After that, the sample was incubated at RT for 5 min. In the next step, 100 µl of chloroform was added and the reaction tube slowly inverted for about 12 s and again incubated for 10 min at RT. After incubation, the sample was centrifuged for 15 min at 15,000 g and 4°C. 250 µl of the aqueous phase was transferred to a new 15 ml tube and precipitated with 125 µl Isopropanol and 125 µl of high salt solution. Thereafter, sample was vortex and incubated for 10 min at RT and further centrifuged for 10 min at 15,000 g and 4°C. The supernatant was discarded, and the pellet was washed with 500 µl 70% (v/v) ethanol. To remove the ethanol, sample was centrifuged at 7500 g and 4°C for 5 min. For complete removal of ethanol, samples were dried for 10 min under the fumigation hood. In the final step, 20 µl of sterilized MilliQ water was added, and the pellet was dissolved for 10 min at 65°C. The concentration of the RNA was measured at a NanoQuant Infinite M200 (Tecan). The integrity of the isolated RNA was determined by running an RNA control gel (1 µg RNA/10 µl on 1% agarose gel), and the isolated RNA was stored at -20°C.

4.6.2.2 First-strand cDNA synthesis from RNA samples

To generate cDNA samples from RNA Revert Aid Reverse Transcriptase (Thermo Scientific) was used according to the manufacturer manual. Following steps and reaction mixture was performed for cDNA synthesis.

Total volume: 20 μ l

RNA	1 - 5 μ g
dNTPs, 10 mM each	1 μ l
Oligo-dT-Primer, 0,5 μ g/ μ l	0,5 - 1 μ l
H ₂ O	add.15 μ l

The sample was incubated for 5 min at 65°C to denature the secondary structure. After chilling the samples on ice for 1 min, the following components were added.

5x reaction buffer	4 μ l
RNase Inhibitor (40 U/ μ l)	5 μ l
Revert Aid MuLV-ReverseTranskriptase (200 U/ μ l)	0,5 μ l

Thereby, mRNA was reverse transcribed for 1 h at 42°C. The reaction was terminated by a heat shock at 70°C for 10 min. The cDNA samples were stored at -20°C until usage.

4.7 Microscopic analysis

4.7.1 Confocal laser scanning microscopy (CLSM)

For confocal laser scanning microscopy of Arabidopsis and *N. benthamiana* tissues, LSM700 (Zeiss), LSM780 and LSM880 microscopes were used. 20x and 40x/1.20 Water immersion objective was used to acquire the image unless stated otherwise. Zen Software (Zeiss) was used to operate the microscope and images were processed using Zen as well as via ImageJ (<http://rsb.info.nih.gov/ij/>). YFP and RFP signal was excited using 514 nm and 555 nm laser, respectively, and emission was detected between 520-550 nm and 560-620 nm wavelength, respectively. For GFP, the 488 nm laser line was used to excite the signal, while emission was detected between 492 to 550 nm. For staining with FM4-64 or PI, samples were incubated in 10 μ M of PI and 50 μ M of Synapto-Red C2, respectively. In case of co-expression, signals were recorded in the sequential mode. FM464 was excited similarly to RFP signals. DAPI and PI staining were visualized by using excitation wavelength of 405 nm and 488/561 nm respectively, and emission was detected between 409-484 nm and 565-720 nm, respectively. The Z-stacks were recorded with a magnification of 0.8x and the close-ups with a magnification of 3.4x.

4.7.2 Whole-mount immunofluorescence and DAPI staining

Whole-mount immunolocalization was performed as described in (Stöckle et al., 2016). 7 day-old Arabidopsis seedlings were transferred to bright mount media (BM) and vacuum-incubated for 1 h in 4% (v/v) paraformaldehyde and 0.01 % (w/v) Triton X100 in microtubule stabilizing buffer (MTSB-50 mM PIPES, 5 mM MgSO₄, 5 mM EGTA, pH, 6.9-7.0) to fix the tissue. Thereafter, seedlings were washed three times for 10 min each with distilled water and placed on super frost microscope slides. Samples were left overnight at RT for drying. Rehydration was performed by applying MTSB for 10 min. Samples were again rehydrated in 2% Driselase in MTSB for 1 h at 37°C, which causes partial digestion of the cell wall. Membranes were permeabilized after four times washing with phosphate saline buffer (PBS-150 mM NaCl, 2, 1 M Na₂HPO₄, 1M NaH₂PO₄) by using 10% DMSO/ 3% NP40 in PBS for 1 h at RT. Subsequently, seedlings were washed 6 times for 5 min each in PBS buffer. Samples were blocked for 2 h at 37 °C in 3-5% (w/v) bovine serum albumin (BSA) dissolved in PBS. After two times washing with PBS, samples were incubated with primary rabbit-anti-GFP (1/200) and rat-anti-tubulin (1/200) antibodies overnight at 4°C. After three times washing, Alexa Fluor 488 goat-anti-rabbit (1/600) and goat anti-rat Cy3 (1/1000) secondary antibodies were applied for GFP antibody and tubulin antibody, respectively, and incubated at 37°C for 3.5 h. Samples were washed four times for 10 min each with PBS and two times for 10 min each with distilled water. Both primary, as well as secondary antibodies, were dissolved in 5% BSA/PBS. DNA was stained with dilution DAPI (1/1000) for 15 min at 37°C. After 6 times washing in distilled water for 5 min each, samples were mounted in Citifluor. Imaging was performed using LSM880.

4.7.3 Subcellular distribution of IQD8-GFP

Dividing cells of Arabidopsis root meristem co-expressing IQD8-GFP along with RFP-MBD were used for quantification. The cells expressing RFP-MBD were used as a reference to determine IQD8-GFP signal in distinct mitotic stages. Based on the microtubule array organization, cells were classified into different cell cycle stages.

4.7.4 Plot profile

Plot profile was determined by using ImageJ software. A line was drawn along the merged images and data from the resulting plot profile were collected in MS Excel to make the final graph.

4.7.5 Microtubule pattern analysis and quantification

For microtubule pattern analysis, immunolocalization of Col-0, *iqd8-1* single, *iqd678* triple and *pIQD8:IQD8-GFP/iqd678* was performed. Intact root was used for analysis. Z-stacks of images at the optimum interval was collected, and single longitudinal sections from the stacks were used for analysis. The angle between the deviated orientation of PPB, spindle, phragmoplast, and expected transverse orientation with respect to the parent cell wall axis was determined. The angle tool of ImageJ was used for analysis. Raw data were collected in MS Excel and used to create the boxplots via BoxPlotR (<http://boxplot.tyerslab.com/>). Significance difference was determined by one-way ANOVA post hoc Tukey HSD. Deviation angle was classified into 3 categories 0-5°, >5° ≤15°, and >15°. Angles in the range of 0° to 5° were considered a normal transverse orientation. 20-25 roots per genotype were used for analysis.

4.7.6 Analysis of width of IQD8-GFP at the division site

Single optical sections were used for analysis. Full width half maximum (FWHM) was used to determine the width of the CDZ/CDS. A plot profile along the line drawn along the lateral wall of cells was determined using ImageJ. FWHM from resulting plot profile was calculated in MS Excel. For FWHM, distance (x) for half of the maximum intensity from both sides of cells was determined. The difference between the two value of distance represented the FWHM. The ratio of the width of CDZ/CDS to the width of the lateral cell wall was determined. Measured values were averaged, and Boxplots were created using BoxPlotR. Significance difference was determined by one-way ANOVA post hoc Tukey HSD. 12 cells were analyzed per genotype. Different letters indicate significant differences.

4.7.7 Localization of IQD6-GFP and IQD8-GFP

For localization studies, we introduced *IQD8-GFP*, *IQD6-GFP* in the *iqd678* triple mutants and *iqd6-1* single mutants, respectively. For clarity, single-cell resolution images are used as representative images. Images were acquired with LSM780/880 confocal. Additionally, for IQD8-GFP localization, Airyscan detector of LSM780 was used. 7-day-old seedlings were used for analysis. 3D rotated views were created by using 3D viewer plugin of ImageJ.

4.7.8 Analysis of cell number, meristem size and root diameter

The single epidermal cell files were used to count epidermal cell numbers. For this purpose, single median longitudinal sections of Arabidopsis roots meristems were used. Cell numbers were measured in single-cell files from QC up to the cell that was twice the length of the immediately preceding cell. The corresponding region was used to measure the meristem

size. The meristems sizes and root diameters were measured in the same optical sections. Lateral root cap tissue was excluded from all studies. The diameters of root meristems were measured at 180 μm from QC. ImageJ was used in all analyses. Data obtained from the measurements were collected in MS Excel to generate boxplots using BoxPlotR, and significant difference was determined using post-hoc Tukey HSD test. Data were collected from at least 8 independent seedlings per genotype. All analysis was performed according to Dello Ioio et al. (2007) and González-García et al. (2011).

4.8 Analysis of growth morphology of mutants and WT

Root length analysis was done by using the segmented line tool of ImageJ. Twenty to thirty roots per genotype were used for the study. Quantification of rosette leaves morphology was done by easy leaf area tools. 15-25 plants were used to compare rosette leaves of WT and mutants. Silique length and area were quantified using Polygon and line tool of ImageJ, respectively. Raw data derived from quantification were used to create boxplot using BoxPlotR. 35-45 siliques per genotype were used in the quantification. The raw data were exported to MS Excel, and Boxplots were generated by using BoxPlotR. One-way ANOVA with the post hoc Tukey HSD was used to determine the significant difference between 2 genotypes.

4.9 Cell wall deviation study and quantification

Deviation angle of Arabidopsis root meristematic cells were quantified using the angle tool of ImageJ. Single longitudinal sections of primary root meristem were used for analysis. Similar region of interest was selected from each genotype. The deviation from the expected transverse orientation with respect to the parent cell wall axis was calculated. Box plots of the measurement data were created using BoxplotR. Boxes represent the mean deviation angle. Gray bar indicates 95% confidence interval of the mean. Centerlines show the median value. Box limits indicate the 25th and 75th percentile. The Tukey-whiskers extend 1.5 times the IQR from the 25th and 75th percentiles. Significance difference was determined by one-way ANOVA post hoc Tukey HSD. Approximately, 300-400 angles from 7-12 seedlings per genotype were measured for the analysis. For complementation analysis, the T3 homozygous line was used. Two independent T3 lines and 12 independent T2 lines were used to confirm the rescue of phenotype. Quantification was done using single T3 representative line.

5 Supplemental figures

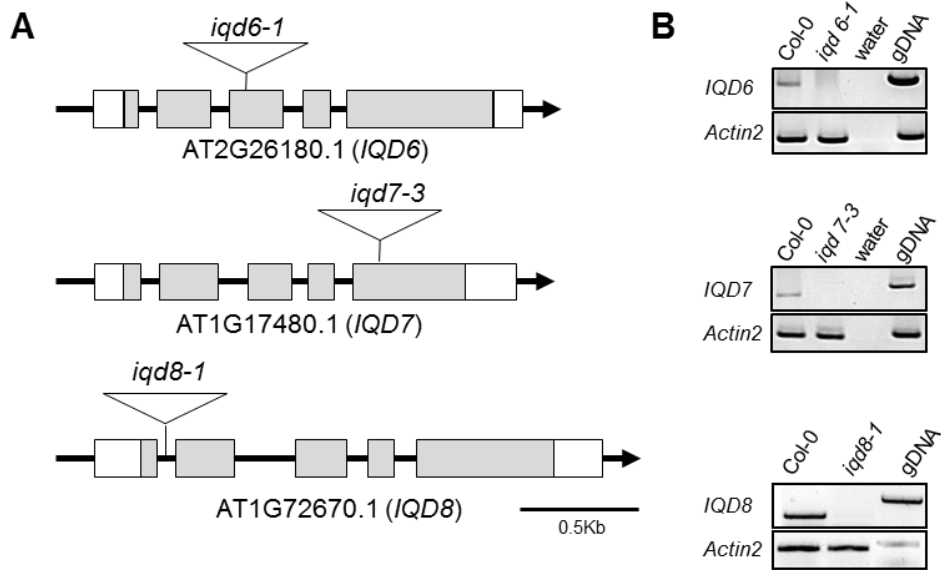


Figure S 1 Gene model and verification of transcript loss.

(A) Schematic diagram showing gene models of *iqd6-1*, *iqd7-1* and *iqd8-1* single mutants. Triangles indicate the position of T-DNA insertions in the mutants. White boxes indicate 5'UTR and 3'UTR. Exons and introns are represented by gray boxes and black lines, respectively. Accession number of gene is indicated in parathesis. Scale bar, 0.5 kb. (B) RT-PCR showing loss of transcript in *iqd6-1*, *iqd7-1* and *iqd8-1* single mutants. *Actin2* was used as a control for determining the integrity of cDNA. Water and gDNA, respectively were used as a positive and negative control of the experiment. RT-PCR was performed by Gina stamm and Dipannita Mitra.

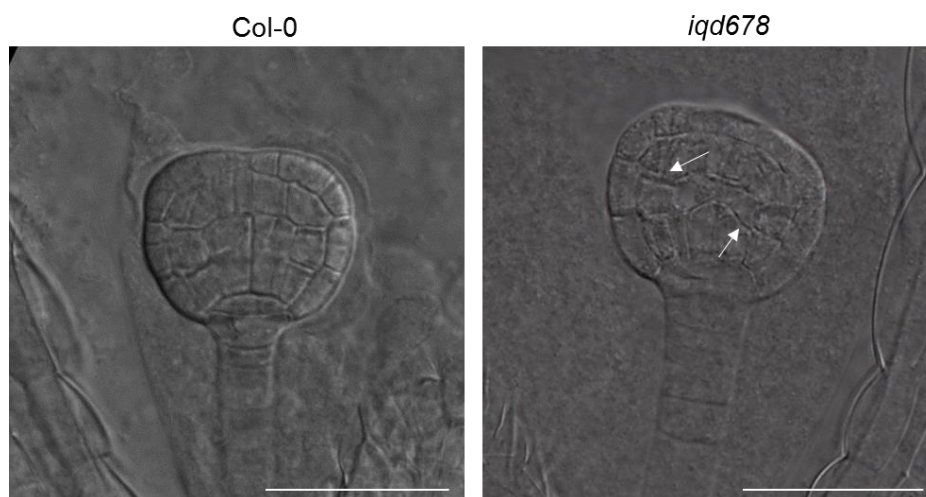


Figure S 2 Cell wall misorientation in *iqd678* triple mutant embryos.

Pattern of cell wall orientation in Col-o (left image) and *iqd678* triple mutants (right image). Embryos were cleared using chloral hydrate and visualized using DIC mode of Nikon microscope. Arrows mark the position of deviated cell wall. Bars, 50 μ m.

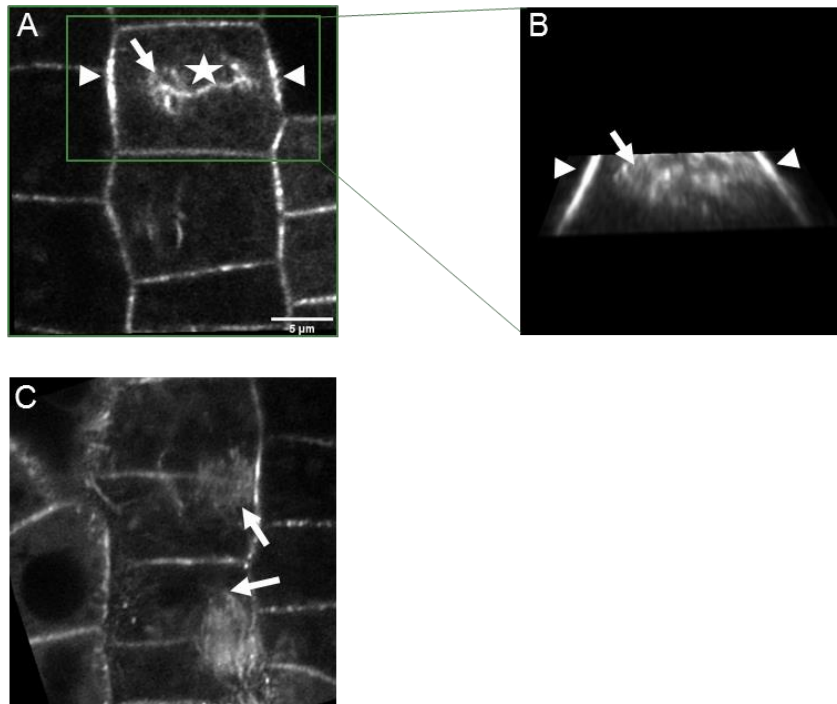


Figure S 3 Localization of IQD8-GFP in cytokinetic cells.

(A) Single-cell resolution images of 5-day-old Arabidopsis root meristematic cells expressing *pIQD8:IQD8-GFP*iqd678** in cytokinetic cells showing IQD8-GFP localization on phragmoplast (arrow), CDS (arrowheads) and cell plate (asterisk). (B) Optical section of 3D projected view showing CDS (arrowheads) and phragmoplast microtubules (arrow). (C) IQD8 localization on exploratory microtubules of phragmoplast (arrows). Images are representative of at least three independent experiments. All images are acquired in LSM780 with airy scan detector. Scale bar, 5 μm.

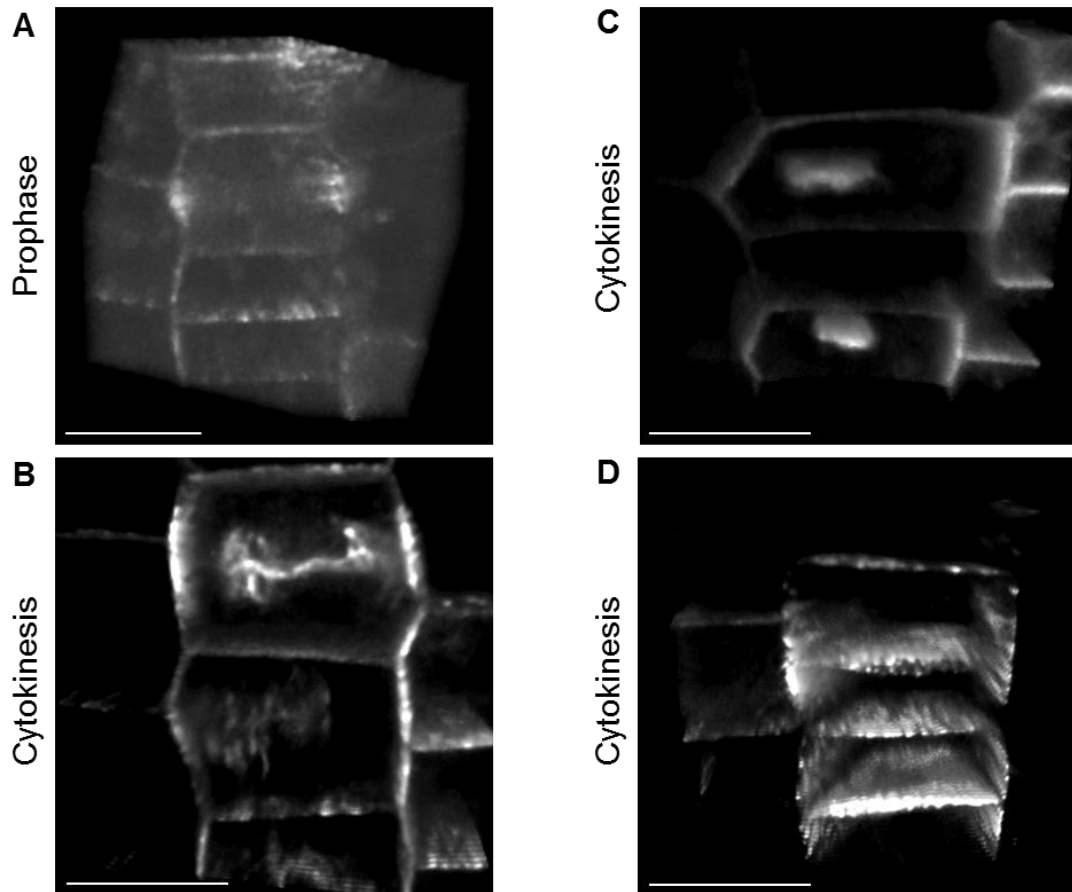


Figure S 4 3D-rotated views showing IQD8-GFP localization patterns during cell division
 (A-D) Single-cell resolution images of 5-day-old Arabidopsis root expressing *pIQD8:IQD8-GFP/iqd678*. 3D-rotated views showing PPB (A), Phragmoplast, CDS (B), and cell plate (C, D). Images were acquired in airyscan mode, and representing the result of at least three independent experiments. Scale bars, 10μm.

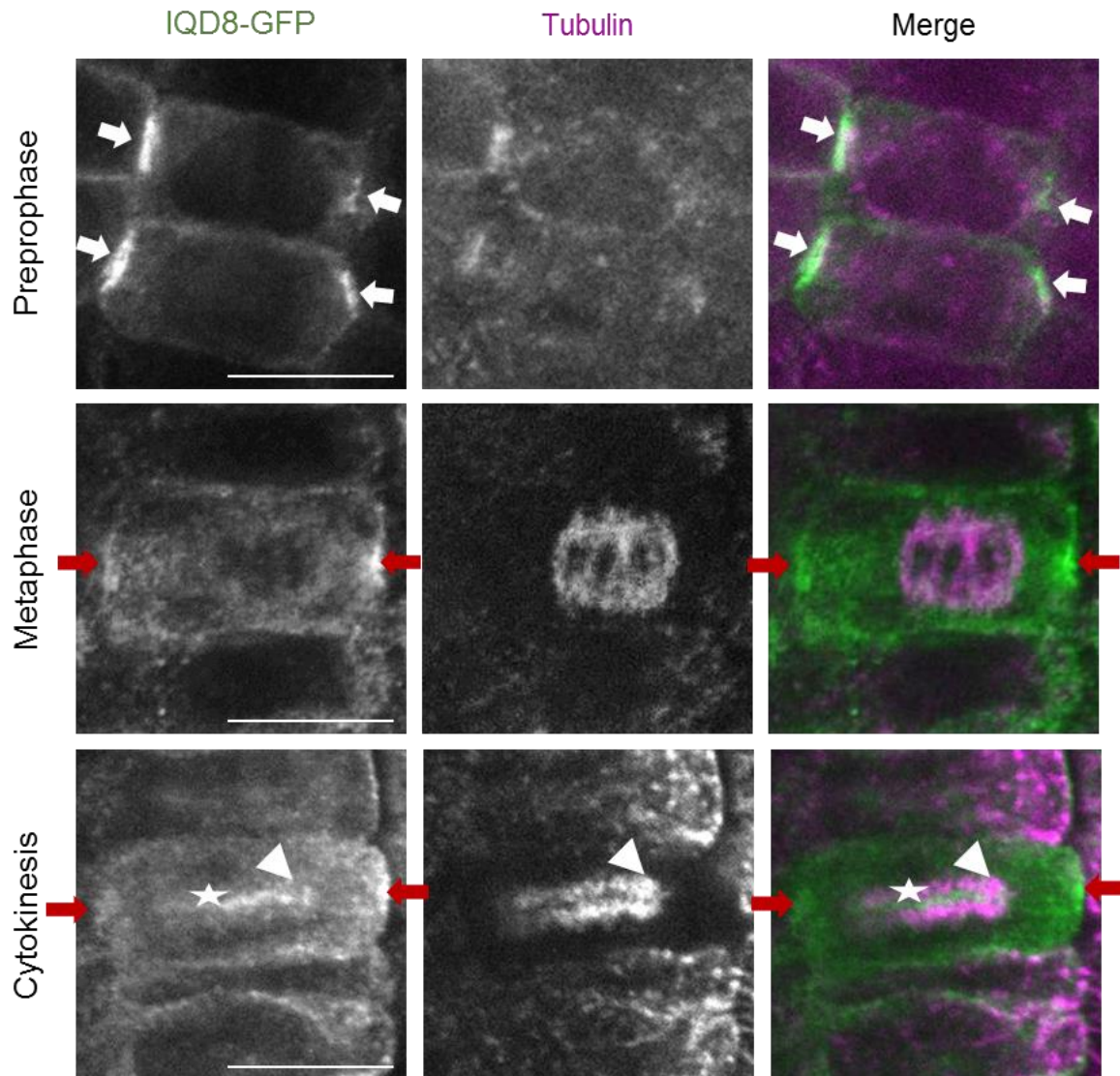


Figure S 5 IQD8 localization study using immunostaining.

Single-cell resolution images showing whole mount immuno labeling of 5-day-old Arabidopsis seedlings expressing *pIQD8:IQD8-GFP* in the *iqd678* triple mutant background. Anti-GFP (Green) and anti-tubulin (magenta) specific antibodies were used to stain IQD8-GFP and microtubules, respectively. Arrows indicate position of PPB (white arrows) and CDZ (red arrows). Arrowheads and asterisks indicate positions of phragmoplast and cell plate, respectively. Images are representative of at least two independent experiments. Scale bars, 10 μ m.

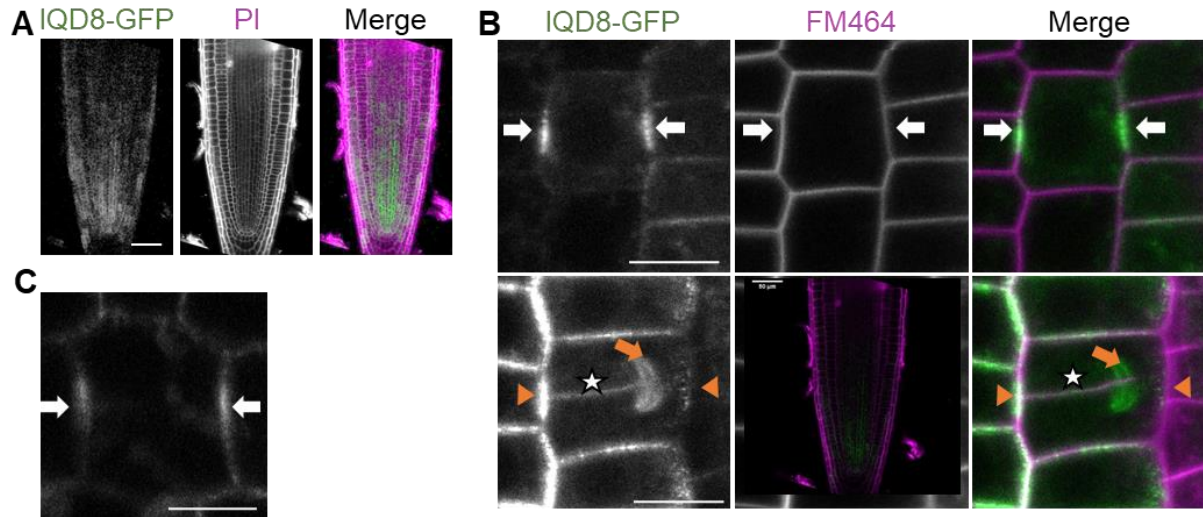


Figure S 6 IQD8 localization during cell division.

(A) Confocal median longitudinal section of 7-day-old-Arabidopsis root tip cells showing overview for the expression of *pIQD8:IQD8-GFP* in the *iqd678* mutant background. (B) Single-cell resolution images showing IQD8-GFP signal at PPB (white arrows), CDZ/CDS (brown arrowheads), phragmoplast (brown arrows) and cell plate (asterisks). (C) Shoot apical meristem cells showing IQD8-GFP signal at PPB (white arrows). PI and FM464 were used to stain cell wall (A) and plasma membrane (B, C), respectively. Images are representative of 8-10 roots from at least three independent experiments. Scale bars, 50 μ m (A), 10 μ m (B, C).

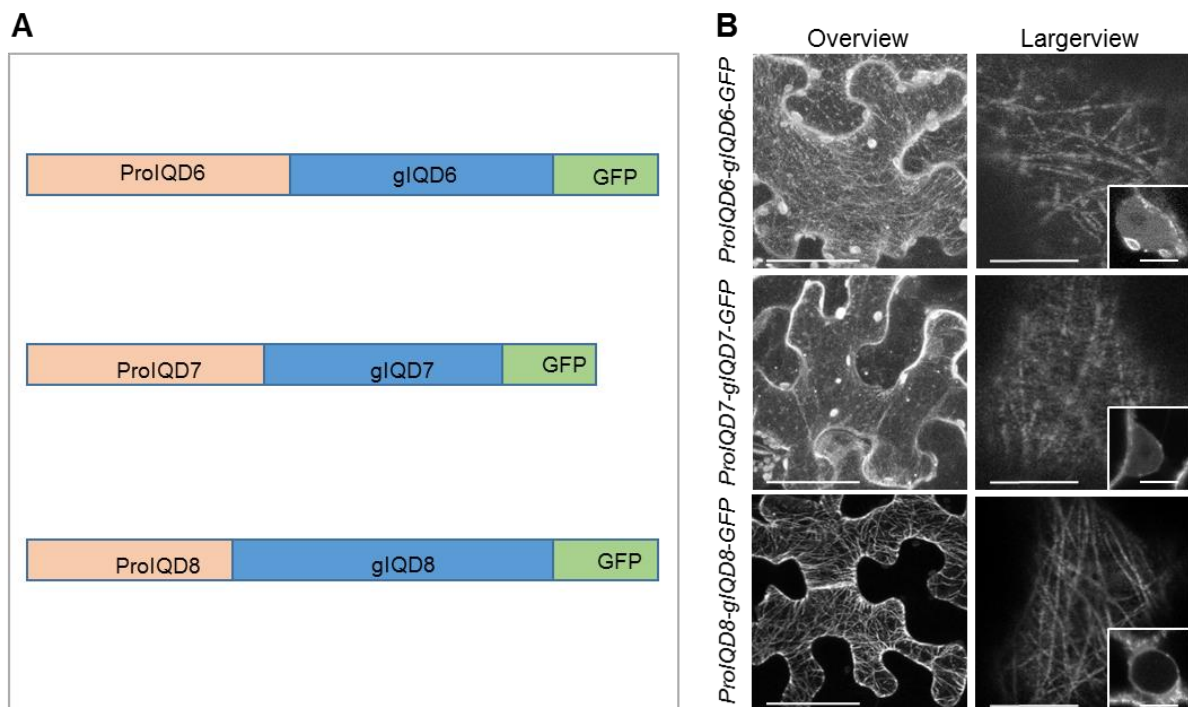


Figure S 7 IQD6, IQD7 and IQD8 localization pattern in heterologous system.

(A) Schematic representation of IQD6, IQD7 and IQD8 cassette under endogenous promoter with C-terminal GFP tag and (B) their transient expression in *N. benthamiana* leaf epidermal cells. Left column shows overview images, right column shows larger magnified views. Images were acquired 2

days after transient transformation and representing the results of two independent experiments. Scale bars, 10 μ m (right column) and 50 μ m (left column).

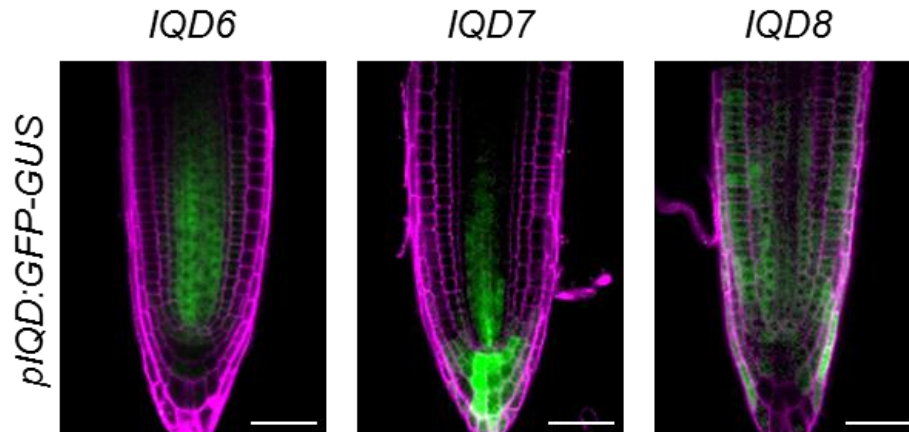


Figure S 8 Promoter activity of IQD8 and related proteins.

Confocal median longitudinal optical section of 4-day-old Arabidopsis seedlings showing GFP expression under the control of endogenous promoter of *IQD6*, *IQD7* and *IQD8*. PI was used to stain cell wall. Scale bar, 50 μ m.

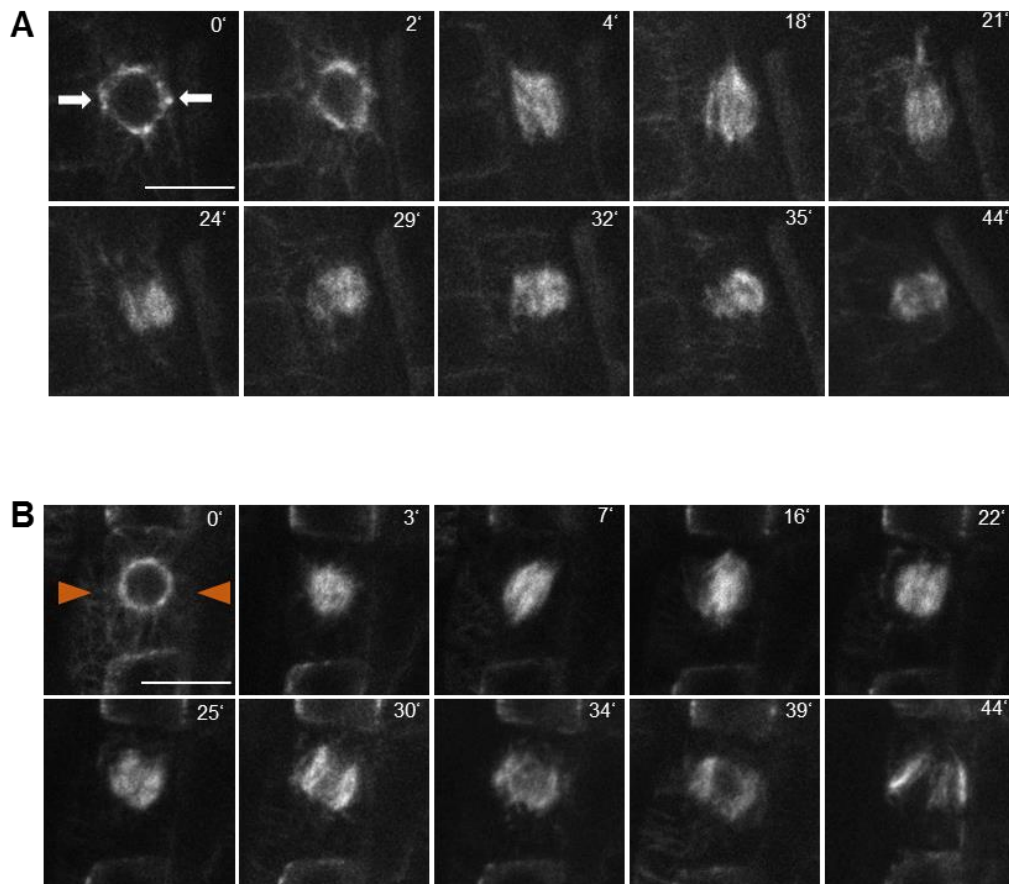


Figure S 9 Cell cycle duration.

Time-lapse imaging of cell cycle progression from 7-day-old Arabidopsis root meristematic cells of WT (A) and *iqd678* (B). White arrows depict the position of PPB, brown arrowheads show PPB loss.

Microtubules were visualized by introducing RFP-MBD marker in *iqd678* and WT background. Time frame indicated in minutes within all images. Scale bars, 10 μ m.

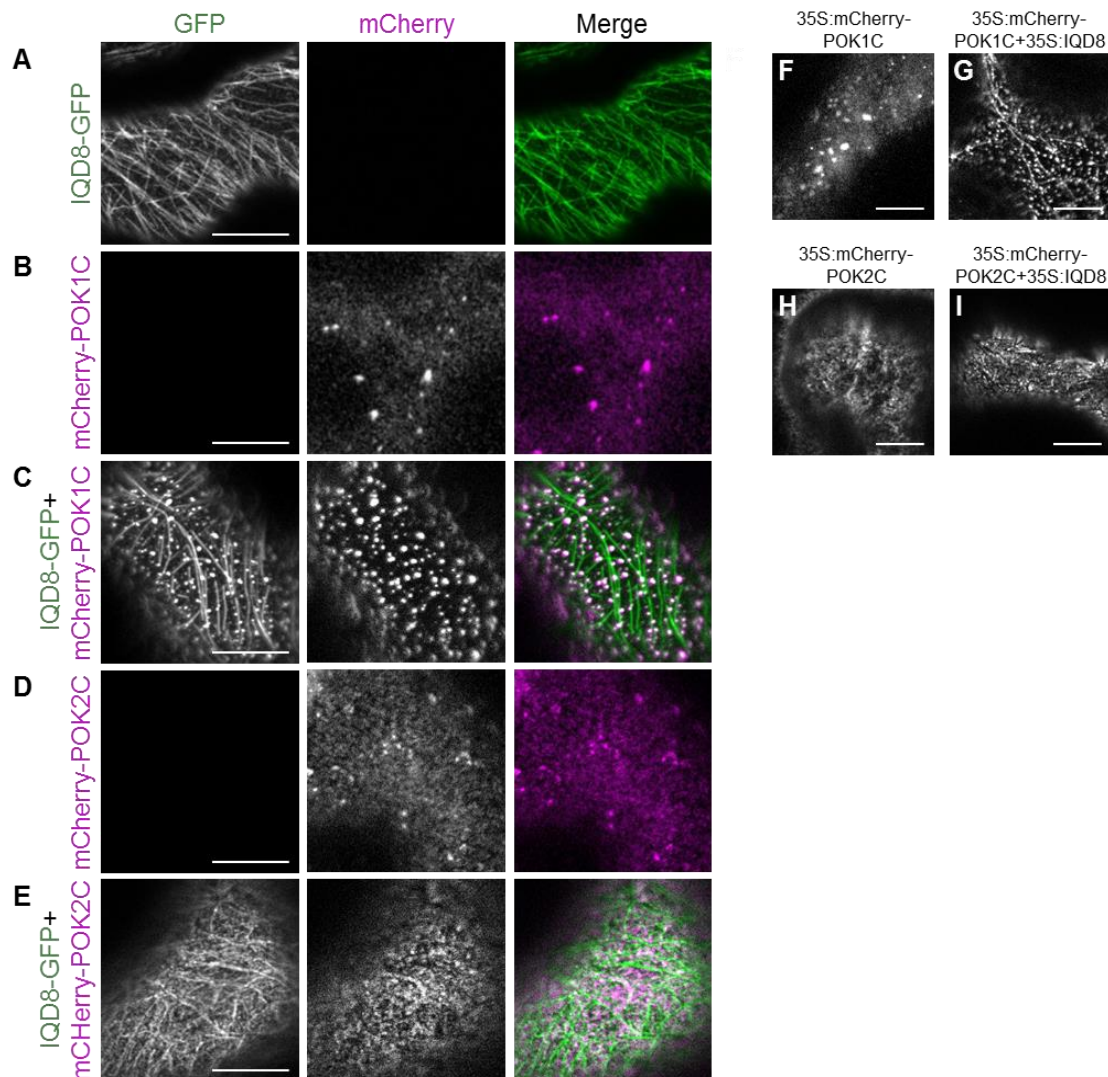


Figure S 10 Co-expression of C-terminally GFP-tagged and untagged variants of IQD8 with POKs.

(A-E) C-terminally GFP-tagged IQD8 are co-expressed transiently with mCherry-POK1 and POK2 C-terminal fragments. Expression of IQD8-GFP, mCherry-POKs and merged images are shown in left column, center column, and rightmost column, respectively. (F-I) mcherry-POKs localization upon their alone expression (F,H) and with untagged IQD8 (G,I). Constructs were expressed under 35S promoter. Images were acquired 2 days after transient transformation of constructs in *N. benthamiana*. All image were acquired with the identical settings. Scale bars, 10 μ m.

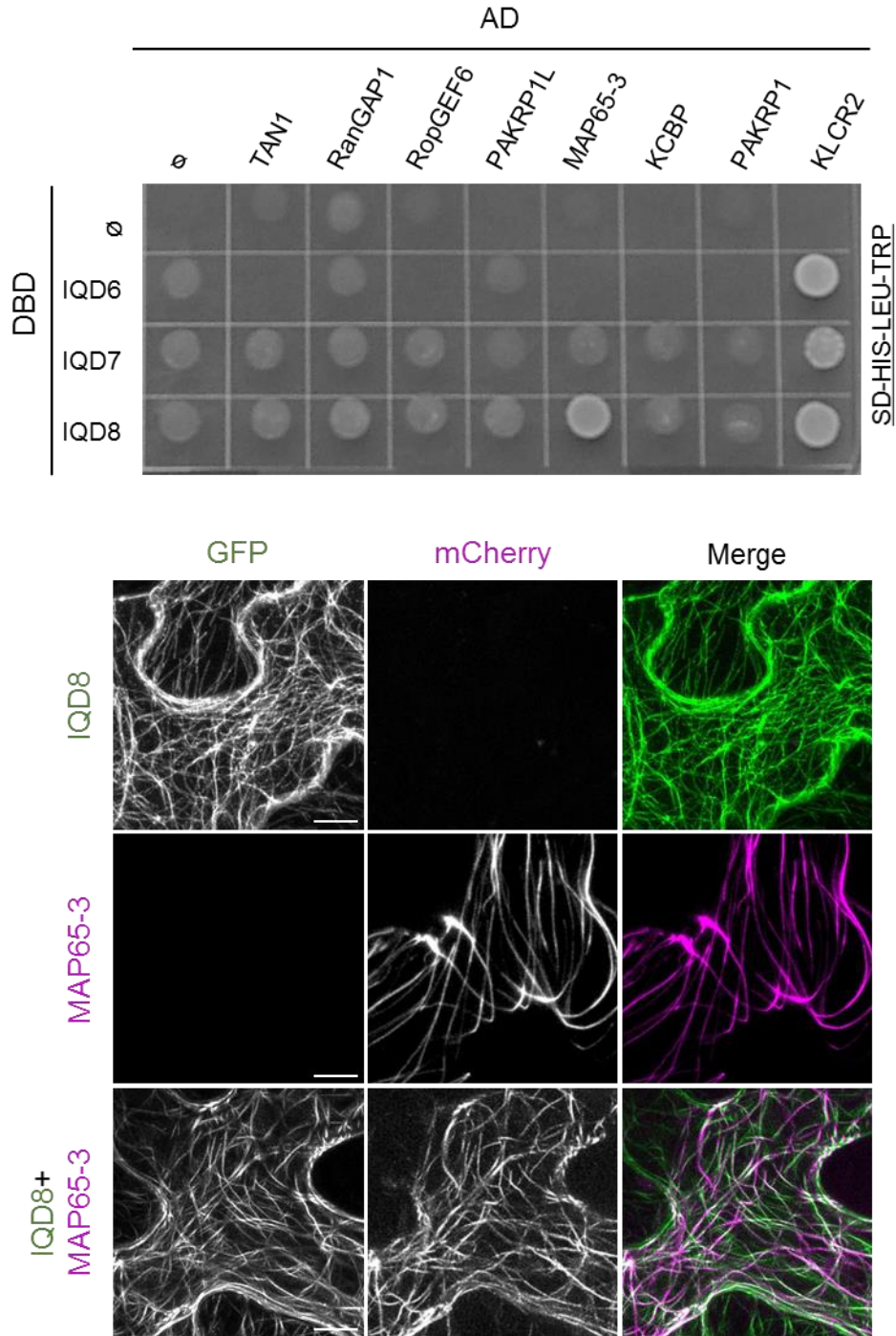


Figure S 11 Interaction of IQD8 and related proteins with key player of cytokinesis.

Yeast cells showing co-expression of IQD6-8 with key players of cytokinesis. (A) Growth of yeast cells on interaction selective, SD-HIS-LEU-TRP triple drop out media indicative of protein-protein interaction. Interaction was analyzed 3 days after spotting. The result represents at least two independent experiments. SD-HIS-LEU-TRP, yeast media lacking histidine, leucine, and tryptophan. (B) Confocal laser scanning microscopy showing expression of GFP-IQD8, mCherry-MAP65-3 (upper and middle rows, respectively) and co-expression of GFP-IQD8 with mCherry-MAP65-3 (lower row). left column shows expression of fusion proteins in GFP channel, center column shows expression of fusion proteins in mCherry channel and right column shows merge images. Constructs were expressed under 35S promoter. Images are acquired 2 days after transient transformation in *N. benthamiana*. Scale bars, 10 μ m.

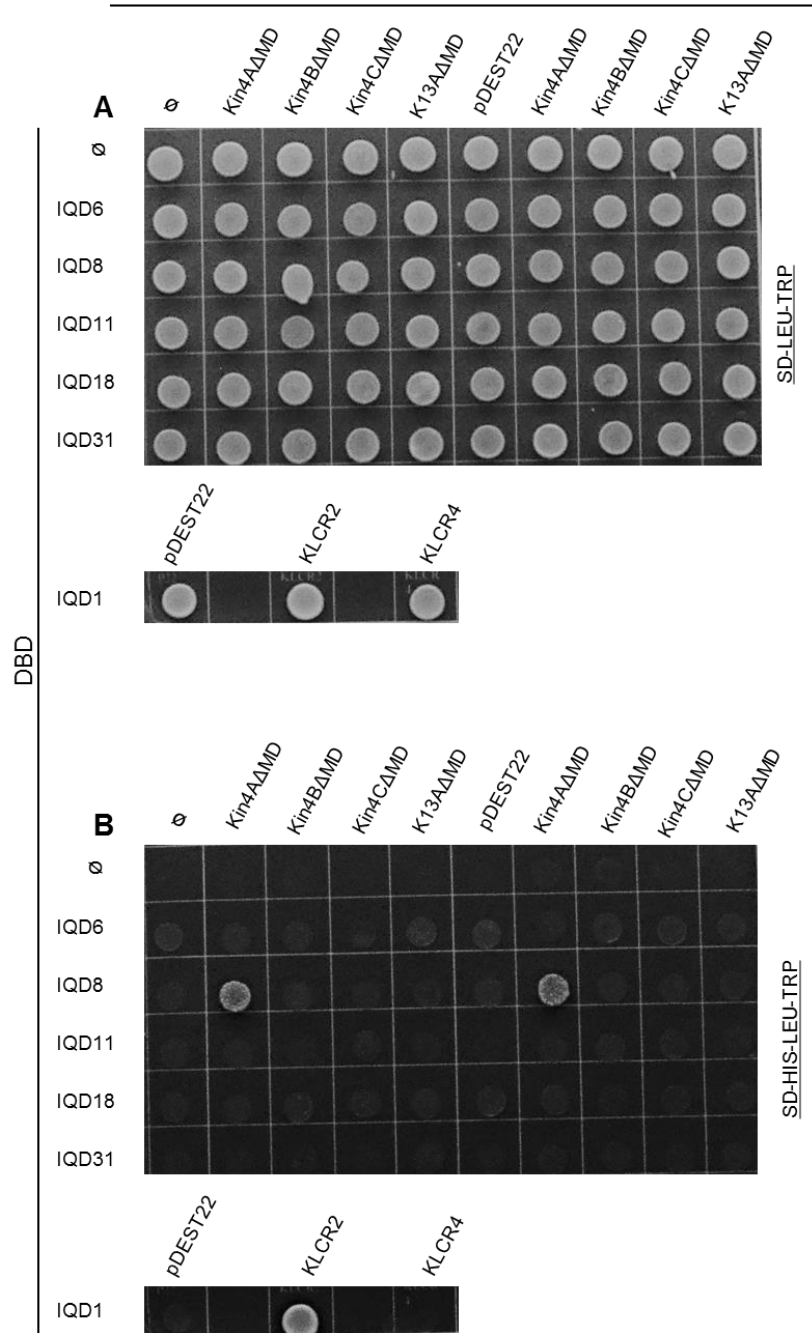


Figure S 12 Interaction of IQDs with other factors outside the cytokinesis.

Yeast cells co-expressing IQDs and kinesins fused to the DBD and AD, respectively of GAL4. Growth of transformed yeast cells on vector selective media (A) and interaction selective media (B). Interaction was analyzed 3 days after spotting. SD-HIS-LEU-TRP, yeast media lacking histidine, leucine, and tryptophan.

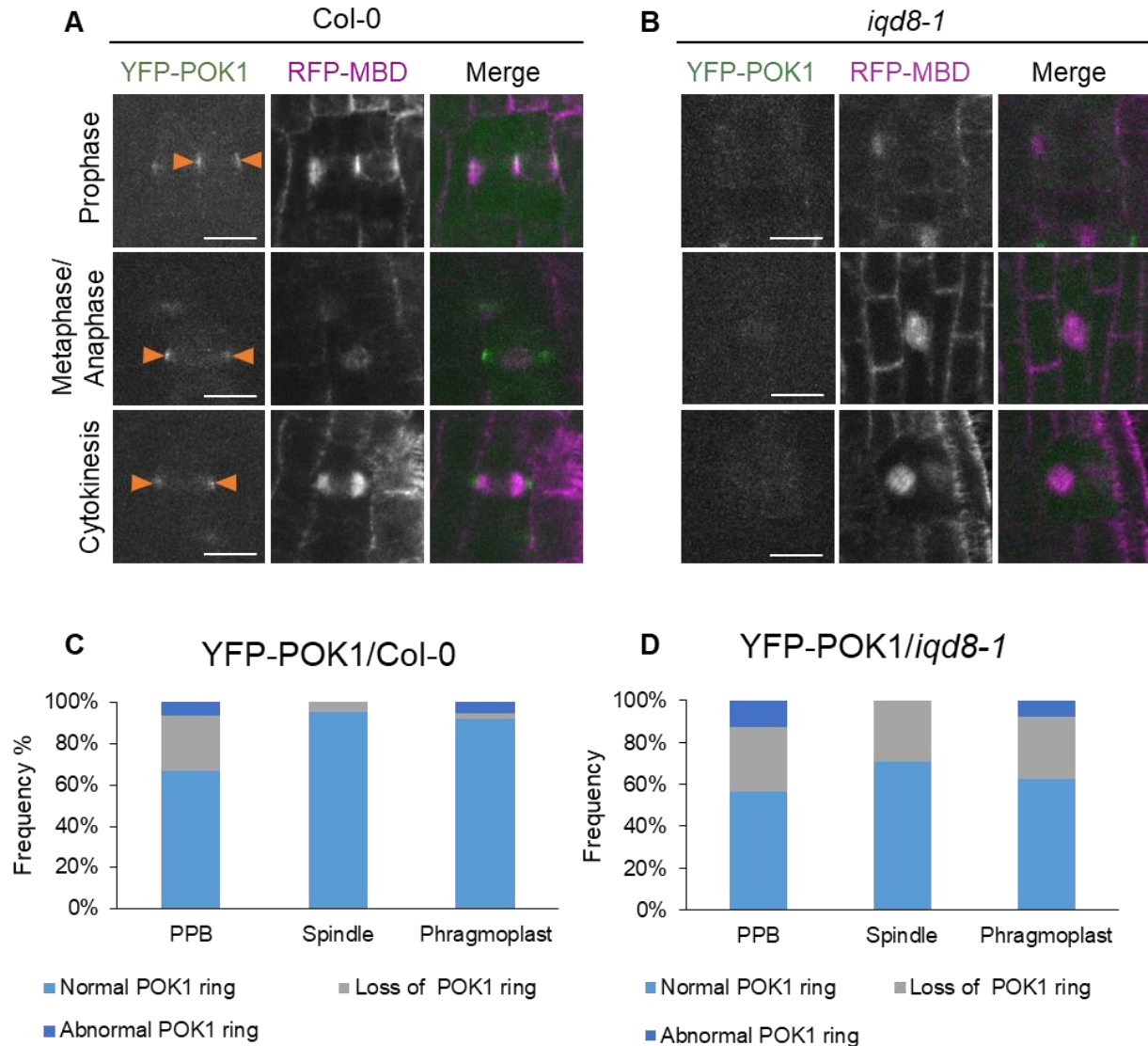


Figure S 13 Dependency of POK1 localization for functional IQD8.

(A-B) YFP-POK1 localization pattern in Arabidopsis root meristem of 7-day-old seedlings of Col-0 (A) and *iqd8-1* single mutant (B) in prophase, metaphase/anaphase and in cytokinetic cells. Scale bars, 10 μ m. Distribution of YFP-POK1 ring in Col-0 (C) and *iqd8-1* single mutant (D) cells showing PPB, spindle and phragmoplast microtubules. RFP-MBD was used to visualize microtubules. Dark blue, light blue and gray color represent 3 categories of cells depending upon localization pattern of YFP-POK1 at division site. Confocal images and quantification data represent 20-25 roots from two independent experiments.

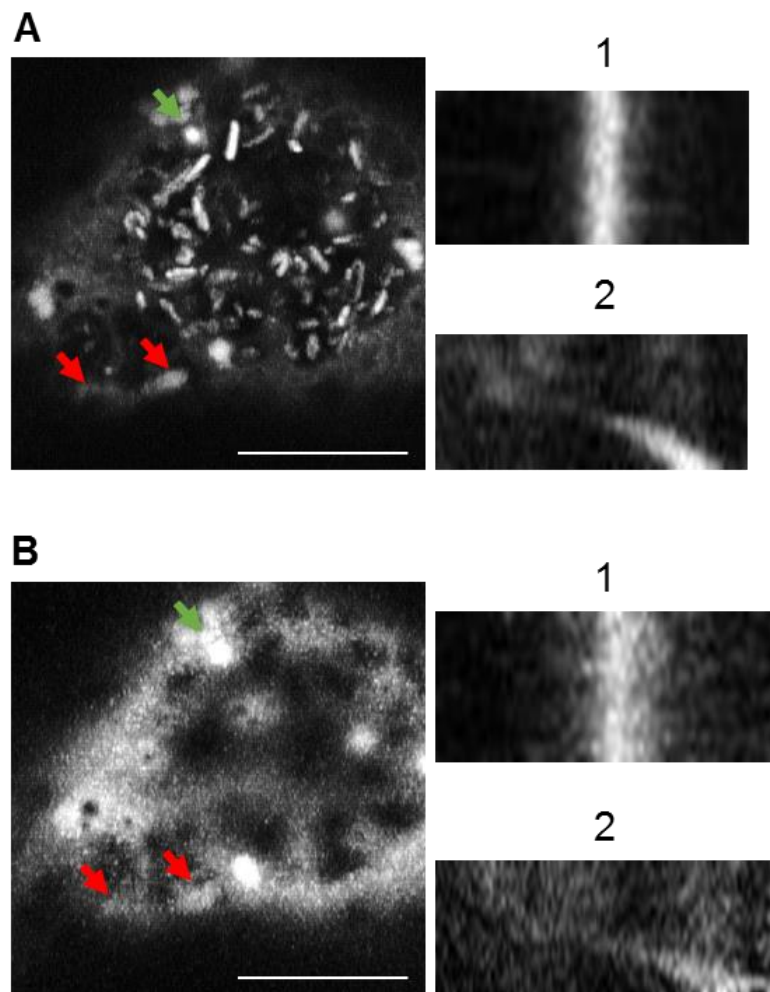


Figure S 14 Kymograph analysis.

Kymograph analysis showing dynamics of Golgi bodies labeled with Golgi marker protein (A) and KIN1 (B). Red arrows indicate the first and last positions of moving bodies and green arrows indicate the positions of static protein bodies. Right column indicates the kymograph of static (1) and moving protein bodies (2). Images are acquired 2 days after transient transformation in *N. benthamiana*. Analysis was performed using 3 cells for each construct. Scale bars, 10 μ m.

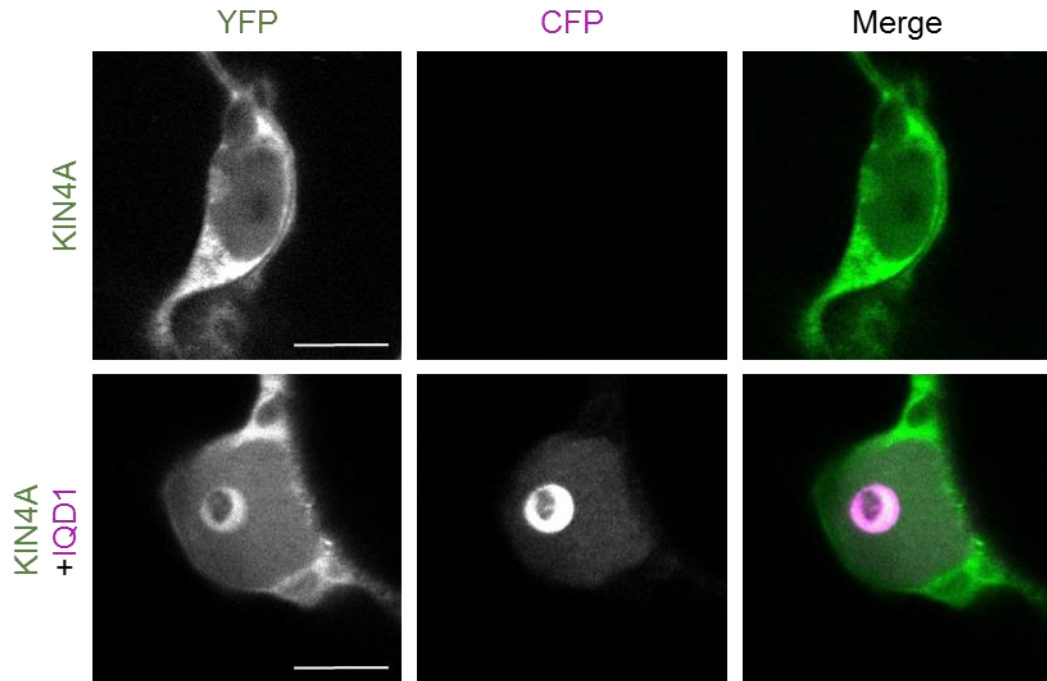


Figure S 15 KIN4A interaction with IQD1.

single optical section of *N. benthamiana* leaf epidermal cells showing expression of KIN4A alone as well as with IQD1. Constructs were expressed under the control of 35S promoter. GFP, CFP and merge signals were shown in left, center, and right columns, respectively. Images are acquired 2 days after transient transformation and representing two independent experiments. Scale bars, 10 μ m.

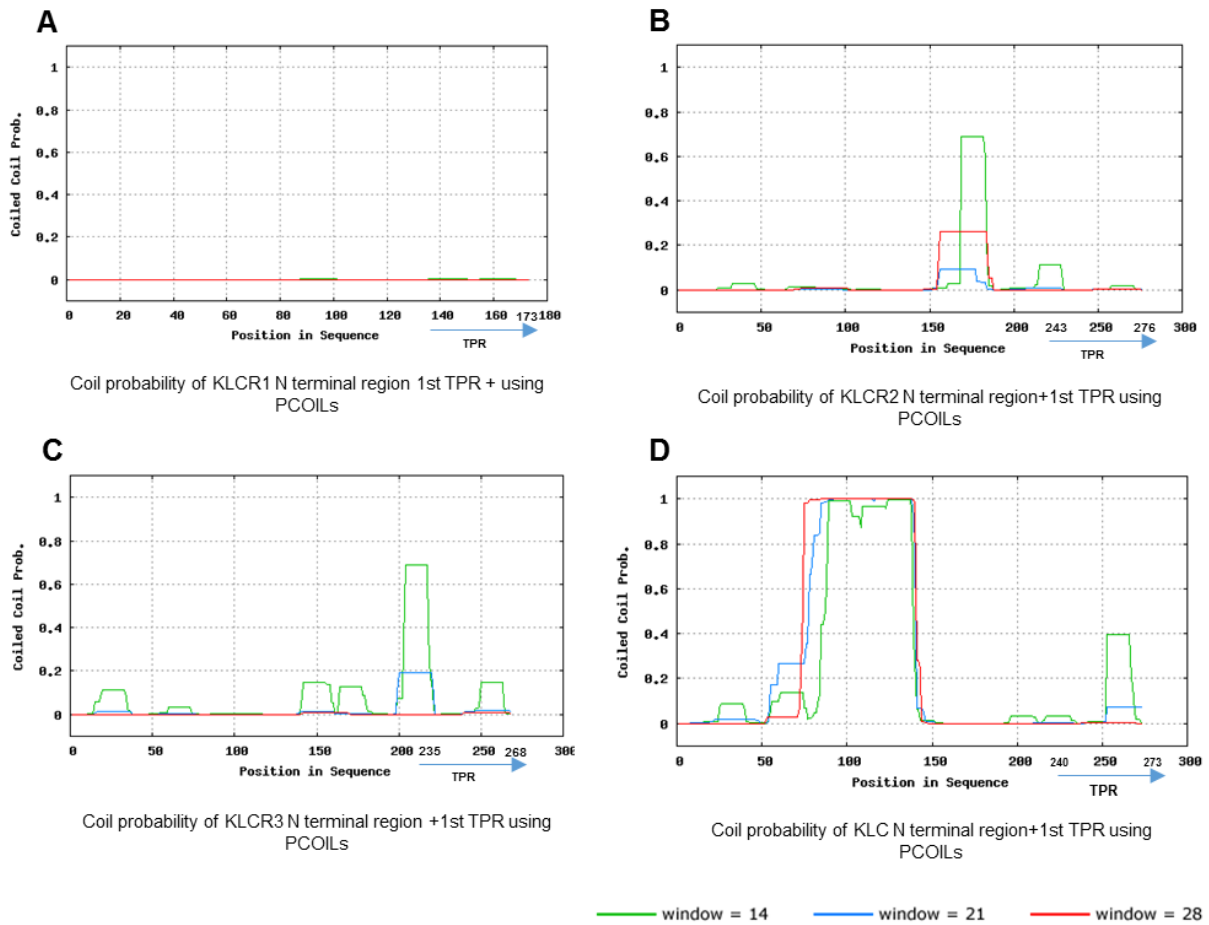


Figure S 16 Coiled coil probability of Arabidopsis KLCRs in comparison to mammalian KLC. Prediction of coiled coil region in Arabidopsis KLCR1 (A), KLCR2 (B), KLCR3 (C) in comparison to animal KLC (D).

References

- Abel, S., Savchenko, T., Levy, M., 2005. Genome-wide comparative analysis of the IQD gene families in *Arabidopsis thaliana* and *Oryza sativa*. *BMC Evol. Biol.* 5, 1–25. <https://doi.org/10.1186/1471-2148-5-72>
- Abu-Abied, M., Belausov, E., Hagay, S., Peremyslov, V., Dolja, V., Sadot, E., 2018. Myosin XI-K is involved in root organogenesis, polar auxin transport, and cell division. *J. Exp. Bot.* 69, 2869–2881. <https://doi.org/10.1093/jxb/ery112>
- Adio, S., Reth, J., Bathe, F., Woehlke, G., 2006. Review: Regulation mechanisms of Kinesin-1. *J. Muscle Res. Cell Motil.* 27, 153–160. <https://doi.org/10.1007/s10974-005-9054-1>
- Aikin, R.A., Ayers, K.L., Thérond, P.P., 2008. The role of kinases in the Hedgehog signalling pathway. *EMBO Rep.* 9, 330–336. <https://doi.org/10.1038/embor.2008.38>
- Akhmanova, A., Hammer, J.A., 2010. Linking molecular motors to membrane cargo. *Curr Opin Cell Biol.* 22, 479–487. <https://doi.org/10.1016/j.ceb.2010.04.008>
- Akhmanova, A., Hoogenraad, C.C., Drabek, K., Stepanova, T., Dortland, B., Verkerk, T., Vermeulen, W., Burgering, B.M., De Zeeuw, C.I., Grosveld, F., Galjart, N., 2001. CLASPs are CLIP-115 and -170 associating proteins involved in the regional regulation of microtubule dynamics in motile fibroblasts. *Cell* 104, 923–935. [https://doi.org/10.1016/S0092-8674\(01\)00288-4](https://doi.org/10.1016/S0092-8674(01)00288-4)
- Amaratungas, A., Morins, P.J., Kosiks, K.S., Fineslil, R.E., 1993. Inhibition of Kinesin Synthesis and Rapid Anterograde Axonal Transport in Vivo by an Antisense Oligonucleotide, *J. Biol. Chem.* <https://doi.org/https://doi.org/10.1046/j.1471-4159.1995.64052374.x>
- Ambrose, J.C., Cyr, R., 2008. Mitotic spindle organization by the preprophase band. *Mol. Plant* 1, 950–960. <https://doi.org/10.1093/mp/ssn054>
- Ambrose, J.C., Cyr, R., 2007. The kinesin ATK5 functions in early spindle assembly in *Arabidopsis*. *Plant Cell* 19, 226–236. <https://doi.org/10.1105/tpc.106.047613>
- Apostolokos, P., Galatis, B., 1985. Studies on the development of the air pores and air chambers of *Marchantia paleacea*. *Protoplasma* 128, 136–146. <https://doi.org/10.1007/BF01276335>
- Ayaydin, F., Vissi, E., Mészáros, T., Miskolczi, P., Kovács, I., Fehér, A., Dombrádi, V., Erdödi, F., Gergely, P., Dudits, D., 2000. Inhibition of serine/threonine-specific protein phosphatases causes premature activation of cdc2MsF kinase at G2/M transition and early mitotic microtubule organisation in alfalfa. *Plant J.* 23, 85–96. <https://doi.org/10.1046/j.1365-313X.2000.00798.x>
- Azimzadeh, J., Nacry, P., Christodoulidou, A., Drevensek, S., Camilleri, C., Amiour, N., Parcy, F., Pastuglia, M., Boucheza, D., 2008. *Arabidopsis* Tonneau1 proteins are essential for preprophase band formation and interact with centrin. *Plant Cell* 20, 2146–2159. <https://doi.org/10.1105/tpc.107.056812>
- Bähler, M., Rhoads, A., 2002. Calmodulin signaling via the IQ motif. *FEBS Lett.* 513, 107–113. [https://doi.org/10.1016/S0014-5793\(01\)03239-2](https://doi.org/10.1016/S0014-5793(01)03239-2)
- Baluška, F., Jasik, J., Edelmann, H.G., Salajová, T., Volkmann, D., 2001. Latrunculin B-induced plant dwarfism: Plant cell elongation is F-actin-dependent. *Dev. Biol.* 231, 113–124. <https://doi.org/10.1006/dbio.2000.0115>
- Bannigan, A., Scheible, W.R., Lukowitz, W., Fagerstrom, C., Wadsworth, P., Somerville, C., Baskin, T.I., 2007. A conserved role for kinesin-5 in plant mitosis. *J. Cell Sci.* 120, 2819–2827. <https://doi.org/10.1242/jcs.009506>
- Bayer, M., Slane, D., Jürgens, G., 2017. Early plant embryogenesis — dark ages or dark matter? *Curr. Opin. Plant Biol.* 35, 30–36. <https://doi.org/10.1016/j.pbi.2016.10.004>
- Belmont, L.D., Hyman, A.A., Sawin, K.E., Mitchison, T.J., 1990. Real-time visualization of cell cycle-dependent changes in microtubule dynamics in cytoplasmic extracts. *Cell* 62, 579–589. [https://doi.org/10.1016/0092-8674\(90\)90022-7](https://doi.org/10.1016/0092-8674(90)90022-7)
- Bergey, D.R., Kandel, R., Tyree, B.K., Dutt, M., Dhekney, S.A., 2014. The Role of Calmodulin and Related Proteins in Plant Cell Function: An Ever-Thickening Plot. *Springer Sci. Rev.* 145–159. <https://doi.org/10.1007/s40362-014-0025-z>
- Berlow, R.B., Dyson, H.J., Wright, P.E., 2015. Functional advantages of dynamic protein disorder. *FEBS Lett.* 589, 2433–2440. <https://doi.org/10.1016/j.febslet.2015.06.003>
- Bertani, G., 1951. Studies on lysogenesis. I. The mode of phage liberation by lysogenic *Escherichia coli*. *J. Bacteriol.* 62, 293–300.
-

-
- Besson, S., Dumais, J., 2011. Universal rule for the symmetric division of plant cells. *Proc. Natl. Acad. Sci.* 108, 6294–6299. <https://doi.org/10.1073/pnas.1011866108>
- Bi, L., Weng, L., Jiang, Z., Xiao, H., 2018. The tomato IQD gene SUN24 regulates seed germination through ABA signaling pathway. *Planta* 248, 919–931. <https://doi.org/10.1007/s00425-018-2950-6>
- Binarová, P., Cenklová, V., Hause, B., Kubátová, E., Lysák, M., Doležel, J., Bögre, L., Dráber, P., 2000. Nuclear γ -Tubulin during Acentriolar Plant Mitosis. *Plant Cell* 12, 433–442. <https://doi.org/10.1105/tpc.12.3.433>
- Bisgrove, S.R., Lee, Y.-R.J., Liu, B., Peters, N.T., Kropf, D.L., 2008. The Microtubule Plus-End Binding Protein EB1 Functions in Root Responses to Touch and Gravity Signals in Arabidopsis. *Plant Cell* 20, 396–410. <https://doi.org/10.1105/tpc.107.056846>
- Blackstone, N.W., 2015. The impact of mitochondrial endosymbiosis on the evolution of calcium signaling. *Cell Calcium*. <https://doi.org/10.1016/j.ceca.2014.11.006>
- Blangy, A., Lane, H.A., D'Herin, P., Harper, M., Kress, S.M., Nigg, E.A., 1995. Phosphorylation by p34cdc2 regulates spindle association of human Eg5, a kinesin-related motor essential for bipolar spindle formation in vivo. *Cell* 83, 1159–1169. [https://doi.org/10.1016/0092-8674\(95\)90142-6](https://doi.org/10.1016/0092-8674(95)90142-6)
- Blasius, T.L., Cai, D., Jih, G.T., Toret, C.P., Verhey, K.J., 2007. Two binding partners cooperate to activate the molecular motor Kinesin-1. *J. Cell Biol.* 176, 11–17. <https://doi.org/10.1083/jcb.200605099>
- Bouché, N., Yellin, A., Snedden, W.A., Fromm, H., 2005. Plant-Specific Calmodulin-Binding Proteins. *Annu. Rev. Plant Biol.* 56, 435–466. <https://doi.org/10.1146/annurev.arplant.56.032604.144224>
- Boudsocq, M., Droillard, M.-J., Regad, L., Laurière, C., 2012. Characterization of Arabidopsis calcium-dependent protein kinases: activated or not by calcium? *Biochem. J.* 447, 291–299. <https://doi.org/10.1042/BJ20112072>
- Browning, K.S., 1996. The plant translational apparatus. *Plant Mol. Biol.* 32, 107–144. <https://doi.org/10.1007/BF00039380>
- Burgess, J. & Northcote, D.H., 1968. The relationship between the endoplasmic reticulum and microtubular aggregation and disaggregation. *Planta* 80, 1–14. <https://doi.org/https://doi.org/10.1007/BF00387183>
- Burk, D.H., Liu, B., Zhong, R., Morrison, W.H., Ye, Z.-H., 2001. A Katanin-like Protein Regulates Normal Cell Wall gBiosynthesis and Cell Elongation. *Plant Cell* 13, 807–827. <https://doi.org/10.1105/tpc.13.4.807>
- Burk, D.H., Zhong, R., Ye, Z.H., 2007. The katanin microtubule severing protein in plants. *J. Integr. Plant Biol.* 49, 1174–1182. <https://doi.org/10.1111/j.1672-9072.2007.00544.x>
- Burssens, S., Van Montagu, M., Inzé, D., 1998. The cell cycle in Arabidopsis. *Plant Physiol. Biochem.* 36, 9–19. [https://doi.org/10.1016/S0981-9428\(98\)80087-9](https://doi.org/10.1016/S0981-9428(98)80087-9)
- Bürstenbinder, K., Möller, B., Plötner, R., Stamm, G., Hause, G., Mitra, D., Abel, S., 2017. The IQD family of calmodulin-binding proteins links calcium signaling to microtubules, membrane subdomains, and the nucleus. *Plant Physiol.* 173, 1692–1708. <https://doi.org/10.1104/pp.16.01743>
- Bürstenbinder, K., Savchenko, T., Müller, J., Adamson, A.W., Stamm, G., Kwong, R., Zipp, B.J., Dinesh, D.C., Abel, S., 2013. Arabidopsis calmodulin-binding protein iq67-domain 1 localizes to microtubules and interacts with kinesin light chain-related protein-1. *J. Biol. Chem.* 288, 1871–1882. <https://doi.org/10.1074/jbc.M112.396200>
- Buschmann, H., Dols, J., Kopischke, S., Peña, E.J., Andrade-Navarro, M.A., Heinlein, M., Szymanski, D.B., Zachgo, S., Doonan, J.H., Lloyd, C.W., 2015. Arabidopsis KCBP interacts with AIR9 but stays in the cortical division zone throughout mitosis via its MyTH4-FERM domain. *J. Cell Sci.* 128, 2033–2046. <https://doi.org/10.1242/jcs.156570>
- Buschmann, H., Fabri, C.O., Hauptmann, M., Hutzler, P., Laux, T., Lloyd, C.W., Schöffner, A.R., 2004. Helical growth of the Arabidopsis mutant *tortifolia1* reveals a plant-specific microtubule-associated protein. *Curr. Biol.* 14, 1515–1521. <https://doi.org/10.1016/j.cub.2004.08.033>
- Buschmann, H., Lloyd, C.W., 2008. Arabidopsis mutants and the network of microtubule-associated functions. *Mol. Plant* 1, 888–898. <https://doi.org/10.1093/mp/ssn060>
- Buschmann, H., Müller, S., 2019. Update on plant cytokinesis: rule and divide. *Curr. Opin. Plant Biol.* 52, 97–105. <https://doi.org/10.1016/j.pbi.2019.07.003>
- Buschmann, H., Zachgo, S., 2016. The Evolution of Cell Division: From Streptophyte Algae to Land Plants. *Trends Plant Sci.* 21, 872–883. <https://doi.org/10.1016/j.tplants.2016.07.004>
-

-
- Cai, D., Hoppe, A.D., Swanson, J.A., Verhey, K.J., 2007. Kinesin-1 structural organization and conformational changes revealed by FRET stoichiometry in live cells. *J. Cell Biol.* 176, 51–63. <https://doi.org/10.1083/jcb.200605097>
- Cai, G., Cresti, M., 2012. Are kinesins required for organelle trafficking in plant cells? *Front. Plant Sci.* 3, 1–10. <https://doi.org/10.3389/fpls.2012.00170>
- Cai, H., Cheng, J., Yan, Y., Xiao, Z., Li, J., Mou, S., Qiu, A., Lai, Y., Guan, D., He, S., 2015. Genome-wide identification and expression analysis of calcium-dependent protein Kinase and its closely related Kinase genes in capsicum Annuum. *Front. Plant Sci.* 6, 1–14. <https://doi.org/10.3389/fpls.2015.00737>
- Cai, R., Zhang, C., Zhao, Y., Zhu, K., Wang, Y., Jiang, H., Xiang, Y., Cheng, B., 2016. Genome-wide analysis of the IQD gene family in maize. *Mol. Genet. Genomics* 291, 543–558. <https://doi.org/10.1007/s00438-015-1122-7>
- Caillaud, M.C., Lecomte, P., Jammes, F., Quentin, M., Pagnotta, S., Andrio, E., Engler, J.D.A., Marfaing, N., Gounon, P., Abad, P., Favery, B., 2008. MAP65-3 microtubule-associated protein is essential for nematode-induced giant cell ontogenesis in Arabidopsis. *Plant Cell* 20, 423–437. <https://doi.org/10.1105/tpc.107.057422>
- Camilleri, C., Azimzadeh, J., Pastuglia, M., Bellini, C., Grandjean, O., Bouchez, D., 2002. The Arabidopsis TONNEAU2 gene encodes a putative novel protein phosphatase 2A regulatory subunit essential for the control of the cortical cytoskeleton. *Plant Cell* 14, 833–845. <https://doi.org/10.1105/tpc.010402>
- Case, R.M., Eisner, D., Gurney, A., Jones, O., Muallem, S., Verkhatsky, A., 2007. Evolution of calcium homeostasis: From birth of the first cell to an omnipresent signalling system. *Cell Calcium* 42, 345–350. <https://doi.org/10.1016/j.ceca.2007.05.001>
- Cervený, L., Strasková, A., Danková, V., Hartlova, A., Cecková, M., Staud, F., Stulik, J., 2013. Tetratricopeptide Repeat Motifs in the World of Bacterial Pathogens: Role in Virulence Mechanisms. *Infect. Immun.* 81, 629–635. <https://doi.org/10.1128/IAI.01035-12>
- Chakraborty, B., Willemsen, V., de Zeeuw, T., Liao, C.Y., Weijers, D., Mulder, B., Scheres, B., 2018. A Plausible Microtubule-Based Mechanism for Cell Division Orientation in Plant Embryogenesis. *Curr. Biol.* 28, 3031–3043.e2. <https://doi.org/10.1016/j.cub.2018.07.025>
- Chan, J., Calder, G., Fox, S., Lloyd, C., 2005. Localization of the microtubule end binding protein EB1 reveals alternative pathways of spindle development in Arabidopsis suspension cells. *Plant Cell* 17, 1737–1748. <https://doi.org/10.1105/tpc.105.032615>
- Chan, J., Calder, G.M., Doonan, J.H., Lloyd, C.W., 2003a. EB1 reveals mobile microtubule nucleation sites in Arabidopsis. *Nat. Cell Biol.* 5, 967–971. <https://doi.org/10.1038/ncb1057>
- Chan, J., Jensen, C.G., Jensen, L.C.W., Bush, M., Lloyd, C.W., 1999. The 65-kDa carrot microtubule-associated protein forms regularly arranged filamentous cross-bridges between microtubules. *Proc. Natl. Acad. Sci.* 96, 14931–14936. <https://doi.org/10.1073/pnas.96.26.14931>
- Chan, J., Mao, G., Smertenko, A., Hussey, P.J., Naldrett, M., Bottrill, A., Lloyd, C.W., 2003b. Identification of a MAP65 isoform involved in directional expansion of plant cells. *FEBS Lett.* 534, 161–163. [https://doi.org/10.1016/S0014-5793\(02\)03848-6](https://doi.org/10.1016/S0014-5793(02)03848-6)
- Chen, X., Grandont, L., Li, H., Hauschild, R., Paque, S., Abuzeineh, A., Rakusová, H., Benkova, E., Perrot-Rechenmann, C., Friml, J., 2014. Inhibition of cell expansion by rapid ABP1-mediated auxin effect on microtubules. *Nature* 516, 90–93. <https://doi.org/10.1038/nature13889>
- Cheung, H.O.-L., Zhang, X., Ribeiro, A., Mo, R., Makino, S., Puvion-Randall, V., Law, K.K.L., Briscoe, J., Hui, C.-C., 2009. The kinesin protein Kif7 is a critical regulator of Gli transcription factors in mammalian hedgehog signaling. *Sci. Signal.* 2, ra29. <https://doi.org/10.1126/scisignal.2000405>
- Cleary, A.L., 1995. F-actin redistributions at the division site in living Tradescantia stomatal complexes as revealed by microinjection of rhodamine-phalloidin. *Protoplasma* 185, 152–165. <https://doi.org/10.1007/BF01272855>
- Cleary, A.L., Gunning, B.E.S., Wasteneys, G.O., Hepler, P.K., 1992. Microtubule and F-actin dynamics at the division site in living Tradescantia stamen hair cells. *J. Cell Sci.* 103, 977–988.
- Cleary, A.L., Smith, L.G., 1998. The Tangled1 gene is required for spatial control of cytoskeletal arrays associated with cell division during maize leaf development. *Plant Cell* 10, 1875–1888. <https://doi.org/10.1105/tpc.10.11.1875>
- Clough, S.J., Bent, A.F., 1998. Floral dip: A simplified method for Agrobacterium-mediated transformation of
-

-
- Arabidopsis thaliana*. Plant J. 16, 735–743. <https://doi.org/10.1046/j.1365-313X.1998.00343.x>
- Colasanti, J., Cho, S.O., Wick, S., Sundaresan, V., 1993. Localization of the functional p34cdc2 homolog of maize in root tip and stomatal complex cells: Association with predicted division sites. Plant Cell 5, 1101–1111. <https://doi.org/10.2307/3869630>
- Coy, D.L., Hancock, W.O., Wagenbach, M., Howard, J., 1999. Kinesin's tail domain is an inhibitory regulator of the motor domain. Nat. Cell Biol. 1, 288–292. <https://doi.org/10.1038/13001>
- Craddock, C., Lavagi, I., Yang, Z., 2012. New insights into Rho signaling from plant ROP/Rac GTPases. Trends Cell Biol. 22, 492–501. <https://doi.org/10.1016/j.tcb.2012.05.002>
- Dagenbach, E.M., 2004. A new kinesin tree. J. Cell Sci. 117, 3–7. <https://doi.org/10.1242/jcs.00875>
- Dammermann, A., Desai, A., Oegema, K., 2003. The minus end in sight. Curr. Biol. 13, 614–624. [https://doi.org/10.1016/S0960-9822\(03\)00530-X](https://doi.org/10.1016/S0960-9822(03)00530-X)
- Das, A.K., Cohen, P.T.W., Barford, D., 1998. The structure of the tetratricopeptide repeats of protein phosphatase 5: implications for TPR-mediated protein-protein interactions. EMBO J. 17, 1192–1199. <https://doi.org/10.1093/emboj/17.5.1192>
- Day, I.S., Reddy, V.S., Shad Ali, G., Reddy, A.S., 2002. Analysis of EF-hand-containing proteins in Arabidopsis. Genome Biol. 3. <https://doi.org/10.1186/gb-2002-3-10-research0056>
- de Keijzer, J., Kieft, H., Ketelaar, T., Goshima, G., Janson, M.E., 2017. Shortening of Microtubule Overlap Regions Defines Membrane Delivery Sites during Plant Cytokinesis. Curr. Biol. 27, 514–520. <https://doi.org/10.1016/j.cub.2016.12.043>
- de Michele, R., McFarlane, H.E., Parsons, H.T., Meents, M.J., Lao, J., González Fernández-Niño, S.M., Petzold, C.J., Frommer, W.B., Samuels, A.L., Heazlewood, J.L., 2016. Free-Flow Electrophoresis of Plasma Membrane Vesicles Enriched by Two-Phase Partitioning Enhances the Quality of the Proteome from *Arabidopsis* Seedlings. J. Proteome Res. 15, 900–913. <https://doi.org/10.1021/acs.jproteome.5b00876>
- Deavours, B.E., Reddy, A.S.N., Walker, R.A., 1998. Ca²⁺/calmodulin regulation of the Arabidopsis kinesin-like calmodulin-binding protein. Cell Motil. Cytoskeleton 40, 408–416. [https://doi.org/10.1002/\(SICI\)1097-0169\(1998\)40:4<408::AID-CM8>3.0.CO;2-6](https://doi.org/10.1002/(SICI)1097-0169(1998)40:4<408::AID-CM8>3.0.CO;2-6)
- Dello Iorio, R., Linhares, F.S., Scacchi, E., Casamitjana-Martinez, E., Heidstra, R., Costantino, P., Sabatini, S., 2007. Cytokinins Determine Arabidopsis Root-Meristem Size by Controlling Cell Differentiation. Curr. Biol. 17, 678–682. <https://doi.org/10.1016/j.cub.2007.02.047>
- Desai, A., Verma, S., Mitchison, T.J., Walczak, C.E., 1999. Kin I kinesins are microtubule-destabilizing enzymes. Cell 96, 69–78. [https://doi.org/10.1016/S0092-8674\(00\)80960-5](https://doi.org/10.1016/S0092-8674(00)80960-5)
- Dhonukshe, P., Gadella, T.W.J., 2003. Alteration of microtubule dynamic instability during preprophase band formation revealed by yellow fluorescent protein-CLIP170 microtubule plus-end labeling. Plant Cell 15, 597–611. <https://doi.org/10.1105/tpc.008961>
- Dhonukshe, P., Kleine-Vehn, J., Friml, J., 2005a. Cell polarity, auxin transport, and cytoskeleton-mediated division planes: Who comes first? Protoplasma 226, 67–73. <https://doi.org/10.1007/s00709-005-0104-8>
- Dhonukshe, P., Mathur, J., Hülskamp, M., Gadella, T.W.J., 2005b. Microtubule plus-ends reveal essential links between intracellular polarization and localized modulation of endocytosis during division-plane establishment in plant cells. BMC Biol. 3, 1–15. <https://doi.org/10.1186/1741-7007-3-11>
- Dibbayawan, T.P., Harper, J.D.I., Marc, J., 2001. A γ -tubulin antibody against a plant peptide sequence localises to cell division-specific microtubule arrays and organelles in plants. Micron 32, 671–678. [https://doi.org/10.1016/S0968-4328\(00\)00064-0](https://doi.org/10.1016/S0968-4328(00)00064-0)
- Dietrich, K.A., Sindelar, C. V., Brewer, P.D., Downing, K.H., Cremo, C.R., Rice, S.E., 2008. The kinesin-1 motor protein is regulated by a direct interaction of its head and tail. Proc. Natl. Acad. Sci. 105, 8938–8943. <https://doi.org/10.1073/pnas.0803575105>
- Ditengou, F.A., Teale, W.D., Kochersperger, P., Flittner, K.A., Kneuper, I., van der Graaff, E., Nziengui, H., Pinosa, F., Li, X., Nitschke, R., Laux, T., Palme, K., 2008. Mechanical induction of lateral root initiation in *Arabidopsis thaliana*. Proc. Natl. Acad. Sci. 105, 18818–18823. <https://doi.org/10.1073/pnas.0807814105>
- Dixit, R., Cyr, R., 2004a. The cortical microtubule array: From dynamics to organization. Plant Cell 16, 2546–2552. <https://doi.org/10.1105/tpc.104.161030>
- Dixit, R., Cyr, R., 2004b. Encounters between dynamic cortical microtubules promote ordering of the cortical array through angle-dependent modifications of microtubule behavior. Plant Cell 16, 3274–3284.
-

<https://doi.org/10.1105/tpc.104.026930>

- Dobney, S., Chiasson, D., Lam, P., Smith, S.P., Snedden, W.A., 2009. The calmodulin-related calcium sensor CML42 plays a role in trichome branching. *J. Biol. Chem.* 284, 31647–31657. <https://doi.org/10.1074/jbc.M109.056770>
- Dodd, A.N., Kudla, J., Sanders, D., 2010. The Language of Calcium Signaling. *Annu. Rev. Plant Biol.* 61, 593–620. <https://doi.org/10.1146/annurev-arplant-070109-104628>
- Doonan, J.H., Cove, D.J., Corke, F.M.K., Lloyd, C.W., 1987. Pre-prophase band of microtubules, absent from tip-growing moss filaments, arises in leafy shoots during transition to intercalary growth. *Cell Motil. Cytoskeleton* 7, 138–153. <https://doi.org/10.1002/cm.970070206>
- Dou, J., Zhao, S., Lu, X., He, N., Zhang, L., Ali, A., Kuang, H., Liu, W., 2018. Genetic mapping reveals a candidate gene (CIFS1) for fruit shape in watermelon (*Citrullus lanatus* L.). *Theor. Appl. Genet.* 131, 947–958. <https://doi.org/10.1007/s00122-018-3050-5>
- Drechsel, D.N., Kirschner, M.W., 1994. The minimum GTP cap required to stabilize microtubules. *Curr. Biol.* 4, 1053–1061. [https://doi.org/10.1016/S0960-9822\(00\)00243-8](https://doi.org/10.1016/S0960-9822(00)00243-8)
- Drevensek, S., Goussot, M., Duroc, Y., Christodoulidou, A., Steyaert, S., Schaefer, E., Duvernois, E., Grandjean, O., Vantard, M., Bouchez, D., Pastuglia, M., 2012. The Arabidopsis TRM1-TON1 interaction reveals a recruitment network common to plant cortical microtubule arrays and eukaryotic centrosomes. *Plant Cell* 24, 178–191. <https://doi.org/10.1105/tpc.111.089748>
- Duan, P., Xu, J., Zeng, D., Zhang, B., Geng, M., Zhang, G., Huang, K., Huang, L., Xu, R., Ge, S., Qian, Q., Li, Y., 2017. Natural Variation in the Promoter of GSE5 Contributes to Grain Size Diversity in Rice. *Mol. Plant* 10, 685–694. <https://doi.org/10.1016/j.molp.2017.03.009>
- Durso, N.A., Cyr, R.J., 1994. A calmodulin-sensitive interaction between microtubules and a higher plant homolog of elongation factor-1alpha. *Plant Cell* 6, 893–905. <https://doi.org/10.1105/tpc.6.6.893>
- Edel and Kudla, 2015, 2015. Increasing complexity and versatility: How the calcium signaling toolkit was shaped during plant land colonization. *Cell Calcium* 57, 231–246. <https://doi.org/http://dx.doi.org/10.1016/j.ceca.2014.10.013>
- Eleftheriou, E.P., Palevitz, B.A., 1992. The effect of cytochalasin D on preprophase band organization in root tip cells of *Allium*. *J. Cell Sci.* 103, 989–998.
- Elliott, A., Shaw, S.L., 2018. Update: Plant Cortical Microtubule Arrays. *Plant Physiol.* 176, 94–105. <https://doi.org/10.1104/pp.17.01329>
- Ems-McClung, S.C., Walczak, C.E., 2010. Kinesin-13s in mitosis: Key players in the spatial and temporal organization of spindle microtubules. *Semin. Cell Dev. Biol.* 21, 276–282. <https://doi.org/10.1016/j.semcdb.2010.01.016>
- Endler, A., Persson, S., 2011. Cellulose synthases and synthesis in arabidopsis. *Mol. Plant* 4, 199–211. <https://doi.org/10.1093/mp/ssq079>
- Endow, S.A., 1999. Microtubule motors in spindle and chromosome motility. *Eur. J. Biochem.* 262, 12–18. <https://doi.org/10.1046/j.1432-1327.1999.00339.x>
- Feiguelman, G., Fu, Y., Yalovsky, S., 2018. ROP GTPases structure-function and signaling pathways. *Plant Physiol.* 176, 57–79. <https://doi.org/10.1104/pp.17.01415>
- Feng, L., Chen, Z., Ma, H., Chen, X., Li, Y., Wang, Y., Xiang, Y., 2014. The IQD Gene Family in Soybean: Structure, Phylogeny, Evolution and Expression. *PLoS One* 9, e110896. <https://doi.org/10.1371/journal.pone.0110896>
- Ferreira, P.C.G., Hemerly, A.S., de Almeida Engler, J., Van Montagu, M., Engler, G., Inze, D., 1994. Developmental expression of the Arabidopsis cyclin gene *cyc1At*. *Plant Cell* 6, 1763–1774. <https://doi.org/10.1105/tpc.6.12.1763>
- Filiz, E., Tombuloglu, H., Ozyigit, I.I., 2013. Genome-wide analysis of IQ67 domain (IQD) gene families in *Brachypodium distachyon*, *Plant OMICS Journal*.
- Fisher, D.D., Gilroy, S., Cyr, R.J., 1996. Evidence for opposing effects of calmodulin on cortical microtubules. *Plant Physiol.* 112, 1079–1087. <https://doi.org/10.1104/pp.112.3.1079>
- Flanders, D.J., Rawlins, D.J., Shaw, P.J., Lloyd, C.W., 1990. Nucleus-associated microtubules help determine the division plane of plant epidermal cells: Avoidance of four-way junctions and the role of cell geometry. *J. Cell Biol.* 110, 1111–1122. <https://doi.org/10.1083/jcb.110.4.1111>

-
- Frey, N., Klotz, J., Nick, P., 2010. A kinesin with calponin-homology domain is involved in premitotic nuclear migration. *J. Exp. Bot.* 61, 3423–3437. <https://doi.org/10.1093/jxb/erq164>
- Friedman, D.S., Vale, R.D., 1999. Single-molecule analysis of kinesin motility reveals regulation by the cargo-binding tail domain. *Nat. Cell Biol.* 1, 293–297. <https://doi.org/10.1038/13008>
- Gaillard, J., Neumann, E., Van Damme, D., Stoppin-Mellet, V., Ebel, C., Barbier, E., Geelen, D., Vantard, M., 2008. Two microtubule-associated proteins of Arabidopsis MAP65s promote antiparallel microtubule bundling. *Mol. Biol. Cell* 19, 4534–4544. <https://doi.org/10.1091/mbc.E08-04-0341>
- Galjart, N., 2005. CLIPs and CLASPs and cellular dynamics. *Nat. Rev. Mol. Cell Biol.* <https://doi.org/10.1038/nrm1664>
- Ganguly, A., Zhu, C., Chen, W., Dixit, R., 2019. FRA1 modulates cortical microtubule localization of CMU proteins. *bioRxiv* 2859, 1–38. <https://doi.org/10.1101/760389>
- Gehl, C., Waadt, R., Kudla, J., Mendel, R.-R., Hänsch, R., 2009. New GATEWAY vectors for High Throughput Analyses of Protein–Protein Interactions by Bimolecular Fluorescence Complementation. *Mol. Plant* 2, 1051–1058. <https://doi.org/10.1093/mp/ssp040>
- Goddard, R.H., Wick, S.M., Silflow, C.D., Snustad, D.P., 1994. Microtubule components of the plant cell cytoskeleton. *Plant Physiol.* <https://doi.org/10.1104/pp.104.1.1>
- Goldstein, L.S.B., Philp, A.V., 1999. The Road Less Traveled: Emerging Principles of Kinesin Motor Utilization. *Annu. Rev. Cell Dev. Biol.* 15, 141–183. <https://doi.org/10.1146/annurev.cellbio.15.1.141>
- González-García, M.P., Vilarrasa-Blasi, J., Zhiponova, M., Divol, F., Mora-García, S., Russinova, E., Caño-Delgado, A.I., 2011. Brassinosteroids control meristem size by promoting cell cycle progression in Arabidopsis roots. *Development* 138, 849–859. <https://doi.org/10.1242/dev.057331>
- Goodbody, K.C., Lloyd, C.W., 1990. Actin filaments line up across Tradescantia epidermal cells, anticipating wound-induced division planes. *Protoplasma* 157, 92–101. <https://doi.org/10.1007/BF01322641>
- Goodbody, K.C., Venverloo, C.J., Lloyd, C.W., 1991. Laser microsurgery demonstrates that cytoplasmic strands anchoring the nucleus across the vacuole of premitotic plant cells are under tension. Implications for division plane alignment. *Development* 113, 931–939.
- Granger, C. L., Cyr, R.J., 2001. Spatiotemporal relationships between growth and microtubule orientation as revealed in living root cells of Arabidopsis thaliana transformed with green-fluorescent-protein gene construct GFP-MBD. *Protoplasma* 216, 201–214. <https://doi.org/10.1007/BF02673872>
- Granger, Cheryl L., Cyr, R.J., 2001. Use of abnormal preprophase bands to decipher division plane determination. *J. Cell Sci.* 114, 599–607.
- Grubb, C.D., Abel, S., 2006. Glucosinolate metabolism and its control. *Trends Plant Sci.* <https://doi.org/10.1016/j.tplants.2005.12.006>
- Grummt, M., Pistor, S., Lottspeich, F., Schliwa, M., 1998. Cloning and functional expression of a “fast” fungal kinesin. *FEBS Lett.* 427, 79–84. [https://doi.org/10.1016/s0014-5793\(98\)00399-8](https://doi.org/10.1016/s0014-5793(98)00399-8)
- GUNNING, B.E.S., WICK, S.M., 1985. Preprophase Bands, Phragmoplasts, and Spatial Control of Cytokinesis. *J. Cell Sci.* 1985, 157–179. https://doi.org/10.1242/jcs.1985.Supplement_2.9
- Hackney, D.D., 2007. Jump-starting kinesin. *J. Cell Biol.* <https://doi.org/10.1083/jcb.200611082>
- Hackney, D.D., Baek, N., Snyder, A.C., 2009. Half-Site Inhibition of Dimeric Kinesin Head Domains by Monomeric Tail Domains †. *Biochemistry* 48, 3448–3456. <https://doi.org/10.1021/bi8022575>
- Hackney, D.D., Levitt, J.D., Suhan, J., 1992. Kinesin undergoes a 9 S to 6 S conformational transition. *J. Biol. Chem.* 267, 8696–701.
- Hackney, D.D., Stock, M.F., 2008. Kinesin tail domains and Mg²⁺ directly inhibit release of ADP from head domains in the absence of microtubules. *Biochemistry* 47, 7770–7778. <https://doi.org/10.1021/bi8006687>
- Hackney, D.D., Stock, M.F., 2000. Kinesin's IAK tail domain inhibits initial microtubule-stimulated ADP release. *Nat. Cell Biol.* 2, 257–260. <https://doi.org/10.1038/35010525>
- Halfter, U., Ishitani, M., Zhu, J.-K., 2000. The Arabidopsis SOS2 protein kinase physically interacts with and is activated by the calcium-binding protein SOS3. *Natl. Acad. Sci.* 97, 3735–3740. <https://doi.org/https://doi.org/10.1073/pnas.97.7.3735>
- Halkier, B.A., Gershenzon, J., 2006. BIOLOGY AND BIOCHEMISTRY OF GLUCOSINOLATES. *Annu. Rev. Plant*
-

Biol. 57, 303–333. <https://doi.org/10.1146/annurev.arplant.57.032905.105228>

- Hamada, T., 2014. Microtubule organization and microtubule-associated proteins in plant cells, in: *International Review of Cell and Molecular Biology*. Elsevier Inc., pp. 1–52. <https://doi.org/10.1016/B978-0-12-800178-3.00001-4>
- Hamada, T., 2007. Microtubule-associated proteins in higher plants. *J. Plant Res.* 120, 79–98. <https://doi.org/10.1007/s10265-006-0057-9>
- Hamada, T., Ueda, H., Kawase, T., Hara-Nishimura, I., 2014. Microtubules Contribute to Tubule Elongation and Anchoring of Endoplasmic Reticulum, Resulting in High Network Complexity in Arabidopsis. *Plant Physiol.* 166, 1869–1876. <https://doi.org/10.1104/pp.114.252320>
- Hanahan, D., 1983. Studies on transformation of *Escherichia coli* with plasmids. *J. Mol. Biol.* 166, 557–580. [https://doi.org/10.1016/S0022-2836\(83\)80284-8](https://doi.org/10.1016/S0022-2836(83)80284-8)
- Hardham, A.R., 2013. Microtubules and biotic interactions. *Plant J.* 75, 278–289. <https://doi.org/10.1111/tpj.12171>
- Hardham, A.R., Gunning, B.E.S., 1978. STRUCTURE IN OF CORTICAL ARRAYS From the Department of Developmental Biology , Research School of Biological Sciences , Australian Serial sectioning was used to track the position and measure the lengths of cortical microtubules in glutaraldehyde-osmium t. *J. Cell Biol.* 77, 14–34. <https://doi.org/https://doi.org/10.1083/jcb.77.1.14>
- Harmon, A.C., Gribskov, M., Harper, J.F., 2000. CDPKs - A kinase for every Ca²⁺ signal? *Trends Plant Sci.* 5, 154–159. [https://doi.org/10.1016/S1360-1385\(00\)01577-6](https://doi.org/10.1016/S1360-1385(00)01577-6)
- Harold, F.M., 2014. In search of cell history : the evolution of life's building blocks, in: *In Search of Cell History*. p. 304.
- Hartman, J.J., Mahr, J., McNally, K., Okawa, K., Iwamatsu, A., Thomas, S., Cheesman, S., Heuser, J., Vale, R.D., McNally, F.J., 1998. Katanin, a microtubule-severing protein, is a novel AAA ATPase that targets to the centrosome using a WD40-containing subunit. *Cell* 93, 277–287. [https://doi.org/10.1016/S0092-8674\(00\)81578-0](https://doi.org/10.1016/S0092-8674(00)81578-0)
- Hashimoto, K., Kudla, J., 2011. Calcium decoding mechanisms in plants. *Biochimie.* <https://doi.org/10.1016/j.biochi.2011.05.019>
- He, J.-X., Gendron, J.M., Yang, Y., Li, J., Wang, Z.-Y., 2002. The GSK3-like kinase BIN2 phosphorylates and destabilizes BZR1, a positive regulator of the brassinosteroid signaling pathway in Arabidopsis. *Proc. Natl. Acad. Sci.* 99, 10185–10190. <https://doi.org/10.1073/pnas.152342599>
- Hepler, P.K., 2016. The cytoskeleton and its regulation by calcium and protons. *Plant Physiol.* 170, 3–22. <https://doi.org/10.1104/pp.15.01506>
- Hepler, P.K., 2005. Calcium: A central regulator of plant growth and development. *Plant Cell* 17, 2142–2155. <https://doi.org/10.1105/tpc.105.032508>
- Hepler, P.K., Wayne, R.O., 1985. Calcium and Plant Development. *Annu. Rev. Plant Physiol.* 36, 397–439. <https://doi.org/10.1146/annurev.pp.36.060185.002145>
- Hepler, P.K., Wolniak, S.M., 1984. Membranes in the mitotic apparatus: Their structure and function. *Int. Rev. Cytol.* VOL. 90, 169–238. [https://doi.org/10.1016/s0074-7696\(08\)61490-4](https://doi.org/10.1016/s0074-7696(08)61490-4)
- Herrington, K.A., Trinh, A.L., Dang, C., O'Shaughnessy, E., Hahn, K.M., Gratton, E., Digman, M.A., Sütterlin, C., 2017. Spatial analysis of Cdc42 activity reveals a role for plasma membrane-associated Cdc42 in centrosome regulation. *Mol. Biol. Cell* 28, 2135–2145. <https://doi.org/10.1091/mbc.E16-09-0665>
- Herrmann, A., Livanos, P., Lipka, E., Gadeyne, A., Hauser, M., Van Damme, D., Müller, S., 2018. Dual localized kinesin- 12 POK 2 plays multiple roles during cell division and interacts with MAP 65- 3 . *EMBO Rep.* 19, 1–16. <https://doi.org/10.15252/embr.201846085>
- Higaki, T., Kutsuna, N., Sano, T., Hasezawa, S., 2008. Quantitative analysis of changes in actin microfilament contribution to cell plate development in plant cytokinesis. *BMC Plant Biol.* 8, 1–15. <https://doi.org/10.1186/1471-2229-8-80>
- Himschoot, E., Beekman, T., Friml, J., Vanneste, S., 2015. Calcium is an organizer of cell polarity in plants. *Biochim. Biophys. Acta - Mol. Cell Res.* 1853, 2168–2172. <https://doi.org/10.1016/j.bbamcr.2015.02.017>
- Hirokawa, N., Noda, Y., Tanaka, Y., Niwa, S., 2009. Kinesin superfamily motor proteins and intracellular transport. *Nat. Rev. Mol. Cell Biol.* 10, 682–696. <https://doi.org/10.1038/nrm2774>
- Ho, C.M.K., Hotta, T., Guo, F., Roberson, R.W., Lee, Y.R.J., Liu, B., 2011. Interaction of antiparallel microtubules
-

-
- in the phragmoplast is mediated by the microtubule-associated protein MAP65-3 in Arabidopsis. *Plant Cell* 23, 2909–2923. <https://doi.org/10.1105/tpc.110.078204>
- Hoeflich, K.P., Ikura, M., 2002. Calmodulin in action: Diversity in target recognition and activation mechanisms. *Cell* 108, 739–742. [https://doi.org/10.1016/S0092-8674\(02\)00682-7](https://doi.org/10.1016/S0092-8674(02)00682-7)
- Horio, T., Murata, T., 2014. The role of dynamic instability in microtubule organization. *Front. Plant Sci.* 5, 1–10. <https://doi.org/10.3389/fpls.2014.00511>
- Hoshino, H., Yoneda, A., Kumagai, F., Hasezawa, S., 2003. Roles of actin-depleted zone and preprophase band in determining the division site of higher-plant cells, a tobacco BY-2 cell line expressing GFP-tubulin. *Protoplasma* 222, 157–165. <https://doi.org/10.1007/s00709-003-0012-8>
- Hrabak, E.M., Chan, C.W.M., Gribskov, M., Harper, J.F., Choi, J.H., Halford, N., Kudla, J., Luan, S., Nimmo, H.G., Sussman, M.R., Thomas, M., Walker-Simmons, K., Zhu, J.-K., Harmon, A.C., 2003. The Arabidopsis CDPK-SnRK Superfamily of Protein Kinases. *Plant Physiol.* 132, 666–680. <https://doi.org/10.1104/pp.102.011999>
- Hu, J.C., Sauer, R.T., 1992. The Basic-Region Leucine-Zipper Family of DNA Binding Proteins, in: *Nucleic Acids and Molecular Biology*. pp. 82–101. https://doi.org/10.1007/978-3-642-77356-3_5
- Huang, Z., Van Houten, J., Gonzalez, G., Xiao, H., Van Der Knaap, E., 2013. Genome-wide identification, phylogeny and expression analysis of SUN, OFP and YABBY gene family in tomato. *Mol. Genet. Genomics* 288, 111–129. <https://doi.org/10.1007/s00438-013-0733-0>
- Hush, J., Wu, L., John, P.C.L., Hepler, L.H., Hepler, P.K., 1996. Plant mitosis promoting factor disassembles the microtubule preprophase band and accelerates prophase progression in *Tradescantia*. *Cell Biol. Int.* 20, 275–287. <https://doi.org/10.1006/cbir.1996.0031>
- Hussey, P.J., Hawkins, T.J., 2001. Plant microtubule-associated proteins: The HEAT is off in temperature-sensitive mor1. *Trends Plant Sci.* 6, 389–392. [https://doi.org/10.1016/S1360-1385\(01\)02090-8](https://doi.org/10.1016/S1360-1385(01)02090-8)
- Hussey, P.J., Ketelaar, T., Deeks, M.J., 2006. Control of the Actin Cytoskeleton in Plant Cell Growth. *Annu. Rev. Plant Biol.* 57, 109–125. <https://doi.org/10.1146/annurev.arplant.57.032905.105206>
- Hutchins, J.R.A., Toyoda, Y., Hegemann, B., Poser, I., Hériché, J.K., Sykora, M.M., Augsburg, M., Hudecz, O., Buschhorn, B.A., Bulkescher, J., Conrad, C., Comartin, D., Schleiffer, A., Sarov, M., Pozniakovsky, A., Slabicki, M.M., Schloissnig, S., Steinmacher, I., Leuschner, M., Ssykor, A., Lawo, S., Pelletier, L., Stark, H., Nasmyth, K., Ellenberg, J., Durbin, R., Buchholz, F., Mechtler, K., Hyman, A.A., Peters, J.M., 2010. Systematic analysis of human protein complexes identifies chromosome segregation proteins. *Science* (80-). 328, 593–599. <https://doi.org/10.1126/science.1181348>
- Ide, Y., Nagasaki, N., Tomioka, R., Suito, M., Kamiya, T., Maeshima, M., 2007. Molecular properties of a novel, hydrophilic cation-binding protein associated with the plasma membrane. *J. Exp. Bot.* 58, 1173–1183. <https://doi.org/10.1093/jxb/erl284>
- Jaillon, O., Aury, J.M., Noel, B., Policriti, A., Clepet, C., Casagrande, A., Choisne, N., Aubourg, S., Vitulo, N., Jubin, C., Vezzi, A., Legeai, F., Huguency, P., Dasilva, C., Horner, D., Mica, E., Jublot, D., Poulain, J., Bruyère, C., Billault, A., Segurens, B., Gouyvenoux, M., Ugarte, E., Cattonaro, F., Anthouard, V., Vico, V., Del Fabro, C., Alaux, M., Di Gaspero, G., Dumas, V., Felice, N., Paillard, S., Juman, I., Moroldo, M., Scalabrin, S., Canaguier, A., Le Clainche, I., Malacrida, G., Durand, E., Pesole, G., Laucou, V., Chatelet, P., Merdinoglu, D., Delledonne, M., Pezzotti, M., Lecharny, A., Scarpelli, C., Artiguenave, F., Pè, M.E., Valle, G., Morgante, M., Caboche, M., Adam-Blondon, A.F., Weissenbach, J., Quétier, F., Wincker, P., 2007. The grapevine genome sequence suggests ancestral hexaploidization in major angiosperm phyla. *Nature* 449, 463–467. <https://doi.org/10.1038/nature06148>
- Jarsch, I.K., Konrad, S.S.A., Stratil, T.F., Urbanus, S.L., Szymanski, W., Braun, P., Braun, K.H., Ott, T., 2014. Plasma membranes are Subcompartmentalized into a plethora of coexisting and diverse microdomains in Arabidopsis and *Nicotiana benthamiana*. *Plant Cell* 26, 1698–1711. <https://doi.org/10.1105/tpc.114.124446>
- Jeong, S.Y., Rose, A., Joseph, J., Dasso, M., Meier, I., 2005. Plant-specific mitotic targeting of RanGAP requires a functional WPP domain. *Plant J.* 42, 270–282. <https://doi.org/10.1111/j.1365-313X.2005.02368.x>
- Jiang, S., Li, M., Xu, T., Ren, D., Liu, G., 2007. Two Kinesins from Arabidopsis, KatB and KatC, Have a Second Microtubule-binding Site in the Tail Domain. *BMB Rep.* 40, 44–52. <https://doi.org/10.5483/BMBRep.2007.40.1.044>
- Jones, M.A., Raymond, M.J., Smirnov, N., 2006. Analysis of the root-hair morphogenesis transcriptome reveals the molecular identity of six genes with roles in root-hair development in Arabidopsis. *Plant J.* 45, 83–100. <https://doi.org/10.1111/j.1365-313X.2005.02609.x>
-

-
- Kaan, H.Y.K., Hackney, D.D., Kozielski, F., 2011. The structure of the kinesin-1 motor-tail complex reveals the mechanism of autoinhibition. *Science* (80-). 333, 883–885. <https://doi.org/10.1126/science.1204824>
- Kang, E., Zheng, M., Zhang, Y., Yuan, M., Yalovsky, S., Zhu, L., Fu, Y., 2017. The microtubule-associated protein MAP18 affects ROP2 GTPase activity during root hair growth. *Plant Physiol.* 174, 202–222. <https://doi.org/10.1104/pp.16.01243>
- Kao, Y.L., Deavours, B.E., Phelps, K.K., Walker, R.A., Reddy, A.S.N., 2000. Bundling of microtubules by motor and tail domains of a kinesin-like calmodulin-binding protein from Arabidopsis: Regulation by Ca²⁺/calmodulin. *Biochem. Biophys. Res. Commun.* 267, 201–207. <https://doi.org/10.1006/bbrc.1999.1896>
- Karahara, I., Staehelin, L.A., Mineyuki, Y., 2010. A role of endocytosis in plant cytokinesis. *Commun. Integr. Biol.* 3, 42–45. <https://doi.org/10.4161/cib.3.1.9634>
- Karahara, I., Suda, J., Tahara, H., Yokota, E., Shimmen, T., Misaki, K., Yonemura, S., Staehelin, L.A., Mineyuki, Y., 2009. The preprophase band is a localized center of clathrin-mediated endocytosis in late prophase cells of the onion cotyledon epidermis. *Plant J.* 57, 819–831. <https://doi.org/10.1111/j.1365-313X.2008.03725.x>
- Kato, M., Aoyama, T., Maeshima, M., 2013. The Ca²⁺-binding protein PCaP2 located on the plasma membrane is involved in root hair development as a possible signal transducer. *Plant J.* 74, 690–700. <https://doi.org/10.1111/tpj.12155>
- Kato, M., Nagasaki-Takeuchi, N., Ide, Y., Maeshima, M., 2010a. An arabidopsis hydrophilic Ca²⁺-binding protein with a pevK-rich domain, pcap2, is associated with the plasma membrane and interacts with calmodulin and phosphatidylinositol phosphates. *Plant Cell Physiol.* 51, 366–379. <https://doi.org/10.1093/pcp/pcq003>
- Kato, M., Nagasaki-Takeuchi, N., Ide, Y., Tomioka, R., Maeshima, M., 2010b. PCaPs, possible regulators of PtdInsP signals on plasma membrane. *Plant Signal. Behav.* 5, 848–850. <https://doi.org/10.4161/psb.5.7.11825>
- Kawamura, E., Himmelspach, R., Rashbrooke, M.C., Whittington, A.T., Gale, K.R., Collings, D.A., Wasteneys, G.O., 2006. MICROTUBULE ORGANIZATION 1 regulates structure and function of microtubule arrays during mitosis and cytokinesis in the Arabidopsis root. *Plant Physiol.* 140, 102–114. <https://doi.org/10.1104/pp.105.069989>
- Kawano, T., Araseki, M., Araki, Y., Kinjo, M., Yamamoto, T., Suzuki, T., 2012. A Small Peptide Sequence is Sufficient for Initiating Kinesin-1 Activation Through Part of TPR Region of KLC1. *Traffic* 13, 834–848. <https://doi.org/10.1111/j.1600-0854.2012.01350.x>
- Kazmierczak, J., Kempe, S., Kremer, B., 2013. Calcium in the Early Evolution of Living Systems: A Biohistorical Approach. *Curr. Org. Chem.* 17, 1738–1750. <https://doi.org/10.2174/13852728113179990081>
- Keech, O., Pesquet, E., Gutierrez, L., Ahad, A., Bellini, C., Smith, S.M., Gardeström, P., 2010. Leaf Senescence Is Accompanied by an Early Disruption of the Microtubule Network in Arabidopsis. *Plant Physiol.* 154, 1710–1720. <https://doi.org/10.1104/pp.110.163402>
- Keith, C., Dipaola, M., Maxfield, F.R., Shelanski, M.L., 1983. Microinjection of Ca²⁺-Calmodulin Causes a Localized Depolymerization of Microtubules. *J. CELL Biol.* 97, 1918–1924. <https://doi.org/https://doi.org/10.1083/jcb.97.6.1918>
- Kirik, A., Ehrhardt, D.W., Kirik, V., 2012. TONNEAU2/FASS regulates the geometry of microtubule nucleation and cortical array organization in interphase Arabidopsis cells. *Plant Cell* 24, 1158–1170. <https://doi.org/10.1105/tpc.111.094367>
- Kirik, V., Herrmann, U., Parupalli, C., Sedbrook, J.C., Ehrhardt, D.W., Hülskamp, M., 2007. CLASP localizes in two discrete patterns on cortical microtubules and is required for cell morphogenesis and cell division in Arabidopsis. *J. Cell Sci.* 120, 4416–4425. <https://doi.org/10.1242/jcs.024950>
- Kirschner, M., Mitchison, T., 1986. Beyond self-assembly: From microtubules to morphogenesis. *Cell.* [https://doi.org/10.1016/0092-8674\(86\)90318-1](https://doi.org/10.1016/0092-8674(86)90318-1)
- Kohoutová, L., Kourová, H., Nagy, S.K., Volc, J., Halada, P., Mészáros, T., Meskiene, I., Bögre, L., Binarová, P., 2015. The Arabidopsis mitogen-activated protein kinase 6 is associated with γ -tubulin on microtubules, phosphorylates EB1c and maintains spindle orientation under nitrosative stress. *New Phytol.* 207, 1061–1074. <https://doi.org/10.1111/nph.13501>
- Kölling, M., Kumari, P., Bürstenbinder, K., 2019. Calcium- and calmodulin-regulated microtubule-associated proteins as signal-integration hubs at the plasma membrane-cytoskeleton nexus. *J. Exp. Bot.* 70, 387–396. <https://doi.org/10.1093/jxb/ery397>
-

-
- Kolukisaoglu, Ü., Weinl, S., Blazevic, D., Batistic, O., Kudla, J., 2004. Calcium Sensors and Their Interacting Protein Kinases: Genomics of the Arabidopsis and Rice CBL-CIPK Signaling Networks. *Plant Physiol.* 134, 43–58. <https://doi.org/10.1104/pp.103.033068>
- Komaki, S., Abe, T., Coutuer, S., Inzé, D., Russinova, E., Hashimoto, T., 2010. Nuclear-localized subtype of end-binding 1 protein regulates spindle organization in Arabidopsis. *J. Cell Sci.* 123, 451–459. <https://doi.org/10.1242/jcs.062703>
- Komis, G., Illés, P., Beck, M., Šamaj, J., 2011. Microtubules and mitogen-activated protein kinase signalling. *Curr. Opin. Plant Biol.* 14, 650–657. <https://doi.org/10.1016/j.pbi.2011.07.008>
- Komis, G., Luptovčiak, I., Ovečka, M., Samakovli, D., Šamajová, O., Šamaj, J., 2017. Katanin effects on dynamics of cortical microtubules and mitotic arrays in Arabidopsis thaliana revealed by advanced live-cell imaging. *Front. Plant Sci.* 8, 1–19. <https://doi.org/10.3389/fpls.2017.00866>
- Kong, Z., Ioki, M., Braybrook, S., Li, S., Ye, Z.H., Julie Lee, Y.R., Hotta, T., Chang, A., Tian, J., Wang, G., Liu, B., 2015. Kinesin-4 Functions in Vesicular Transport on Cortical Microtubules and Regulates Cell Wall Mechanics during Cell Elongation in Plants. *Mol. Plant* 8, 1011–1023. <https://doi.org/10.1016/j.molp.2015.01.004>
- Korinek, W.S., 2000. Molecular Linkage Underlying Microtubule Orientation Toward Cortical Sites in Yeast. *Science (80-.)*. 287, 2257–2259. <https://doi.org/10.1126/science.287.5461.2257>
- Kosetsu, K., de Keijzer, J., Janson, M.E., Goshima, G., 2013. MICROTUBULE-ASSOCIATED PROTEIN65 is essential for maintenance of phragmoplast bipolarity and formation of the cell plate in Physcomitrella patens. *Plant Cell* 25, 4479–4492. <https://doi.org/10.1105/tpc.113.117432>
- Kosetsu, K., Murata, T., Yamada, M., Nishina, M., Boruc, J., Hasebe, M., Van Damme, D., Goshima, G., 2017. Cytoplasmic MTOCs control spindle orientation for asymmetric cell division in plants. *Proc. Natl. Acad. Sci.* 114, E8847–E8854. <https://doi.org/10.1073/pnas.1713925114>
- Kudla, J., Batistič, O., Hashimoto, K., 2010. Calcium signals: The Lead Currency of plant information processing. *Plant Cell* 22, 541–563. <https://doi.org/10.1105/tpc.109.072686>
- Kusumi, A., Fujiwara, T.K., Chadda, R., Xie, M., Tsunoyama, T.A., Kalay, Z., Kasai, R.S., Suzuki, K.G.N., 2012. Dynamic Organizing Principles of the Plasma Membrane that Regulate Signal Transduction: Commemorating the Fortieth Anniversary of Singer and Nicolson's Fluid-Mosaic Model. *Annu. Rev. Cell Dev. Biol.* 28, 215–250. <https://doi.org/10.1146/annurev-cellbio-100809-151736>
- Lamb, J.R., Tugendreich, S., Hieter, P., 1995. Tetratricopeptide repeat interactions: to TPR or not to TPR? *Trends Biochem. Sci.* 20, 257–259. [https://doi.org/10.1016/S0968-0004\(00\)89037-4](https://doi.org/10.1016/S0968-0004(00)89037-4)
- Lansbergen, G., Akhmanova, A., 2006. Microtubule plus end: A hub of cellular activities. *Traffic* 7, 499–507. <https://doi.org/10.1111/j.1600-0854.2006.00400.x>
- Lawrence, C.J., Dawe, R.K., Christie, K.R., Cleveland, D.W., Dawson, S.C., Endow, S.A., Goldstein, L.S.B., Goodson, H. V., Hirokawa, N., Howard, J., Malmberg, R.L., McIntosh, J.R., Miki, H., Mitchison, T.J., Okada, Y., Reddy, A.S.N., Saxton, W.M., Schliwa, M., Scholey, J.M., Vale, R.D., Walczak, C.E., Wordeman, L., 2004. A standardized kinesin nomenclature. *J. Cell Biol.* 167, 19–22. <https://doi.org/10.1083/jcb.200408113>
- Ledbetter, M.C., Porter, K.R., 1963. A “microtubule” in plant cell fine structure. *J. Cell Biol.* 19, 239–250. <https://doi.org/10.1083/jcb.19.1.239>
- Lee, Y.C., Wolff, J., 1982. Two opposing effects of calmodulin on microtubule assembly depend on the presence of microtubule-associated proteins. *J. Biol. Chem.* 257, 6306–6310.
- Lee, Y.K., Kim, G.T., Kim, I.J., Park, J., Kwak, S.S., Choi, G., Chung, W. Il, 2006. LONGIFOLIA1 and LONGIFOLIA2, two homologous genes, regulate longitudinal cell elongation in Arabidopsis. *Development* 133, 4305–4314. <https://doi.org/10.1242/dev.02604>
- Lee, Y.R.J., Li, Y., Liu, B., 2007. Two Arabidopsis phragmoplast-associated kinesins play a critical role in cytokinesis during male gametogenesis. *Plant Cell* 19, 2595–2605. <https://doi.org/10.1105/tpc.107.050716>
- Lee, Y.R.J., Liu, B., 2019. Microtubule nucleation for the assembly of acentrosomal microtubule arrays in plant cells. *New Phytol.* 222, 1705–1718. <https://doi.org/10.1111/nph.15705>
- Lee, Y.R.J., Liu, B., 2000. Identification of a phragmoplast-associated kinesin-related protein in higher plants. *Curr. Biol.* 10, 797–800. [https://doi.org/10.1016/S0960-9822\(00\)00564-9](https://doi.org/10.1016/S0960-9822(00)00564-9)
- Lee, Y.R.J., Qiu, W., Liu, B., 2015. Kinesin motors in plants: From subcellular dynamics to motility regulation. *Curr. Opin. Plant Biol.* <https://doi.org/10.1016/j.pbi.2015.10.003>
-

-
- Levy, M., Wang, Q., Kaspi, R., Parrella, M.P., Abel, S., 2005. Arabidopsis IQD1, a novel calmodulin-binding nuclear protein, stimulates glucosinolate accumulation and plant defense. *Plant J.* 43, 79–96. <https://doi.org/10.1111/j.1365-313X.2005.02435.x>
- Li, H., Sun, B., Sasabe, M., Deng, X., Machida, Y., Lin, H., Julie Lee, Y.R., Liu, B., 2017. Arabidopsis MAP65-4 plays a role in phragmoplast microtubule organization and marks the cortical cell division site. *New Phytol.* 215, 187–201. <https://doi.org/10.1111/nph.14532>
- Li, J., Jiang, J., Qian, Q., Xu, Y., Zhang, C., Xiao, J., Du, C., Luo, W., Zou, G., Chen, M., Huang, Y., Feng, Y., Cheng, Z., Yuan, M., Chong, K., 2011. Mutation of rice BC12/GDD1, which encodes a kinesin-like protein that binds to a GA biosynthesis gene promoter, leads to dwarfism with impaired cell elongation. *Plant Cell* 23, 628–640. <https://doi.org/10.1105/tpc.110.081901>
- Li, S., Sun, T., Ren, H., 2015. The functions of the cytoskeleton and associated proteins during mitosis and cytokinesis in plant cells. *Front. Plant Sci.* 6, 1–7. <https://doi.org/10.3389/fpls.2015.00282>
- Li, Wang, X., Qin, T., Zhang, Y., Liu, X., Sun, J., Zhou, Y., Zhu, L., Zhang, Z., Yuan, M., Mao, T., 2011. MDP25, A Novel Calcium Regulatory Protein, Mediates Hypocotyl Cell Elongation by Destabilizing Cortical Microtubules in Arabidopsis. *Plant Cell* 23, 4411–4427. <https://doi.org/10.1105/tpc.111.092684>
- Liang, H., Zhang, Y., Martinez, P., Rasmussen, C.G., Xu, T., Yang, Z., 2018. The microtubule-associated protein IQ67 DOMAIN5 modulates microtubule dynamics and pavement cell shape. *Plant Physiol.* 177, 1555–1568. <https://doi.org/10.1104/pp.18.00558>
- Lingwood, D., Simons, K., 2010. Lipid rafts as a membrane-organizing principle. *Science* (80-.). 327, 46–50. <https://doi.org/10.1126/science.1174621>
- Lipka, E., Gadeyne, A., Stöckle, D., Zimmermann, S., De Jaeger, G., Ehrhardt, D.W., Kirik, V., Van Damme, D., Müller, S., 2014. The phragmoplast-orienting kinesin-12 class proteins translate the positional information of the preprophase band to establish the cortical division zone in Arabidopsis thaliana. *Plant Cell* 26, 2617–2632. <https://doi.org/10.1105/tpc.114.124933>
- Lipka, E., Herrmann, A., Mueller, S., 2015. Mechanisms of plant cell division. *Wiley Interdiscip. Rev. Dev. Biol.* 4, 391–405. <https://doi.org/10.1002/wdev.186>
- Liu, B., Cyr, R.J., Palevitz, B.A., 1996. A kinesin-like protein, KatAp, in the cells of arabidopsis and other plants. *Plant Cell* 8, 119–132. <https://doi.org/10.2307/3870073>
- Liu, B., Joshi, H.C., Wilson, T.J., Silflow, C.D., Palevitz, B.A., Snustad, D.P., 1994. gamma-Tubulin in Arabidopsis: gene sequence, immunoblot, and immunofluorescence studies. *Plant Cell* 6, 303–314. <https://doi.org/10.1105/tpc.6.2.303>
- Liu, B., Marc, J., Joshi, H.C., Palevitz, B.A., 1993. A gamma-tubulin-related protein associated with the microtubule arrays of higher plants in a cell cycle-dependent manner. *J. Cell Sci.* 104 (Pt 4, 1217–28.
- Liu, B., Palevitz, B.A., 1992. Organization of cortical microfilaments in dividing root cells. *Cell Motil. Cytoskeleton* 23, 252–264. <https://doi.org/10.1002/cm.970230405>
- Liu, J., Chen, J., Zheng, X., Wu, F., Lin, Q., Heng, Y., Tian, P., Cheng, Z.J., Yu, X., Zhou, K., Zhang, X., Guo, X., Wang, J., Wang, H., Wan, J., 2017. GW5 acts in the brassinosteroid signalling pathway to regulate grain width and weight in rice. *Nat. Plants* 3, 1–7. <https://doi.org/10.1038/nplants.2017.43>
- Liu, Z., Persson, S., Zhang, Y., 2015. The connection of cytoskeletal network with plasma membrane and the cell wall. *J. Integr. Plant Biol.* 57, 330–340. <https://doi.org/10.1111/jipb.12342>
- Liu, Z., Schneider, R., Kesten, C., Zhang, Yi, Somssich, M., Zhang, Youjun, Fernie, A.R., Persson, S., 2016. Cellulose-Microtubule Uncoupling Proteins Prevent Lateral Displacement of Microtubules during Cellulose Synthesis in Arabidopsis. *Dev. Cell* 38, 305–315. <https://doi.org/10.1016/j.devcel.2016.06.032>
- Livanos, P., Müller, S., 2019. Division Plane Establishment and Cytokinesis. *Annu. Rev. Plant Biol.* 70, 239–267. <https://doi.org/10.1146/annurev-arplant-050718-100444>
- Lloyd, C., Hussey, P., 2001. Microtubule-associated proteins in plants - Why we need a map. *Nat. Rev. Mol. Cell Biol.* 2, 40–47. <https://doi.org/10.1038/35048005>
- Lloyd, C.W., 1991. How does the cytoskeleton read the laws of geometry in aligning the division plane of plant cells? *Development* 112, 55–65.
- Lloyd, C.W., Traas, J.A., 1988. The role of F-actin in determining the division plane of carrot suspension cells. *Drug studies. Development* 102, 211–221.
- Lu, B., Roegiers, F., Jan, L.Y., Jan, Y.N., 2001. Adherens junctions inhibit asymmetric division in the Drosophila
-

-
- epithelium. *Nature* 409, 522–525. <https://doi.org/10.1038/35054077>
- Lu, L., Lee, Y.R.J., Pan, R., Maloof, J.N., Liu, B., 2005. An internal motor kinesin is associated with the golgi apparatus and plays a role in trichome morphogenesis in *Arabidopsis*. *Mol. Biol. Cell* 16, 811–823. <https://doi.org/10.1091/mbc.E04-05-0400>
- Luan, S., Kudla, J., Rodriguez-Concepcion, M., Yalovsky, S., Goussery, W., 2002. Calmodulins and Calcineurin B-like Proteins: Calcium Sensors for Specific Signal Response Coupling in Plants. *Plant Cell* S389–S400. <https://doi.org/10.1105/tpc.001115>
- Lyle, K., Kumar, P., Wittmann, T., 2009. SnapShot: Microtubule Regulators II. *Cell* 136, 566.e1–566.e2. <https://doi.org/10.1016/j.cell.2009.01.011>
- Ma, H., Feng, L., Chen, Z., Chen, X., Zhao, H., Xiang, Y., 2014. Genome-wide identification and expression analysis of the IQD gene family in *Populus trichocarpa*. *Plant Sci.* 229, 96–110. <https://doi.org/10.1016/j.plantsci.2014.08.017>
- Maiato, H., Fairley, E.A.L., Rieder, C.L., Swedlow, J.R., Sunkel, C.E., Earnshaw, W.C., 2003. Human CLASP1 is an outer kinetochore component that regulates spindle microtubule dynamics. *Cell* 113, 891–904. [https://doi.org/10.1016/S0092-8674\(03\)00465-3](https://doi.org/10.1016/S0092-8674(03)00465-3)
- Malinsky, J., Opekarová, M., Grossmann, G., Tanner, W., 2013. Membrane Microdomains, Rafts, and Detergent-Resistant Membranes in Plants and Fungi. *Annu. Rev. Plant Biol.* 64, 501–529. <https://doi.org/10.1146/annurev-arplant-050312-120103>
- Marcum, J.M., Dedman, J.R., Brinkley, B.R., Means, A.R., 1978. Control of microtubule assembly-disassembly by calcium-dependent regulator protein. *Proc. Natl. Acad. Sci.* 75, 3771–3775. <https://doi.org/10.1073/pnas.75.8.3771>
- Marcus, A.I., Dixit, R., Cyr, R.J., 2005. Narrowing of the preprophase microtubule band is not required for cell division plane determination in cultured plant cells. *Protoplasma* 226, 169–174. <https://doi.org/10.1007/s00709-005-0119-1>
- Marquès-Bueno, M.M., Morao, A.K., Cayrel, A., Platre, M.P., Barberon, M., Caillieux, E., Colot, V., Jaillais, Y., Roudier, F., Vert, G., 2016. A versatile Multisite Gateway-compatible promoter and transgenic line collection for cell type-specific functional genomics in *Arabidopsis*. *Plant J.* 85, 320–333. <https://doi.org/10.1111/tpj.13099>
- Martinez, P., Dixit, R., Balkunde, R.S., O'Leary, S.E., Brakke, K.A., Rasmussen, C.G., 2019. TANGLED1 mediates interactions between microtubules that may promote spindle organization and phragmoplast guidance to the division site in maize. *bioRxiv*. <https://doi.org/10.1101/711796>
- Máthé, E., Inoue, Y.H., Palframan, W., Brown, G., Glover, D.M., 2003. Orbit/Mast, the CLASP orthologue of *Drosophila*, is required for asymmetric stem cell and cystocyte divisions and development of the polarised microtubule network that interconnects oocyte and nurse cells during oogenesis. *Development*. <https://doi.org/10.1242/dev.00315>
- Mazumdar, M., Misteli, T., 2005. Chromokinesins: Multitalented players in mitosis. *Trends Cell Biol.* 15, 349–355. <https://doi.org/10.1016/j.tcb.2005.05.006>
- McCartney, B.M., McEwen, D.G., Grevengoed, E., Maddox, P., Bejsovec, A., Peifer, M., 2001. *Drosophila* APC2 and Armadillo participate in tethering mitotic spindles to cortical actin. *Nat. Cell Biol.* 3, 933–938. <https://doi.org/10.1038/ncb1001-933>
- McClinton, R.S., Sung, Z.R., 1997. Organization of cortical microtubules at the plasma membrane in *Arabidopsis* *Regina*. *Planta* 201, 252–260. <https://doi.org/https://doi.org/10.1007/s004250050064>
- McCormack, E., Tsai, Y.C., Braam, J., 2005. Handling calcium signaling: *Arabidopsis* CaMs and CMLs. *Trends Plant Sci.* 10, 383–389. <https://doi.org/10.1016/j.tplants.2005.07.001>
- McNally, F.J., Vale, R.D., 1993. Identification of katanin, an ATPase that severs and disassembles stable microtubules. *Cell* 75, 419–429. [https://doi.org/10.1016/0092-8674\(93\)90377-3](https://doi.org/10.1016/0092-8674(93)90377-3)
- Miki, H., Okada, Y., Hirokawa, N., 2005. Analysis of the kinesin superfamily: insights into structure and function. *Trends Cell Biol.* 15, 467–476. <https://doi.org/10.1016/j.tcb.2005.07.006>
- Mineyuki, Y., Gunning, B.E.S., 1990. A role of preprophase bands of microtubules in maturation of new cell walls, and a general proposal on the function of preprophase band sites in cell division in higher plants. *J. Cell Sci.* 97, 527–537.
- Mineyuki, Y., Murata, T., Wada, M., 1991. Experimental obliteration of the preprophase band alters the site of cell division, cell plate orientation and phragmoplast expansion in *Adiantum protonemata*. *J. Cell Sci.* 551–557.
-

-
- Mineyuki, Y., Palevitz, B.A., 1990. Relationship between preprophase band organization, F-actin and the division site in *Allium*. Fluorescence and morphometric studies on cytochalasin-treated cells. *J. Cell Sci.* 97, 283–295.
- Mitra, D., Klemm, S., Kumari, P., Quegwer, J., Möller, B., Poeschl, Y., Pflug, P., Stamm, G., Abel, S., Bürstenbinder, K., 2019. Microtubule-associated protein IQ67 DOMAIN5 regulates morphogenesis of leaf pavement cells in *Arabidopsis thaliana*. *J. Exp. Bot.* 70, 529–543. <https://doi.org/10.1093/jxb/ery395>
- Möller, B.K., Ten Hove, C.A., Xiang, D., Williams, N., López, L.G., Yoshida, S., Smit, M., Datla, R., Weijers, D., 2017. Auxin response cell-autonomously controls ground tissue initiation in the early *Arabidopsis* embryo. *PNAS* 114, E2533–E2539. <https://doi.org/10.1073/pnas.1616493114>
- Monshausen, G.B., Miller, N.D., Murphy, A.S., Gilroy, S., 2011. Dynamics of auxin-dependent Ca²⁺ and pH signaling in root growth revealed by integrating high-resolution imaging with automated computer vision-based analysis. *Plant J.* 65, 309–318. <https://doi.org/10.1111/j.1365-313X.2010.04423.x>
- Moore, R.C., Durso, N.A., Cyr, R.J., 1998. Elongation factor-1 α stabilizes microtubules in a calcium/calmodulin-dependent manner. *Cell Motil. Cytoskeleton* 41, 168–180. [https://doi.org/10.1002/\(SICI\)1097-0169\(1998\)41:2<168::AID-CM7>3.0.CO;2-A](https://doi.org/10.1002/(SICI)1097-0169(1998)41:2<168::AID-CM7>3.0.CO;2-A)
- Moore, C.A., Milligan, R.A., 2006. Lucky 13 - Microtubule depolymerisation by kinesin-13 motors. *J. Cell Sci.* 119, 3905–3913. <https://doi.org/10.1242/jcs.03224>
- Mucha, E., Hoefle, C., Hüchelhoven, R., Berken, A., 2010. RIP3 and AtKinesin-13A – A novel interaction linking Rho proteins of plants to microtubules. *Eur. J. Cell Biol.* 89, 906–916. <https://doi.org/10.1016/j.ejcb.2010.08.003>
- Mukhtar, M.S., Carvunis, A., Dreze, M., Epple, P., Steinbrenner, J., Moore, J., Tasan, M., Galli, M., Hao, T., Nishimura, M.T., Pevzner, S.J., Donovan, S.E., Ghamsari, L., Santhanam, B., Romero, V., Poulin, M.M., Gebreab, F., Gutierrez, B.J., Tam, S., Monachello, D., Boxem, M., Harbort, C.J., McDonald, N., Gai, L., Chen, H., He, Y., Union, E., Consortium, E., Vandenhoute, J., Roth, F.P., Hill, D.E., Ecker, J.R., Vidal, M., Beynon, J., 2011. Plant Immune System Network. *Science* (80-). 333, 596–601. <https://doi.org/10.1126/science.1203659>.Independently
- Müller, S., Han, S., Smith, L.G., 2006. Two Kinesins Are Involved in the Spatial Control of Cytokinesis in *Arabidopsis thaliana*. *Curr. Biol.* 16, 888–894. <https://doi.org/10.1016/j.cub.2006.03.034>
- Müller, S., Smertenko, A., Wagner, V., Heinrich, M., Hussey, P.J., Hauser, M.-T., 2004. The Plant Microtubule-Associated Protein AtMAP65-3/PLE Is Essential for Cytokinetic Phragmoplast Function. *Curr. Biol.* 14, 412–417. <https://doi.org/10.1016/j.cub.2004.02.032>
- Müller, S., Wright, A.J., Smith, L.G., 2009. Division plane control in plants: new players in the band. *Trends Cell Biol.* 19, 180–188. <https://doi.org/10.1016/j.tcb.2009.02.002>
- Murata, T., Sano, T., Sasabe, M., Nonaka, S., Higashiyama, T., Hasezawa, S., Machida, Y., Hasebe, M., 2013. Mechanism of microtubule array expansion in the cytokinetic phragmoplast. *Nat. Commun.* 4, 1–12. <https://doi.org/10.1038/ncomms2967>
- Murata, T., Sonobe, S., Baskin, T.I., Hyodo, S., Hasezawa, S., Nagata, T., Horio, T., Hasebe, M., 2005. Microtubule-dependent microtubule nucleation based on recruitment of γ -tubulin in higher plants. *Nat. Cell Biol.* 7, 961–968. <https://doi.org/10.1038/ncb1306>
- Murata, T., Wada, M., 1991. Effects of centrifugation on preprophase-band formation in *Adiantum protonemata*. *Planta* 183, 391–398. <https://doi.org/10.1007/BF00197738>
- Nagasaki, N., Tomioka, R., Maeshima, M., 2008. A hydrophilic cation-binding protein of *Arabidopsis thaliana*, AtPCaP1, is localized to plasma membrane via N-myristoylation and interacts with calmodulin and the phosphatidylinositol phosphates PtdIns(3,4,5)P₃ and PtdIns(3,5)P₂. *FEBS J.* 275, 2267–2282. <https://doi.org/10.1111/j.1742-4658.2008.06379.x>
- Nakamura, M., Ehrhardt, D.W., Hashimoto, T., 2010. Microtubule and katanin-dependent dynamics of microtubule nucleation complexes in the acentrosomal *Arabidopsis* cortical array. *Nat. Cell Biol.* 12, 1064–1070. <https://doi.org/10.1038/ncb2110>
- Nakamura, M., Hashimoto, T., 2009. A mutation in the *Arabidopsis* γ -tubulin-containing complex causes helical growth and abnormal microtubule branching. *J. Cell Sci.* 122, 2208–2217. <https://doi.org/10.1242/jcs.044131>
- Nakamura, M., Lindeboom, J.J., Saltini, M., Mulder, B.M., Ehrhardt, D.W., 2018. SPR2 protects minus ends to promote severing and reorientation of plant cortical microtubule arrays. *J. Cell Biol.* 217, 915–927. <https://doi.org/10.1083/jcb.201708130>
-

-
- Narasimhulu, S.B., Reddy, A.S.N., 1998. Characterization of microtubule binding domains in the arabidopsis kinesin-like calmodulin binding protein. *Plant Cell* 10, 957–965. <https://doi.org/10.1105/tpc.10.6.957>
- Ni, C.Z., Wang, H.Q., Xu, T., Qu, Z., Liu, G.Q., 2005. AtKP1, a kinesin-like protein, mainly localizes to mitochondria in *Arabidopsis thaliana*. *Cell Res.* 15, 725–733. <https://doi.org/10.1038/sj.cr.7290342>
- Nick, P., 2013. Microtubules, signalling and abiotic stress. *Plant J.* 75, 309–323. <https://doi.org/10.1111/tbj.12102>
- Nishihama, R., Soyano, T., Ishikawa, M., Araki, S., Tanaka, H., Asada, T., Irie, K., Ito, M., Terada, M., Banno, H., Yamazaki, Y., Machida, Y., 2002. Expansion of the cell plate in plant cytokinesis requires a kinesin-like protein/MAPKKK complex. *Cell* 109, 87–99. [https://doi.org/10.1016/S0092-8674\(02\)00691-8](https://doi.org/10.1016/S0092-8674(02)00691-8)
- Nogales, E., Wang, H.W., 2006. Structural mechanisms underlying nucleotide-dependent self-assembly of tubulin and its relatives. *Curr. Opin. Struct. Biol.* <https://doi.org/10.1016/j.sbi.2006.03.005>
- Obayashi, T., Aoki, Y., Tadaka, S., Kagaya, Y., Kinoshita, K., 2018. ATTED-II in 2018: A Plant Coexpression Database Based on Investigation of the Statistical Property of the Mutual Rank Index. *Plant Cell Physiol.* 59, e3. <https://doi.org/10.1093/pcp/pcx191>
- Oda, Y., 2018. Emerging roles of cortical microtubule–membrane interactions. *J. Plant Res.* 131, 5–14. <https://doi.org/10.1007/s10265-017-0995-4>
- Oda, Y., Fukuda, H., 2013. Rho of plant GTPase signaling regulates the behavior of *Arabidopsis* kinesin-13A to establish secondary cell wall patterns. *Plant Cell* 25, 4439–4450. <https://doi.org/10.1105/tpc.113.117853>
- Oh, S.A., Allen, T., Kim, G.J., Sidorova, A., Borg, M., Park, S.K., Twell, D., 2012. *Arabidopsis* fused kinase and the kinesin-12 subfamily constitute a signalling module required for phragmoplast expansion. *Plant J.* 72, 308–319. <https://doi.org/10.1111/j.1365-313X.2012.05077.x>
- Ohta, K., Toriyama, M., Endo, S., Sakai, H., 1988. Localization of mitotic-apparatus-associated 51-kD protein in unfertilized and fertilized sea urchin eggs. *Cell Motil. Cytoskeleton* 10, 496–505. <https://doi.org/10.1002/cm.970100406>
- Otegui, M., Staehelin, L.A., 2000. Cytokinesis in flowering plants: More than one way to divide a cell. *Curr. Opin. Plant Biol.* 3, 493–502. [https://doi.org/10.1016/S1369-5266\(00\)00119-9](https://doi.org/10.1016/S1369-5266(00)00119-9)
- Otegui, M.S., Noh, Y.-S., Martínez, D.E., Vila Petroff, M.G., Andrew Staehelin, L., Amasino, R.M., Guimmet, J.J., 2005. Senescence-associated vacuoles with intense proteolytic activity develop in leaves of *Arabidopsis* and soybean. *Plant J.* 41, 831–844. <https://doi.org/10.1111/j.1365-313X.2005.02346.x>
- Otegui, M.S., Staehelin, L.A., 2004. Electron tomographic analysis of post-meiotic cytokinesis during pollen development in *Arabidopsis thaliana*. *Planta* 218, 501–515. <https://doi.org/10.1007/s00425-003-1125-1>
- Palevitz, B.A., Hepler, P.K., 1974. The control of the plane of division during stomatal differentiation in *Allium* - II. Drug studies. *Chromosoma* 46, 327–341. <https://doi.org/10.1007/BF00284885>
- Pan, R., Lee, Y.R.J., Liu, B., 2004. Localization of two homologous *Arabidopsis* kinesin-related proteins in the phragmoplast. *Planta* 220, 156–164. <https://doi.org/10.1007/s00425-004-1324-4>
- Pan, Y., Liang, X., Gao, M., Liu, H., Meng, H., Weng, Y., Cheng, Z., 2017. Round fruit shape in W17239 cucumber is controlled by two interacting quantitative trait loci with one putatively encoding a tomato SUN homolog. *Theor. Appl. Genet.* 130, 573–586. <https://doi.org/10.1007/s00122-016-2836-6>
- Panteris, E., Adamakis, I.D.S., Voulgari, G., Papadopoulou, G., 2011. A role for katanin in plant cell division: Microtubule organization in dividing root cells of *fra2* and *lue1* *Arabidopsis thaliana* mutants. *Cytoskeleton* 68, 401–413. <https://doi.org/10.1002/cm.20522>
- Panteris, E., Apostolakos, P., Galatis, B., 1995. The effect of taxol on *Triticum* preprophase root cells: preprophase microtubule band organization seems to depend on new microtubule assembly. *Protoplasma* 186, 72–78. <https://doi.org/10.1007/BF01276938>
- Panteris, E., Apostolakos, P., Quader, H., Galatis, B., 2004. A cortical cytoplasmic ring predicts the division plane in vacuolated cells of *Coleus*: The role of actomyosin and microtubules in the establishment and function of the division site. *New Phytol.* 163, 271–286. <https://doi.org/10.1111/j.1469-8137.2004.01125.x>
- Paredes, A.R., Somerville, C.R., Ehrhardt, D.W., 2006. Visualization of cellulose synthase demonstrates functional association with microtubules. *Science* (80-.). 312, 1491–1495. <https://doi.org/10.1126/science.1126551>
- Peaucelle, A., Wightman, R., Höfte, H., 2015. The Control of Growth Symmetry Breaking in the *Arabidopsis* Hypocotyl. *Curr. Biol.* 25, 1746–1752. <https://doi.org/10.1016/j.cub.2015.05.022>
-

-
- Peremyslov, V. V., Prokhnevsky, A.I., Avisar, D., Dolja, V. V., 2008. Two class XI myosins function in organelle trafficking and root hair development in Arabidopsis. *Plant Physiol.* 146, 1109–1116. <https://doi.org/10.1104/pp.107.113654>
- Perrin, R.M., Wang, Y., Yuen, C.Y.L., Will, J., Masson, P.H., 2007. WVD2 is a novel microtubule-associated protein in Arabidopsis thaliana. *Plant J.* 49, 961–971. <https://doi.org/10.1111/j.1365-313X.2006.03015.x>
- Pickett-Heaps, J.D., Northcote, D.H., 1966. Organization of microtubules and endoplasmic reticulum during mitosis and cytokinesis in wheat meristems. *J. Cell Sci.* 1, 109–120.
- Puthenveedu, M.A., Bachert, C., Puri, S., Lanni, F., Linstedt, A.D., 2006. GM130 and GRASP65-dependent lateral cisternal fusion allows uniform Golgi-enzyme distribution. *Nat. Cell Biol.* 8, 238–248. <https://doi.org/10.1038/ncb1366>
- Qin, T., Liu, X., Li, J., Sun, J., Song, L., Mao, T., 2014. Arabidopsis microtubule-destabilizing protein 25 functions in pollen tube growth by severing actin filaments. *Plant Cell* 26, 325–339. <https://doi.org/10.1105/tpc.113.119768>
- Raffaele, S., Mongrand, S., Gamas, P., Niebel, A., Ott, T., 2007. Genome-wide annotation of remorins, a plant-specific protein family: Evolutionary and functional perspectives. *Plant Physiol.* 145, 593–600. <https://doi.org/10.1104/pp.107.108639>
- Ranty, B., Aldon, D., Galaud, J.P., 2006. Plant calmodulins and calmodulin-related proteins: Multifaceted relays to decode calcium signals. *Plant Signal. Behav.* 1, 96–104. <https://doi.org/10.4161/psb.1.3.2998>
- Rashotte, A.M., Carson, S.D.B., To, J.P.C., Kieber, J.J., 2003. Expression profiling of cytokinin action in Arabidopsis. *Plant Physiol.* 132, 1998–2011. <https://doi.org/10.1104/pp.103.021436>
- Rasmussen, C.G., Humphries, J.A., Smith, L.G., 2011a. Determination of Symmetric and Asymmetric Division Planes in Plant Cells. *Annu. Rev. Plant Biol.* 62, 387–409. <https://doi.org/10.1146/annurev-arplant-042110-103802>
- Rasmussen, C.G., Sun, B., Smith, L.G., 2011b. Tangled localization at the cortical division site of plant cells occurs by several mechanisms. *J. Cell Sci.* 124, 270–279. <https://doi.org/10.1242/jcs.073676>
- Rasmussen, C.G., Wright, A.J., Müller, S., 2013. The role of the cytoskeleton and associated proteins in determination of the plant cell division plane. *Plant J.* 75, 258–269. <https://doi.org/10.1111/tpj.12177>
- Ray, S., Agarwal, P., Arora, R., Kapoor, S., Tyagi, A.K., 2007. Expression analysis of calcium-dependent protein kinase gene family during reproductive development and abiotic stress conditions in rice (*Oryza sativa* L. ssp. *indica*). *Mol. Genet. Genomics* 278, 493–505. <https://doi.org/10.1007/s00438-007-0267-4>
- Reddy, A.S.N., 2001. Molecular motors and their functions in plants, in: *International Review of Cytology*. Academic Press Inc., pp. 97–178. [https://doi.org/10.1016/S0074-7696\(01\)04004-9](https://doi.org/10.1016/S0074-7696(01)04004-9)
- Reddy, A.S.N., Ben-Hur, A., Day, I.S., 2011. Experimental and computational approaches for the study of calmodulin interactions. *Phytochemistry* 72, 1007–1019. <https://doi.org/10.1016/j.phytochem.2010.12.022>
- Reddy, A.S.N., Day, I.S., 2001. Kinesins in the Arabidopsis genome: A comparative analysis among eukaryotes. *BMC Genomics* 2. <https://doi.org/10.1186/1471-2164-2-2>
- Reddy, A.S.N., Day, I.S., 2000. The role of the cytoskeleton and a molecular motor in trichome morphogenesis. *Trends Plant Sci.* 5, 503–505. [https://doi.org/10.1016/S1360-1385\(00\)01792-1](https://doi.org/10.1016/S1360-1385(00)01792-1)
- Reddy, A.S.N., Narasimhulu, S.B., Safadi, F., Golovkin, M., 1996. A plant kinesin heavy chain-like protein is a calmodulin-binding protein. *Plant J.* 10, 9–21. <https://doi.org/10.1046/j.1365-313X.1996.10010009.x>
- Reddy, V.S., Day, I.S., Thomas, T., Reddy, A.S.N., 2004. KIC, a Novel Ca²⁺ Binding Protein with One EF-Hand Motif, Interacts with a Microtubule Motor Protein and Regulates Trichome Morphogenesis 16, 185–200. <https://doi.org/10.1105/tpc.016600.2>
- Reichelt, S., Knight, A.E., Hodge, T.P., Baluska, F., Samaj, J., Volkmann, D., Kendrick-Jones, J., 1999. Characterization of the unconventional myosin VIII in plant cells and its localization at the post-cytokinetic cell wall. *Plant J.* 19, 555–567. <https://doi.org/10.1046/j.1365-313X.1999.00553.x>
- Richardson, D.N., Simmons, M.P., Reddy, A.S.N., 2006. Comprehensive comparative analysis of kinesins in photosynthetic eukaryotes, *BMC Genomics*. <https://doi.org/10.1186/1471-2164-7-18>
- Rodrigo-Peirís, T., Xu, X.M., Zhao, Q., Wang, H.J., Meier, I., 2011. RanGAP is required for post-meiotic mitosis in female gametophyte development in Arabidopsis thaliana. *J. Exp. Bot.* 62, 2705–2714. <https://doi.org/10.1093/jxb/erq448>
-

-
- Rogers, S.L., Rogers, G.C., Sharp, D.J., Vale, R.D., 2002. *Drosophila* EB1 is important for proper assembly, dynamics, and positioning of the mitotic spindle. *J. Cell Biol.* 158, 873–884. <https://doi.org/10.1083/jcb.200202032>
- Romeis, T., Ludwig, A.A., Martin, R., Jones, J.D.G., 2001. Calcium-dependent protein kinases play an essential role in a plant defence response. *EMBO J.* 20, 5556–5567. <https://doi.org/10.1093/emboj/20.20.5556>
- Sabelli, P.A., Larkins, B.A., 2009. The Development of Endosperm in Grasses. *Plant Physiol.* 149, 14–26. <https://doi.org/10.1104/pp.108.129437>
- Sabharwal, V., Koushika, S.P., 2019. Crowd Control: Effects of Physical Crowding on Cargo Movement in Healthy and Diseased Neurons. *Front. Cell. Neurosci.* 13, 1–17. <https://doi.org/10.3389/fncel.2019.00470>
- Saijo, Y., Hata, S., Kyojuka, J., Shimamoto, K., Izui, K., 2000. Over-expression of a single Ca²⁺-dependent protein kinase confers both cold and salt/drought tolerance on rice plants. *Plant J.* 23, 319–327. <https://doi.org/10.1046/j.1365-313X.2000.00787.x>
- Sakai, T., Honing, H. Van Der, Nishioka, M., Uehara, Y., Takahashi, M., Fujisawa, N., Saji, K., Seki, M., Shinozaki, K., Jones, M.A., Smirnov, N., Okada, K., Wasteneys, G.O., 2008. Armadillo repeat-containing kinesins and a NIMA-related kinase are required for epidermal-cell morphogenesis in *Arabidopsis*. *Plant J.* 53, 157–171. <https://doi.org/10.1111/j.1365-313X.2007.03327.x>
- Sanders, D., Brownlee, C., Harper, J.F., 1999. Communicating with calcium. *Plant Cell* 11, 691–706. <https://doi.org/10.1105/tpc.11.4.691>
- Sanders, D., Pelloux, J., Brownlee, C., Harper, J.F., 2002. Calcium at the Crossroads of Signaling Calcium Signals: A Central Paradigm in. *Plant Cell* 401–417. <https://doi.org/10.1105/tpc.002899.Calcium>
- Sano, T., Higaki, T., Oda, Y., Hayashi, T., Hasezawa, S., 2005. Appearance of actin microfilament “twin peaks” in mitosis and their function in cell plate formation, as visualized in tobacco BY-2 cells expressing GFP-fimbrin. *Plant J.* 44, 595–605. <https://doi.org/10.1111/j.1365-313X.2005.02558.x>
- Sasabe, M., Machida, Y., 2012. Regulation of organization and function of microtubules by the mitogen-activated protein kinase cascade during plant cytokinesis. *Cytoskeleton* 69, 913–918. <https://doi.org/10.1002/cm.21072>
- Sawin, K.E., Mitchison, T.J., 1995. Mutations in the kinesin-like protein Eg5 disrupting localization to the mitotic spindle. *Proc. Natl. Acad. Sci. U. S. A.* 92, 4289–4293. <https://doi.org/10.1073/pnas.92.10.4289>
- Schaefer, E., Belcram, K., Uyttewaal, M., Duroc, Y., Goussot, M., Legland, D., Laruelle, E., De Tauzia-Moreau, M.L., Pastuglia, M., Bouchez, D., 2017. The preprophase band of microtubules controls the robustness of division orientation in plants. *Science* (80-.). 356, 186–189. <https://doi.org/10.1126/science.aal3016>
- Schmiedel, G., Reiss, H.D., Schnepf, E., 1981. Associations between membranes and microtubules during mitosis and cytokinesis in caulonema tip cells of the moss *Funaria hygrometrica*. *Protoplasma* 108, 173–190. <https://doi.org/10.1007/BF01276891>
- Sedbrook, J.C., 2004. MAPs in plant cells: Delineating microtubule growth dynamics and organization. *Curr. Opin. Plant Biol.* <https://doi.org/10.1016/j.pbi.2004.09.017>
- Sedbrook, J.C., Kaloriti, D., 2008. Microtubules, MAPs and plant directional cell expansion. *Trends Plant Sci.* 13, 303–310. <https://doi.org/10.1016/j.tplants.2008.04.002>
- Seguí-Simarro, J.M., Otegui, M.S., Austin, J.R., Staehelin, L.A., 2007. Plant cytokinesis - Insights gained from electron tomography studies. *Plant Cell Monogr.* 9, 251–287. https://doi.org/10.1007/7089_2007_131
- Shaw, S.L., 2003. Sustained Microtubule Treadmilling in *Arabidopsis* Cortical Arrays. *Science* (80-.). 300, 1715–1718. <https://doi.org/10.1126/science.1083529>
- Sheen, J., 1996. Ca²⁺-dependent protein kinases and stress signal transduction in plants. *Science* (80-.). 274, 1900–1902. <https://doi.org/10.1126/science.274.5294.1900>
- Shen, Z., Collatos, A.R., Bibeau, J.P., Furt, F., Vidali, L., 2012. Phylogenetic analysis of the kinesin superfamily from *Physcomitrella*. *Front. Plant Sci.* 3. <https://doi.org/10.3389/fpls.2012.00230>
- Shu, H.B., Joshi, H.C., 1995. γ -Tubulin can both nucleate microtubule assembly and self-assemble into novel tubular structures in mammalian cells. *J. Cell Biol.* 130, 1137–1147. <https://doi.org/10.1083/jcb.130.5.1137>
- Sinnott, E.W., Bloch, R., 1940. Cytoplasmic Behavior during Division of Vacuolate Plant Cells. *Proc. Natl. Acad. Sci.* 26, 223–227. <https://doi.org/10.1073/pnas.26.4.223>
- Skoufias, D.A., Cole, D.G., Wedaman, K.P., Scholey, J.M., 1994. The carboxyl-terminal domain of kinesin heavy
-

-
- chain is important for membrane binding. *J. Biol. Chem.* 269, 1477–85.
- Smertenko, A., Hewitt, S.L., Jacques, C.N., Kacprzyk, R., Liu, Y., Marcec, M.J., Moyo, L., Ogden, A., Oung, H.M., Schmidt, S., Serrano-Romero, E.A., 2018. Phragmoplast microtubule dynamics - A game of zones. *J. Cell Sci.* 131, 1–11. <https://doi.org/10.1242/jcs.203331>
- Smertenko, A.P., Chang, H.-Y., Wagner, V., Kaloriti, D., Fenyk, S., Sonobe, S., Lloyd, C., Hauser, M.-T., Hussey, P.J., 2004. The Arabidopsis Microtubule-Associated Protein AtMAP65-1: Molecular Analysis of Its Microtubule Bundling Activity. *Plant Cell* 16, 2035–2047. <https://doi.org/10.1105/tpc.104.023937>
- Smertenko, A.P., Chang, H.Y., Sonobe, S., Fenyk, S.I., Weingartner, M., Bögre, L., Hussey, P.J., 2006. Control of the AtMAP65-1 interaction with microtubules through the cell cycle. *J. Cell Sci.* 119, 3227–3237. <https://doi.org/10.1242/jcs.03051>
- Smertenko, A.P., Piette, B., Hussey, P.J., 2011. The origin of phragmoplast asymmetry. *Curr. Biol.* 21, 1924–1930. <https://doi.org/10.1016/j.cub.2011.10.012>
- Smith, L.G., 2001. Plant cell division: Building walls in the right places. *Nat. Rev. Mol. Cell Biol.* 2, 33–39. <https://doi.org/10.1038/35048050>
- Smith, L.G., Gerttula, S.M., Han, S., Levy, J., 2001. TANGLED1: A microtubule binding protein required for the spatial control of cytokinesis in maize. *J. Cell Biol.* 152, 231–236. <https://doi.org/10.1083/jcb.152.1.231>
- Smith, L.G., Hake, S., Sylvester, A.W., 1996. The tangled-1 mutation alters cell division orientations throughout maize leaf development without altering leaf shape. *Development* 122, 481–489.
- Song, H., Golovkin, M., Reddy, A.S.N., Endow, S.A., 1997. In vitro motility of AtkCBP, a calmodulin-binding kinesin protein of Arabidopsis. *Proc. Natl. Acad. Sci. U. S. A.* 94, 322–327. <https://doi.org/10.1073/pnas.94.1.322>
- Spector, D.L., Lamond, A.I., 2011. Nuclear Speckles. *Cold Spring Harb. Perspect. Biol.* 3, a000646–a000646. <https://doi.org/10.1101/cshperspect.a000646>
- Spinner, L., Gadeyne, A., Belcram, K., Goussot, M., Moison, M., Duroc, Y., Eeckhout, D., De Winne, N., Schaefer, E., Van De Slijke, E., Persiau, G., Witters, E., Gevaert, K., De Jaeger, G., Bouchez, D., Van Damme, D., Pastuglia, M., 2013. A protein phosphatase 2A complex spatially controls plant cell division. *Nat. Commun.* 4, 1–13. <https://doi.org/10.1038/ncomms2831>
- Spinner, L., Pastuglia, M., Belcram, K., Pegoraro, M., Goussot, M., Bouchez, D., Schaefer, D.G., 2010. The function of TONNEAU1 in moss reveals ancient mechanisms of division plane specification and cell elongation in land plants. *Development* 137, 2733–2742. <https://doi.org/10.1242/dev.043810>
- Spira, F., Mueller, N.S., Beck, G., von Olshausen, P., Beig, J., Wedlich-Söldner, R., 2012. Patchwork organization of the yeast plasma membrane into numerous coexisting domains. *Nat. Cell Biol.* 14, 640–648. <https://doi.org/10.1038/ncb2487>
- Staehelein, L.A., Hepler, P.K., 1996. Cytokinesis in Higher Plants Minireview. *Cell* 84, 821–824.
- Steinberg, G., Schliwa, M., 1995. The Neurospora organelle motor: A distant relative of conventional kinesin with unconventional properties. *Mol. Biol. Cell* 6, 1605–1618. <https://doi.org/10.1091/mbc.6.11.1605>
- Steinberg, G., Schliwa, M., Lehmler, C., Böcker, M., Kahmann, R., McIntosh, J.R., 1998. Kinesin from the plant pathogenic fungus *Ustilago maydis* is involved in vacuole formation and cytoplasmic migration. *J. Cell Sci.* 111, 2235–2246.
- Stock, M.F., Guerrero, J., Cobb, B., Eggers, C.T., Huang, T.-G., Li, X., Hackney, D.D., 1999. Formation of the Compact Conformer of Kinesin Requires a COOH-terminal Heavy Chain Domain and Inhibits Microtubule-stimulated ATPase Activity. *J. Biol. Chem.* 274, 14617–14623. <https://doi.org/10.1074/jbc.274.21.14617>
- Stöckle, D., Herrmann, A., Lipka, E., Lauster, T., Gavidia, R., Zimmermann, S., Müller, S., 2016. Putative RopGAPs impact division plane selection and interact with kinesin-12 POK1. *Nat. Plants* 2, 1–6. <https://doi.org/10.1038/nplants.2016.120>
- Stoppin-Mellet, V., Gaillard, J., Vantard, M., 2002. Functional evidence for in vitro microtubule severing by the plant katanin homologue. *Biochem. J.* 365, 337–342. <https://doi.org/10.1042/BJ20020689>
- Strompen, G., El Kasmi, F., Richter, S., Lukowitz, W., Assaad, F.F., Jürgens, G., Mayer, U., 2002. The Arabidopsis HINKEL Gene Encodes a Kinesin-Related Protein Involved in Cytokinesis and Is Expressed in a Cell Cycle-Dependent Manner. *Curr. Biol.* 12, 153–158. [https://doi.org/10.1016/S0960-9822\(01\)00655-8](https://doi.org/10.1016/S0960-9822(01)00655-8)
- Suetsugu, N., Yamada, N., Kagawa, T., Yonekura, H., Uyeda, T.Q.P., Kadota, A., Wada, M., 2010. Two kinesin-like proteins mediate actin-based chloroplast movement in Arabidopsis thaliana. *Proc. Natl. Acad. Sci.* 107,
-

- Sugiyama, Y., Wakazaki, M., Toyooka, K., Fukuda, H., Oda, Y., 2017. A Novel Plasma Membrane-Anchored Protein Regulates Xylem Cell-Wall Deposition through Microtubule-Dependent Lateral Inhibition of Rho GTPase Domains. *Curr. Biol.* 27, 2522–2528.e4. <https://doi.org/10.1016/j.cub.2017.06.059>
- Takahashi, Y., Soyano, T., Kosetsu, K., Sasabe, M., Machida, Y., 2010. HINKEL kinesin, ANP MAPKKs and MKK6/ANQ MAPKK, which phosphorylates and activates MPK4 MAPK, constitute a pathway that is required for cytokinesis in *Arabidopsis thaliana*. *Plant Cell Physiol.* 51, 1766–1776. <https://doi.org/10.1093/pcp/pcq135>
- Takeuchi, M., Karahara, I., Kajimura, N., Takaoka, A., Murata, K., Misaki, K., Yonemura, S., Staehelin, L.A., Mineyuki, Y., 2016. Single microfilaments mediate the early steps of microtubule bundling during preprophase band formation in onion cotyledon epidermal cells. *Mol. Biol. Cell* 27, 1809–1820. <https://doi.org/10.1091/mbc.E15-12-0820>
- Tamura, K., Nakatani, K., Mitsui, H., Ohashi, Y., Takahashi, H., 1999. Characterization of *katD*, a kinesin-like protein gene specifically expressed in floral tissues of *Arabidopsis thaliana*. *Gene* 230, 23–32. [https://doi.org/10.1016/S0378-1119\(99\)00070-0](https://doi.org/10.1016/S0378-1119(99)00070-0)
- Tanaka, H., Ishikawa, M., Kitamura, S., Takahashi, Y., Soyano, T., Machida, C., Machida, Y., 2004. The *AtNACK1/HINKEL* and *STUD/TETRASPORE/AtNACK2* genes, which encode functionally redundant kinesins, are essential for cytokinesis in *Arabidopsis*. *Genes to Cells* 9, 1199–1211. <https://doi.org/10.1111/j.1365-2443.2004.00798.x>
- Teixidó-Travesa, N., Villén, J., Lacasa, C., Bertran, M.T., Archinti, M., Gygi, S.P., Caelles, C., Roig, J., Lüders, J., 2010. The γ TuRC Revisited: A Comparative Analysis of Interphase and Mitotic Human γ TuRC Redefines the Set of Core Components and Identifies the Novel Subunit GCP8. *Mol. Biol. Cell* 21, 3963–3972. <https://doi.org/10.1091/mbc.e10-05-0408>
- Tian, G.W., Smith, D., Glück, S., Baskin, T.I., 2004. Higher Plant Cortical Microtubule Array Analyzed in Vitro in the Presence of the Cell Wall. *Cell Motil. Cytoskeleton* 57, 26–36. <https://doi.org/10.1002/cm.10153>
- Tian, J., Han, L., Feng, Z., Wang, G., Liu, W., Ma, Y., Yu, Y., Kong, Z., 2015. Orchestration of microtubules and the actin cytoskeleton in trichome cell shape determination by a plant-unique kinesin. *Elife* 4, 1–22. <https://doi.org/10.7554/eLife.09351>
- Tiezzi, A., Moscatelli, A., Cai, G., Bartalesi, A., Cresti, M., 1992. An immunoreactive homolog of mammalian kinesin in *Nicotiana tabacum* pollen tubes. *Cell Motil. Cytoskeleton* 21, 132–137. <https://doi.org/10.1002/cm.970210206>
- Tirnauer, J.S., 2002. EB1-Microtubule Interactions in *Xenopus* Egg Extracts: Role of EB1 in Microtubule Stabilization and Mechanisms of Targeting to Microtubules. *Mol. Biol. Cell* 13, 3614–3626. <https://doi.org/10.1091/mbc.02-04-0210>
- Tompa, P., 2014. Multiteric regulation by structural disorder in modular signaling proteins: An extension of the concept of allostery. *Chem. Rev.* 114, 6715–6732. <https://doi.org/10.1021/cr4005082>
- Torres-Ruiz, R.A., Jürgens, G., 1994. Mutations in the *FASS* gene uncouple pattern formation and morphogenesis in *Arabidopsis* development. *Development* 120, 2967–2978.
- Traas, J., Bellini, C., Nacry, P., Kronenberger, J., Bouchez, D., Caboche, M., 1995. Normal differentiation patterns in plants lacking microtubular preprophase bands. *Nature* 375, 676–677. <https://doi.org/10.1038/375676a0>
- Vale, R.D., 2003. The molecular motor toolbox for intracellular transport. *Cell* 112, 467–480. [https://doi.org/10.1016/S0092-8674\(03\)00111-9](https://doi.org/10.1016/S0092-8674(03)00111-9)
- Vale, R.D., 1991. Severing of stable microtubules by a mitotically activated protein in *xenopus* egg extracts. *Cell* 64, 827–839. [https://doi.org/10.1016/0092-8674\(91\)90511-V](https://doi.org/10.1016/0092-8674(91)90511-V)
- Vale, R.D., Fletterick, R.J., 1997. THE DESIGN PLAN OF KINESIN MOTORS, *Annu. Rev. Cell Dev. Biol.*
- Vale, R.D., Reese, T.S., Sheetz, M.P., 1985. Identification of a novel force-generating protein, kinesin, involved in microtubule-based motility. *Cell* 42, 39–50. [https://doi.org/10.1016/S0092-8674\(85\)80099-4](https://doi.org/10.1016/S0092-8674(85)80099-4)
- Valster, A.H., Hepler, P.K., 1997. Caffeine inhibition of cytokinesis: Effect on the phragmoplast cytoskeleton in living *Tradescantia* stamen hair cells. *Protoplasma* 196, 155–166. <https://doi.org/10.1007/BF01279564>
- Van Bruaene, N., Joss, G., Van Oostveldt, P., 2004. Reorganization and in Vivo Dynamics of Microtubules during *Arabidopsis* Root Hair Development. *Plant Physiol.* 136, 3905–3919. <https://doi.org/10.1104/pp.103.031591>
- Van Damme, D., 2009. Division plane determination during plant somatic cytokinesis. *Curr. Opin. Plant Biol.* 12,

- Van Damme, D., Bouget, F.Y., Van Poucke, K., Inzé, D., Geelen, D., 2004. Molecular dissection of plant cytokinesis and phragmoplast structure: A survey of GFP-tagged proteins. *Plant J.* 40, 386–398. <https://doi.org/10.1111/j.1365-313X.2004.02222.x>
- Van Leene, J., Stals, H., Eeckhout, D., Persiau, G., Van de Slijke, E., Van Isterdael, G., De Clercq, A., Bonnet, E., Laukens, K., Remmerie, N., Henderickx, K., De Vijlder, T., Abdelkrim, A., Pharazyn, A., Van Onckelen, H., Inzé, D., Witters, E., De Jaeger, G., 2007. A tandem affinity purification-based technology platform to study the cell cycle interactome in *Arabidopsis thaliana*. *Mol. Cell. Proteomics* 6, 1226–1238. <https://doi.org/10.1074/mcp.M700078-MCP200>
- Vanstraelen, M., Torres Acosta, J.A., De Veylder, L., Inzé, D., Geelen, D., 2004. A Plant-Specific Subclass of C-Terminal Kinesins Contains a Conserved A-Type Cyclin-Dependent Kinase Site Implicated in Folding and Dimerization. *Plant Physiol.* 135, 1417–1429. <https://doi.org/10.1104/pp.104.044818>
- Vanstraelen, M., Van Damme, D., De Rycke, R., Mylle, E., Inzé, D., Geelen, D., 2006. Cell cycle-dependent targeting of a kinesin at the plasma membrane demarcates the division site in plant cells. *Curr. Biol.* 16, 308–314. <https://doi.org/10.1016/j.cub.2005.12.035>
- Venverloo, C.J., Libbenga, K.R., 1987. Regulation of the Plane of Cell Division in Vacuolated Cells I. The Function of Nuclear Positioning and Phragmosome Formation. *J. Plant Physiol.* 131, 267–284. [https://doi.org/10.1016/S0176-1617\(87\)80166-9](https://doi.org/10.1016/S0176-1617(87)80166-9)
- Verde, F., Dogterom, M., Stelzer, E., Karsenti, E., Leibler, S., 1992. Control of microtubule dynamics and length by cyclin A- and cyclin B-dependent kinases in *Xenopus* egg extracts. *J. Cell Biol.* 118, 1097–1108. <https://doi.org/10.1083/jcb.118.5.1097>
- Verhey, K.J., Hammond, J.W., 2009. Traffic control: Regulation of kinesin motors. *Nat. Rev. Mol. Cell Biol.* 10, 765–777. <https://doi.org/10.1038/nrm2782>
- Verhey, K.J., Kaul, N., Soppina, V., 2011. Kinesin Assembly and Movement in Cells. *Annu. Rev. Biophys.* 40, 267–288. <https://doi.org/10.1146/annurev-biophys-042910-155310>
- Vermeer, J.E.M., Geldner, N., 2015. Lateral root initiation in *Arabidopsis thaliana*: a force awakens. *F1000Prime Rep.* 7, 1–7. <https://doi.org/10.12703/P7-32>
- Vinogradova, M. V., Malanina, G.G., Reddy, A.S.N., Fletterick, R.J., 2009. Structure of the complex of a mitotic kinesin with its calcium binding regulator. *Proc. Natl. Acad. Sci.* 106, 8175–8179. <https://doi.org/10.1073/pnas.0811131106>
- Vos, J.W., Dogterom, M., Emons, A.M.C., 2004. Microtubules Become More Dynamic but Not Shorter during Preprophase Band Formation: A Possible “Search-and-Capture” Mechanism for Microtubule Translocation. *Cell Motil. Cytoskeleton* 57, 246–258. <https://doi.org/10.1002/cm.10169>
- Vos, J.W., Safadi, F., Reddy, A.S.N., Hepler, P.K., 2000. The kinesin-like calmodulin binding protein is differentially involved in cell division. *Plant Cell* 12, 979–990. <https://doi.org/10.1105/tpc.12.6.979>
- Vosolsobě, S., Petrášek, J., Schwarzerová, K., 2017. Evolutionary plasticity of plasma membrane interaction in DREPP family proteins. *Biochim. Biophys. Acta - Biomembr.* 1859, 686–697. <https://doi.org/10.1016/j.bbmem.2017.01.017>
- Walczak, C.E., Heald, R., 2008. Mechanisms of Mitotic Spindle Assembly and Function, in: *International Review of Cytology*. Academic Press Inc., pp. 111–158. [https://doi.org/10.1016/S0074-7696\(07\)65003-7](https://doi.org/10.1016/S0074-7696(07)65003-7)
- Walker, K.L., Müller, S., Moss, D., Ehrhardt, D.W., Smith, L.G., 2007. *Arabidopsis* TANGLED Identifies the Division Plane throughout Mitosis and Cytokinesis. *Curr. Biol.* 17, 1827–1836. <https://doi.org/10.1016/j.cub.2007.09.063>
- Wang, Adler, R., 1995. Chromokinesin: A DNA-binding, kinesin-like nuclear protein. *J. Cell Biol.* 128, 761–768. <https://doi.org/10.1083/jcb.128.5.761>
- Wang, H., Liu, R., Wang, J., Wang, P., Shen, Y., Liu, G., 2014. The *Arabidopsis* kinesin gene *AtKin-1* plays a role in the nuclear division process during megagametogenesis. *Plant Cell Rep.* 33, 819–828. <https://doi.org/10.1007/s00299-014-1594-7>
- Wang, H.W., Nogales, E., 2005. Nucleotide-dependent bending flexibility of tubulin regulates microtubule assembly. *Nature* 435, 911–915. <https://doi.org/10.1038/nature03606>
- Wang, X., Schwarz, T.L., 2009. The Mechanism of Ca²⁺-Dependent Regulation of Kinesin-Mediated Mitochondrial Motility. *Cell* 136, 163–174. <https://doi.org/10.1016/j.cell.2008.11.046>

-
- Wang, X., Zhu, L., Liu, B., Wang, C., Jin, L., Zhao, Q., Yuan, M., 2007. Arabidopsis microtubule-associated protein18 functions in directional cell growth by destabilizing cortical microtubules. *Plant Cell* 19, 877–889. <https://doi.org/10.1105/tpc.106.048579>
- Wang, Y., Wang, B., Gilroy, S., Chehab, E.W., Braam, J., 2011. CML24 is Involved in Root Mechanoresponses and Cortical Microtubule Orientation in Arabidopsis. *J. Plant Growth Regul.* 30, 467–479. <https://doi.org/10.1007/s00344-011-9209-9>
- WASTENEYS, G., WILLIAMSON, R., 1989. Reassembly of microtubules in *Nitella tasmanica*: quantitative analysis of assembly and orientation. *J. Cell Biol.* 50, 76–83.
- Wasteneys, G.O., Yang, Z., 2004. New Views on the Plant Cytoskeleton. *Plant Physiol.* 136, 3884–3891. <https://doi.org/10.1104/pp.104.900133>
- Wei, L., Zhang, W., Liu, Z., Li, Y., 2009. AtKinesin-13A is located on Golgi-associated vesicle and involved in vesicle formation/budding in Arabidopsis root-cap peripheral cells. *BMC Plant Biol.* 9, 1–8. <https://doi.org/10.1186/1471-2229-9-138>
- Weingartner, M., Binarova, P., Drykova, D., Schweighofer, A., David, J., Heberle-bors, E., Doonan, J., Bögre, L., Weingartner, M., Binarova, P., Drykova, D., Schweighofer, A., David, J., 2017. Dynamic Recruitment of Cdc2 to Specific Microtubule Structures during Mitosis Published by: American Society of Plant Biologists (ASPB) Linked references are available on JSTOR for this article: Dynamic Recruitment of Cdc2 to Specific Microtubule Stru. *Plant Cell* 13, 1929–1943. <https://doi.org/10.1105/tpc.010109>
- Weisenberg, R.C., 1972. Microtubule formation in vitro in solutions containing low calcium concentrations. *Science* (80-). 177, 1104–1105. <https://doi.org/10.1126/science.177.4054.1104>
- Wendrich, J.R., Möller, B.K., Li, S., Saiga, S., Sozzani, R., Benfey, P.N., De Rybel, B., Weijers, D., 2017. Framework for gradual progression of cell ontogeny in the Arabidopsis root meristem. *Proc. Natl. Acad. Sci. U. S. A.* 114, E8922–E8929. <https://doi.org/10.1073/pnas.1707400114>
- Wendrich, J.R., Yang, B.-J., Mijnhout, P., Xue, H.-W., Rybel, B. De, Weijers, D., 2018. IQD proteins integrate auxin and calcium signaling to regulate microtubule dynamics during Arabidopsis development. *bioRxiv* 275560. <https://doi.org/10.1101/275560>
- Whitaker, M., 2008. Calcium signalling in early embryos. *Philos. Trans. R. Soc. B Biol. Sci.* 363, 1401–1418. <https://doi.org/10.1098/rstb.2008.2259>
- Whitaker, M., 2006. Calcium microdomains and cell cycle control. *Cell Calcium* 40, 585–592. <https://doi.org/10.1016/j.ceca.2006.08.018>
- Whittington, A.T., Vugrek, O., Wei, K.J., Hasenbein, N.G., Sugimoto, K., Rashbrooke, M.C., Wasteneys, G.O., 2001. MOR1 is essential for organizing cortical microtubules in plants. *Nature* 411, 610–613. <https://doi.org/10.1038/35079128>
- Wick, S.M., Duniec, J., 1983. Immunofluorescence microscopy of tubulin and microtubule arrays in plant cells. I. Preprophase band development and concomitant appearance of nuclear envelope-associated tubulin. *J. Cell Biol.* 97, 235–243. <https://doi.org/10.1083/jcb.97.1.235>
- Willemsen, V., Friml, J., Grebe, M., Toorn, A. Van Den, Palme, K., Scheres, B., 2003. Cell Polarity and PIN Protein Positioning in Arabidopsis Require. *Society* 15, 612–625. <https://doi.org/10.1105/tpc.008433.1999>
- Williamson, R.E., 1993. Organelle movements. *Annu. Rev. Plant Physiol. Plant Mol. Biol.* 44, 181–202. <https://doi.org/10.1146/annurev.pp.44.060193.001145>
- Williamson, R.E., 1986. Organelle Movements along Actin Filaments and Microtubules. *Plant Physiol.* 82, 631–634. <https://doi.org/10.1104/pp.82.3.631>
- Wilson, A.K., Pickett, F.B., Turner, J.C., Estelle, M., 1990. A dominant mutation in Arabidopsis confers resistance to auxin, ethylene and abscisic acid. *MGG Mol. Gen. Genet.* 222, 377–383. <https://doi.org/10.1007/BF00633843>
- Wittmann, T., Waterman-Storer, C.M., 2005. Spatial regulation of CLASP affinity for microtubules by Rac1 and GSK3 β in migrating epithelial cells. *J. Cell Biol.* 169, 929–939. <https://doi.org/10.1083/jcb.200412114>
- Wong, Y.L., Dietrich, K.A., Naber, N., Cooke, R., Rice, S.E., 2009. The Kinesin-1 Tail Conformationally Restricts the Nucleotide Pocket. *Biophys. J.* 96, 2799–2807. <https://doi.org/10.1016/j.bpj.2008.11.069>
- Wong, Y.L., Rice, S.E., 2010. Kinesin's light chains inhibit the head- and microtubule-binding activity of its tail. *Natl. Acad. Sci.* 107, 11781–11786. <https://doi.org/10.1073/pnas.1005854107>
- Wright, A.J., Gallagher, K., Smith, L.G., 2009. *Discordia1* and Alternative *Discordia1* Function Redundantly At the
-

-
- Cortical Division Site To Promote Preprophase Band Formation and Orient Division Planes in Maize. *Plant Cell* 21, 234–247. <https://doi.org/10.1105/tpc.108.062810>
- Wu, M., Li, Y., Chen, D., Liu, H., Zhu, D., Xiang, Y., 2016. Genome-wide identification and expression analysis of the IQD gene family in moso bamboo (*Phyllostachys edulis*). *Sci. Rep.* 6. <https://doi.org/10.1038/srep24520>
- Wu, N., Hanson, S.M., Francis, D.J., Vishnivetskiy, S.A., Thibonnier, M., Klug, C.S., Shoham, M., Gurevich, V. V., 2006. Arrestin Binding to Calmodulin: A Direct Interaction Between Two Ubiquitous Signaling Proteins. *J. Mol. Biol.* 364, 955–963. <https://doi.org/10.1016/j.jmb.2006.09.075>
- Wu, S., Xiao, H., Cabrera, A., Meulia, T., van der Knaap, E., 2011. SUN regulates vegetative and reproductive organ shape by changing cell division patterns. *Plant Physiol.* 157, 1175–1186. <https://doi.org/10.1104/pp.111.181065>
- Wu, S.Z., Bezanilla, M., 2014. Myosin VIII associates with microtubule ends and together with actin plays a role in guiding plant cell division. *Elife* 3, 1–20. <https://doi.org/10.7554/eLife.03498>
- Xiao, H., Jiang, N., Schaffner, E., Stockinger, E.J., Knaap, E. Van Der, 2008. Variation of Tomato Fruit. *Science* (80-.). 319, 1527–1530. <https://doi.org/10.1016/j.plantsci.2016.10.001>
- Xu, T., Qu, Z., Yang, X., Qin, X., Xiong, J., Wang, Y., Ren, D., Liu, G., 2009. A cotton kinesin GhKCH2 interacts with both microtubules and microfilaments. *Biochem. J.* 421, 171–180. <https://doi.org/10.1042/BJ20082020>
- Xu, W., Huang, W., 2017. Calcium-dependent protein Kinases in phytohormone signaling pathways. *Int. J. Mol. Sci.* 18, 6–10. <https://doi.org/10.3390/ijms18112436>
- Xu, X.M., Zhao, Q., Rodrigo-Peiris, T., Brkljacic, J., He, C.S., Muller, S., Meier, I., 2008. RanGAP1 is a continuous marker of the Arabidopsis cell division plane. *Proc. Natl. Acad. Sci.* 105, 18637–18642. <https://doi.org/10.1073/pnas.0806157105>
- Yamada, M., Tanaka-Takiguchi, Y., Hayashi, M., Nishina, M., Goshima, G., 2017. Multiple kinesin-14 family members drive microtubule minus end-directed transport in plant cells. *J. Cell Biol.* 216, 1705–1714. <https://doi.org/10.1083/jcb.201610065>
- Yamashita, Y.M., Jones, D.L., Fuller, M.T., 2003. Orientation of asymmetric stem cell division by the APC tumor suppressor and centrosome. *Science* (80-.). 301, 1547–1550. <https://doi.org/10.1126/science.1087795>
- Yan, X., Habedanck, R., Nigg, E.A., 2006. A Complex of Two Centrosomal Proteins, CAP350 and FOP, Cooperates with EB1 in Microtubule Anchoring. *Mol. Biol. Cell* 17, 634–644. <https://doi.org/10.1091/mbc.e05-08-0810>
- Yang, B., Wendrich, J.R., Rybel, B. De, Weijers, D., Xue, H., 2019. Rice microtubule-associated protein IQ67-DOMAIN14 regulates rice grain shape by modulating microtubule cytoskeleton dynamics. *Plant Biotechnol. J. pbi.13279*. <https://doi.org/10.1111/pbi.13279>
- Yang, G., Gao, P., Zhang, H., Huang, S., Zheng, Z.L., 2007. A mutation in MRH2 kinesin enhances the root hair tip growth defect caused by constitutively activated ROP2 small GTPase in Arabidopsis. *PLoS One* 2. <https://doi.org/10.1371/journal.pone.0001074>
- Yip, Y.Y., Pernigo, S., Sanger, A., Xu, M., Parsons, M., Steiner, R.A., Dodding, M.P., 2016. The light chains of kinesin-1 are autoinhibited. *Proc. Natl. Acad. Sci.* 113, 2418–2423. <https://doi.org/10.1073/pnas.1520817113>
- Yoshida, S., BarbierdeReuille, P., Lane, B., Bassel, G.W., Prusinkiewicz, P., Smith, R.S., Weijers, D., 2014. Genetic control of plant development by overriding a geometric division rule. *Dev. Cell* 29, 75–87. <https://doi.org/10.1016/j.devcel.2014.02.002>
- Zentella, R., Zhang, Z.L., Park, M., Thomas, S.G., Endo, A., Murase, K., Fleet, C.M., Jikumaru, Y., Nambara, E., Kamiya, Y., Sun, T.P., 2007. Global Analysis of DELLA Direct Targets in Early Gibberellin Signaling in Arabidopsis. *Plant Cell* 19, 3037–3057. <https://doi.org/10.1105/tpc.107.054999>
- Zhang, D., Wadsworth, P., Hepler, P.K., 1990. Microtubule dynamics in living dividing plant cells: confocal imaging of microinjected fluorescent brain tubulin. *Proc. Natl. Acad. Sci.* 87, 8820–8824. <https://doi.org/10.1073/pnas.87.22.8820>
- Zhang, M., Zhang, B., Qian, Q., Yu, Y., Li, R., Zhang, J., Liu, X., Zeng, D., Li, J., Zhou, Y., 2010. Brittle Culm 12, a dual-targeting kinesin-4 protein, controls cell-cycle progression and wall properties in rice. *Plant J.* 63, 312–328. <https://doi.org/10.1111/j.1365-313X.2010.04238.x>
- Zhang, Y., Iakovidis, M., Costa, S., 2016. Control of patterns of symmetric cell division in the epidermal and cortical tissues of the Arabidopsis root. *Development* 143, 978–982. <https://doi.org/10.1242/dev.129502>
-

-
- Zhang, Y., Kang, E., Yuan, M., Fu, Y., Zhu, L., 2015. PCaP2 regulates nuclear positioning in growing *Arabidopsis thaliana* root hairs by modulating filamentous actin organization. *Plant Cell Rep.* 34, 1317–1330. <https://doi.org/10.1007/s00299-015-1789-6>
- Zhong, R., Burk, D.H., Morrison, W.H., Ye, Z.H., 2002. A kinesin-like protein is essential for oriented deposition of cellulose microfibrils and cell wall strength. *Plant Cell* 14, 3101–3117. <https://doi.org/10.1105/tpc.005801>
- Zhou, S., Wang, Yang, Li, W., Zhao, Z., Ren, Y., Wang, Yong, Gu, S., Lin, Q., Wang, D., Jiang, L., Su, N., Zhang, X., Liu, L., Cheng, Z., Lei, C., Wang, J., Guo, X., Wu, F., Ikehashi, H., Wang, H., Wan, J., 2011. Pollen semi-sterility1 encodes a kinesin-1-like protein important for male meiosis, anther dehiscence, and fertility in rice. *Plant Cell* 23, 111–129. <https://doi.org/10.1105/tpc.109.073692>
- Zhu, C., Dixit, R., 2012. Functions of the *Arabidopsis* kinesin superfamily of microtubule-based motor proteins. *Protoplasma* 249, 887–899. <https://doi.org/10.1007/s00709-011-0343-9>
- Zhu, C., Ganguly, A., Baskin, T.I., McClosky, D.D., Anderson, C.T., Foster, C., Meunier, K.A., Okamoto, R., Berg, H., Dixit, R., 2015. The Fragile Fiber1 Kinesin Contributes to Cortical Microtubule-Mediated Trafficking of Cell Wall Components. *Plant Physiol.* 167, 780–792. <https://doi.org/10.1104/pp.114.251462>
- Zhu, L., Zhang, Y., Kang, E., Xu, Q., Wang, M., Rui, Y., Liu, B., Yuan, M., Fu, Y., 2013. MAP18 regulates the direction of pollen tube growth in *Arabidopsis* by modulating F-actin organization. *Plant Cell* 25, 851–867. <https://doi.org/10.1105/tpc.113.110528>

Acknowledgements

I would like to take this opportunity to thank those people who directly or indirectly contribute to the successful completion of this thesis. At the very first, I want to acknowledge to Prof. Dr. Steffen Abel for accepting me as a doctoral student. I would like to thank Dr Katharina Bürstenbinder to supervise on my research work and keeping her doors open for scientific suggestions. I would like to thank Professor Dr Ingo Heilmann for his guidance as my second supervisor.

Institution Colleagues

I would like to acknowledge for constant support and care by Gina Stamm, Marlene Zimmer, Michael Niemeyer, and Stefan Mielke during my PhD. My special thanks to Antje Hellmuth for her constant support, I would also like to thank to Malte Kölling, for his suggestions to this thesis. I owe deep gratitude to Sandra, Michael and Marcus, Paul Pflug, Jacob Quegwer and Lukas müller for their support during my PhD work. I would also like to thank Dr LuZ Irina A. Calderon Villalobos and Dr Debora Gasperini for their innovative scientific discussion. Big thanks to Gardeners of the greenhouse and taking care of my huge number of plants. I would also like to acknowledge Mrs. Anshu khatri and Mrs. Dipannita Mitra for their support. I would like to give my great regards and thanks to Hagen Stellmach for the technical support in microscopy.

Collaborators

I would like to thank to Dr. Sabine Müller to provide me opportunity to work in her laboratory. My special thanks to Dr. Pantelis Livanos and Dr. Arvid Herrmann for their scientific suggestion.

Funding

I would like to thank the Erasmus Mundus BRAVE program of the European Union for initial funding (three years) of my research work. I would like to acknowledge the BRAVE coordinator Dr. Andreas Voloudakis (AUA, Greece) and Prof. Dr. Sven Erik Behrens (MLU, Germany) for their constant support during the funding period.

Friends and family

I appreciate the efforts of BRAVE fellows in Halle for making my social life enjoy full during the stay in *Halle an der Saale*. I would like to special thanks to Prodyut Mondal and Dr. Archana to always be on my side in all situations. I owe my deep sense of gratitude to my parents and my in-laws for their love and patience during my research stay. Also thanks to my sisters and my brother for their continuous encouragement and support. A beyond thanks to dearest husband Mr. Harish Kumar Rai for his continuous support. I could not even think to finish my thesis without his enormous support.

CURRICULUM VITAE

Name: Pratibha Kumari
Nationality: Indian
Date of birth: 20.05.1990
Place of birth: Buxar, Bihar, India

RESEARCH EXPERIENCE

PhD Research - Dec-2014 – until now, Leibniz Institute of Plant Biochemistry, Halle, Germany Dept. Molecular Signal Processing, Prof. Dr. Steffen Abel, Dr. Katharina Bürstenbinder

Topic: Investigating the role of IQD proteins in cell wall positioning.

Scientific Visit - Worked as visiting scientist for one month in the lab of Dr. Sabine Müller, University of Tübingen, Germany

M. Sc. Research - Sep-2013 – Aug-2014, Jawaharlal Nehru University, New Delhi-110067, India Plant Transformations Laboratory, Prof. Dr. Neera Bhalla Sarin

Topic: Development of transgenic *Brassica juncea* overexpressing HSF3 gene for abiotic stress Tolerance

EDUCATIONS

M. Sc. (Life sciences) - July-2014, School of Life Sciences, Jawaharlal Nehru University, New Delhi, India

B. Sc. (Biotechnology) - Mar-2011, Ranchi Women's College, Ranchi, India.

PUBLICATIONS

Peer-Reviewed Journals

Calcium- and calmodulin-regulated microtubule-associated proteins as signal- integration hubs at the plasma membrane–cytoskeleton nexus.

Malte Kölling*, **Pratibha Kumari***, and Katharina Bürstenbinder†, Journal of exp. Botany (2019), 70:387-396, *these authors contributed equally

Microtubule-associated protein IQ67 DOMAIN5 regulates morphogenesis of leaf pavement cells in *Arabidopsis thaliana*.

Dipannita Mitra*, Sandra Klemm*, **Pratibha Kumari***, and Katharina Bürstenbinder†, Journal of exp. Botany, (2019) 70:529-543, *these authors contributed equally

Book Chapter:

Enhancing Cold Tolerance in Horticultural Plants Using In vitro Approaches.

Samira Chugh, Shweta Sharma, Anjana Rustogi, **Pratibha Kumari**, Aayushi Agrawal and Deepak Kumar†, Springer, (2018), <https://doi.org/10.1007/978-981-10-7479-0>.

Erklärung zur Dissertation

Name

Pratibha Kumari

Geburtsdatum, -ort:

20.05.1990; Buxar, Bihar, (Indien)

Eidesstattliche Erklärung zu meiner Dissertation mit dem Titel: "Dissecting functions of *Arabidopsis thaliana* IQD and KLCR proteins in the control of microtubule-related processes"

Sehr geehrte Damen und Herren,

Hiermit erkläre ich, dass ich die beigefügte Dissertation selbstständig verfasst und keine anderen als die angegebenen Hilfsmittel genutzt habe. Alle wörtlich oder inhaltlich übernommenen Stellen habe ich als solche gekennzeichnet.

Ich versichere außerdem, dass ich die beigefügte Dissertation nur in diesem und keinem anderen Promotionsverfahren eingereicht habe und, dass diesem Promotionsverfahren keine endgültig gescheiterten Promotionsverfahren vorausgegangen sind.

Halle (Saale), 18/12/2019

Ort, Datum

Pratibha Kumari

Unterschrift